Economic Model Predictive Control for Spray Drying Plants

Petersen, Lars Norbert

Publication date:
2016

Document Version
Publisher's PDF, also known as Version of record

Economic Model Predictive Control for Spray Drying Plants

Lars Norbert Petersen

Kongens Lyngby 2016
PHD-2016-403

Technical University of Denmark
Department of Applied Mathematics and Computer Science
Richard Petersens Plads, building 324,
2800 Kongens Lyngby, Denmark
Phone +45 4525 3031
compute@compute.dtu.dk
www.compute.dtu.dk

PHD-2016-403, ISSN 0909-3192

Preface

This thesis is submitted at the Department of Applied Mathematics and Computer Science at the Technical University of Denmark in partial fulfillment of the requirements for acquiring the PhD degree in engineering. The project has been funded by GEA Process Engineering A/S and Innovation Fund Denmark under the Industrial PhD program, project 12-128720.

The thesis deals with the development and application of new models and Model Predictive Control (MPC) strategies to optimize the operation of four-stage spray dryers. We develop first-principle dynamic models of a four-stage spray dryer that facilitates development and comparison of control strategies. We develop MPCs that are tailored for the process to optimize the cost of operation by maximizing the production rate while minimizing the energy consumption and producing powder at given quality specifications. The proposed linear tracking MPC with steady-state optimal targets (RTO) and the Economic Nonlinear MPC (E-MPC) control strategies are compared by closed-loop simulations. In these simulations, the conventional PI controller serves as a benchmark for the performance comparison. Moreover, we industrially implement and demonstrate the application of the proposed MPC with RTO for control of a full sized industrial milk powder spray dryer.

The thesis consists of a summary report and a collection of nine research papers written during the project period October 2012 to January 2016. Seven papers have been published at international peer-reviewed scientific conferences. Two journal papers are currently under review for publication in peer-reviewed scientific journals.

Kgs. Lyngby, 31-January-2016

Lars Norbert Petersen

Acknowledgements

The advisors of the thesis are John B. Jørgensen, Niels K. Poulsen, Hans Henrik Niemann and Christer Utzen. I am thankful to my main supervisor, John B. Jørgensen, for his high scientific ambitions and expertise in control matters. From him I have drawn scientific knowledge, had fruitful discussions and got my guidance during the project. Thanks also goes to Niels K. Poulsen and Hans Henrik Niemann for always keeping a door open when I needed their suggestions. I want to thank my industrial supervisor, Christer Utzen, for initiating this project, helping me in many technical matters and promoting the project at GEA. Also, I would like to thank him for bringing the fun and joy into the work, both during travel and at the office. Many thanks also goes to my other colleagues Emil Sokoler, Sabrina L. Wendt, Gianluca Frison and Emil S. Christensen. In particular thanks to Rasmus Halvgaard for our hours of technical discussions.

I would also like to thank Prof. James B. Rawlings for taking good care of me during my research stay at University of Wisconsin–Madison. I would like to thank him for the valuable guidance and for co-authoring a paper.

Finally, I would like to thank my friends and family, in particular my girlfriend, Ditte Kirstine Andersen. She has been a constant support, given me love and strength.

Summary (English)

The main challenge in cost optimal operation of a spray dryer, is to maximize the production rate while minimizing the energy consumption, keeping the residual moisture content of the powder below a maximum limit and avoiding that the powder sticks to the chamber walls. The conventional PI control strategy is simple, but known to be insufficient at providing optimal operation in the presence of variations in the feed and the ambient air humidity. This motivates our investigation of Model Predictive Control (MPC) strategies.

In this thesis, we consider the development and application of new models and MPC strategies to optimize the operation of four-stage spray dryers. The models are first-principle dynamic models with parameters identified from dryer specific experiments and powder properties identified from laboratory tests. A simulation model is used for detailed closed-loop simulations and a complexity reduced control model is used for state estimation and prediction in the controllers. These models facilitate development and comparison of control strategies. We develop two MPC strategies; a linear tracking MPC with a Real-Time Optimization layer (MPC with RTO) and an Economic Nonlinear MPC (E-MPC). We tailor these for the spray drying process to optimize the cost of operation by adjustments to the inputs of the dryer according to the present disturbances and process constraints. Simulations show that the MPC strategies improve the profit of operation by up to 9.69%, the production of powder by up to 9.61%, the residual moisture content by up to 3.37%, the energy efficiency by up to 6.06% and the specific energy consumption is decreased by up to 6.72% while the produced powder is within the given quality specifications and sticky powder on the walls of the chamber is avoided. Thus, we are able to improve the cost of operation significantly compared to the conventional PI control strategy.

The proposed MPC strategies are based on a feedback control algorithm that explicitly handles constrained control inputs and uses a model to predict and optimize the future behavior of the dryer. The solution of the control problem results in a sequence of inputs for a finite horizon, out of which only the first input is applied to the dryer. This procedure is repeated at each sample instant and is solved numerically in real-time. The MPC with RTO tracks a target that optimizes the cost of operation at steady-state. The E-MPC optimizes the cost of operation directly by having this objective directly in the controller. The need for the RTO layer is then eliminated.

We demonstrate the industrial application of the proposed MPC with RTO to control a GEA MSD$^{\text{TM}}$-1250 spray dryer, which produces approximately 7500 kg/hr of enriched milk powder. Compared to the conventional PI controller, our first results shows that the MPC improves the profit of operation by approximately 228,000 €/year, the product rate by 4.44% (322 kg/hr), the residual moisture content by 6.31% (0.166 p.p.) and decreases the specific energy consumption by 3.10%. The demonstrated MPC with RTO is fully integrated in the daily operation of the spray dryer today.

Our primary objectives in the thesis are: 1) Spray dryer modeling of a small-scale four-stage spray dryer. The purpose of the models are to enable simulations of the spray drying process at different operating points, such that the models facilitate development and comparison of control strategies; 2) Development of MPC strategies that automatically adjust the dryer to variations in the feed and the ambient air humidity, such that the energy consumption is minimized, the residual moisture content in the powder is controlled within the specifications and sticky powder is avoided from building up on the dryer walls; 3) Demonstrate the industrial application of an MPC strategy to a full-scale industrial four-stage spray dryer.

The main scientific contributions can be summarized to:

- Modeling of a four-stage spray dryer. We develop new first-principles engineering models for simulation of a four-stage spray dryer. These models enables simulations of the spray dryer at different operating points with high accuracy.
- Development and simulation of control strategies. We develop two control strategies, the MPC with RTO and the E-MPC strategy. The performance of the controllers is studied and evaluated by simulation.
- Industrial application of MPC to a spray dryer. We demonstrate that our proposed MPC with RTO is applicable to an industrial GEA MSD$^{\text{TM}}$-1250 spray dryer, that produces enriched milk powder.

Summary (Danish)

Den største udfordring i omkostningsoptimal drift af en spraytørrer er at maksimere produktionen af pulver, samtidig med at energiforbruget minimeres, restfugtindholdet i pulveret holdes under en maksimumgrænse og at afsætninger på kammervæggene undgås. Den konventionelle PI-reguleringsstrategi er enkel, men kendt for at være utilstrækkelige ved variationer i føden og den omgivende luftfugtighed. Dette motiverer vores undersøgelse af Model Prædiktive Kontrol (MPC)-strategier.

I denne afhandling, behandler vi udviklingen af nye modeller og brugen af MPC til fire-trins-spraytørrere. Modellerne er fysik-basseret dynamiske modeller med parametre identificeret fra spraytørrerspecifikke eksperimenter og pulver egenskaber identificeret fra laboratorieforsøg. En simuleringsmodel anvendes til detaljerede simuleringer og en simplere reguleringsmodel bruges til tilstandsestimering og forudsigelse i regulatorerne. Tilsammen letter modellerne udvikling og sammenligning af reguleringsstrategier. Vi udvikler to MPC strategier; en lineær MPC med et realtids optimeringslag (MPC med RTO) og en økonomisk ulineær MPC (E-MPC). Vi skræddersyer disse til spraytørringsprocessen med det mål at optimere driftsomkostningerne ved at justere spraytørreren til forstyrrelser og procesbegrænsninger. Simuleringer viser, at MPC strategierne kan forbedre driftoverskudet med op til 9,69%, produktionen af pulver med op til 9,61%, restfugtindholdet med op til 3,37%, energieffektiviteten med op til 6,06% og reducere det specifikke energi forbrug med op til 6,72%, mens det producerede pulver er inden for de givne kvalitetskrav og pulverafsætninger undgås. Således er vi i stand til at forbedre driftsomkostningerne betydeligt sammenlignet med den konventionelle PI-reguleringsstrategi.

De foreslåede MPC strategier er baseret på en algoritme til tilbagekoblingsregulering, som håndterer begrænsningerne i styresignalerne og benytter modellerne til at forudsige og optimere det fremtidige respons af spraytørren. Resultatet af reguleringsproblemet er en sekvens af inputs over en endelig horisont, hvoraf kun det første input benyttes på spraytørreren. Denne procedure gentages og løses numerisk i realtid. MPC med RTO følger en reference der optimerer driftsomkostningerne ved stationær tilstand. E-MPC optimerer driftsomkostningerne ved at have dette mål direkte i objektivfunktionen af regulatoren. Behovet for RTO fjernes derved.

Vi demonstrerer anvendelsen af den foreslåede MPC med RTO på en industriel GEA MSD^{TM} -1250 spraytørre, der producerer ca. 7500 kg/time mælkepulver. Sammenlignet med den konventionelle PI-reguleringsstrategi, viser vores første resultater at MPC forbedrer driftsoverskuddet med ca. 1,7 mill. kr/år, produktion af pulver med 4,44% (322 kg/time), restfugtindholdet med 6,31% (0,166 p.p.), og det specifikke energi forbrug med 3,10%. Den demonstrerede MPC med RTO er i dag fuldt integreret i den daglige drift af spraytørreren.

Vores primære mål i afhandlingen er: 1) Modellering af en mindre fire-trins-spraytørre. Formålet med modellerne er at lave simuleringer af spraytørringsprocessen ved forskellige operationsområder, således at modellerne fremmer udvikling og sammenligning af reguleringsstrategier; 2) Udvikling af MPC strategier, der automatisk justerer spraytørreren til variationer i føden og den omgivende luftfugtighed, således at produktionen af pulver maksimeres mens energiforbruget minimeres, restfugtindholdet i pulveret holdes inden for grænserne og pulverafsætninger på kammervæggene undgås; 3) Industriel demonstrering af en foreslået MPC strategi på et fuldskala industrielt fire-trins spraytørringsanlæg.

De vigtigste videnskabelige bidrag kan sammenfattes til:

- Modellering af en fire-trins-spraytørrer. Vi udvikler fysik-baserede modeller til simulering af en fire-trins-spraytørrer. Disse modeller muliggør simuleringer af spraytørreren ved forskellige arbejdspunkter med stor nøjagtighed.
- Udvikling og simulering af reguleringsstrategier. Vi udvikler to reguleringsstrategier, en MPC med RTO og en E-MPC strategi. Effektiviteten af regulatorerne undersøges og evalueres ved simulering.
- Industriel anvendelse af MPC til en spraytørrer. Vi viser, at vores foreslåede MPC med RTO kan benyttes på et industrielt GEA MSD^{TM}-1250 spraytørringsanlæg, der producerer beriget mælkepulver.

List of publications

International journals

The following papers were submitted for publication in international peer-reviewed journals during the project period. They constitute the main contributions of the PhD project. We advice the reader to pick up on the specific details in the papers after reading the summary report.

[A] Petersen, Lars Norbert; Poulsen, Niels Kjølstad; Niemann, Hans Henrik; Utzen, Christer; Jørgensen, John Bagterp An experimentally validated simulation model for a four stage spray dryer. *Journal of Process Control, pp. submitted, 2016.*

[B] Petersen, Lars Norbert; Poulsen, Niels Kjølstad; Niemann, Hans Henrik; Utzen, Christer; Jørgensen, John Bagterp Comparison of Control Strategies for Optimization of Spray Dryer Operation *Journal of Process Control, pp. submitted, 2016.*

Peer-reviewed conferences

In addition to the papers listed above, the following peer-reviewed conference contributions were also published during the project period.

[C] Petersen, Lars Norbert; Poulsen, Niels Kjølstad; Niemann, Hans Henrik; Utzen, Christer; Jørgensen, John Bagterp A Grey-Box Model for Spray Drying Plants. *10th IFAC International Symposium on Dynamics and Control of Process Systems (DYCOPS 2013), Mumbai, pp. 559–564, 2013.*

[D] Petersen, Lars Norbert; Jørgensen, John Bagterp Real-time economic optimization for a fermentation process using Model Predictive Control. *13th European Control Conference (ECC 2014), Strasbourg, pp. 1831–1836, 2014.*

[E] Petersen, Lars Norbert; Poulsen, Niels Kjølstad; Niemann, Hans Henrik; Utzen, Christer; Jørgensen, John Bagterp Application of Constrained Linear MPC to a Spray Dryer. *IEEE Multi-conference on Systems and Control (MSC 2014), Antibes, pp. 2120–2126, 2014.*

[F] Petersen, Lars Norbert; Poulsen, Niels Kjølstad; Niemann, Hans Henrik; Utzen, Christer; Jørgensen, John Bagterp Economic Optimization of Spray Dryer Operation using Nonlinear Model Predictive Control. *53rd IEEE Conference on Decision and Control (CDC 2014), Los Angeles, pp. 6794–6800, 2014.*

[G] Petersen, Lars Norbert; Jørgensen, John Bagterp; Rawlings, James B. Economic Optimization of Spray Dryer Operation using Nonlinear Model Predictive Control with State Estimation. *9th International Symposium on Advanced Control of Chemical Processes (ADCHEM 2015), Whistler, pp. 507–513, 2015.*

[H] Petersen, Lars Norbert; Poulsen, Niels Kjølstad; Niemann, Hans Henrik; Utzen, Christer; Jørgensen, John Bagterp Comparison of Linear and Nonlinear Model Predictive Control for Optimization of Spray Dryer Operation. *5th IFAC Conference on Nonlinear Model Predictive Control (NMPC 2015), Seville, pp. 218–223, 2015.*

[I] Petersen, Lars Norbert; Poulsen, Niels Kjølstad; Niemann, Hans Henrik; Utzen, Christer; Jørgensen, John Bagterp Industrial Application of Model Predictive Control to a Milk Powder Spray Drying Plant. *15th European Control Conference (ECC 2016), Aalborg, pp. accepted, 2016.*

Contents

Part I

Summary Report

Chapter 1

Introduction

In this chapter we motivate the need for Model Predictive Control (MPC) for spray drying plants. First, we present the megatrends that drives the food industry and explain how MPC can play an important role in leveraging the future challenges. We briefly motivate and describe the objective of the research project, highlight the state-of-the-art and give an outline of the thesis.

1.1 Megatrends in the Food Industry

The world is currently undergoing major interrelated global changes such as population growth, urbanization, climate change etc. These pose challenges that have implications for human life and every industry all over the world. Thereby also for the food processing industry. Fig. 1.1 shows three megatrends that are expected in particularly to shape the future of the food industry. These are the urbanization and population growth, food quality and safety concerns and rising energy costs [GEA].

Urbanization and Population Growth
The growing population and urbanization require ever increasing amounts of food to be collected, processed, shipped and stored before reaching the end

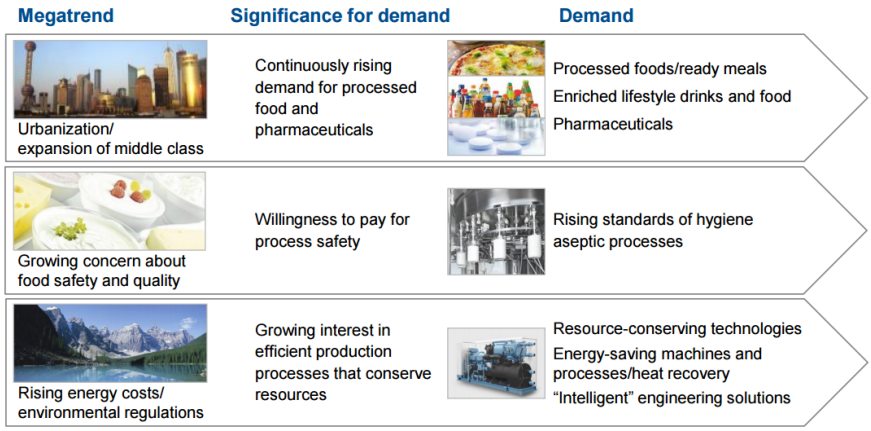

Figure 1.1: Megatrends expected to shape the future of the food industry [GEA].

consumer. Globally, human population growth amounts to around 75 million annually, or 1.1% per year. This means that the total global population is expected to grow from 7 billion in 2012 to a total population of 8.4 billion by mid-2030 and 9.6 billion by mid-2050 [EY15]. Furthermore, it is expected that urbanization will make almost two-thirds of the world's population reside in cities by 2030, compared to just under one-third in 2009. The increased number of formerly self-sufficient rural families, that now lives in the cities, have significantly increased spending power and changed lifestyle. With this development follows an increased consumption of processed foods and in increased amounts per person [Mur07]. Based on the population growth and urbanization, it is estimated that a 50% increase in food production will be necessary to feed the world population [Chi14]. In the future, the food production must therefore grow, particularly in the developing countries, to meet the food demand. At the same time climate changes and water scarcity will demand that the food is produced using less raw material and water.

Food Quality and Safety Concerns

Recent concerns also relate to the food quality and safety. The increased number of process-steps in the food industry increase the time from farmer to end consumer. This allows for bacterial growth and eventual product spoiling. Food quality e.g. the product water content that dictates the bacterial growth, must therefore be strictly monitored and controlled in all parts of the industry. Food safety is a constant concern. A Chinese food scandal from 2008 illustrates the importance of food safety, as melamine-tainted milk powder led to the deaths of six infants and hundreds more being hospitalized [Dug15]. The mistrust towards Chinese-produced milk powder still remains, leading to high demand for

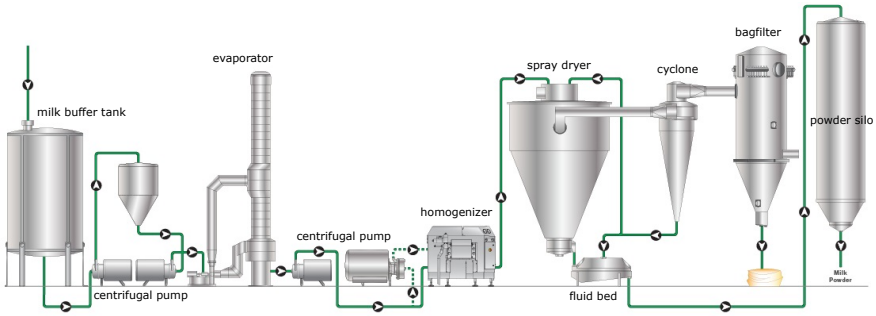

Figure 1.2: Simple sketch of a milk processing powder plant. Milk is concentrated and dried to powder in the spray dryer [Flo].

imported milk powder products.

Rising Energy Costs
The climate challenge that the world currently faces calls for reductions in carbon emissions. Technological developments within energy efficiency is an effective way to reduce the emissions. The energy efficiency is also key to increase the often tight profit margins in the food industry. Fossil fuel-based energy sources will be with us for some time, particularly given recent technological advances, but renewable fuels are booming at the same time [EY15]. Renewable energy, carried in form of electricity in a so-called smart-grid [Hal14], may be a carbon free alternative in the future.

1.2 Milk Processing Powder Plant

The production of milk powder perfectly illustrates the importance of food processing in a global context. For example, raw milk spoils within a day or two if left in a cupboard, while powdered milk provides a long shelf-life and ease of transportation and form a base ingredient in many consumer products. Every day several million liters of milk are processed into powders. The process ensures that areas with a surplus of milk can transport it to areas with a shortage. Milk powder is often shipped to the developing countries that may not have a strong dairy base, transportation system or processing capabilities to meet the population's need for liquid milk. In addition, many of the homes in these countries have no refrigerators. Powdered milk is therefore a good alternative to fresh milk.

Milk powder is produced in a milk processing powder plant. Fig. 1.2 shows a

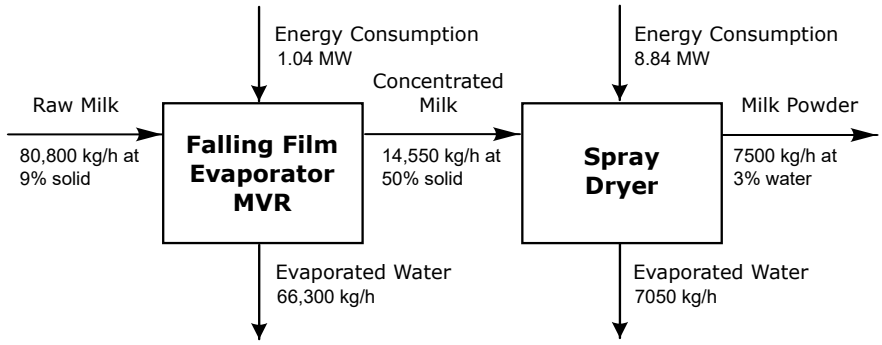

Figure 1.3: Example of combining the MVR and the spray drying technologies. The MVR technology is significantly more efficient than the spray drying process.

schematic of a milk powder process, from standardized raw milk to final milk powder. The production of milk powder requires large amounts of energy, particularly in the spray drying process, due to the high latent heat of vaporization and the inherent inefficiency of using hot air as the drying medium [Muj12, VdJ03]. Drying processes are known to be the most energy consuming processes used in the food industry. For example, the Dutch dairy industry required 1.4 PJ for drying its whey and milk powder in 2007 [FASdJ10]. In order to save energy, an intermediate falling film evaporator is added to remove a large portion of the water from the milk before it is sent to the spray dryer [VdJ03].

A Mechanical Vapor Re-compression (MVR) evaporator consumes only 55 MJ/ton evaporated water which gives an energy efficiency of above 40 (4000%). The spray dryer consumes 4500 MJ/ton evaporated water leading to an energy efficiency of 0.5 (50%). Thus, considerably lower than what can be achieved in the MVR [FASdJ10]. Fig. 1.3 illustrates the inherent advantage of combining an evaporator and a spray dryer. In the example, we assume that a milk powder plant produces 7500 kg/h of skim milk powder with 3% residual moisture content while receiving skim milk at 9% solids content. The product flows are then given for the two processes assuming an intermediate milk concentration of 50%. The energy consumption is computed according to the above efficiencies [FASdJ10]. As can be seen, the raw milk flow intake sums to 80,800 kg/h, which is considerably more than the 7500 kg/h of final powder. Also, notice that 66,300 kg/h of water is evaporated in the evaporator while only consuming 1.04 MW of energy, compared to 7050 kg/h of water evaporated in the spray dryer while consuming 8.84 MW of energy. Thus, we seek to maximize the evaporation in the evaporator to save energy in the spray drying process. As a consequence, the evaporator should produce as high an intermediate milk concentration as possible [FASdJ10]. However, at a certain milk concentration fouling starts in

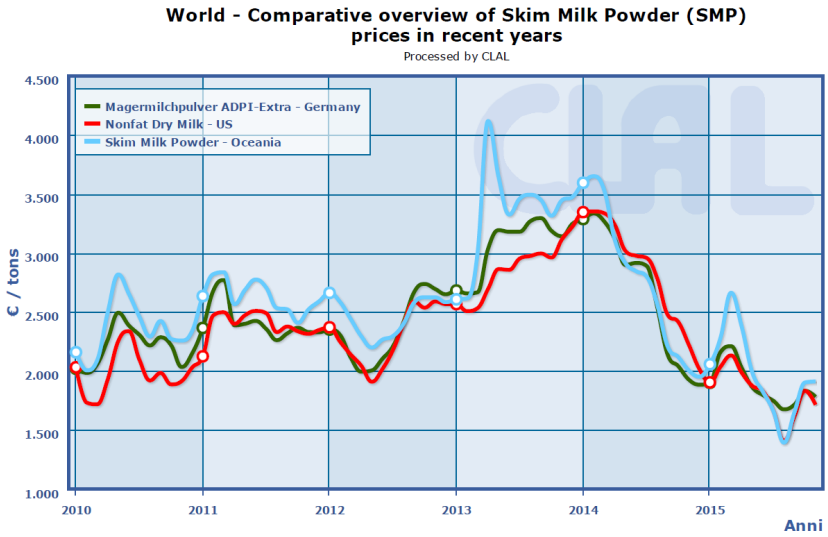

Figure 1.4: Skim milk powder (SMP) prices are currently at a six-year low. Prices provided by Clal [Cla]

the evaporator. Therefore, there is an upper limit to the amount of water that can be removed in the evaporator [VdJ03]. The milk powder moisture content should also be maximized to reduce the necessary amount of evaporation in the spray dryer [VdJ03]. The shelf-life of the powder limits the maximum moisture content.

Milk powder processing plants must stay profitable to form a sustainable business case. Profitability is given by the price of the produced powder minus the cost of running the process i.e. raw material and energy costs. Fig. 1.4 shows that the milk powder price has recently fallen to a six-year low. The profit is therefore squished to a minimum, motivating the producers to maximize profit by decreasing running costs e.g. through a better utilization of the energy and raw materials.

1.3 Spray Drying

Spray drying as a concept can be tracked back to a filed patent in the 1860s. However, it took nearly 50 years for the first commercial successful dryer design to be developed and operated [Mas02]. The latest development is the four-stage spray dryer (marketed by GEA Process Engineering A/S as a Multi-Stage Dryer,

MSD^{TM}) which is widely used for production of milk powder and other food powders. It combines drying in four stages to increase the energy efficiency and the product quality.

Fig. 1.5 illustrates the four-stage spray dryer with an integrated (static) fluid bed and an external (vibrating) fluid bed. The four-stage spray dryer consists of the primary spray drying stage (SD), the static fluid bed stage (SFB), the hot vibrating fluid bed stage (VFBh) and the cold vibrating fluid bed stage (VFBc).

The hot main air is let into the upper section of the SD around a set of high pressure nozzles. The nozzles disperse the liquid feed into droplets. The heat is transferred from the hot air to the droplets which makes the water evaporate from the droplets. In that process, the air temperature and the residual moisture content of the droplets decrease. During drying there is a transfer of evaporated water from the feed to the air in the dryer. The dried product then enters the SFB and is dried further while being fluidized by hot air. After drying in the SFB, the powder is transported to the VFB for gentle drying and cooled to the temperature desired for handling and storage. The exhaust air from the chamber and VFB is passed through a cyclone, separating the powder contained in the air. The fine powder is returned to the chamber to form agglomerated powder particles. The exit air is passed through a bag filter, not shown in Fig. 1.5, to remove any particles left before the air can be discharged.

The spray drying operation accounts for the largest energy consumption in the milk powder process. In the daily operation, minimizing the raw material use and the energy consumption is the primary objective to stay competitive. Optimal use of a spray dryer is a challenging task. One must maximize energy efficiency and production while minimizing down time [KM07]. These two goals are often conflicting, as increased production and efficiency may lead to an increase in the hours lost on process-related problems such as plugging, powder build-up, cleaning in place (CIP) etc. The main challenge in operating a spray dryer is to bring the residual moisture content below a maximum limit and to avoid that the powder sticks to the chamber walls at high ambient air humidities. To achieve that, the operation of the spray dryer must continuously be adjusted to variations in the feed concentration and the ambient air humidity. The conventional PI control strategy is simple, but known to be insufficient at making these adjustments. The operator must then manually perform the adjustments to the spray dryer. These adjustments are hardly ever performed, as the operator have other important tasks to perform. Instead the spray dryer is operated in a conservative non-optimal way. Thus, automatic control systems to perform the adjustments are needed.

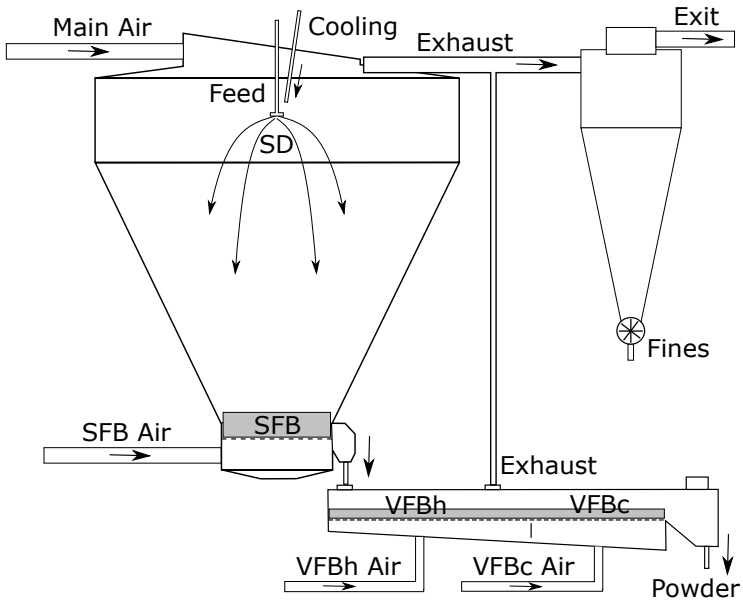

Figure 1.5: Principle diagram of the four-stage spray dryer with an integrated static fluid bed and an external vibrating fluid bed.

1.4 Model Predictive Control

For a long time linear Model Predictive Control (MPC) has been considered the preferred control methodology in the process industries and academia for complex processes. MPC provides an integrated solution for controlling processes with multivariate and cross-coupled dynamics, time delays and constraints on both the inputs and the states [DHN09, RAB12]. Forecasts of the disturbances are also naturally utilized in MPC. In general, these features allows operation closer to the process constraints which may lead to greater profits and/or better performance. Fig. 1.6 illustrates how optimal control can reduce the variance of the controlled outputs, making it possible to squeeze and shift the target to a more profitable value. In spray drying, the profit significantly benefit from reducing the variance of the residual moisture content. This makes it possible to shift the moisture content to a slightly higher level which increase the yield, by selling more water as product, while reducing the energy consumption due to less evaporation. To illustrate the idea, we assume that MPC is able to increase the average residual moisture content by only 0.2 p.p. at a milk powder plant that produces 7500 kg/h of skim milk powder (from Fig. 1.3). The annual profit

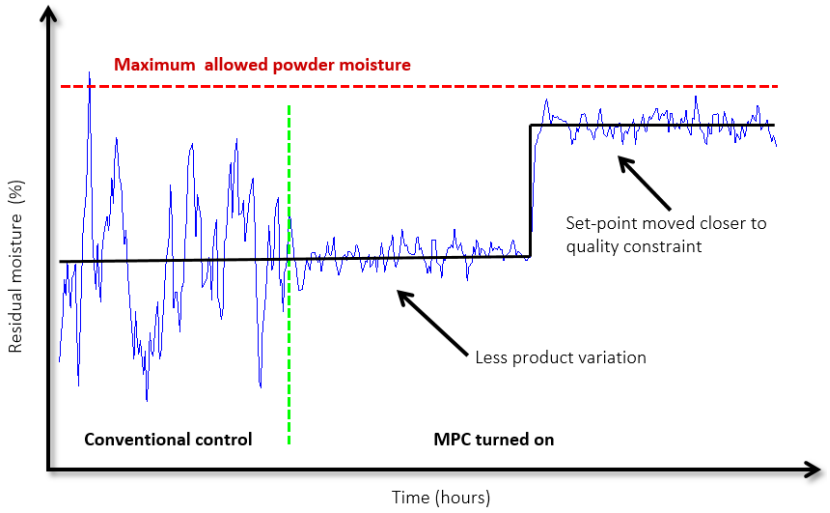

Figure 1.6: MPC makes it possible to squeeze and shift the residual moisture content to a more profitable value.

increase is then

$$= 0.2 \text{ p.p.} \cdot 7500 \text{ kg/hr} \cdot 7200 \text{ hr/year} \cdot 2.5 \text{ €/kg}$$
$$= 224,100 \text{ €/year}$$

The profit increase illustrates the importance of optimal control well.

MPC refers to a control algorithm that explicitly incorporates a process model, to predict the future response of the controlled process and take appropriate action through optimization. Traditionally, MPC is designed using objective functions penalizing deviations from a given target and fast movements in the inputs. Often MPC is combined with a Real-Time Optimization (RTO) layer [FCB15, Eng07, DNJN11, AO10, EH01], in a so-called two-layer structure. The upper-level RTO system provides targets under different conditions such as feed compositions, production rates, energy availability, feed and product prices to the lower-level control system in order to maintain the process operation as close as possible to the economic optimum [AG10]. The RTO layer and the MPC layer have different time scales and the RTO layer assumes that the closed-loop process will reach a steady-state. Transients, such as target transitions and the inherent effect of disturbances, may thus lead to loss of economical efficiency. Recent advances within process optimization focus on optimizing the higher-level objectives, such as economics, directly in the objective function of the MPC, known as Economic MPC (E-MPC) [RA09, RAB12, AAR12, Grü13, Grü12]. Thus, the E-MPC eliminates the presented drawbacks. E-MPC is

maturing and has now been successfully applied to an increasing number of continuous processes.

MPC is the natural choice to automatically optimize the operation of spray dryers, as it naturally handles the dryers multiple and cross-coupled inputs and outputs, time delays, process constraints and feed-forward of disturbances such as the feed concentration and the ambient air humidity. The MPC will then allow operation closer to the process constraints which may increase profits without violating the process constraints. The application of MPC to spray dryers can therefore be an effective way to support the operators in the challenging task of optimizing the spray dryer operation.

1.5 Thesis Objective

The aim of this project is to investigate the application of MPC to optimize the operation of four-stage spray dryers. To facilitate this goal, new models and MPC strategies for the process will be developed.

Spray Dryer Modeling
One of the key objectives is to develop first-principles dynamic models of a four-stage spray dryer. The purpose of the simulation model is to enable detailed closed-loop simulations of the spray dryer at different operating points, such that the model can facilitate development and comparison of control strategies. The purpose of the control model is to provide a simpler model that can be used for state estimation and prediction in the controllers. We perform experiments on a GEA MSD^{TM}-20 spray dryer to identify the model parameters and validate the model accuracy for this dryer. Powder characteristics are identified by laboratory tests. The models provide the key performance indicators (KPIs) such as the profit of operation, the energy consumption, the energy efficiency, the product flow rate and the stickiness of the powder in the spray dryer. These features are important for comparison of the different control strategies.

Model Predictive Control
A key objective is to automatically adjust the dryer to variations in the feed and the ambient air humidity, such that the profit of operation is maximized while the energy consumption is minimized, the residual moisture content in the powder is controlled below the specification and sticky powder is prevented from building up on the dryer walls. We do this by first developing a traditional linear target tracking MPC algorithm with an RTO layer for calculation of cost optimal targets. This is the conventional approach and may perform well in many cases. Secondly, we develop an Economic Nonlinear MPC that brings economic costs

directly into the objective function of the controller. The controller will then constantly bring the process to the most cost efficient state of operation, while considering constraints of the process such as stickiness and moisture limits of the powder. The MPCs include a state estimator (soft-sensor) for estimation of the current state of the dryer. A second goal is therefore to investigate the design and tuning of this state estimator, such that missing observations are handled well. The observations that can be missing for shorter periods are the exhaust air humidity and the residual moisture content of the powder, which must be handled accordingly.

Application of MPC to an Industrial Spray Dryer
A key objective is to demonstrate the MPC strategy on a full-scale industrial four-stage spray dryer. In that effort, we will document the complete standalone MPC solution i.e. the spray dryer setup, the MPC algorithm, the model identification and tuning etc. We also document the KPIs obtained during the demonstration experiments. Our goal is that the MPC strategy will be widely used as part of the commercial control solution.

1.6 State-of-the-Art

In this section, we provide an overview of the state-of-the-art and give some references to important literature in the fields that are addressed in this thesis. The collection of papers written during the project, included in Part II, also contain literature studies and references relevant to the specific paper.

1.6.1 Spray Dryer Modeling and Control

Mathematical modeling and control of spray dryers have been subjects of research for many decades. The models have traditionally been classified into static and dynamic models. Mathematical models of spray dryers exist as detailed computational fluid dynamics (CFD) models for static design oriented simulation [CPO01, PCLA09, WDM$^+$08a, Kie97], and as models for dynamic simulation. The models for dynamic simulation are linear models for control design that are also used for closed-loop simulation [Cla88, TTA09, TIKT11] and lumped first-principles engineering models [SH08, Sha06, ZGS$^+$88, ZPC91, PCF95, GJC$^+$94]. The purpose of the dynamic simulation models is often to facilitate analysis and synthesis of advanced control schemes.

Clarke [Cla88] designs a Generalized Predictive Controller (GPC) for a spray

dryer and base the controller on the CARIMA model, but does not provide a simulation model. Tan *et al* [TTA09, TIKT11] provide continuous transfer functions of first order with a delay that they use for PI controller design as well as closed loop simulation. They report models for spray drying of full cream milk [TTA09] as well as spray drying of whole milk and orange juice [TIKT11].

A lumped first-principles model of a single-stage spray dryer is developed in [SH08, Sha06]. Mass and energy balances describe the air temperature, the mean particle size and the residual moisture content of the powder. Based on the model PI controllers are developed to control the mean particle size and the residual moisture content of the powder. A mathematical model based on mass, energy and momentum equations are formulated and solved in [ZGS$^+$88]. The model describes the moisture content and particle size of a single spray dried powder particle and fits the experimental data within 10-15% error. In [ZPC91] a dynamic model of a single-stage spray dryer is developed from first-principles and is validated experimentally to assist in control simulation studies. The model provides the moisture content and particle size of the powder as well as the exhaust air temperature and humidity. The inferred moisture content is controlled in a cascade PI configuration to mitigate the effect of disturbances. Reference [PCF95] extends the model in [ZPC91] by further developing the model for drying of milk powder, and controls the exhaust air humidity to indirectly control the powder moisture content. A single-stage dynamic model is developed by [GJC$^+$94] for the simulation of the residual moisture control and air temperatures in an industrial detergent spray drying process. A linear-quadratic-Gaussian (LQG) controller for residual moisture control is reported. The moisture content for drying of milk powders in a spouted bed dryer is described by a physical-mathematical model in [VFF15]. The evaporation term is estimated using a neural network and the inferred powder moisture content is controlled by adjusting the inlet air temperature with a PI controller. A detailed review of the status and future of modeling and control for spray drying of dairy products is given in [OC05].

The above first-principles models simulate single-stage spray dryers or a spouted bed dryer. In-line powder residual moisture sensors are often not available. Therefore, the above models are based on irregularly sampled off-line laboratory measurements of the residual moisture. We present models and control strategies for a four-stage spray dryer that is validated against in-line residual moisture measurements and control strategies that utilizes in-line measurements.

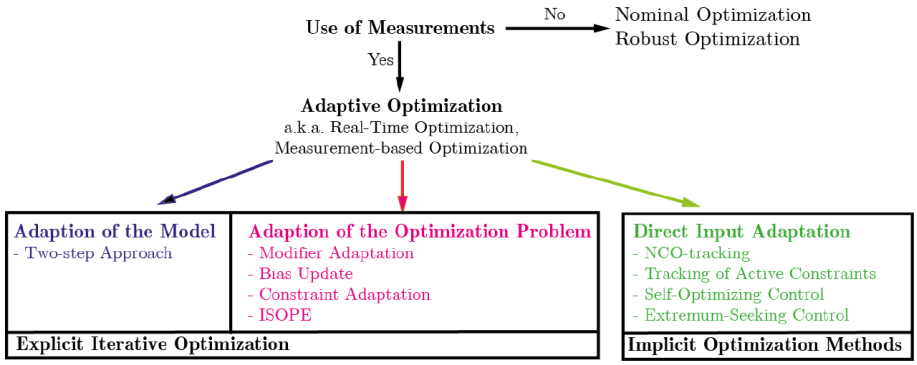

Figure 1.7: Classification of RTO methods and their Philosophies [FCB15].

1.6.2 Model Predictive Control

The use of tracking MPC in conjunction with an RTO layer (the so-called two-layer structure) dates back to the late 1970s-1980s [Eng07, DNJN11]. Since then the MPC with an RTO layer has become the standard approach for implementing steady-state economic optimization in processes that operate around nominal steady-states. The RTO methods aim to reject the effect of model uncertainty on the economic performance by the use of process measurements. As indicated by Fig. 1.7, the RTO methods divide into two classes, explicit and implicit iterative optimization methods [FCB15,EH01]. Explicit methods utilize a model and measured disturbances for computing the optimal operating point. The explicit methods further divide into two main classes; adaptation of the model and adaptation of the optimization problem. In model adaptation, the measurements can be used to refine the model by updating the model parameters. Correction terms to the optimization problem are determined in optimization problem adaptation. No model parameter identification is performed. The two methods both rely on the repeated solving of a model-based optimization problem. Thus, rather accurate models are needed, but the model information can be used to achieve better economic performance. Implicit methods seek to optimize the profit of operation, without the use of a rigorous model. Well known examples of implicit methods are extremum-seeking [AK03] and self-optimizing controllers [Sko00]. Extremum-seeking methods impose small changes to the steady-state of the process, and a cost function gradient is estimated. On that basis, steps towards a lower cost are taken. The advantage is that no model is required, but the method can be slow and requires the process to reach steady-state before a new step can be taken.

The two-layer structure has some inherent drawbacks. As the optimization is only performed intermittently at a low sampling rate, the adaptation of the operating conditions is slow [Eng07]. Furthermore, the RTO layer assumes that the closed-loop process will reach a steady-state. Transients, such as target transitions and the inherent effect of disturbances, may thus lead to loss of economical efficiency.

In E-MPC, the traditional target tracking objective function in the MPC is exchanged with an economic objective function from the RTO layer. The idea of using economic objectives in the dynamic regulation problem has been proposed in many works [Amr11, RAB12, RA09, AAR12, Grü13, Grü12]. Computational studies and analysis of processes have been published [RAB12]. The earliest work on optimal economic control problems dates back to 1920s, in which the objective was to determine optimal savings rates to maximize capital accumulation [Amr11] and 1975 in connection to closed-loop control [CD75]. E-MPC can present some difficulties [RA09], e.g. that it can yield a turnpike which forces the use of a long prediction horizon. The turnpike property is well known in the field of E-MPC and is an active research area [Grü13, FKJB14]. Also, unlike target tracking MPC, research shows that E-MPC may lead to closed-loop periodic/cyclic operation [Amr11, AAR12, ZGD13]. Such periodic operation may be economically favorable compared to the best steady-state economic solution on a time average. Fig. 1.8 illustrates such closed-loop periodic operation. Highly time-varying inputs may pose safety issues to the process, and attempts are reported to prevent rapid changes by imposing rate of change constraints on the inputs [QB03, SMTR12]. Stability proofs on E-MPC is an ongoing research topic. [Grü12] presents a survey of recent results on stability, performance and feasibility of nonlinear E-MPC with and without terminal constraints. An analysis of performance in the absence of any terminal constraints is provided in [Grü13].

E-MPC has been applied to a growing variety of continuous processes. Often the application of E-MPC emerges from research in connection with the future energy system, refereed to as the smart-grid [SPJS13, Hal14, SEJ15]. In particular large-scale power management and production planning in power systems have been studied for application of E-MPC to provide flexible consumption or load shedding [SESJ13,SPJS13,SEJ15]. Some interesting applications are industrial refrigeration [HLJB12], building climate control, charging and discharging of electric vehicles including electricity price forecasts [HPM$^+$12, MCH10], residential heat pumps exploiting load shedding [PEH$^+$13, Hal14] and many more. E-MPC has also been studied in connection to batch processes, such as production optimization of oil recovery from oil fields by controlling the water flooding [Cap13, BJ04] and chemical batch processes [ARB13]. Progress has been reported on improving the control of spray dryers, but to our knowledge E-MPC has not been studied for the process of spray drying before now.

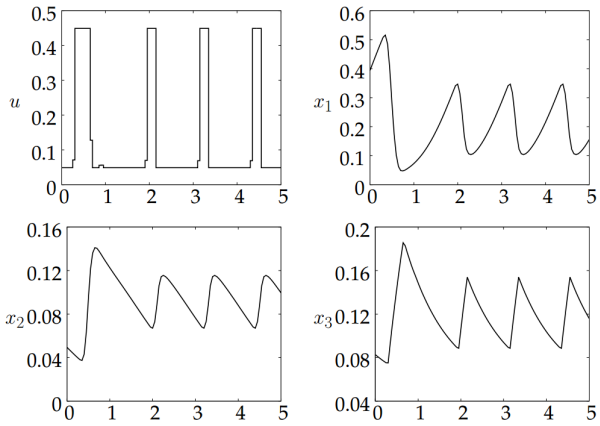

Figure 1.8: Closed-loop simulation of a system under periodic E-MPC [Amr11].

1.6.3 Application of MPC to an Industrial Spray Dryer

Attempts have been made to improve the industrial control of spray dryers over time. The solutions fall mainly into two groups; the extension of the conventional PI control strategy and the MPC strategies with target optimization. PI control strategies are reported in patents [Nie13, SB11]. These adjust the exhaust air temperature or exhaust air humidity to maintain a stable powder residual moisture content. [GJC+94] develop an LQG controller for residual moisture control in an industrial detergent spray drying process. Industrial MPCs are reported and seem to rely on empirically based step-response models and least-squares methods for estimation of the residual moisture content of the powder [Vai, Roc]. [Vai] reports up to 20% increase in production capacity.

1.7 Thesis Contribution

The key contributions of this thesis are described in the following three sections.

1. **Modeling of a four-stage spray dryer**

   We develop two first-principles engineering models of a four-stage spray dryer. The simulation and control models combines physical knowledge of the process with unknown parameters identified from an experiment.

The novelty of the proposed models lies in three main features: 1) The models enable simulations of the spray dryer at different operating points with high accuracy and is validated against in-line measurements of the powder residual moisture content. 2) The key performance indicators (KPIs) such as the profit of operation, the product flow rate, the energy consumption and the energy efficiency are provided. 3) In addition, the models offer stickiness constraints of the powder in each stage of the spray dryer.

To the author's knowledge, there does not exist such a model that combines all three features for a four-stage spray dryer. These features make the simulation model well suited for closed-loop comparison of the process economics associated to different control strategies. The complexity reduced control model, based on the simulation model, is well suited for state estimation and predictions in the MPCs.

2. **Development and simulation of control strategies**

   We develop and demonstrate by simulation two proposed control strategies and compare them against the conventional PI control strategy; the two strategies are based on the MPC with an RTO layer strategy and the E-MPC strategy. The performance of the controllers are studied and evaluated according to the performance indicators above.

   The novelty of the proposed MPC with RTO control strategy lies in three main features: 1) It offers independent control of the exhaust air temperature, the exhaust air humidity, the SFB powder temperature and the residual moisture content of the powder. This enables control of the spray dryer such that the stickiness of the powder and the residual moisture content can be operated closer to its limits. 2) It offers significantly improved economical performance and reduced energy consumption while avoiding violation of the process constraints. 3) In addition, the state estimator offers a built-in method for handling missing observations as a so-called soft-sensor.

   The novelty of the proposed E-MPC control strategy consists of the two main features: 1) It combines the MPC and RTO layers into one E-MPC control layer, such that the economical performance is constantly maximized while avoiding violation of the process constraints. 2) It provides an even further improved profit of operation compared to the MPC with RTO control strategy. It also offers a state estimator that handles missing observations.

   To the author's knowledge, there does not exist such a comprehensive study and evaluation of the economic benefits of using MPC with RTO as well as E-MPC for a four-stage spray dryer. Furthermore, we have not seen any comparison of such control strategies to the conventional PI control strategy.

3. **Application of MPC to an industrial spray dryer**

   We demonstrate that the proposed MPC with an RTO layer is applicable to an industrial four-stage spray dryer. The industrial dryer is a GEA MSD^{TM}-1250 type producing enriched milk powder.

   The novelty of the industrial implementation of the MPC with an RTO layer lies in 1) The fully integrated and functioning solution, that is used in the daily operation of the milk powder spray dryer. During the project, we participated in the development and installation of the in-line instruments for the measurement of the exhaust air humidity and the residual moisture content of the powder. These provide high quality measurements and are actively used in the MPC. 2) We document in detail the installation and workings of the industrial MPC solution. 3) The performance of the controller is evaluated and show that the profit of operation, product flow rate and the energy efficiency are improved significantly compared to conventional PI control. This confirms the results obtained by the closed-loop simulations of the MPC with RTO control strategy.

   Industrial MPC solutions exists, but to the author's knowledge, there has not been published any detailed data of the performance of these nor has the MPC strategies been as well documented as in this work. It is our experience that the industrial MPC solutions seldom incorporate in-line measurements of the exhaust air humidity and powder residual moisture content.

We address these contributions in Part I, the summary report, and in Part II, the published papers.

1.8 Thesis Organization

The thesis is divided into two parts. Part I is comprised of a summary report which gives an overview of the main results and contributions of the thesis. Part I is composed of the chapters 1 to 8. Chapter 1 provides an introduction and the background for the thesis. It presents the four-stage spray drying process and the MPC algorithm in general terms. Chapter 2 provides a short description of the modeling of the spray dryer. Chapter 3 provides an overview of the three control strategies considered in Chapter 4-6. Chapter 4 presents the conventional PI control strategy, Chapter 5 presents the MPC with RTO control strategy and Chapter 6 presents the E-MPC control strategy. Application of MPC to an industrial spray dryer is presented in Chapter 7. Conclusions are provided in Chapter 8. Part II is comprised of the research papers published and submitted during the project period.

Chapter 2

Four-Stage Spray Dryer Models

In this chapter, we describe the four-stage spray dryer and present two experiments conducted on the dryer and laboratory tests on the final powder. We formulate a nonlinear index-1 differential algebraic equations (DAE) model for simulation purposes and a simpler nonlinear ordinary differential equation (ODE) model for design of model based controllers. A linear model is also provided for design of linear model based controllers. The model parameters are identified based on the experiments and we show that the models fit the experimental data well.

The chapter is a summary of Paper A, Paper C, Paper E, and Paper G.

2.1 Equipment Setup

The four-stage spray dryer that is used in this project combines drying in four stages to increase the energy efficiency and the product quality; spray drying at the top of the dryer chamber (SD), drying in an integrated static bed at the bottom of the dryer chamber (SFB) and drying in an external vibrating fluidized bed (VFB). Fig. 2.1 illustrates the working principle of the four-stage

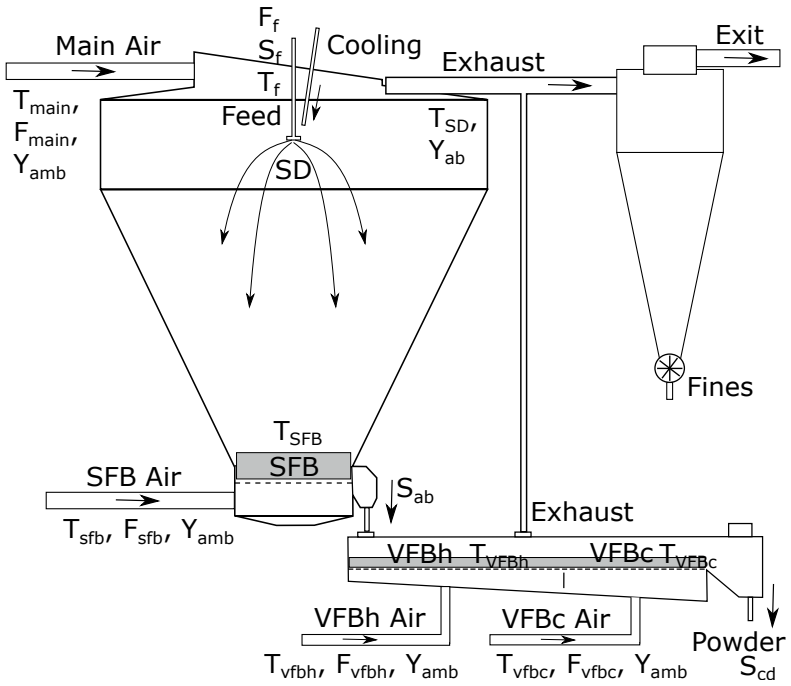

Figure 2.1: Principle diagram of the four-stage spray dryer with indication of the inputs, disturbances and outputs.

spray dryer as well as the inputs, disturbances and outputs. The outputs are the exhaust and stage temperatures, T_{SD}, T_{SFB}, T_{VFBh} and T_{VFBc}, the exhaust air humidity, Y_{ab}, and the SFB and VFBc stage residual moisture content of the powder, S_{ab} and S_{cd}. The inputs are the feed flow rate, F_{f}, the main inlet air temperature, T_{main}, the SFB inlet air temperature, T_{sfb} and the VFBh inlet air temperature, T_{vfbh}. The main disturbances are the ambient air humidity, Y_{amb}, the feed solids concentration, S_{f}, and the feed temperature, T_{f}. The other disturbances are the main inlet air flow rate, F_{main}, the SFB inlet air flow rate, F_{sfb}, and the VFBh inlet air flow rate, F_{vfbh}. The cooling of the powder is performed with unheated ambient air in the VFBc stage at an inlet air flow rate, F_{vfbc}, and temperature, T_{vfbc}.

The experiments in this project are conducted on a small-scale industrial type GEA MSD$^{\mathrm{TM}}$-20 spray dryer. Fig. 2.2 shows a picture of the dryer at the test-station. The control room, the VFB, the feed tank and the feed pump are located on the ground floor. The SFB is located at the first floor and the spray dryer chamber is located on the first and above floors. The bag filter is the unit to the right in the picture.

Figure 2.2: The picture of the MSD^{TM}-20 spray dryer seen from the ground floor.

Fig. 2.3 shows the inside of the dryer chamber, divided into an upper SD part (left) and the lower SFB part (right). The pictures are taken after the experiment was conducted and shows none to small signs of powder deposits on the cone of the dryer chamber.

The dryer is fitted with an abundance of temperature sensors, pressure sensors and air mass-flow meters. We note that all the inlet air mass-flow meters have an offset in the readings. This offset is identified from an air humidity mass balance of the spray dryer using measurements of the air flow rates, the feed flow rate and the air humidity. We estimated the offset to be 5%, which we subtracted from the readings before these are used in the model. A combined feed mass-flow and density meter is fitted to the feedline. The feed solids concentration is estimated

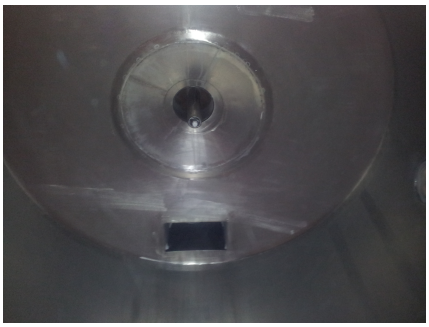

(a) The SD stage with nozzle and exhaust air outlet.

(b) The SFB at the bottom of the dryer chamber.

Figure 2.3: Picture of the SD and SFB stages. The picture is taken after the experiments and shows none to small signs powder deposits.

from the feed density and feed temperature, as we know the density of the individual components in the feed i.e. the solids and water. We fitted residual moisture instruments to the SFB and VFB powder outlets and an exhaust air humidity instrument to the exhaust air duct. We also fit vapor injectors to the inlet air streams, to control the ambient air humidity supplied to the dryer. The manipulated inputs are the reference temperature of the electric heaters on the main, SFB and VFBh inlet air streams. The feed pump speed is controlled directly. All these sensors, instruments as well as actuators are connected and handled by a single SIEMENS S7 PLC system and a Wonderware^{TM} Intouch v10.5 SCADA system from Schneider Electric.

The experiments are based on drying of maltodextrin DE-18. Maltodextrin is a starch based polysaccharide that is used as a food additive. Maltodextrin is used because the feed can then be re-wetted and the composition is well defined. We use maltodextrin DE-18 as a substitute to milk because milk is difficult to handle over longer periods due to natural deterioration. Stickiness and drying properties are sought to be comparable to milk by the selection of the DE-18 type. The DE number indicates the stickiness and drying properties of the maltodextrin.

The residual moisture content is measured using two ProFoss^{TM} in-line analyzers placed at the SFB and VFBc powder outlets. Fig. 2.4 shows the position of the residual moisture instruments. The SFB sensor is placed after the powder discharge piston and the VFBc sensor is placed after the final powder outlet. The powder from the VFBc powder outlet is collected in a container.

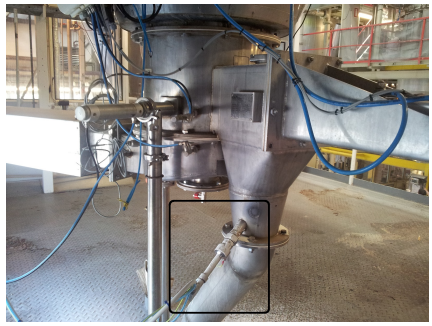

(a) The SFB powder discharge.

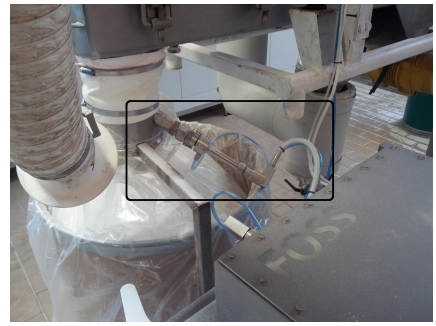

(b) The VFB final powder outlet.

Figure 2.4: Picture of the SFB and VFB powder outlets with installed in-line ProFoss^{TM} NIR analyzers marked with black boxes.

The air humidity is measured using an industrial air humidity sensor fitted with pre-filtering. The pre-filtering of the exhaust air prevents it from blocking due to the fine powder particles in the exhaust air.

2.2 Experimental Tests

Two experiments were made in consecutive order without stops. The data from the first experiment is used for estimation, while the data from the second experiment is used for validation.

A number of steps are performed during the two experiments to excite the spray dryer outputs. The nominal inputs and the steps to the spray dryer are provided in Table 2.1. The nominal operating point and the step size of the inputs are selected based on operator process knowledge and experience from previous experiments using maltodextrin DE-18.

During the estimation experiment an exhaustive number of steps is performed. In this experiment, we want to be sure that all possible inputs and disturbances are identified and excited. The validation experiment is made from a repetition of the estimation experiment, but omitting the steps in the inlet air flow rates and the feed temperature. These are normally kept constant during operation. The first experiment is therefore the longest of the two experiments and contains the most information due to the increased number of excited inputs. The data from both experiments are well excited and covers a large operation range. Each step lasts about 1 hour and the feed flow steps lasts 1.5 hours. The estimation

Table 2.1: The table show the nominal inputs and the input steps that are used during the estimation and validation experiments.

	Nominal	Estimation Step		Validation Step	
	Input	Down	Up	Down	Up
F_{f}	85 kg/hr	65 kg/hr	120 kg/hr	70 kg/hr	117 kg/hr
T_{f}	50°C	42°C	60°C	-	-
S_{f}	50%	40%	-	40%	-
F_{main}	1700 kg/h	1500 kg/h	1900 kg/h	-	-
T_{main}	170°C	160°C	180°C	160°C	180°C
Y_{main}	3 g/kg	-	$15-25$ g/kg	-	15 g/kg
F_{sfb}	470 kg/h	330 kg/h	570 kg/h	-	600 kg/h
T_{sfb}	90°C	80°C	100°C	80°C	100°C
Y_{sfb}	3 g/kg	-	$15-25$ g/kg	-	15 g/kg
F_{vfbh}	280 kg/h	-	410 kg/h	-	-
T_{vfbh}	60°C	-	80°C	-	80°C
Y_{vfbh}	3 g/kg	-	-	-	-
F_{vfbc}	280 kg/h	-	-	-	-
T_{vfbc}	35°C	-	-	-	-
Y_{vfbc}	3 g/kg	-	-	-	-

experiment lasts in total 28 hours and the validation experiment lasts in total 17 hours.

Appendix A reports the recorded inputs, disturbances and outputs for the estimation and validation experiments.

2.3 Laboratory Tests

The powder equilibrium moisture content, X_{eq}, is a product dependent function that describes the moisture content at which water cannot be evaporated from the powder any longer. The dynamic models, presented later, make extensive use of this function. We identify this function based on already dried powder in the laboratory by *adsorption* isotherms studies. We fit the Guggenheim-Anderson-de Boer (GAB) equation [BSM06], which has a theoretical background based on equilibrium assumptions. The GAB function has the form

$$X_{\mathrm{eq}} = \frac{C \cdot K \cdot X_{\mathrm{m}} \cdot \mathrm{RH}}{(1 - K \cdot \mathrm{RH})(1 - K \cdot \mathrm{RH} + C \cdot K \cdot \mathrm{RH})} \tag{2.1}$$

in which X_{m}, C and K are temperature dependent Arrhenius expressions and RH is the relative humidity of the air. Fig. 2.5(a) illustrates 15 laboratory data

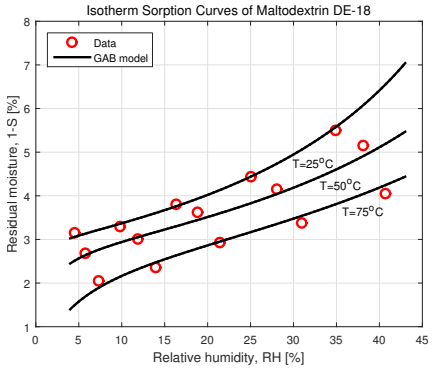

(a) The equilibrium moisture content.

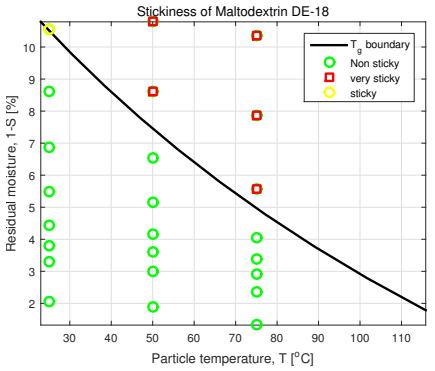

(b) The stickiness boundary.

Figure 2.5: Maltodextrin DE-18 laboratory data made from *adsorption* isotherm experiments. The black lines indicate fitted equations.

points and the fitted GAB function. Temperatures were fixed at $T = 25°\text{C}$, $T = 50°C$ and $T = 75°\text{C}$ with relativity humidities between RH $= 4.5\%$ and RH $= 40.1\%$. The simulation model presented in Section 2.4 uses the GAB function fitted to the data in Fig. 2.5(a). The control model presented in Section 2.5 was developed later in the project, which made it possible to conduct a second experiment with data points at higher temperatures. Thus, the control model uses a different GAB function fitted to the that data (not presented here). In the literature, models already exist for maltodextrin [WDM+08b, FOS01, PCLA09]. However, these models do not fit our data well.

Stickiness of powder can be predicted using the glass transition temperature, T_g, computed by the Gordon–Taylor equation (a mass-proportion-mixing rule) as [BBH04]

$$T_g = \frac{T_{\text{gp}} + kZT_{\text{gw}}}{1 + kZ} \tag{2.2}$$

$T_{\text{gp}} = 144.8°\text{C}$ (maltodextrin DE-18) and $T_{\text{gw}} = -137°\text{C}$ (water) are the glass transition temperatures, T_g, of the solid and water fractions, respectively. Z is the dry base residual moisture content at the surface of the powder. We fit (2.2) by estimation of a single constant, $k = 6.296$, to data from an additional experiment that indicates whether the powder in Fig. 2.5(a) has turned sticky after being exposed to the specific temperature and air humidity conditions [BBH04]. Fig. 2.5(b) shows the experiment results and the predicted glass transition temperature. Powder with a temperature above T_g is sticky. The predicted glass transition temperatures in (2.2) coincide well with the measurements.

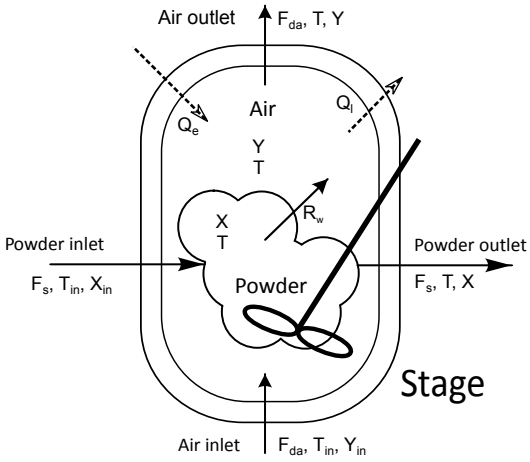

Figure 2.6: Sketch of a general single stage.

2.4 Simulation Model

In this section, we present the four-stage spray dryer model used for simulation at a wide set of operating points with high accuracy. The model combines physical knowledge of the process with unknown parameters identified from the estimation experiment.

The dryer is divided into four stages; a SD, a SFB, a VFBh and a VFBc stage. The model describes the evolution of the temperatures, air humidities as well as the residual moistures of the dried product in each of these stages. All stages are based on the same mass and energy balance principles, thus the stages can, in short, be presented as one general stage. This will illustrate the modeling concept well. The full detailed description of the model is given in Paper A.

2.4.1 Conservation Equations

The evolution of the dry base powder moisture content, X, the air humidity, Y, and the temperature, T, in the stage are determined by the conservation equations

$$\frac{dm_{\mathrm{w}}}{dt} = \overbrace{X_{\mathrm{in}}F_{\mathrm{s}}}^{\text{water in}} - \overbrace{XF_{\mathrm{s}}}^{\text{water out}} - \overbrace{R_{\mathrm{w}}}^{\text{water evaporation rate}} \tag{2.3a}$$

$$\frac{dm_{\mathrm{v}}}{dt} = \overbrace{Y_{\mathrm{in}}F_{\mathrm{da}}}^{\text{vapor in inlet air}} - \overbrace{YF_{\mathrm{da}}}^{\text{vapor in outlet air}} + \overbrace{R_{\mathrm{w}}}^{\text{water evaporation rate}} \tag{2.3b}$$

$$\begin{aligned}\frac{dU}{dt} = &\overbrace{(h_{a,\mathrm{in}} - h_{a,\mathrm{out}})F_{\mathrm{da}}}^{\text{enthalpy of air flows}} + \overbrace{(h_{p,\mathrm{in}} - h_{p,\mathrm{out}})F_{\mathrm{s}}}^{\text{enthalpy of powder flows}} + \\ &\overbrace{\Delta H_{\mathrm{e}}^{\mathrm{in2out}}}^{\text{enthalpy of mass exchange}} - \overbrace{Q_{\mathrm{e}}^{\mathrm{in2out}}}^{\text{heat exchange}} - \overbrace{Q_{\mathrm{l}}}^{\text{heat loss}}\end{aligned} \tag{2.3c}$$

where the state variables are the functions

$$m_{\mathrm{w}} = m_{\mathrm{s}}X \tag{2.4a}$$

$$m_{\mathrm{v}} = m_{\mathrm{da}}Y \tag{2.4b}$$

$$U = m_{\mathrm{da}}(h_a - RT) + m_{\mathrm{s}}h_p + m_{\mathrm{m}}h_m \tag{2.4c}$$

The mass balance (2.3a) governs the amount of water in the powder, m_{w}, and (2.3b) governs the amount of vapor, m_{v}, in the air. The energy balance, (2.3c), governs the accumulated heat, U, in the stage. Note, that the model is an index-1 DAE model, as U in (2.4c) depends on the state Y in h_{a} and X in h_{p}. m_{da} is the mass of dry air, m_{s} is the mass of powder solids and m_{m} is the mass of metal.

F_{s} is the flow of feed solids which is equal in all stages. X_{in} and X are the dry base concentration of the in- and outlet powder flows. R_{w} is the product drying rate that describes the flow of evaporated water to vapor. Y_{in} and Y are the vapor concentration of the air in- and outlet air flows, respectively. F_{da} is the dry inlet air flow to the stage. The advantage of using dry base air flows and dry base powder flows is evident as the hold up of dry air and powder solids are fixed and the notation thereby simplifies the equations. The relation between humid and dry air flows as well as total powder and powder solid flows are given in Paper A. In case more air flows are flowing to the same stage, the inflow of vapor is a sum of multiple $Y_{\mathrm{in}}F_{\mathrm{da}}$ vapor flows and F_{da} out of the stage is the sum of all the dry inlet air flows. $h_{a,\mathrm{in}} = h_{\mathrm{a}}(Y_{\mathrm{in}}, T_{\mathrm{in}})$ and $h_{a,\mathrm{out}} = h_{\mathrm{a}}(Y, T)$ are specific enthalpies of the inlet and outlet air flows. The specific enthalpy of the powder inlet is $h_{p,\mathrm{in}} = h_{\mathrm{p}}(X_{\mathrm{in}}, T_{\mathrm{in}})$ and the powder outlet is $h_{p,\mathrm{out}} = h_{\mathrm{p}}(X, T)$. T_{in} is the temperature of the inlet air flows. The specific enthalpy is calculated as described in Paper A. The enthalpies describe the heat exchange due to the flow of mass, i.e. air flows and powder flows. In case more air flows are flowing to the same stage, the inflow of energy is a sum of multiple $(h_{a,\mathrm{in}} - h_{a,\mathrm{out}})F_{\mathrm{da}}$ terms. $\Delta H_{\mathrm{e}}^{\mathrm{in2out}}$ is the enthalpy of mass exchange due to powder transport between the SD and SFB stages. The stages are connected by steel ducts and plates giving rise to a heat conduction between the stages. We model this transfer by $Q_{\mathrm{e}}^{\mathrm{in2out}}$. Finally, we model the heat loss to the surroundings by Q_{l}.

2.4.2 Constitutive Equations

The constitutive equations define the relations in the conservation equations. The product drying rate is governed by the thin layer equation. The thin layer equation models evaporation as a diffusion process [Lew21]

$$R_{\mathrm{w}} = k_1 D_{\mathrm{w}}(X - X_{\mathrm{eq}}) m_{\mathrm{s}} \tag{2.5}$$

X is the stage powder moisture content and $X_{\mathrm{eq}} = X_{\mathrm{eq}}(T, Y) + X_{\mathrm{add}}$ is the equilibrium moisture content described in Section 2.3. T is the stage temperature and Y is the stage air humidity. The free moisture content, $X - X_{\mathrm{eq}}$, describes the moisture content that is free to evaporate. This expression renders a lower bound for the possible moisture removal and drives the drying process.

The diffusion term, $D_{\mathrm{w}} = D_{\mathrm{w}}(T, X)$, describes the friction of evaporation and depends on the product being dried [HAPB07, YSW01]. D_{w} contains an Arrhenius like relation to compensate for temperature dependencies and is also a function of the residual moisture content. Consequently, we describe diffusion by

$$D_{\mathrm{w}}(T, X) = \exp\left(-\frac{c_1}{R}\left(\frac{1}{T} - \frac{1}{T_0}\right)\right)\frac{X}{c_2 + X} \tag{2.6}$$

where R is the ideal gas constant and T_0 is the reference temperature given in Paper A. c_1 and c_2 are constants that must be identified.

The SFB is supplied with air from below and a proportion of the powder in the SFB stage is therefore blown off the fluid bed and back into the SD stage. Thus, there is an exchange of heat and mass between the SD and SFB stages. We simplify the description of this phenomenon and model the heat exchange only, described by $\Delta H_{\mathrm{e}}^{\mathrm{in2out}}$. The heat transfer, due to conduction, $Q_{\mathrm{e}}^{\mathrm{in2out}}$, between these two stages is negligible. The SFB, VFBh and VFBc stages have no continuous exchange of powder, thus we neglect $\Delta H_{\mathrm{e}}^{\mathrm{in2out}}$ and only model the heat conduction between the stages, $Q_{\mathrm{e}}^{\mathrm{in2out}}$.

The conductive heat loss, Q_{l}, is modeled by

$$Q_{\mathrm{l}} = k_{\mathrm{UA}}(T - T_{\mathrm{amb}}) \tag{2.7}$$

in which T_{amb} denotes the ambient air temperature. k_{UA} is a heat transfer coefficient that must be estimated.

2.4.3 Key Performance Indicators

The key performance indicators (KPIs) in spray drying are the profit of operation, p, the energy consumption, Q_{tot}, the specific energy consumption, $Q_{\text{tot}}/F_{\text{p}}$, the energy efficiency, η, the product residual moisture content, $1-S$, and the product flow rate, F_{p}. The profit of operation is given by the value of the product minus the raw material and energy costs

$$p(\cdot) = p_{\text{p}}F_{\text{p}} - p_{\text{f}}F_{\text{f}} - p_{\text{E}}Q_{\text{tot}} \tag{2.8a}$$

p_{p} is the unit value of the product, p_{f} is the unit cost of feed material and p_{H} is the unit energy cost. We assume that the bulk price of skimmed milk powder (SMP) is $p_{\text{p}} = 2.5$ €/kg, the feed price is $p_f = 0.1p_{\text{p}}$ and the price of energy is $p_{\text{E}} = 12.9$ €/(MWhr). $F_{\text{p}} = F_{\text{s}}(1 + X^{\text{d}})$ is the flow rate of powder out of the dryer and $F_{\text{f}} = F_{\text{s}}(1 + X_{\text{f}})$ is the feed flow rate. $X^{\text{d}} = (1-S)/S$ is the moisture content in the VFBc stage and X_{f} is the moisture content in the feed on the dry base concentration.

Q_{tot} is the total energy consumption of the dryer

$$\begin{aligned} Q_{\text{tot}} = F_{\text{main}}(h_{a,\text{main}} - h_{\text{amb}}) + F_{\text{sfb}}(h_{a,\text{sfb}} - h_{\text{amb}}) + \\ F_{\text{vfbh}}(h_{a,\text{vfbh}} - h_{\text{amb}}) + F_{\text{vfbc}}(h_{a,\text{vfbc}} - h_{\text{amb}}) \end{aligned} \tag{2.8b}$$

where h_{amb} is the specific enthalpy of the air at outdoor temperature and humidity. The specific enthalpy is calculated as described in Paper A. The specific energy consumption is computed as $Q_{\text{tot}}/F_{\text{p}}$.

We adopt the definition of energy efficiency provided by [Kud12,KP10]. The energy required for evaporation is relative to the total energy supplied for heating the air

$$\eta = \frac{\lambda(T_0)F_{\text{s}}(X_{\text{f}} - X^{\text{d}})}{Q_{\text{tot}}} \tag{2.8c}$$

The energy required for evaporation of the water in the feed is $\lambda(T_0)F_{\text{s}}(X_{\text{f}} - X^{\text{d}})$.

The flow rate of powder out of the dryer is given by

$$F_{\text{p}} = F_{\text{s}}(1 + X^{\text{d}}) \tag{2.8d}$$

Note that these measures can be computed without a model, as they only depend on measured outputs.

2.4.4 Constraints

The maximum capacity of the feed pump limits the feed flow. The inlet temperatures must be higher than the ambient temperature, T_{amb}, and the risk of scorched particles creates upper limits on the allowable inlet temperatures. Consequently, we use

$$0 \text{ kg/hr} \leq F_{\text{f}} \leq 140 \text{ kg/hr} \tag{2.9a}$$
$$T_{\text{amb}} \leq T_{\text{main}} \leq 220^{\circ}\text{C} \tag{2.9b}$$
$$T_{\text{amb}} \leq T_{\text{sfb}} \leq 120^{\circ}\text{C} \tag{2.9c}$$
$$T_{\text{amb}} \leq T_{\text{vfbh}} \leq 70^{\circ}\text{C} \tag{2.9d}$$

In addition, the model includes stickiness constraints of the powder in each stage of the spray dryer. Stickiness of the powder is computed by the glass transition temperature given in Section 2.3. The surface moisture content, Z, in (2.2) is

$$Z = \begin{cases} 0.53X^a & \text{for the SD} \\ X^b & \text{for the SFB} \\ X^c & \text{for the VFBh} \\ X^d & \text{for the VFBc} \end{cases} \tag{2.10}$$

in which the superscript a, b, c and d refers to the SD, SFB, VFBh and VFBc stages, respectively. The surface moisture content, Z, of the powder in the SD stage is subject to a correction term of 0.53. The constant is manually selected and compensates for the crisper surface of the particles that makes the powder less sticky. We experienced none to small signs of powder deposits during the experiments, thus 0.53 is selected to reflect this fact. The constant can only be exactly determined as a result of dryer specific empirical inspection of the chamber walls after deposits have actually formed [HFOS10].

2.4.5 Summary

The presented model, also provided in Paper A, describes the four-stage spray dryer as a deterministic index-1 differential algebraic equations (DAE) model. For simulation purposes, we construct a stochastic DAE model, with two piecewise stochastic inputs, which may be represented in discrete form

$$x_{k+1} = F(x_k, u_k + w_{\text{u},k}, d_k + w_{\text{d},k}, \theta) \tag{2.11a}$$
$$y_k = h_{\text{y}}(x_k) + v_k \tag{2.11b}$$

in which $F(\cdot)$ is the solution of the system of differential equations

$$x(t_k) = x_k \tag{2.12a}$$

$$\frac{d}{dt}g(x(t)) = f(x(t), u_k + w_{\mathrm{u},k}, d_k + w_{\mathrm{d},k}, \theta) \quad t_k \leq t \leq t_{k+1} \tag{2.12b}$$

$$x_{k+1} = x(t_{k+1}) \tag{2.12c}$$

Equation (2.12) is solved efficiently by explicit singly diagonally implicit Runge-Kutta (ESDIRK) methods. We use the ESDIRK4(3) method with variable step-size [KJTJ04, VJTS10]. The state function $g(x(t))$ represents hold-up of mass and energy and $f(x(t), u(t), d(t), \theta)$ is the flux of mass and energy. The two piecewise stochastic inputs, $u_k + w_{u,k}$ and $d_k + w_{d,k}$, are constant for $t_k \leq t \leq t_{k+1}$. The output equation, $h_{\mathrm{y}}(x_k)$, is corrupted by measurement noise, v_k. The noises are given by the stochastic variables $w_{\mathrm{u},k} \sim N_{\mathrm{iid}}(0, R_{\mathrm{u}})$, $w_{\mathrm{d},k} \sim N_{\mathrm{iid}}(0, R_{\mathrm{d}})$, and $v_k \sim N_{\mathrm{iid}}(0, R_{\mathrm{v}})$. The covariances, ($R_{\mathrm{u}}$, R_{d}, R_{v}), are estimated from the covariances of u, d, and y, respectively. θ is the unknown parameter vector that has to be estimated from data. θ is identified by minimization of the sum of squared simulation errors.

The measurement vector, y, the input vector, u, the disturbance vector, d, and the state vector, x, are

$$\begin{aligned} y(t) &= [T^a \quad T^b \quad Y^a \quad T^c \quad T^d \quad S^b \quad S^d]^T \\ &= \begin{bmatrix} T_{\mathrm{SD}} & T_{\mathrm{SFB}} & Y_{\mathrm{ab}} & T_{\mathrm{VFBh}} & T_{\mathrm{VFBc}} & S_{\mathrm{ab}} & S_{\mathrm{cd}} \end{bmatrix}^T \end{aligned} \tag{2.13a}$$

$$\begin{aligned} u(t) = [&F_{\mathrm{f}} \quad T_{\mathrm{f}} \quad S_{\mathrm{f}} \quad F_{\mathrm{main}} \quad T_{\mathrm{main}} \quad Y_{\mathrm{main}} \quad ... \\ &F_{\mathrm{sfb}} \quad T_{\mathrm{sfb}} \quad Y_{\mathrm{sfb}} \quad F_{\mathrm{vfbh}} \quad T_{\mathrm{vfbh}} \quad Y_{\mathrm{vfbh}} \quad ... \\ &F_{\mathrm{vfbc}} \quad T_{\mathrm{vfbc}} \quad Y_{\mathrm{vfbc}}]^T \end{aligned} \tag{2.13b}$$

$$d(t) = [T^{ab}_{\mathrm{amb}} \quad T^{cd}_{\mathrm{amb}}]^T \tag{2.13c}$$

$$\begin{aligned} x(t) = [&T^a \quad Y^a \quad X^a \quad T^b \quad Y^b \quad X^b \quad ... \\ &T^c \quad Y^c \quad X^c \quad T^d \quad Y^d \quad X^d]^T \end{aligned} \tag{2.13d}$$

The superscript a, b, c and d refers to the SD, SFB, VFBh and VFBc stages, respectively.

2.5 Complexity Reduced Control Model

In this section, we present the four-stage spray dryer model that is used for design of the controllers i.e. in the state estimator and for prediction in the controller. The model provide simulations of the outputs with an emphasis

on the residual moisture content of the final powder and describes the data well, while being simple due to the lumped modeling approach. Compared to the simulation model this model contains fewer states and parameters, thus simplifying the computational demand and identification complexity. The dryer is divided into two parts; a SD and a SFB part and a VFBh and a VFBc part. The model is described in full in Paper G.

2.5.1 Spray Dryer and Static Fluid Bed Model

The evolution of the SFB powder moisture content, X_{ab}, the SD air humidity, Y_{ab}, and the temperatures, T_{SD} and T_{SFB}, in the stages are determined by the lumped conservation equations

$$m_{\mathrm{b}}\frac{dX_{\mathrm{ab}}}{dt} = \overbrace{F_{\mathrm{s}}(X_{\mathrm{f}} - X_{\mathrm{ab}})}^{\text{water in and out flows}} - \overbrace{R_{\mathrm{aw}}}^{\text{water evaporation rate}} \tag{2.14a}$$

$$m_{\mathrm{a}}\frac{dY_{\mathrm{ab}}}{dt} = \overbrace{(F_{\mathrm{main}} + F_{\mathrm{sfb}})(Y_{\mathrm{amb}} - Y_{\mathrm{ab}})}^{\text{vapor in and out flows}} + \overbrace{F_{\mathrm{add}}(Y_{\mathrm{add}} - Y_{\mathrm{ab}})}^{\text{vapor correction flows}} + \overbrace{R_{\mathrm{aw}}}^{\text{water evaporation rate}} \tag{2.14b}$$

$$\begin{aligned} C_{\mathrm{a}}\frac{dT_{\mathrm{SD}}}{dt} = &- \overbrace{\lambda R_{\mathrm{aw}}}^{\text{heat of evaporation}} + \overbrace{F_{\mathrm{main}}h_{a_{\mathrm{in}}} + F_{\mathrm{sfb}}h_{b_{\mathrm{out}}} + F_{\mathrm{add}}h_{a_{\mathrm{add}}}}^{\text{enthalpy of inlet air flows}} \\ &- \overbrace{(F_{\mathrm{main}} + F_{\mathrm{sfb}} + F_{\mathrm{add}})h_{a_{\mathrm{out}}}}^{\text{enthalpy of outlet air flow}} + \overbrace{F_{\mathrm{s}}(h_{\mathrm{f}}^{p} - h_{a}^{p})}^{\text{enthalpy of powder flow}} \\ &- \overbrace{Q_{\mathrm{ab}}}^{\text{heat exchange}} - \overbrace{Q_{\mathrm{a}}}^{\text{heat loss}} \end{aligned} \tag{2.14c}$$

$$\begin{aligned} C_{\mathrm{b}}\frac{dT_{\mathrm{SFB}}}{dt} = &\overbrace{F_{\mathrm{sfb}}(h_{b_{\mathrm{in}}}^{a} - h_{b_{\mathrm{out}}}^{a})}^{\text{enthalpy of air flows}} + \overbrace{F_{\mathrm{s}}(h_{a}^{p} - h_{b}^{p})}^{\text{enthalpy of powder flow}} \\ &+ \overbrace{Q_{\mathrm{ab}} - Q_{\mathrm{bc}}}^{\text{heat exchange}} - \overbrace{Q_{\mathrm{b}}}^{\text{heat loss}} \end{aligned} \tag{2.14d}$$

where the constitutive equations are

$$\begin{aligned} h_{\mathrm{a_{in}}}^{a} &= (c_{\mathrm{da}} + c_{\mathrm{v}}Y_{\mathrm{amb}})T_{\mathrm{main}}, \quad h_{\mathrm{a_{out}}}^{a} = (c_{\mathrm{da}} + c_{\mathrm{v}}Y_{\mathrm{ab}})T_{\mathrm{SD}} \\ h_{b_{\mathrm{in}}}^{a} &= (c_{\mathrm{da}} + c_{\mathrm{v}}Y_{\mathrm{amb}})T_{\mathrm{sfb}}, \quad h_{b_{\mathrm{out}}}^{a} = (c_{\mathrm{da}} + c_{\mathrm{v}}Y_{\mathrm{amb}})T_{\mathrm{SFB}} \\ h_{\mathrm{a_{add}}}^{a} &= (c_{\mathrm{da}} + c_{\mathrm{v}}Y_{\mathrm{add}})T_{\mathrm{add}}, \quad h_{\mathrm{f}}^{p} = (c_{\mathrm{s}} + c_{\mathrm{w}}X_{\mathrm{f}})T_{\mathrm{f}} \\ h_{a}^{p} &= (c_{\mathrm{s}} + c_{\mathrm{w}}X_{\mathrm{ab}})T_{\mathrm{SD}}, \quad h_{b}^{p} = (c_{\mathrm{s}} + c_{\mathrm{w}}X_{\mathrm{ab}})T_{\mathrm{SFB}} \\ Q_{\mathrm{ab}} &= k_1(T_{\mathrm{SD}} - T_{\mathrm{SFB}}) + k_2X_{\mathrm{f}} + k_3T_{\mathrm{f}} - k_4 \\ Q_{\mathrm{a}} &= k_5(T_{\mathrm{SD}} - T_{\mathrm{amb}}), \quad Q_{\mathrm{b}} = k_6(T_{\mathrm{SFB}} - T_{\mathrm{amb}}) \end{aligned} \tag{2.14e}$$

m_a is the mass of dry air and m_b is the mass of dry powder. C_a and C_b are the heat capacities of the hold-up of air and powder. The mass balance (2.14a) governs the amount of water in the powder. $F_\mathrm{s} = F_\mathrm{f} S_\mathrm{f}$ is the flow of feed solids. $X_\mathrm{f} = (1 - S_\mathrm{f})/S_\mathrm{f}$ is the dry base feed concentration and T_f is the feed temperature. R_{aw} is the product drying rate. The mass balance (2.14b) governs the amount of vapor in the air. F_main and F_sfb are the dry base inlet air flows. Y_amb is the vapor concentration of the inlet air. The parameters Y_add, F_add and T_add are used to compensate for air leakages and un-modeled inlet air flows such as nozzle cooling air. The energy balance, (2.14c) and (2.14d), governs the accumulated heat in the stages. The specific enthalpies from the air flows are, $h^a_{\{\cdot\}}$, and the specific enthalpies of the powder flows are, $h^p_{\{\cdot\}}$. Q_ab describes the heat exchange between the SD and the SFB stages. Q_bc is the heat exchange between the SFB and the VFBh stages. Q_a and Q_b are heat losses to the surroundings. The heat capacities are given at the reference temperature, T_0, and computed as described in Paper A.

We assume that the evaporation takes place in the SD stage only with the drying rate determined from the powder conditions in the SFB stage. The product drying rate is governed by the thin layer equation, describing evaporation due to diffusion [Lew21]

$$R_{aw} = k_7 \frac{k_8}{k_8 + F_\mathrm{s}} \left(\frac{T_\mathrm{f}}{T_0} \right)^{k_9} (X_\mathrm{ab} - X_\mathrm{eq}) m_b$$

The equilibrium moisture content, $X_\mathrm{eq} = X_\mathrm{eq}(T_\mathrm{SFB}, Y_\mathrm{ab})$, describes the moisture content at which the water cannot be evaporated any longer and is described in Section 2.3 and in Paper G.

2.5.2 Vibrating Fluid Bed Model

The evolution of the VFB powder moisture content, X_cd, the VFB air humidity, Y_cd, and the temperatures, T_VFBh and T_VFBc, in the stages are determined by the lumped conservation equations

$$m_\mathrm{d} \frac{dX_\mathrm{cd}}{dt} = \overbrace{F_\mathrm{s}(X_\mathrm{ab} - X_\mathrm{cd})}^{\text{water in and out flows}} - \overbrace{R_\mathrm{cw}}^{\text{water evaporation rate}} \tag{2.15a}$$

$$m_\mathrm{c} \frac{dY_\mathrm{cd}}{dt} = \overbrace{(F_\mathrm{vfbh} + F_\mathrm{vfbc})(Y_\mathrm{amb} - Y_\mathrm{cd})}^{\text{vapor in and out flows}} + \overbrace{R_\mathrm{cw}}^{\text{water evaporation rate}} \tag{2.15b}$$

$$C_{\mathrm{cd}}\frac{dT_{\mathrm{VFBh}}}{dt} = -\overbrace{\lambda R_{\mathrm{cw}}}^{\text{heat of evaporation}} + \overbrace{F_{\mathrm{vfbh}}(h^a_{c_{\mathrm{in}}} - h^a_{c_{\mathrm{out}}})}^{\text{enthalpy of air flows}} + \overbrace{F_{\mathrm{s}}(h^p_b - h^p_c)}^{\text{enthalpy of powder flow}} + \overbrace{Q_{\mathrm{bc}}}^{\text{heat exchange}} - \overbrace{Q_{\mathrm{c}}}^{\text{heat loss}} \tag{2.15c}$$

$$C_{\mathrm{cd}}\frac{dT_{\mathrm{VFBc}}}{dt} = \overbrace{F_{\mathrm{vfbc}}(h^a_{d_{\mathrm{in}}} - h^a_{d_{\mathrm{out}}})}^{\text{enthalpy of air flows}} + \overbrace{F_{\mathrm{s}}(h^p_c - h^p_d)}^{\text{enthalpy of powder flow}} - \overbrace{Q_{\mathrm{d}}}^{\text{heat loss}} \tag{2.15d}$$

where

$$\begin{aligned}
h^a_{c_{\mathrm{in}}} &= (c_{\mathrm{da}} + c_{\mathrm{v}}Y_{\mathrm{amb}})T_{\mathrm{vfbh}}, \quad h^a_{c_{\mathrm{out}}} = (c_{\mathrm{da}} + c_{\mathrm{v}}Y_{\mathrm{cd}})T_{\mathrm{VFBh}} \\
h^a_{d_{\mathrm{in}}} &= (c_{\mathrm{da}} + c_{\mathrm{v}}Y_{\mathrm{amb}})T_{\mathrm{vfbc}}, \quad h^a_{d_{\mathrm{out}}} = (c_{\mathrm{da}} + c_{\mathrm{v}}Y_{\mathrm{cd}})T_{\mathrm{VFBc}} \\
h^p_c &= (c_{\mathrm{s}} + c_{\mathrm{w}}X_{\mathrm{cd}})T_{\mathrm{VFBh}}, \quad h^p_d = (c_{\mathrm{s}} + c_{\mathrm{w}}X_{\mathrm{cd}})T_{\mathrm{VFBc}} \\
Q_{\mathrm{c}} &= k_{11}(T_{\mathrm{VFBh}} - T_{\mathrm{amb}}), \quad Q_{\mathrm{d}} = k_{12}(T_{\mathrm{VFBc}} - T_{\mathrm{amb}}) \\
Q_{\mathrm{bc}} &= k_{10}(T_{\mathrm{SFB}} - T_{\mathrm{VFBh}})
\end{aligned} \tag{2.15e}$$

m_{c} is the mass of dry air and m_{d} is the mass of dry powder. C_{cd} is the heat capacity of the hold-up of air and powder in both the VFBh and VFBc stage. The mass balance (2.15a) governs the amount of water in the powder. F_{s} is the flow of feed solids. X_{ab} is the dry base feed concentration of the inlet powder. R_{cw} is the product drying rate, that renders the flow of evaporated water to vapor. Water is assumed only to evaporate from the VFBh stage. The mass balance (2.15b) governs the amount of vapor in the air. F_{vfbh} and F_{vfbc} are the dry base inlet air flows. Y_{amb} is the vapor concentration of the inlet air. The energy balance, (2.15c) and (2.15d), governs the accumulated heat in the stages. The specific enthalpies from the air flows are, $h^a_{\{\cdot\}}$, and the specific enthalpies of the powder flows are, $h^p_{\{\cdot\}}$. Q_{bc} describes the heat exchange between the SFB and the VFBh stages. Q_{c} and Q_{d} are heat losses to the surroundings.

The product drying rate is governed by the thin layer equation and a constant term

$$R_{\mathrm{cw}} = k_{13}(X_{\mathrm{cd}} - X_{\mathrm{eq}})m_{\mathrm{d}} - k_{14}m_{\mathrm{d}}$$

The equilibrium moisture content is $X_{\mathrm{eq}} = X_{\mathrm{eq}}(T_{\mathrm{VFBh}}, Y_{\mathrm{cd}})$

2.5.3 Key Performance Indicators

The profit of operation is given by the value of the product minus the raw material and energy costs

$$p(\cdot) = p_{\mathrm{p}}F_{\mathrm{p}} - p_{\mathrm{f}}F_{\mathrm{f}} - p_{\mathrm{E}}Q_{\mathrm{tot}} \tag{2.16a}$$

in which $F_{\mathrm{p}} = F_{\mathrm{s}}(1 + X_{\mathrm{cd}})$ is the flow rate of powder out of the dryer and $F_{\mathrm{f}} = F_{\mathrm{s}}(1 + X_{\mathrm{f}})$ is the feed flow rate. p_{p}, p_{f} and p_{E} are the prices presented in Section 2.4.3. Q_{tot} is the total energy consumption of the dryer

$$\begin{aligned} Q_{\mathrm{tot}} = F_{\mathrm{main}}(h^a_{a_{\mathrm{in}}} - h^a_{\mathrm{amb}}) + F_{\mathrm{sfb}}(h^a_{b_{\mathrm{in}}} - h^a_{\mathrm{amb}}) \\ + F_{\mathrm{vfbh}}(h^a_{c_{\mathrm{in}}} - h^a_{\mathrm{amb}}) + F_{\mathrm{vfbc}}(h^a_{d_{\mathrm{in}}} - h^a_{\mathrm{amb}}) \end{aligned} \tag{2.16b}$$

in which $h^a_{\mathrm{amb}} = (c_{\mathrm{da}} + c_{\mathrm{v}} Y_{\mathrm{amb}}) T_{\mathrm{amb}}$ is the specific enthalpy of the outdoor air. $h^a_{a_{\mathrm{in}}}$, $h^a_{b_{\mathrm{in}}}$, $h^a_{c_{\mathrm{in}}}$ and $h^a_{d_{\mathrm{in}}}$ are the specific enthalpy of the inlet air.

2.5.4 Constraints

As with the simulation model, the inputs are constrained by (2.9).

This model also includes stickiness constraints of the powder in each stage of the spray dryer. Stickiness of the powder is computed by the glass transition temperature in (2.2) with the surface moisture content, Z, given by

$$Z = \begin{cases} (A_p + B_p\ T_{\mathrm{SD}}) \exp\left(C_p\ \mathrm{RH}_{\mathrm{SD}}\right) & \text{for SD} \\ X_{\mathrm{ab}} & \text{for SFB} \\ X_{\mathrm{cd}} & \text{for VFBh} \\ X_{\mathrm{cd}} & \text{for VFBc} \end{cases} \tag{2.17}$$

in which $A_p = 0.193$, $B_p = -0.000435$ and $C_p = 4.51$. $RH_{\mathrm{SD}} = \mathrm{RH}(T_{\mathrm{SD}}, Y_{\mathrm{ab}})$ is the relative air humidity. The moisture content of the powder in the SD stage is estimated by an experimentally determined expression related to the equilibrium moisture, X_{eq}, as the residual moisture in the SD stage is un-modeled.

Additionally, the SFB stage temperature is constrained by $65°\mathrm{C} \leq T_{\mathrm{SFB}} \leq 75.5°\mathrm{C}$ as the operators have experienced that operation between these temperatures provide a low risk of powder lumps forming in the SFB.

2.5.5 Summary

The presented model, also provided in Paper G, describes the four-stage spray dryer as a deterministic system of ordinary differential equations (ODEs). The ODE model may be represented in discrete form

$$x_{k+1} = F(x_k, u_k, d_k, \theta) \tag{2.18a}$$

$$y_k = h_{\mathrm{y}}(x_k) \tag{2.18b}$$

in which $F(\cdot)$ is the solution of the system of differential equations

$$x(t_k) = x_k \tag{2.19a}$$

$$\frac{d}{dt}x(t) = f(x(t), u_k, d_k, \theta) \quad t_k \leq t \leq t_{k+1} \tag{2.19b}$$

$$x_{k+1} = x(t_{k+1}) \tag{2.19c}$$

Equation (2.19) is solved using the ESDIRK4(3) method with variable step-size [VJTS10]. The state $x(t)$ represents hold-up of mass and energy and $f(x(t), u_k, d_k, \theta)$ is the flux of mass and energy. $h_{\mathrm{y}}(x_k)$ is the measurement equation. θ is the unknown parameter vector that has to be estimated from data. θ is identified by minimization of the sum of squared simulation errors.

The measurement and output vector, y, the input vector, u, the disturbance vector, d, and the state vector, x, are

$$y = \begin{bmatrix} T_{\mathrm{SD}} & T_{\mathrm{SFB}} & Y_{\mathrm{ab}} & T_{\mathrm{VFBh}} & T_{\mathrm{VFBc}} & S_{\mathrm{ab}} & S_{\mathrm{cd}} \end{bmatrix}^T \tag{2.20a}$$

$$u = \begin{bmatrix} F_{\mathrm{f}} & T_{\mathrm{main}} & T_{\mathrm{sfb}} & T_{\mathrm{vfbh}} \end{bmatrix}^T \tag{2.20b}$$

$$d = \begin{bmatrix} S_{\mathrm{f}} & T_{\mathrm{f}} & Y_{\mathrm{amb}} & F_{\mathrm{main}} & F_{\mathrm{sfb}} & F_{\mathrm{vfbh}} & F_{\mathrm{vfbc}} & T_{\mathrm{amb}} & T_{\mathrm{vfbc}} \end{bmatrix}^T \tag{2.20c}$$

$$x = \begin{bmatrix} T_{\mathrm{SD}} & T_{\mathrm{SFB}} & Y_{\mathrm{ab}} & X_{\mathrm{ab}} & T_{\mathrm{VFBh}} & T_{\mathrm{VFBc}} & Y_{\mathrm{cd}} & X_{\mathrm{cd}} \end{bmatrix}^T \tag{2.20d}$$

2.6 Discrete Time State-Space Model

Linear models take many forms and may be identified directly from data or by linearization of first-principles models. Examples of linear input-output models are the finite impulse response (FIR) models, autoregressive exogenous (ARX) models, autoregressive moving average exogenous (ARMAX) models, step response models, impulse response models, transfer-function models etc.

In general, all these models can be represented as linear discrete time state-space models. The state-space models have the form

$$x_{k+1} = Ax_k + Bu_k + Ed_k + \sigma_{\mathrm{x}} \tag{2.21a}$$

$$y_k = C_{\mathrm{y}}x_k + \sigma_{\mathrm{y}} \tag{2.21b}$$

in which x_k is the state vector, u_k is the input vector, d_k is the disturbance vector and y_k is the measurement vector. (A,B,E,C_{y}) are the state-space matrices. σ_{x} and σ_{y} contain the constants related to the linearisation of the model, i.e. $\sigma_{\mathrm{x}} = x_{\mathrm{ss}} - Ax_{\mathrm{ss}} - Bu_{\mathrm{ss}} - Ed_{\mathrm{ss}}$ and $\sigma_{\mathrm{y}} = y_{\mathrm{ss}} - C_{\mathrm{y}}x_{\mathrm{ss}}$.

In Paper B, Paper E and Paper H we identify state-space models by linearization of the control model in Section 2.5. In Paper I we get the state-space model from a transfer-function model identified solely from data to ease the required modeling work, as we do not know the accuracy of the nonlinear control model on milk products and industrial sized dryers. Discretization of the model is performed using the matrix exponential, assuming a zero-order-hold sampling system.

2.7 Model Validation

In this section, we asses the quality of the deterministic simulation and control models by comparing its outputs with the estimation and validation experiment. The simulation model is described in Section 2.4 and the control models are described in Section 2.5 and 2.6.

Fig. 2.7 shows the outputs of the estimation experiment which is used to identify the parameters. Fig. 2.8 shows the validation experiment. The deterministic model simulations are shown for each model in the same figure. The inputs and disturbances of the two experiments are shown in Appendix A.

All three simulations show good agreement with the estimation experiment. The transients and the steady-states are well described by the models. The simulation model renders all the outputs well compared to the data. The stage temperatures, T, and the air humidity in the SD stage, Y, fit the data well. The powder moisture contents, S, also fit the data well, but deviates slightly at low residual moisture levels. The nonlinear and linear control models simulate the stage temperatures, T, and the air humidity in the SD stage, Y, well. The powder residual moisture content, S, in the SFB stage do not render the same high accuracy as seen for the simulation model. The VFBc outlet moisture content fit the data well. The simulation accuracy of the SFB moisture content is not as important as the VFBc moisture content, as it is seldom measured and used for control anyway. The nonlinear and linear control models show almost equal simulation abilities, except for very large steps in the ambient air humidity. This is due to the non-linearity in the model of the equilibrium moisture content.

The moisture content is in general difficult to estimate at low moisture contents, due to an increasing dependency on the equilibrium moisture content, X_{eq}, in (2.1). The equilibrium moisture content is estimated based on laboratory tests, which do not render the conditions in a spray dryer well. Thus, we expect some deviation as the equilibrium moisture content becomes significant.

The VFBc stage is not sealed from the surrounding air, since the powder naturally has to be emptied from the VFBc stage. The residual moisture content may therefore be subject to an unknown disturbance. Note, that the communication to the VFBc residual moisture sensor dropped out in the period t=16.5 hours and t=18.2 hours due to a malfunction.

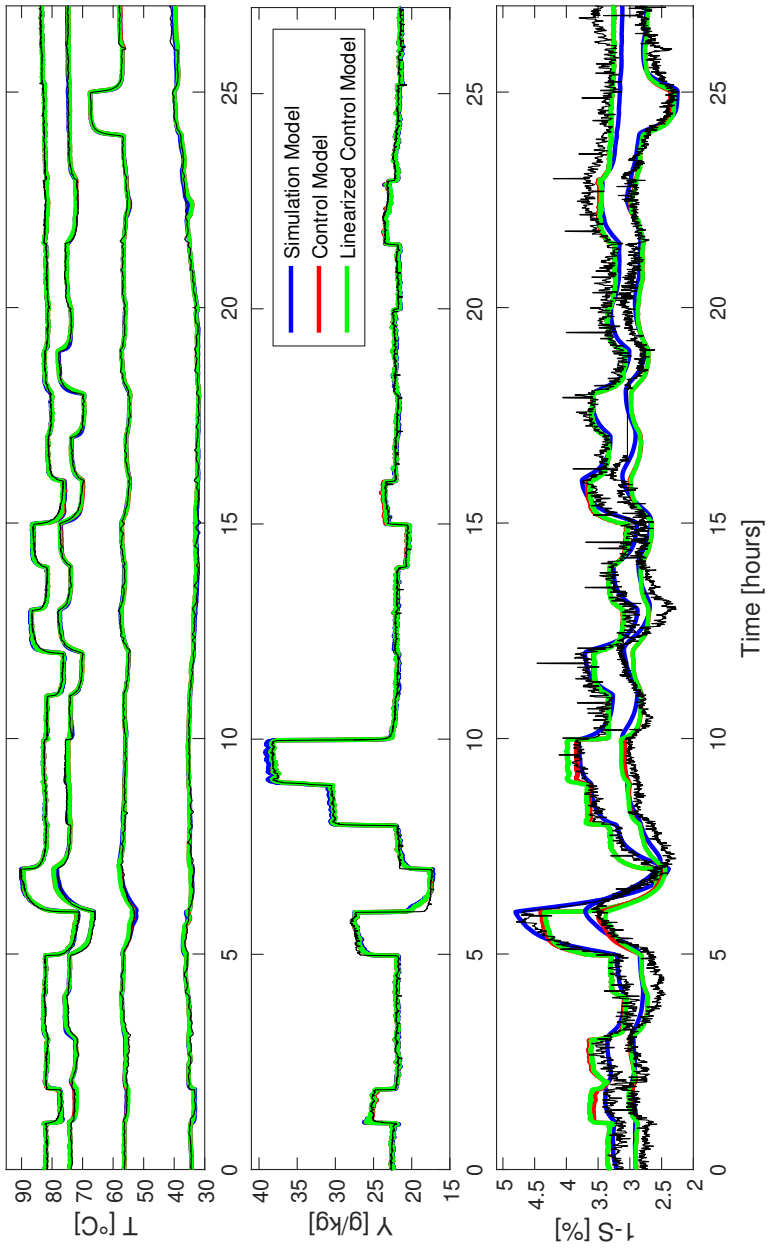

Figure 2.7: Plot of the estimation experiment outputs and the simulated outputs of each model. T and Y are the temperatures and abs. humidities of the air. $1 - S$ is the residual moisture contents.

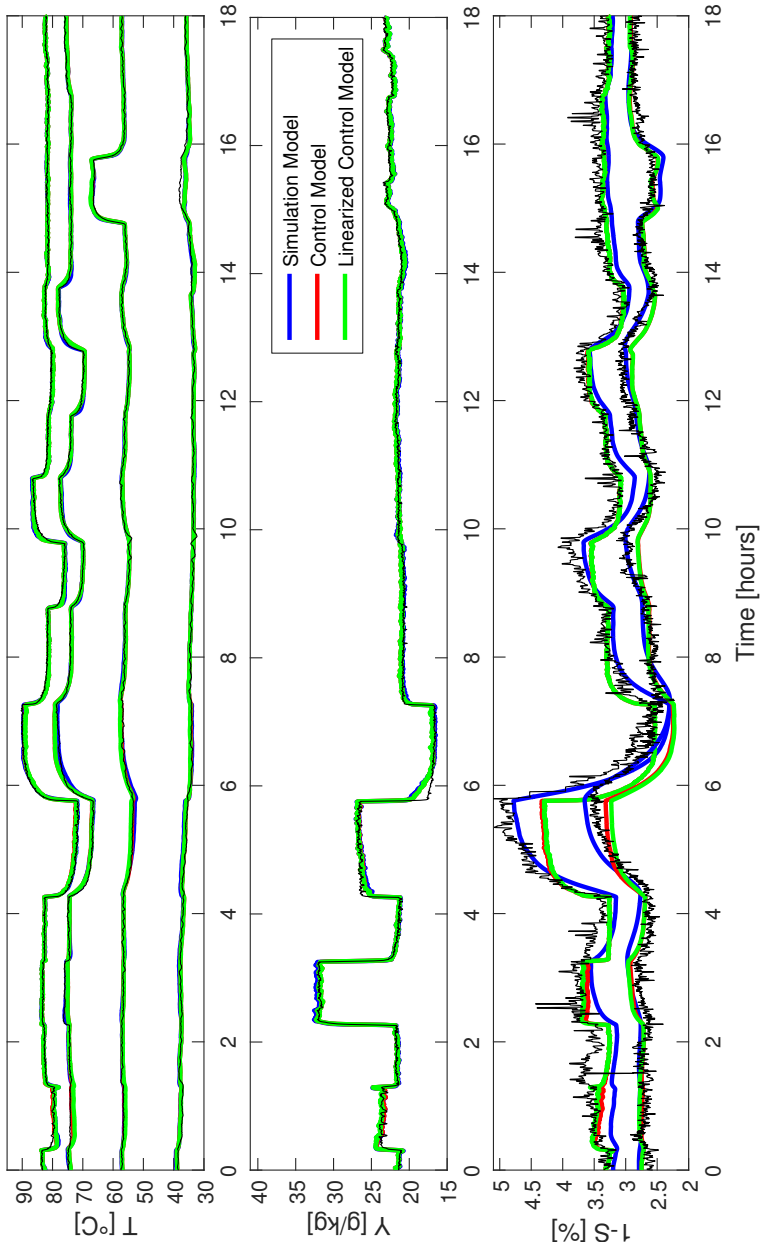

Figure 2.8: Plot of the validation experiment outputs and the simulated outputs of each model. T and Y are the temperatures and abs. humidities of the air. $1 - S$ is the residual moisture contents.

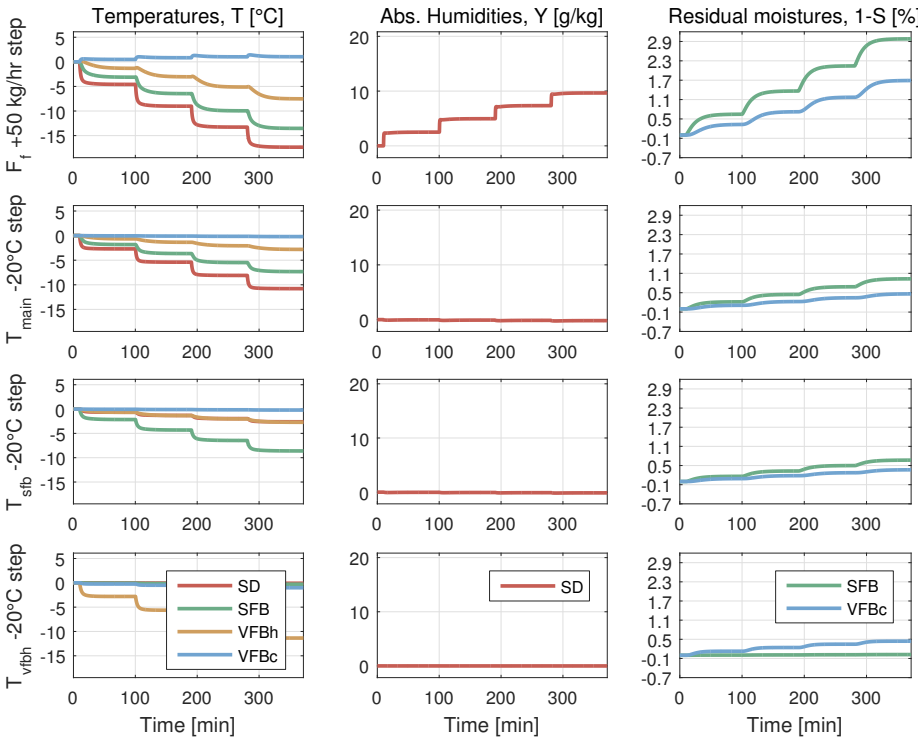

Figure 2.9: Simulated responses to several steps in the inputs.

The three simulations also show good agreement with the validation experiment. The transients and the steady-states are well described by the models. The temperatures and air humidity, T and Y, fit the data well during both disturbance and input steps. The powder moisture content, S, from the simulation model is estimated well, but some in-accuracies are present at low residual moisture contents. As for the estimation experiment, the control models do not render the SFB powder moisture content well. The VFBc moisture content fits the data well.

2.8 Step responses

Fig. 2.9 shows the step responses of the simulated outputs to the inputs. The responses are simulated using the simulation model of the four-stage spray dryer in Section 2.4. The control models provide similar responses. The initial offset

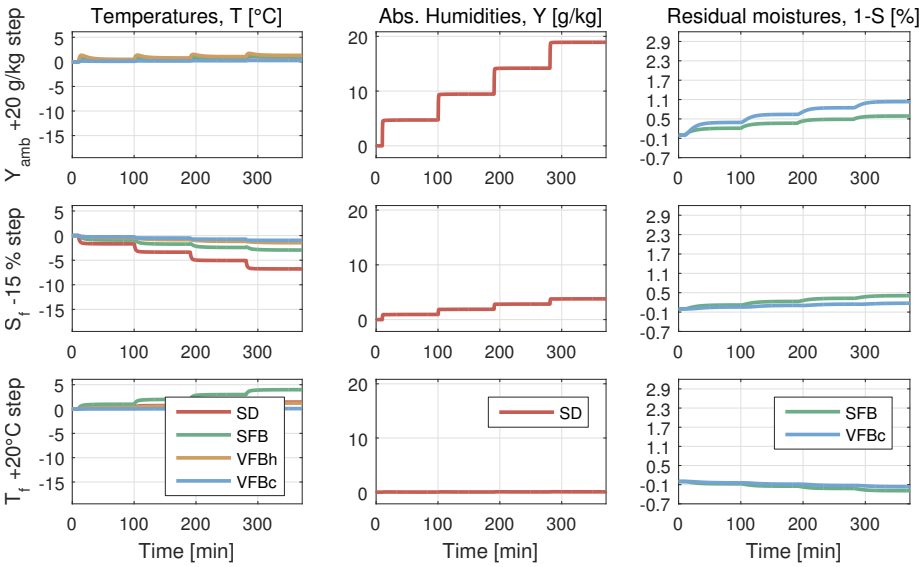

Figure 2.10: Simulated responses to several steps in the selected disturbances.

in the outputs is removed and every 90 minutes the step-size of the inputs is increased. This makes it possible to identify the effect of the non-linearities in the model. In the first row of Fig. 2.9, a 50 kg/hr increase in the feed flow rate, F_{f}, is shown to have a significant effect on all outputs. When the feed flow rate increases, the temperatures decrease, the air humidity increase, and the residual moisture content in the powder increase. The temperatures decrease because more water and feed need to be evaporated and heated with the same amount of energy from the inlet air. The air humidity increase as a consequence of the increased evaporation of water from the powder. The residual moisture content in the powder increase because the stage temperatures decrease and the air humidity increase. The plots in the second, third and last row of Fig. 2.9 indicate the step responses to a 20°C reduction in the main hot inlet air temperature, T_{main}, the inlet air to the SFB stage, T_{sfb}, and the inlet air to the VFBh stage. T_{main} and T_{sfb} both significantly affects the temperatures in the SD stage and the SFB stage. The similar effect is due to the mixing of the air in these two stages of the four-stage spray dryer. T_{main} and T_{sfb} hardly affects the temperature in the VFBh stage and in the VFBc stage. T_{vfbh} mainly affects the temperature in the VFBh stage of the four-stage spray dryer. T_{main} and T_{sfb} decrease the residual moisture of the powder at the SFB stage and the VFBc stage. T_{vfbh} only decreases the residual moisture content at the VFBc stage. This is as expected given the design and flows of the four-stage spray dryer.

Fig. 2.10 shows the step responses of the simulated outputs to the main disturbances of the four-stage spray dryer. These disturbances vary during production and a controller must adjust the inputs to compensate for these disturbances. The ambient air humidity, Y_{amb}, varies due to changing weather conditions and the feed, S_{f} and T_{f}, varies due to variations in the upstream processes. The first row of plots in Fig. 2.10 shows the responses to a 20 g/kg step increase in the ambient air humidity, Y_{amb}, in the SD, SFB and VFBh inlet air streams. The VFBc inlet air is assumed dehumidified as is often the case. The ambient air humidity has a direct effect on the outlet air humidity in the SD stage. The stage temperatures are only marginally affected. The ambient air humidity leads to a significant increase in the residual moisture of the powder in both the SFB stage and the VFBc stage. The second row of plots in Fig. 2.10 illustrates the response to step decreases in the feed solid concentration, S_{f}. This decreases the air temperatures in particularly the SD stage and the SFB stage, increases the SD air humidity and increases the residual moisture content of the powder. The third row of plots in Fig. 2.10 demonstrates that the feed temperature, T_{f}, has an effect on the residual moisture of the powder. It also affects the temperature at the SFB stage, but hardly at the other stages and has only a limited effect on the SD air humidity.

Fig. 2.9 and Fig. 2.10 do not indicate the presence of severe non-linearities. Non-linearities would show as a change in the relative step-change of the resulting simulated outputs or a change in the time to steady-state. The figures on the other hand clearly indicate a highly cross-coupled system model, in which one input has an affect on several simulated outputs. We conclude, based on the simulations and step responses, that the use of linear models can be used to accurately simulate the outputs of the four-stage spray dryer.

2.9 Summary

In this chapter, we developed a simulation and a control model for an MSD$^{\text{TM}}$-20 four-stage spray dryer.

- We introduced the experimental dryer setup and presented an estimation and a validation experiment conducted on the spray dryer. The experiments provide the basis for identification and validation of the models with well excited inputs and disturbances. Laboratory tests were conducted to identify the equilibrium moisture content and stickiness of the powder.
- We presented a first-principles index-1 DAE model, based on mass and energy balance principles, for simulation purposes. The model describes

the evolution of the air temperatures, the air humidity and the powder moisture contents in each state. The model provides simulations that fits the validation data well.

- We developed a lumped ODE model, based on mass and energy balance principles, for design of the controllers. The model describes the evolution of the control relevant outputs only and fits the validation data well. Compared to the simulation model this model contains fewer states and parameters, thus simplifying the computational demand and identification complexity.
- We showed that linear models of the spray dryer simulates the outputs well and that the models have strong input-output cross-couplings. A linear control model is also provided based on the lumped ODE model.
- Deposits caused by stickiness of the powder is predicted in both models by the glass-transition temperature.
- The KPIs are computed as part of both models.

Chapter 3

Control Strategies

In the following, we briefly provide an overview of the three control strategies that are investigated in this thesis i.e. the conventional PI control strategy, the MPC with RTO strategy and the E-MPC strategy. In all three control strategies the inputs, u, are kept at their setpoints by low level PI controllers. These are not considered further in this thesis. Fig. 3.1 illustrates the working principles of the high-level controllers. Fig. 3.2 illustrates the conceptual control performance of the controlled outputs.

Fig. 3.1(a) illustrates the single input and single output PI control strategy. The PI controller measures and controls the spray dryer temperature, $y = T_{\mathrm{SD}}$, to the target, r, by manipulating the feed flow rate, $u = F_{\mathrm{f}}$. The inlet temperatures, $(T_{\mathrm{main}}, T_{\mathrm{sfb}}, T_{\mathrm{vfbh}})$, are not manipulated in the PI control strategy. Fig. 3.2(a) illustrates that the controlled outputs in the PI control strategy have fixed constraints for relatively long times of operation as the setpoint, r, is only changed manually. Furthermore, the PI control strategy has a relative large output variance such that the required back-off from the constraint is larger than for the advanced process control strategies (MPC with RTO and E-MPC). As a consequence the uncontrolled outputs, i.e. the residual moisture content and stickiness of the powder, have a large variance and the profit of operation is as a consequence significantly decreased most of time.

Fig. 3.1(b) illustrates that the MPC with RTO is a two layer optimization

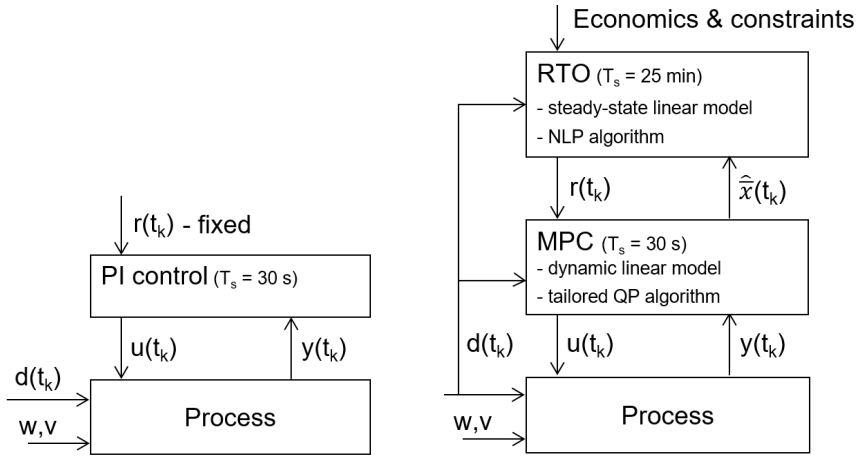

(a) PI control

(b) MPC with RTO

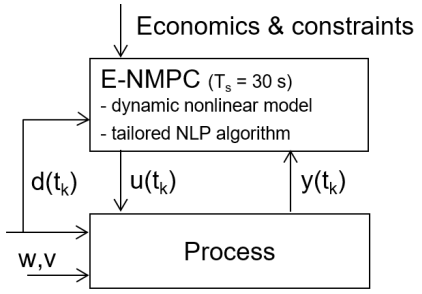

(c) E-MPC

Figure 3.1: Illustration of the working principle of the three control strategies.

based controller. Using the measured disturbances, d, the estimated states, $\hat{\hat{x}}$, the operating profit function, the constraints, and a steady-state linear model, the RTO layer computes the optimal setpoints, r, for the ouputs, z, by solving a steady-state optimization problem. The MPC layer in the MPC with RTO solves a weighted and regularized least-squares problem with constraints using a dynamic linear model. The MPC is based on feedback from the measurement, y, and feed-forward from the measured disturbances, d. The MPC brings the controlled outputs, z, to the target, r, by manipulating, u. As illustrated in Fig. 3.2(b), the RTO adjusts the setpoints including the corresponding back-off to the variations in the disturbances. The back-off of the MPC with RTO is smaller than the back-off of the PI control strategy due to better regulation by the MPC. We apply an explicit iterative optimization method with bias update adaptation in the RTO layer to determine the setpoints [FCB15]. The economic

value of the MPC with RTO stems from the adjustment of setpoints to the actual disturbances and less back-off as a consequence of better regulation with less output variance.

Fig. 3.1(c) illustrates that the E-MPC is a one layer optimization based controller. Based on the measurements, y, the measured disturbances, d, the profit function, the constraints, and a nonlinear model, the E-MPC computes the inputs, u, at each sample time to maximize the predicted profit of operation. Fig. 3.2(c) shows that E-MPC does not compute targets directly, but maximizes operating profits subject to constraints. This implies that the optimal controlled outputs corresponding to the optimal inputs, u, are adjusted and predicted at each sample time. The back-off in E-MPC may be implemented directly or by solving stochastic versions of E-MPC using soft constraints with penalty functions representing the economic cost of violating a constraint. In this thesis, we used a certainty-equivalence E-MPC and did not explicitly consider back-off from the constraints.

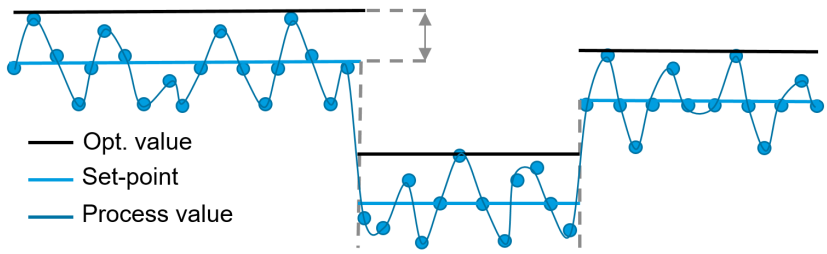

(a) PI control

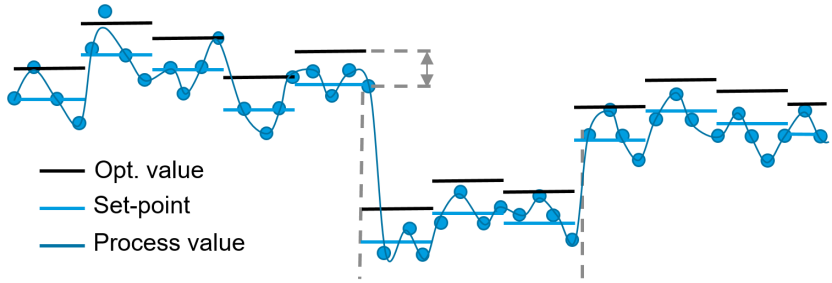

(b) MPC with RTO

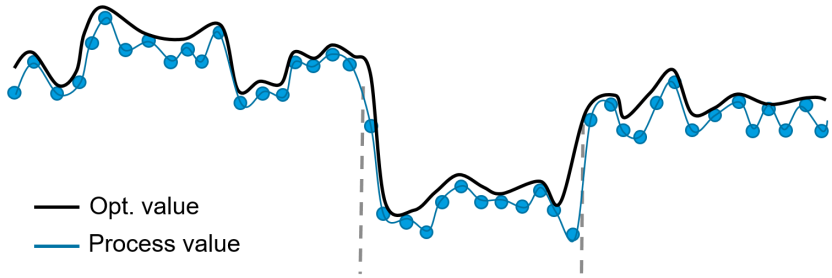

(c) E-MPC

Figure 3.2: The sketches illustrates the control of the outputs, the corresponding setpoints (if relevant), r, and the corresponding constraints for the three controllers.

Chapter 4

Proportional and integral (PI) Control

In the following, we briefly present the conventional PI control strategy for control of the four-stage spray dryer. This control method is the reference to which we compare the performance of the MPC strategies. The PI control strategy is the standard control method used in the spray drying industry.

4.1 Control principles of PI Control

Proportional and integral (PI) control offer a simple solution to steer a controlled value to a target and reject disturbances. It counteracts the measured error by a proportional gain and ensures offset-free tracking by integral action.

In the conventional PI control strategy, a number of low level PI controllers keep the inlet temperatures constant during operation. These low level PI controllers maintain the main inlet air temperature, the SFB inlet air temperature, and the VFB inlet air temperature at a fixed setpoint by adjusting the power of the heaters for the respective inlet air streams. The main controller in the PI control strategy is a high level PI controller that controls the chamber exhaust air temperature, T_{SD}, to a fixed target, T_{sp}, by manipulating the feed flow rate,

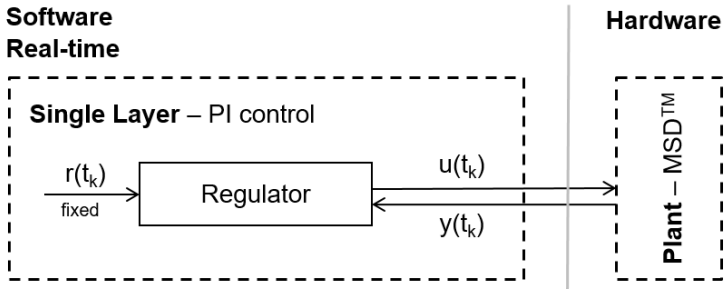

Figure 4.1: Illustration of the PI control strategy.

F_{f}. The inlet air temperatures are controlled constant at T_{main}, T_{sfb} and T_{vfbh}. The main disturbances are the absolute ambient air humidity, Y_{amb}, the feed solids concentration, S_{f}, and the feed temperature, T_{f}. No feed-forward of the disturbances are needed as the exhaust air temperature is tracking the setpoint well.

The measurement and output vector, y, and the input vector, u, are

$$y = T_{\mathrm{SD}} \qquad u = F_{\mathrm{f}} \tag{4.1}$$

Fig. 4.1 illustrates the PI control strategy for control of the exhaust air temperature and Fig. 2.1 provides an overview of the spray dryer, the symbols and the naming convention.

The PI control strategy is simple, but does not control the residual moisture and does not control the stickiness of the powder in the chamber. This implies that the residual moisture cannot be guaranteed to satisfy the quality constraints and that deposits may form on the chamber walls due to sticky powder inside the dryer. The additional inputs and outputs of the dryer that are related to control of these properties are highly cross-coupled and long process delays may be present. These features make it difficult to optimally operate the spray dryer using additional PI controllers. The cross-coupled dynamics also makes the process difficult to operate under the current PI control strategy for the operator. The operators therefore tend to fix the exhaust air temperature target at a high level, resulting in extensively dried powder, to meet the residual moisture constraint and avoid stickiness of the powder at all time. Thus, the energy consumption is increased, the energy efficiency is decreased and the powder residual moisture content is often very low.

Algorithm 1 PI Algorithm

Require: y_k, r_k, I_k
$e_k = r_k - y_k$
$u_k = K_c e_k + I_k$
$u_k = \min(u_{\max}, \max(u_{\min}, u_k))$
$I_{k+1} = I_k + (T_s K_c/\tau_c)\, e_k$
return u_k, I_{k+1}

4.2 Regulator

The main challenge in using PI control is tuning of the gain and integral time. We used the SIMC tuning method with good results [Sko03]. Using input-output data of the simulation model in Section 2.4, we approximate the transfer function from F_f to T_SD with the first order model

$$Y(s) = \frac{K_\mathrm{p}}{\tau_\mathrm{p} s + 1} U(s) \tag{4.2}$$

$K_\mathrm{p} = -0.35$ °C/(kg/h) and $\tau_\mathrm{p} = 122$ s. In continuous-time the PI control law is

$$U(s) = K_c \frac{\tau_c s + 1}{\tau_c s} \left(R(s) - Y(s)\right) \tag{4.3}$$

Aiming for at closed-loop time constant of $\tau_{cl} = 50$ s we get the following PI control parameters using the SIMC tuning rule: $K_\mathrm{c} = (1/K_\mathrm{p})\tau_\mathrm{p}/\tau_\mathrm{cl} = -6.97$ (kg/h)/°C and $\tau_\mathrm{c} = \min\{\tau_\mathrm{p}, 4\tau_\mathrm{cl}\} = 122$ s.

Algorithm 1 transforms the continuous-time PI controller (4.3) to a discrete time PI controller using the explicit Euler method [ÅH06, Årz12]. The implementation outlined in Algorithm 1 provides bumpless parameter changes and handles control signal saturation. Bumpless transfer between manual and automatic mode is obtained by setting $I_0 = u_0 - K_c(r_0 - y_0)$ when the PI controller is switched on to automatic mode. In the implementation we do not consider anti-windup nor setpoint weighting. For the PI control strategy we use a sample time of $T_\mathrm{s} = 30$ s, $u_{\min} = 0$ kg/hr and $u_{\max} = 140$ kg/hr.

4.3 Closed-loop Simulation

The performance of the PI control strategy has been investigated by a closed-loop simulation. The simulation model presented in Section 2.4 is used with the

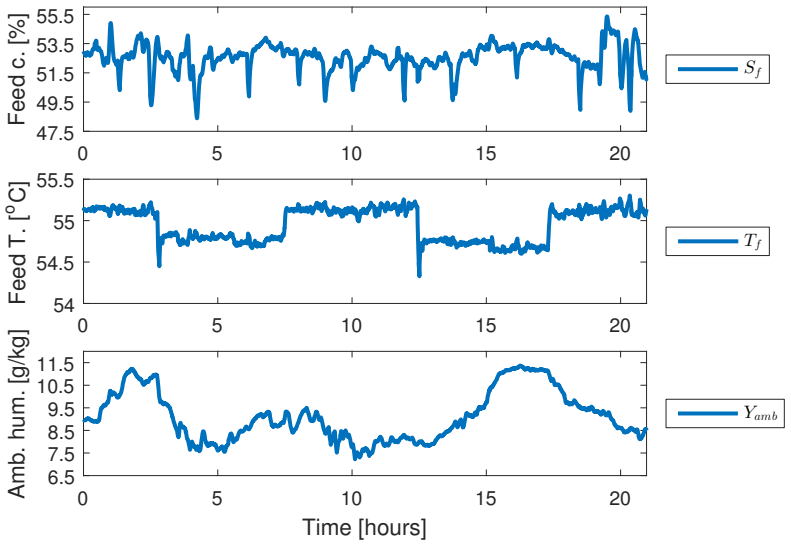

Figure 4.2: Industrially recorded disturbance scenario.

above PI controller fitted to control the exhaust air temperature, T_{SD}, to the target, T_{sp}, using the feed flow rate, F_{f}.

We use an industrially recorded disturbance scenario in order to produce realistic simulations and concluding performance measures. The three control strategies in this thesis are compared using the same disturbance scenario shown in Fig. 4.2. The feed solids concentration, S_{f}, the feed temperature, T_{f}, and the ambient air humidity, Y_{amb}, are recorded disturbances from a larger dairy spray dryer. The feed solids concentration, S_{f}, have a relatively large variance where as the feed temperature, T_{f}, is well controlled compared to other dryers. The ambient air humidity, Y_{amb}, resembles the variations from a normal humid summer day. The disturbances, F_{main}, F_{sfb}, F_{vfbh}, F_{vfbc}, T_{vfbc} and T_{amb} are constant.

Fig. 4.3 shows the measured outputs, the target and the inputs of the closed-loop simulation. The simulation shows that the PI controller is able to maintain a stable exhaust air temperature, T_{SD}, and avoids violation of the stickiness constraint, i.e. the glass transition temperature. Notice the mismatch between the stickiness constraint predicted by the simulation model, T_g^{SD}, and the control model, $\bar{T}_g^{\mathrm{SD}}$. By design, $\bar{T}_g^{\mathrm{SD}}$, which we use for control purposes is conservatively made compared to T_g^{SD} at all time. The exhaust air humidity, Y_{ab}, and the residual moisture content, S_{cd}, are not controlled and fluctuates according to the disturbances. With the conventional PI control methodology no correcting action is made, because the ambient air humidity, affects the air humidity,

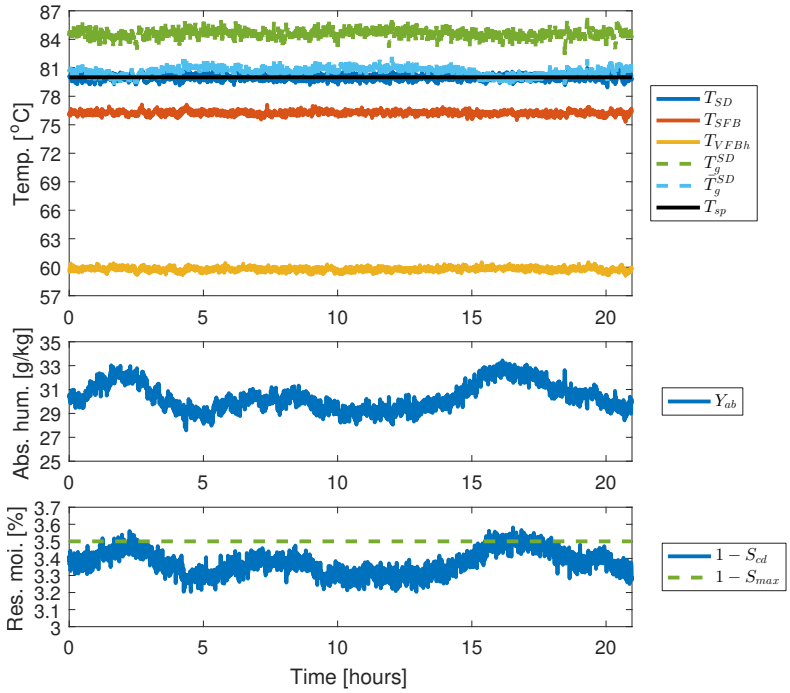

(a) Measured output variables and target.

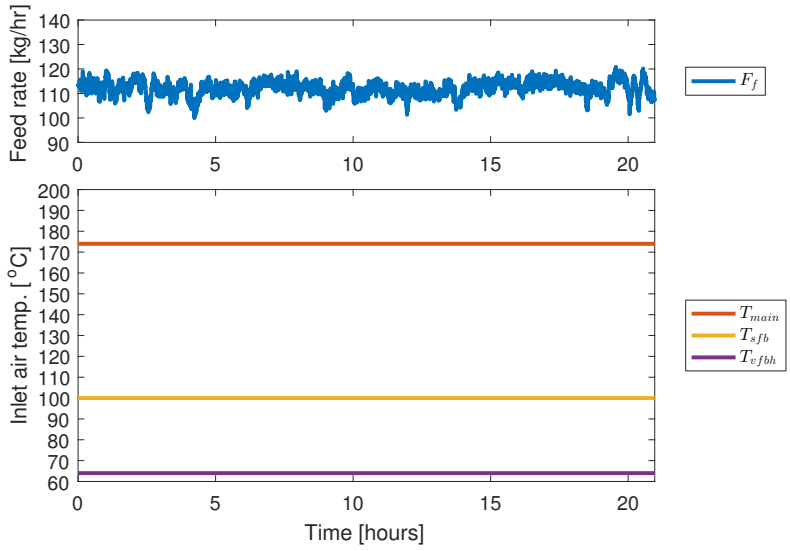

(b) Input variables.

Figure 4.3: Simulation of the PI control strategy subject to the disturbance scenario given in Fig. 4.2.

Table 4.1: Average KPIs for the PI controller.

KPIs	Unit	PI
Product flow rate	F_{p}	60.95 kg/hr
Energy consumption	Q_{tot}	87.2 kW
Specific energy consum.	$\frac{Q_{\mathrm{tot}}}{F_{\mathrm{p}}}$	5.16 MJ/kg
Residual moisture	$1 - S$	3.37 %
Energy efficiency	η	40.2 %
Profit of operation	p	123.25 €/hr

Y_{ab} and the residual moisture content, S_{cd}, not the exhaust air temperature. Changes in the feed concentration, S_{f}, is better handled as the amount of water entering the chamber directly affects the exhaust air temperature, T_{SD}. The exhaust air temperature is largely dictated by the evaporation rate, and the controller basically maintains a fixed rate of evaporation. The variations in S_{cd} and Y_{ab} require on average the dryer to dry the powder more than necessary to keep the powder moisture content below the maximum limit and avoid violation of the stickiness constraint at all time. The powder is therefore dried more extensively, to meet the residual moisture limit, which increases the energy consumption, decreases the energy efficiency and the yield of the production. In typical industrial operation, the operators have no in-line measurement of the exhaust air humidity, Y_{ab}, and the residual moisture content, S_{cd}. Thus, they are running almost in blind and must back-off even further from the process constraints. This again increases the cost of operation.

The target of the high level PI-controller, $T_{\mathrm{sp}} = 80°\mathrm{C}$, and the low level controllers are selected by hand to render the best possible profit of operation. The closed-loop simulation in Fig. 4.3 therefore shows the most optimistic performance that may be achieved by the conventional PI control strategy.

Table 4.1 shows the key performance indicators (KPIs) of the closed-loop simulation presented in Fig. 4.3. The PI controller provides on average a product flow rate at 60.95 kg/hr, an energy consumption of 87.2 kW, a specific energy consumption of 5.16 MJ/kg, a residual moisture content in the powder of 3.37% and an energy efficiency of 40.2%. This is the benchmark for comparison of the following MPC strategies.

4.4 Summary

In this chapter, we described the PI control strategy and performed a closed-loop simulation for benchmark using the simulation model.

- We showed that the chamber exhaust air temperature, T_{SD}, is controlled constant by manipulating the feed flow rate, F_{f}.
- The PI control approach is simple, but insufficient for controlling the residual moisture content and the powder can turn sticky inside the dryer.
- We showed that the variations in S_{cd} and Y_{ab} requires on average the dryer to dry the powder more than necessary to satisfy the residual moisture specifications and stickiness constraint at all time.
- The average KPIs provide the best possible performance that can be achieved by the PI control strategy. Industrial practice may be worse.

Chapter 5

Tracking Model Predictive Control with an RTO layer

In this chapter, we present the Model Predictive Control (MPC) algorithm that combines a target tracking MPC and a Real-Time Optimization layer (MPC with RTO), for control of the four-stage spray dryer. The MPC with RTO is based on the linearized control model in Section 2.6. The MPC with RTO manipulate four inputs and control four outputs to a target. The target is adjusted by an RTO layer to provide the best steady-state economic performance within the given process constraints.

The chapter provides a summary of Paper B, Paper E and Paper I.

5.1 Control principles of MPC with RTO

The basic concept of MPC is to solve an optimization problem, incorporating a dynamic model to forecast the model outputs, to produce the best control move at the current time. To do that, an initial state of the model must be estimated based on past recorded measurements [RM09]. The setpoint of the MPC can be manually selected or computed automatically in the RTO layer. Fig. 5.1 illustrates the components of the MPC with RTO algorithm and shows

the signal paths between the hardware, software and the individual software elements.

In the MPC with RTO control strategy we control four outputs by manipulation of four inputs. The outputs are the exhaust and SFB stage air temperatures, T_{SD} and T_{SFB}, the exhaust air humidity, Y_{ab} and the VFBc stage residual moisture content of the powder, S_{cd}. The inputs are the feed flow rate, F_{f}, the main inlet air temperature, T_{main}, the SFB inlet air temperature, T_{sfb}, and the VFBh inlet air temperature, T_{vfbh}. The main disturbances are the ambient air humidity Y_{amb}, the feed solids concentration, S_{f}, and the feed temperature, T_{f}. The selection of these outputs makes it possible to avoid deposits of sticky particles on the spray dryer surfaces, avoid lumps of powder to form in the SFB and control the residual moisture content below and close to the maximum limit. The dryer inlet air temperatures are controlled, as opposed to controlling the inlet air flows, in order to adjust the drying of the powder without compromising the flow patterns of air inside the dryer and fluid beds.

The measurement vector, y, the output vector, z, the input vector, u, and the main disturbance vector, d, are

$$y = \begin{bmatrix} T_{\mathrm{SD}} & T_{\mathrm{SFB}} & Y_{\mathrm{ab}} & T_{\mathrm{VFBh}} & T_{\mathrm{VFBc}} & S_{\mathrm{cd}} \end{bmatrix}^T \tag{5.1a}$$

$$z = \begin{bmatrix} T_{\mathrm{SD}} & T_{\mathrm{SFB}} & Y_{\mathrm{ab}} & S_{\mathrm{cd}} \end{bmatrix}^T \tag{5.1b}$$

$$u = \begin{bmatrix} F_{\mathrm{f}} & T_{\mathrm{main}} & T_{\mathrm{sfb}} & T_{\mathrm{vfbh}} \end{bmatrix}^T \tag{5.1c}$$

$$d = \begin{bmatrix} S_{\mathrm{f}} & T_{\mathrm{f}} & Y_{\mathrm{amb}} \end{bmatrix}^T \tag{5.1d}$$

Fig. 2.1 provides an overview of the spray dryer, the symbols and the naming convention of the outputs, inputs and disturbances.

Algorithm 2 lists the on-line computations in the MPC with RTO algorithm, consisting of a state estimator with a filter and a one-step-ahead predictor step, a regulator and an RTO layer. The sample time is $T_s = 30$ s. The target in the RTO layer is computed every 25 min. At each sample, the state estimator provides the initial state of the dynamic model, which in combination with the model is used in the regulator to compute the future input trajectory. The optimization in the regulator results in a sequence of inputs for a finite horizon (the control and prediction horizon), out of which only the first input is applied to the dryer. This procedure is repeated at each sample instant. The optimization problem has to be implemented efficiently and robustly, as it is repeatedly solved numerically in real-time. The target of the target tracking MPC is computed by the RTO layer and the MPC then steers the dryer to that target. The RTO seeks to optimize the process economics while satisfying the process constraints. In this way, the MPC reduces the variance of the controlled outputs, making it

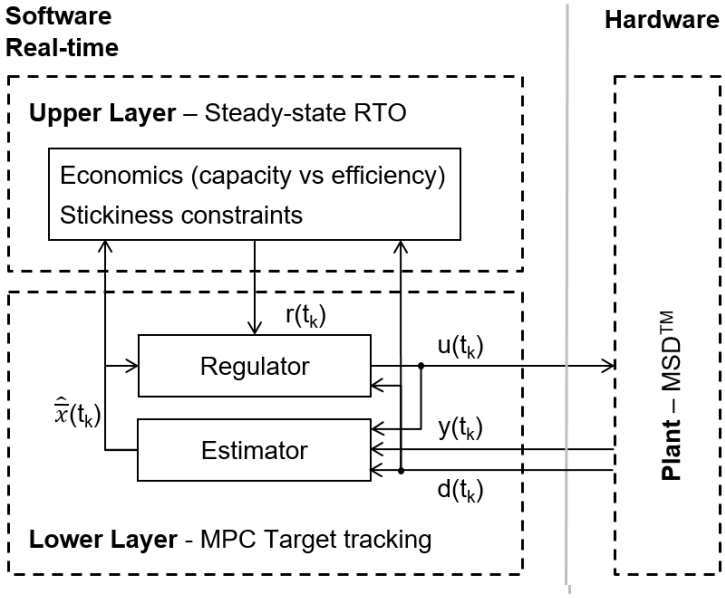

Figure 5.1: Illustration of the MPC with an RTO layer.

possible to squeeze and shift the target, computed in the RTO layer, to a more profitable value.

We use the so-called separation and certainty equivalence principle [Wit71, The57, Mal69] in the formulation of the MPC with RTO. This means that the state estimation and the regulation problem can be decoupled (separated) and that the random variables in the regulation problem can be replaced by the conditional expectations of the costs, predictions of the states, disturbances etc. Thus, the control model simplifies to a deterministic model. The key advantage is that the computational load is significantly reduced compared to for instance a mean-variance approach based on Monte Carlo simulations. The repeated optimization procedure in the MPC provides feedback and form a closed-loop input trajectory. This enables the MPC to counteract model uncertainties, model mismatch and unknown disturbances.

5.2 Linear Model

The linear model, which is used in the state estimator, the regulator and the RTO, is a linearization of the nonlinear control model with reduced complexity

Algorithm 2 MPC with RTO Algorithm

Require: y_k, d_k, $\hat{\bar{x}}_{k|k-1}$, $\bar{P}_{k|k-1}$, u_{k-1}
Filter:
Compute the one-step ahead measurement prediction
$\hat{y}_{k|k-1} = \bar{C}_{\mathrm{y},k}\hat{\bar{x}}_{k|k-1} + \sigma_{\mathrm{y},k}$,
Compute the filtered state
$R_{\mathrm{e},k} = \bar{C}_{\mathrm{y},k}\bar{P}_{k|k-1}\bar{C}_{\mathrm{y},k}^T + R_{\mathrm{v},k}$
$\bar{K}_{\mathrm{fx},k} = \bar{P}_{k|k-1}\bar{C}_{\mathrm{y},k}^T R_{\mathrm{e},k}^{-1}$
$\hat{\bar{x}}_{k|k} = \hat{\bar{x}}_{k|k-1} + \bar{K}_{\mathrm{fx},k}(y_k - \hat{y}_{k|k-1})$
$\bar{P}_{k|k} = \bar{P}_{k|k-1} - \bar{K}_{\mathrm{fx},k}R_{\mathrm{e},k}\bar{K}_{\mathrm{fx},k}^T$
RTO:
$r_k = \rho(\hat{\bar{x}}_{k|k}, d_k, k)$
Regulator:
$u_k = \mu(r_k, \hat{\bar{x}}_{k|k}, u_{k-1}, d_k)$
One-step predictor:
Compute the one-step ahead state, $\hat{\bar{x}}_{k+1|k}$, using
$\hat{\bar{x}}_{k+1|k} = \bar{A}\hat{\bar{x}}_{k|k} + \bar{B}u_k + \bar{E}d_k + \bar{\sigma}_{\mathrm{x}}$
$\bar{P}_{k+1|k} = \bar{A}\bar{P}_{k|k}\bar{A}^T + \bar{G}\bar{R}_{\mathrm{w}}\bar{G}^T$
return u_k, $\hat{\bar{x}}_{k+1|k}$, $\bar{P}_{k+1|k}$

compared to the model used for simulation of the spray dryer. Section 2.5 describes the nonlinear model from which the linear model presented in Section 2.6 in the MPC with RTO is derived. Compared to the simulation model in Section 2.4, the nonlinear model that is used to derive the linear model of the MPC with RTO contains fewer states and parameters. This simplifies the parameter estimation and identification of the model. The model parameters in the complexity reduced model are identified from data produced by the simulation model as outlined in Section 2.4.5 subject to step-inputs. The complexity reduced model is linearized at steady-state and close to the operating point of the controller. The model could as well be identified directly from process or simulation data and with alternative black-box models.

To achieve offset-free output estimation (and control) at steady-state, in the presence of plant/model mismatch and/or un-modeled disturbances, the model is augmented by integrating disturbance states [PR03, PGA15]. In Paper B, Paper E and Paper H we select pure input disturbances, i.e. $C_{\mathrm{d}} = 0$ and B_{d} to subject the energy- and the vapor mass balances to the disturbance integration. In Paper I we select pure output disturbances, i.e. $C_{\mathrm{d}} = I$ and $B_{\mathrm{d}} = 0$.

The augmented linear control model is

$$\bar{x}_{k+1} = \bar{A}\bar{x}_k + \bar{B}u_k + \bar{E}d_k + \bar{G}\bar{w}_k + \bar{\sigma}_{\mathrm{x}} \tag{5.2a}$$

$$y_k = \bar{C}_\mathrm{y}\bar{x}_k + \sigma_\mathrm{y} + v_k \tag{5.2b}$$
$$z_k = \bar{C}_\mathrm{z}\bar{x}_k + \sigma_\mathrm{z} \tag{5.2c}$$

where $\bar{x}_k = [x;\, x_d]_k \in \mathbb{R}^{n_{\bar{x}}}$ is the augmented state vector, $u_k \in \mathbb{R}^{n_u}$ is the inputs, $d_k \in \mathbb{R}^{n_d}$ is the measured disturbances, and $y_k \in \mathbb{R}^{n_y}$ is the measurement vector. The measurement vector may vary in size, because the exhaust air humidity and residual moisture measurements may be lacking for several samples. $z_k \in \mathbb{R}^{n_z}$ is the controlled outputs. The augmented process noise is $\bar{w}_k \sim N_\mathrm{iid}\left(0, \bar{R}_\mathrm{w}\right)$ and the measurement noise is $v_k \sim N_\mathrm{iid}(0, R_\mathrm{v})$. $\bar{G} = I$ is the noise to state matrix. The augmented state-space matrices are

$$\bar{A} = \begin{bmatrix} A & B_\mathrm{d} \\ 0 & I \end{bmatrix} \; \bar{B} = \begin{bmatrix} B \\ 0 \end{bmatrix} \; \bar{E} = \begin{bmatrix} E \\ 0 \end{bmatrix} \; \bar{C}_\mathrm{y} = \begin{bmatrix} C_\mathrm{y} & C_\mathrm{d} \end{bmatrix} \; \bar{C}_\mathrm{z} = \begin{bmatrix} C_\mathrm{z} & C_\mathrm{d} \end{bmatrix} \tag{5.3}$$

$\bar{\sigma}_\mathrm{x}$, σ_y and σ_z contain the constants related to the linearisation of the model, i.e. $\bar{\sigma}_\mathrm{x} = \bar{x}_\mathrm{ss} - \bar{A}\bar{x}_\mathrm{ss} - \bar{B}u_\mathrm{ss} - \bar{E}d_\mathrm{ss}$, $\sigma_\mathrm{y} = y_\mathrm{ss} - \bar{C}_\mathrm{y}\bar{x}_\mathrm{ss}$ and $\sigma_\mathrm{z} = z_\mathrm{ss} - \bar{C}_\mathrm{z}\bar{x}_\mathrm{ss}$. The augmented state vector is $\bar{x}_\mathrm{ss} = [x_\mathrm{ss};\, 0]$. The state-space matrices (A,B,E,C_y) are provided in (2.21). C_z and σ_z are formed by row selection of C_y and σ_y.

5.3 State Estimation

A Linear Time Variant (LTV) Kalman filter is used to estimate the state of the model based on the measurements, y_k, and the inputs, u_k. The measurement, y_k, may vary in size due to missing observations e.g. the residual moisture content in the powder. We use the time variance of the Kalman filter to enable the estimator to handle these missing measurements.

Algorithm 2 provides the state estimator equations. The filtering part corrects $\bar{x}_k$ using the latest measurement, y_k. The filter part enables handling of missing observations by constructing the measurement related properties ($\bar{C}_{\mathrm{y},k}$, $\sigma_{\mathrm{y},k}$, $R_{\mathrm{v},k}$) from ($\bar{C}_\mathrm{y}$, σ_y, R_v) according to the measurement vector, y_k, at sample k. ($\bar{C}_\mathrm{y}$, σ_y, R_v) is the matrices for all possible measurements in (5.2b), while ($\bar{C}_{\mathrm{y},k}$, $\sigma_{\mathrm{y},k}$, $R_{\mathrm{v},k}$) are the matrices corresponding to the actual measurements available at sample k. The filtered state is subsequently used in the regulator as the initial state and in the RTO layer. The predictor part uses the model to predict $\bar{x}_{k+1}$.

5.3.1 Maximum Likelihood (ML) Tuning

The noise variance matrices, $\bar{R}_{\mathrm{w}}$ and R_{v}, are estimated using the Maximum Likelihood (ML) method [KMJ04, JJ07b, JJ07a]. Let $\bar{\theta} = [\bar{\theta}_{\mathrm{w}}; \theta_{\mathrm{v}}]$ be the diagonal elements so $\bar{R}_{\mathrm{w}} = \mathrm{diag}(\bar{\theta}_{\mathrm{w}})$ and $R_{\mathrm{v}} = \mathrm{diag}(\theta_{\mathrm{v}})$. $\bar{R}_{\mathrm{w}}$ and R_{v}, needed for the Kalman filter computations, minimize the negative log likelihood function [JJ07b, JJ07a]

$$V_{\mathrm{ML}}(\bar{\theta}) = \frac{\ln(2\pi)}{2} \sum_{k=1}^{N} n_{y,k} + \frac{1}{2} \sum_{k=1}^{N} \left(\ln[\det(R_{\mathrm{e},k})] + \epsilon_k^T R_{\mathrm{e},k}^{-1} \epsilon_k \right) \tag{5.4}$$

with the innovation, $\epsilon_k = \epsilon_k(\bar{\theta}) = y_k - \hat{y}_{k|k-1}(\bar{\theta})$, and its covariance, $R_{\mathrm{e},k} = R_{\mathrm{e},k}(\bar{\theta})$, computed by Kalman filter iterations i.e. Algorithm 2 without the regulator and RTO computations, using recorded or simulated data. The ML estimate of the variances is determined by solving the nonlinear (nonconvex) optimization problem

$$\min_{\bar{\theta}} V_{\mathrm{ML}}(\bar{\theta}) \tag{5.5a}$$

$$s.t. \;\; \bar{\theta}_l \leq \bar{\theta} \leq \bar{\theta}_u \tag{5.5b}$$

with the lower and upper bounds, $\bar{\theta}_l$ and $\bar{\theta}_u$. Having the optimal $\bar{\theta} = [\bar{\theta}_{\mathrm{w}}; \theta_{\mathrm{v}}]$ provides the noise covariances, $\bar{R}_{\mathrm{w}} = \mathrm{diag}(\bar{\theta}_{\mathrm{w}})$, and $R_{\mathrm{v}} = \mathrm{diag}(\theta_{\mathrm{v}})$.

The model (5.2) and the estimated covariances, $\bar{R}_{\mathrm{w}}$ and R_{v}, enables the computation of the stationary state covariance, $\bar{P}$, of the augmented system by solution of a discrete algebraic Riccati equation. The LTV Kalman filter is initialized using $\bar{P}_{0|-1} = \bar{P}$ and $\hat{\bar{x}}_{0|-1} = \bar{x}_{\mathrm{ss}} = [x_{\mathrm{ss}}; 0]$, where x_{ss} is the steady-state also used for linearization of the model.

Knowledge of the model (5.2), the covariances, $\bar{R}_{\mathrm{w}}$ and R_{v}, and the measurement, y_k, enables the filter to estimate the current states, i.e. computation of $\hat{\bar{x}}_{k|k}$. The filtered state, $\hat{\bar{x}}_{k|k}$, is used by the RTO, the regulator part of the MPC, and the one-step prediction.

The ML method is computational expensive and the solution of (5.5) may not always converge [ORR06, RR09], but the method has shown to provide good results and naturally handles missing observations. The method is explored in Paper B, Paper H and Paper I and showed to estimate $\bar{R}_{\mathrm{w}}$ and R_{v} well.

5.3.2 Autocovariance Least Squares (ALS) Tuning

An alternative method is the correlation technique, Autocovariance Least Squares (ALS) tuning method [ORR06, RR09, ÅJPJ08]. The method has attractive features, as it provides unbiased and positive semi-definite covariance estimates. The computational burden of the method is also minimal even for large dimension systems and shows good convergence properties as well as noise estimation properties [ORR06, RR09]. The method is explored in Paper G and also showed to estimate $\bar{R}_{\mathrm{w}}$ and R_{v} well. The drawback is that the method cannot handle missing observations in a natural way [ORR06, RR09]. Therefore, we mainly focus on the ML tuning method in this thesis.

5.4 Regulator

The regulator tracks the target, r_k, provided by the RTO and rejects measured disturbances, d_k, as well as unmeasured disturbances by solving the regularized output tracking problem with input constraints. This problem may be formulated as the convex quadratic program (QP)

$$\min_{\{u_{k+j}\}_{j=0}^{N-1}} \quad \phi = \frac{1}{2}\sum_{j=1}^{N} \|z_{k+j} - r_k\|_{2,Q_z}^2 + \frac{1}{2}\sum_{j=0}^{N-1} \|\Delta u_{k+j}\|_{2,S_u}^2 \tag{5.6a}$$

$$\text{s.t.} \quad \bar{x}_k = \hat{\bar{x}}_{k|k}, \tag{5.6b}$$

$$\bar{x}_{k+j+1} = \bar{A}\bar{x}_{k+j} + \bar{B}u_{k+j} + \bar{E}d_k + \bar{\sigma}_{\mathrm{x}}, \qquad j \in \mathcal{N}_u \tag{5.6c}$$

$$z_{k+j} = \bar{C}_{\mathrm{z}}\bar{x}_{k+j} + \sigma_{\mathrm{z}}, \qquad j \in \mathcal{N}_z \tag{5.6d}$$

$$u_{\min} \leq u_{k+j} \leq u_{\max}, \qquad j \in \mathcal{N}_u \tag{5.6e}$$

in which $\Delta u_{k+j} = u_{k+j} - u_{k+j-1}$, $\mathcal{N}_z = \{1, 2 \ldots, N\}$ and $\mathcal{N}_u = \{0, 1 \ldots, N-1\}$ [Jør05]. The control and prediction horizons are, $N = 30\ \mathrm{min}/T_s = 60$. N is selected sufficiently long such that any end effects have no influence on the solution in the beginning of the horizon. (5.6c) and (5.6d) are the model constraints where ($\bar{A}$,$\bar{B}$,$\bar{E}$,$\bar{C}_{\mathrm{z}}$) and the offset constants, $\bar{\sigma}_{\mathrm{x}}$ and σ_{z}, are given in (5.2). These constraints provide the model predictions of the augmented model. The estimated current state, $\hat{\bar{x}}_{k|k}$, is assigned to the initial state by (5.6b). The constraint in (5.6e) expresses the input limits. The objective function, (5.6a), is a convex quadratic function and the optimization problem is a convex optimization problem. No forecasts are available for the target, r_k, and the measured disturbances, d_k. Therefore we use the same-as-now predictions in (5.6). The tuning parameters, Q_{z} and S_{u}, are selected by trial and error to obtain an acceptable compromise between robustness and agility. The highest weight is associated to the residual moisture content.

The objective function in (5.6a) penalizes deviations from a target and includes a regularization term on the control input. One may provide targets for both the output variables and the input variables, but such formulations require a separate target calculator to achieve offset-free control [Raw00]. Regularization is important to make the closed-loop trajectory of the controlled process well-behaved [PJ09, HLJB12]. The regularization term may be a linear or quadratic penalty, where quadratic regularization favors smooth solutions [BV04]. In this thesis we only use quadratic regularization.

5.4.1 Optimal Control Problem

The optimal control problem (OCP) in (5.6) is solved by formulating the corresponding boxed constrained QP with dense matrices. We use state elimination and achieve a problem structure similar to the formulations in [Mac02, PJ09, JRH11, HPJJ10, HPJJ12]. State elimination is favorable when the number of states, $n_{\bar{x}}$, is large compared to the number of inputs, n_u, and for relatively short prediction horizons, N [FJ13]. The number of states may be large in our problem due to the potential incorporation of large delays and the Hankel matrix realization of the state-space matrices.

The state, $\bar{x}_k$, in (5.6) is eliminated by repeated substitution of the state predictor in (5.6c) such that

$$\bar{x}_{k+j} = \bar{A}^j \bar{x}_k + \sum_{i=0}^{j-1} \bar{A}^{j-1-i} \bar{B} u_{k+i} + \sum_{i=0}^{j-1} \bar{A}^{j-1-i} \bar{E} d_k + \sum_{i=0}^{j-1} \bar{A}^{j-1-i} \bar{\sigma}_{\mathrm{x}} \tag{5.7}$$

which by (5.6d) results in the output predictions

$$\begin{aligned} z_{k+j} = \bar{C}_{\mathrm{z}} \bar{A}^j \bar{x}_k + \sum_{i=0}^{j-1} \bar{C}_{\mathrm{z}} \bar{A}^{j-1-i} \bar{B} u_{k+i} + \sum_{i=0}^{j-1} \bar{C}_{\mathrm{z}} \bar{A}^{j-1-i} \bar{E} d_k \\ + \sum_{i=0}^{j-1} \bar{C}_{\mathrm{z}} \bar{A}^{j-1-i} \bar{\sigma}_{\mathrm{x}} + \sigma_{\mathrm{z}} \end{aligned} \tag{5.8}$$

The integrating disturbance states are fixed during the prediction horizon. Recall, that the augmented state vector is $\bar{x}_k = [x_k; x_{d,k}]$ and the augmented

system in (5.3), then the state predictor can be rewritten as

$$\begin{aligned} z_{k+j} &= C_{\mathrm{z}}A^{j}x_k + \sum_{i=0}^{j-1} C_{\mathrm{z}}A^{j-1-i}Bu_{k+i} + \sum_{i=0}^{j-1} C_{\mathrm{z}}A^{j-1-i}Ed_k \\ &\qquad + \sum_{i=0}^{j-1} C_{\mathrm{z}}A^{j-1-i}\left(\sigma_{\mathrm{x}} + B_{\mathrm{d}}x_{d,k}\right) + \left(\sigma_{\mathrm{z}} + C_{\mathrm{d}}x_{d,k}\right) \end{aligned} \tag{5.9}$$

$$\begin{aligned} &= C_{\mathrm{z}}A^{j}x_k + \sum_{i=0}^{j-1} H_{u,i}u_{k+i} + \sum_{i=0}^{j-1} H_{d,i}d_k + \\ &\qquad \sum_{i=0}^{j-1} H_{\sigma,i}\left(\sigma_{\mathrm{x}} + B_{\mathrm{d}}x_{d,k}\right) + \left(\sigma_{\mathrm{z}} + C_{\mathrm{d}}x_{d,k}\right) \end{aligned} \tag{5.10}$$

where $H_{u,i} = C_{\mathrm{z}}A^{j-1-i}B$, $H_{d,i} = C_{\mathrm{z}}A^{j-1-i}E$ and $H_{\sigma,i} = C_{\mathrm{z}}A^{j-1-i}$. (5.10) is an affine function which only depend on the initial state, $\bar{x}_k = \hat{\bar{x}}_{k|k}$, the input, u_{k+i}, and the disturbance, d_k.

Define the vectors Z, R, U and D as

$$Z_k = \begin{bmatrix} z_{k+1} \\ z_{k+2} \\ \vdots \\ z_{k+N} \end{bmatrix} \qquad R_k = \begin{bmatrix} r_k \\ r_k \\ \vdots \\ r_k \end{bmatrix} \qquad U_k = \begin{bmatrix} u_k \\ u_{k+1} \\ \vdots \\ u_{k+N-1} \end{bmatrix} \qquad D_k = \begin{bmatrix} d_k \\ d_k \\ \vdots \\ d_k \end{bmatrix}$$

Then the predictions, (5.10), in vector-matrix notation are

$$Z_k = \Phi_x x_k + \Gamma_u U_k + \Gamma_d D_k + \Omega\Sigma_x + \Sigma_z$$

Using the predictions in vector-matrix notation we can write the objective function as

$$\begin{aligned} \phi &= \frac{1}{2}\sum_{j=1}^{N} \|z_{k+j} - r_k\|_{Q_z}^2 + \frac{1}{2}\sum_{j=0}^{N-1} \|\Delta u_{k+j}\|_{S_u}^2 \\ &= \frac{1}{2}\|Z_k - R_k\|_{\mathcal{Q}_z}^2 + \frac{1}{2}\|U_k - U_{k-1}\|_{\mathcal{S}_u}^2 \\ &= \frac{1}{2}\|\Gamma_u U_k - (R_k + b)\|_{\mathcal{Q}_z}^2 + \frac{1}{2}\|\Lambda U_k - I_0 u_{k-1}\|_{\mathcal{S}_u}^2 \\ &= \frac{1}{2}U_k^T H U_k + g^T U_k + \rho \end{aligned}$$

where

$$
\begin{aligned}
H &= \Gamma_u^T \mathcal{Q}_z \Gamma_u + \Lambda^T \mathcal{S}_u \Lambda \\
g &= -\Gamma_u^T \mathcal{Q}_z \left(R_k - b\right) - \Lambda^T \mathcal{S}_u I_0 u_{k-1} \\
\rho &= \frac{1}{2}\| - b - R_k\|_{\mathcal{Q}_z}^2 + \frac{1}{2}\|I_0 u_{k-1}\|_{S_u}^2 \\
b &= -\Phi_x x_k - \Gamma_d D_k - \Omega \Sigma_x - \Sigma_z
\end{aligned}
$$

and the matrices; $\mathcal{Q}_z = \texttt{diag}(Q_z, ..., Q_z)$, $\mathcal{S}_u = \texttt{diag}(S_u, ..., S_u)$

$$
\Phi_x = \begin{bmatrix} C_z A \\ C_z A^2 \\ \vdots \\ C_z A^N \end{bmatrix} \qquad
\Gamma_u = \begin{bmatrix} H_{u,1} & & & \\ H_{u,2} & H_{u,1} & & \\ \vdots & \vdots & \ddots & \\ H_{u,N} & \cdots & H_{u,2} & H_{u,1} \end{bmatrix}
$$

$$
\Gamma_d = \begin{bmatrix} H_{d,1} & & & \\ H_{d,2} & H_{d,1} & & \\ \vdots & \vdots & \ddots & \\ H_{d,N} & \cdots & H_{d,2} & H_{d,1} \end{bmatrix} \qquad
\Omega = \begin{bmatrix} H_{\sigma,1} & & & \\ H_{\sigma,2} & H_{\sigma,1} & & \\ \vdots & \vdots & \ddots & \\ H_{\sigma,N} & \cdots & H_{\sigma,2} & H_{\sigma,1} \end{bmatrix}
$$

$$
\Lambda = \begin{bmatrix} I & & & \\ -I & I & & \\ & \ddots & \ddots & \\ & & -I & I \end{bmatrix} \quad
I_0 = \begin{bmatrix} I \\ 0 \\ \vdots \\ 0 \end{bmatrix} \quad
\Sigma_x = \begin{bmatrix} \sigma_x + B_d x_{d,k} \\ \sigma_x + B_d x_{d,k} \\ \vdots \\ \sigma_x + B_d x_{d,k} \end{bmatrix} \quad
\Sigma_z = \begin{bmatrix} \sigma_z + C_d x_{d,k} \\ \sigma_z + C_d x_{d,k} \\ \vdots \\ \sigma_z + C_d x_{d,k} \end{bmatrix}
$$

$H_{u,i}$ and $H_{d,i}$ are the impulse response matrices. The terms originating from $i = 0$ are neglected, as there are no direct terms in the predictors [Mac02].

The constraints are assumed constant over the prediction horizon and $u_{min} \leq u_{k+j} \leq u_{max}$ may be written as

$$
U_{\min} \leq U_k \leq U_{\max}
$$

where $U_{\min} = \begin{bmatrix} (u_{\min})^T & \dots & (u_{\min})^T \end{bmatrix}^T$ and $U_{\max} = \begin{bmatrix} (u_{\max})^T & \dots & (u_{\max})^T \end{bmatrix}^T$.

We solve the tracking problem by solution to the following QP.

$$
\min_{U_k} \quad \frac{1}{2} U_k^T H U_k + g^T U_k + \rho \tag{5.11a}
$$

$$
\text{s.t.} \quad U_{\min} \leq U_k \leq U_{\max} \tag{5.11b}
$$

Given the solution, $U_k^* = \begin{bmatrix} (u_k^*)^T & (u_{k+1}^*)^T & \dots & (u_{k+N-1}^*)^T \end{bmatrix}^T$, the regulator only apply the first u_k^* to the process. The open-loop optimization is repeated at the next sample where it utilizes the new state estimate, $\hat{\hat{x}}_{k|k}$.

5.4.2 Optimization Methods

Many methods exists for solving the QP related to the control problem in (5.11). The best choice of solver highly depends on the structure of the problem and the accuracy requirements. The QP may be solved using algorithms such as active-set methods [BB06, FKP$^+$14, JRJ04], interior-point methods [RWR98, NW06, BV04, ESJ09, Wri97, WB10, FSD13] and first-order gradient methods [Nes09, CSZ$^+$12, RJM09]. Active-set methods updates the working set of the active constraints until convergence is reached. These methods can be fast when the working set does not change much. Interior-point methods reaches the solution by traversing the interior of the feasible region. Interior-point methods produce high-accuracy solutions using a few, but relatively computationally expensive iterations. The solution is less depended on the starting point (which is also allowed to be infeasible) and the number of active constraints. First-order gradient methods have proven fast for large-scale distributed MPC problems with dynamically coupled systems. These methods have slow convergence rates compared to high order methods, but are favorable for less accurate solutions and scales very well for large problems.

Warm starting of the solvers, i.e. re-using previous solutions, and early termination, i.e. stopping the optimization algorithm at less accurate solutions, can be used to speed up the solution time significantly [SSF$^+$13, Sta15].

We use a primal-dual interior-point QP-solver for solution of (5.11) based on Mehrotra's predictor-corrector algorithm [NW06,BV04] tailored to the QP structure [ESJ09, JRJ04]. Warm starting is used. The QP-solver reduces the computation time considerably compared to general purpose QP-solvers.

The solution of (5.11) is defined by the function

$$u_k = \mu(r_k, \hat{\hat{x}}_{k|k}, u_{k-1}, d_k) \tag{5.12}$$

in which u_k is the first u_k^* of U_k^*. The function defines the on-line computations of the regulator, provided in Algorithm 3, and used in Algorithm 2.

5.5 Steady-state Real-Time Optimization

The steady-state Real-Time Optimization (RTO) layer determines the target that optimizes the cost of operation subject to the process constraints and conditions such as feed compositions, production rates, energy availability, feed and product prices [FCB15, Eng07, DNJN11, AO10, AG10]. The RTO is based on the

Algorithm 3 Regulator Algorithm, $\mu(\cdot)$

Require: r_k, $\hat{\hat{x}}_{k|k}$, u_{k-1}, d_k
Calculate g:
$R_k = \{r_k\}_{i=1}^{N}$, $D_k = \{d_k\}_{i=0}^{N-1}$
$[x_k; x_{d,k}] = \hat{\hat{x}}_{k|k}$
$\Sigma_x = [\sigma_x + B_{\mathrm{d}} x_{d,k};\ \ldots\ ; \sigma_x + B_{\mathrm{d}} x_{d,k}]$
$\Sigma_z = [\sigma_z + C_{\mathrm{d}} x_{d,k};\ \ldots\ ; \sigma_z + C_{\mathrm{d}} x_{d,k}]$
$b = -\Phi_x x_k - \Gamma_d D_k - \Omega\Sigma_x - \Sigma_z$
$g = -\Gamma_u^T \mathcal{Q}_z (R_k - b) - \Lambda^T \mathcal{S}_u I_0 u_{k-1}$
Solve QP:
u_k= QPSolver(H,g,$U_{\min}$,$U_{\max}$)
return u_k

assumption that the process and the disturbance transients can be neglected as the process under control will reach and maintain steady-state operation.

Various RTO methods exist for on-line optimization of the process economics. Implicit RTO methods e.g. the extremum-seeking control method, may be applied. But the slow process transients and long process delays in spray drying may lead to a slow propagation towards the optimal residual moisture content. We apply an explicit iterative optimization method with bias update adaptation [FCB15] in the RTO layer, see Fig. 1.7. This method is effective as the same linear and fixed state-space model in the MPC can be used in the RTO. The adaptation of correction terms are performed by the state estimator. Fig. 5.2 illustrates how model uncertainties are mitigated by the adaption of correction terms. The process profit function and the constraints are measurable from the outputs, inputs and disturbances of the process providing a good estimate of the optimum. Optimum mismatch will still be present due to measurement errors and unknown disturbances, i.e. the optimum is only an estimate. The driving force of the RTO is then to minimize the difference between the predicted and the measured profit function. The explicit method can be fast as it can estimate the steady-state of the process from the model. The MPC with RTO two-layer structure has some inherent drawbacks. The adaptation of the operating conditions is slow as the optimization is only performed intermittently at a low sampling rate [Eng07]. Furthermore, the RTO layer assumes that the closed-loop process will reach a steady-state. Transients, such as target transitions and the inherent effect of disturbances, may thus lead to loss of economical efficiency.

The RTO solves the steady-state economic optimization problem

$$\min_{u_{\mathrm{ss}}, z_{\mathrm{ss}}, s} \quad \phi_{\mathrm{ss}} = -p(z_{\mathrm{ss}}, u_{\mathrm{ss}}, d_k) + \phi_s(s) \tag{5.13a}$$

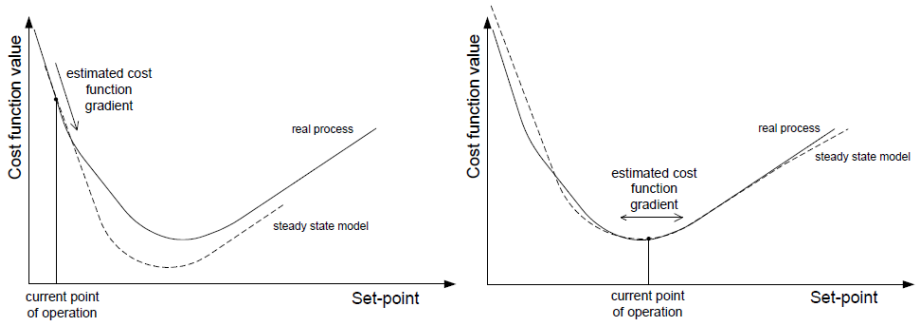

Figure 5.2: The left figure shows a situation with model mismatch. The right figure shows the optimum is reached and the offset between the real process and the model is corrected [Lar06].

$$\text{s.t.} \qquad [0\ I]\bar{x}_{\text{ss}} = [0\ I]\hat{\bar{x}}_{k|k} \tag{5.13b}$$

$$\bar{x}_{\text{ss}} = \bar{A}\bar{x}_{\text{ss}} + \bar{B}u_{\text{ss}} + \bar{E}d_k + \bar{\sigma}_{\text{x}} \tag{5.13c}$$

$$z_{\text{ss}} = \bar{C}_{\text{z}}\bar{x}_{\text{ss}} + \sigma_{\text{z}} \tag{5.13d}$$

$$u_{\min} + \delta_u \leq u_{\text{ss}} \leq u_{\max} - \delta_u \tag{5.13e}$$

$$c(z_{\text{ss}}) - \delta_z + s \geq 0 \tag{5.13f}$$

$$s \geq 0 \tag{5.13g}$$

The target is set to the optimal controlled output value, $r_k = z_{ss}$, when (5.13) is solved. At the samples between the 25 minutes execution, (5.13) is not solved and the target is set to the previous target, $r_k = r_{k-1}$. We denote this function for the RTO by $r_k = \rho(\hat{\bar{x}}_{k|k}, d_k, k)$.

The objective function, ϕ_{ss}, is the sum of the profit function, $p(z_{\text{ss}}, u_{\text{ss}}, d_k)$, and a penalty function, $\phi_s(s)$, that penalizes violations of the output constraints. The profit function, $p(z_{\text{ss}}, u_{\text{ss}}, d_k)$, is provided in Section 2.5.3. The penalty function, $\phi_s(s)$, is an $\ell_2 - \ell_1$-penalty function defined as

$$\phi_s(s) = \frac{1}{2}\|s\|^2_{2,S_W} + \|s\|_{1,s_w} \tag{5.14}$$

This penalty function is used to treat the output constraints (5.13f) as soft constraints [MRRS00]. The soft ℓ_1 penalty is s_w and the soft ℓ_2 penalty is $S_W = \text{diag}(s_w)$. s_w is selected sufficiently large to avoid violation of the constraints in general.

The integrating disturbance states, $x_{d,k} = [0\ I]\hat{\bar{x}}_{k|k}$, are fixed to their current values by (5.13b). These are not necessarily steady-state values. The linear

model (5.2) is used in the constraints (5.13c)-(5.13d) to determine the steady-state relation between the inputs, u_{ss}, and the controlled outputs, z_{ss}. The linear model (5.2) is used in the RTO for the spray dryer as the nonlinear effects are mostly related to the output constraints. Note, that the model cannot and do not contain pure integrators, as the steady-state computation implies the inversion $(I - A)^{-1}$. The nonlinear process constraints, $c(z_{\text{ss}})$, given in Section 2.5.4, contains the stickiness constraints of the powder and the operator defined limits on the outputs. $u_{\min}$ and $u_{\max}$ define the process input constraints. Together these constraints provide a region in which safe operation is guaranteed. δ_u contains a 2.5°C back-off in the input temperatures to avoid saturation and loss of controllability. δ_z contains a 0.05 °C back-off in the stickiness constraint and 0.02 % back-off in the residual moisture. δ_z is selected to provide constraint violations that are similar to the E-MPC strategy.

We use a Sequential Quadratic Programming (SQP) method for solution of (5.13). The SQP method is a quasi-Newton implementation with linesearch for step-size selection and BFGS update of the Hessian. In Paper B and H the gradients are computed by a centered finite difference method and in Paper I the gradients are computed analytically. We use the Matlab® function `fmincon` [Mat15] to solve the SQP. This method performs well in terms of efficiency, accuracy and percentage of successful solutions. An optimal solution is reported by the SQP algorithm if the KKT conditions are satisfied to a relative and absolute tolerance of 10^{-12}. In Paper B and H we solve (5.13) with the outputs and states eliminated from the NLP. In Paper I we eliminate only the state. The problem size is relatively small, with 4 inputs and 4 outputs, thus the computational time difference is marginal.

The solution of (5.13) is defined by the function

$$r_k = \psi(\hat{\hat{x}}_{k|k}, d_k, k) \tag{5.15}$$

in which $\hat{\hat{x}}_{k|k}$ is the current state estimate where only the offset states are utilized for model corrections and d_k is the measured disturbances. Algorithm 4 lists the on-line computations of the RTO.

5.6 Closed-loop Simulation

The performance of the MPC with RTO control strategy has been investigated by a closed-loop simulation. Fig. 5.3 shows the measured outputs, the targets and the inputs of the closed-loop simulation. Fig. 4.2 shows the disturbances. The simulation shows that the MPC is able to control the process outputs related to stickiness of the powder, T_{SD} and Y_{ab}, the SFB stage temperature, T_{SFB},

Algorithm 4 RTO Algorithm, $\psi(\cdot)$

Require: $\hat{\bar{x}}_{k|k}$, d_k, k
  Solve NLP:
  $x^* = \text{NLPSolver}(\text{problem}(X_{\text{init}}, d_k, \hat{\bar{x}}_{k|k}))$
  $[u_{ss}, z_{ss}, s] = \text{unpack}(x^*)$
  $r_k = z_{ss}$
  return r_k

Require: $[q, c_{eq}, c_{ineq}]$=problem$(x, d_k, \hat{\bar{x}}_{k|k})$
  $[u, z, s] = \text{unpack}(x)$
  Compute the cost function
  $q = -p(z, u, d_k) + \frac{1}{2} s^T S_W s + s^T s_w$
  Compute the equality constraints
  $x_{d,k} = [0\ I]\hat{\bar{x}}_{k|k}$
  $x_{ss} = (I - A)^{-1}(Bu + Ed_k + B_{\text{d}} x_{d,k} + \sigma_{\text{x}})$
  $z_{ss} = C_{\text{y}} x_{ss} + C_{\text{d}} x_{d,k} + \sigma_{\text{z}}$
  $c_{eq} = z - z_{ss}$
  Compute the inequality constraints
  $c_{ineq} = [c(z) + \delta_z + s \geq 0; s \geq 0; u_{\min} + \delta_u \leq u \leq u_{\max} - \delta_u]$

and the residual moisture content, S_{cd}, to their targets. The effect of the disturbances are rejected by constant adjustments of the inputs. The targets used are generated by the RTO layer. These are feasible and the regulator is tracking these targets well. It turns out, that the economics of drying are optimized by minimizing the exhaust air temperature, T_{SD}, in order to save energy and maximize the exhaust air humidity, Y_{ab}, to increase the product flow rate. The lower limit of T_{SD} and upper limit of Y_{ab} are determined according to the stickiness constraint of the powder. The powder moisture content, S_{cd}, is increased until it reaches its upper limit. The energy consumption is further minimized by shifting the drying from the top of the spray dryer to the more efficient fluid bed stages. Thus, the supply of hot air to the SFB and VFB stages are favored compared to the SD stage. This leads to a high SFB stage temperature that is controlled close to its maximum temperature $T_{\text{SFB}} \leq 75.5°\text{C}$.

The MPC with RTO does not operate at the maximum production rate, at all times. At time t=1 hour to t=2 hour, t=4 hour, t=5 hour, t=7.5 hours and between t=19 hours to t=21 hours, the RTO reduces the production rate. The RTO problem (5.13) contains back-offs in the controlled inputs. The MPC with RTO compensates for the decreased VFB inlet air temperature, T_{vfbh}, by increasing the SFB inlet air temperature, T_{sfb}. Consequently, the SFB stage temperature, T_{SFB}, increases and the upper limit on the SFB stage temperature, $T_{\text{SFB}} \leq 75.5$ °C, becomes active. When the SFB temperature limit is

Table 5.1: Average KPIs for the MPC with RTO controller.

KPIs	Unit	MPC-RTO	% inc. to PI
Product flow rate	F_{p}	66.21 kg/hr	8.63 %
Energy consumption	Q_{tot}	89.1 kW	2.21 %
Specific energy consum.	$\frac{Q_{\mathrm{tot}}}{F_{\mathrm{p}}}$	4.81 MJ/kg	-6.72 %
Residual moisture	$1-S$	3.48 %	3.21 %
Energy efficiency	η	42.7 %	6.06 %
Profit of operation	p	133.98 €/hr	8.71 %

active, the MPC with RTO decreases the production rate as well as the energy supply from the main inlet air and the SFB inlet air, to maintain a stable SFB stage temperature. Simultaneously, the decreased production rate allows the SD temperature, T_{SD}, to be decreased along the stickiness constraint to save energy and increase the energy efficiency.

The glass transition temperature at the SD stage as estimated by the simulation model, $T_{\mathrm{g}}^{\mathrm{SD}}$, and the control model, $\bar{T}_{\mathrm{g}}^{\mathrm{SD}}$, describes whether the powder sticks in the SD stage of the spray dryer. The powder is non-sticky when $T_{\mathrm{SD}} \leq T_{\mathrm{g}}^{\mathrm{SD}}$. Otherwise, the powder is sticky. Due to stochastic disturbances, the SD temperature occasionally violate $\bar{T}_{\mathrm{g}}^{\mathrm{SD}}$. Therefore, the stickiness constraint used by the controller, $\bar{T}_{\mathrm{g}}^{\mathrm{SD}}$, is designed to have a back-off from $T_{\mathrm{g}}^{\mathrm{SD}}$.

All in all, the MPC with RTO strategy maximizes the throughput and the residual moisture content while minimizing the supply of energy from the inlet air. Note that the given process constraints already have back-off incorporated. We therefore allow only to restrict the estimated controlled outputs to stay within the process constraints.

Table 5.1 shows the key performance indicators (KPIs) of the closed-loop simulation presented in Fig. 5.3. Compared to the PI controller, the MPC with RTO provides on average an increased product flow rate of 8.63% and a decreased specific energy consumption of 6.72%. The energy consumption is increased due to the increased product flow rate. The powder moisture content is increased by 3.21% (0.108 p.p.) and the energy efficiency is increased by 6.06% (2.44 p.p.). The profit of operation is improved by 8.71%. Clearly, despite an increase in energy consumption, the MPC with RTO perform better than the conventional PI control.

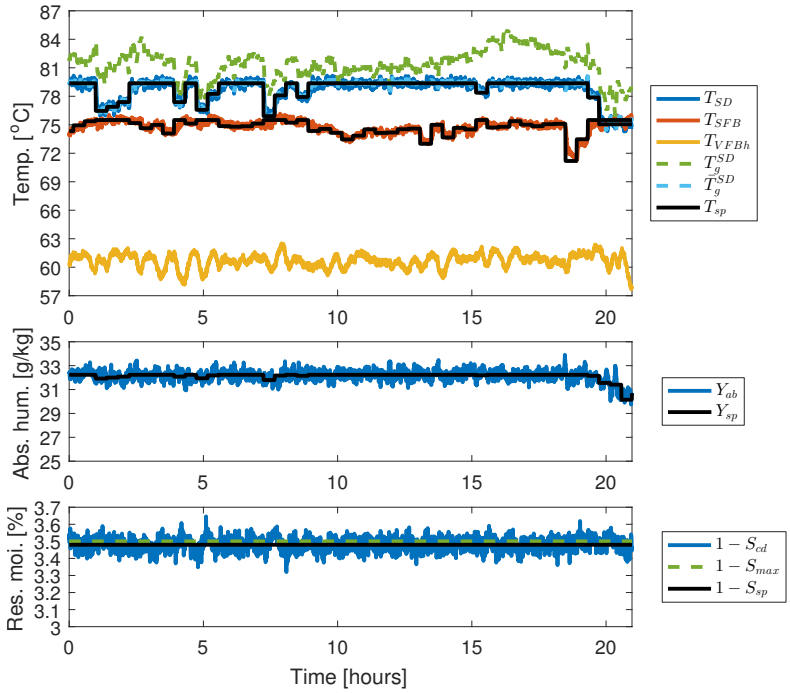

(a) Measured output variables and targets.

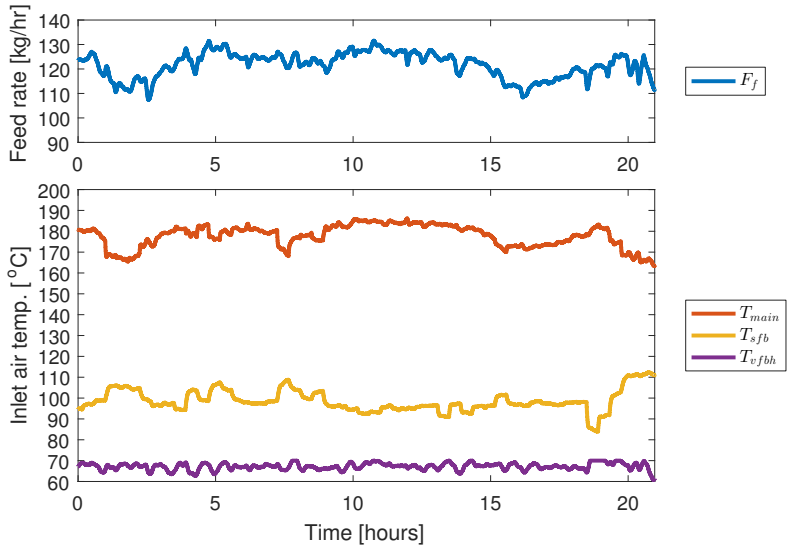

(b) Input variables.

Figure 5.3: Simulation of the MPC with an RTO layer subject to the disturbance scenario given in Fig. 4.2.

5.7 Summary

In this chapter, we described the MPC with RTO control strategy and performed a closed-loop simulation.

- We described the state estimator, the regulator and the RTO layer to form a complete MPC with RTO control strategy applicable for real-time use. Tuning of the state estimator was also presented.
- We showed that the MPC with RTO provides significantly improved control of the residual moisture content compared to the conventional PI control and avoids that the powder sticks to the walls of the chamber.
- Compared to conventional PI control strategy, the product flow rate is improved by 8.63%, the specific energy consumption is decreased by 6.72%, and the powder moisture content is improved by 3.21%.
- The MPC with RTO improves the profit of operation by 8.71%. Thus, the MPC with RTO control strategy perform better than the conventional PI control.

Chapter 6

Economic Model Predictive Control

In this chapter, we present the Economic Model Predictive Control (E-MPC) algorithm, utilizing a nonlinear objective, a nonlinear control model and a constraint function from Section 2.5 for control of the four-stage spray dryer.

The chapter provides a summary of Paper B, Paper F, Paper G and Paper H.

6.1 Control principles of E-MPC

In Chapter 5 we presented the hierarchical approach to economic optimization and control, the MPC with RTO, which is widely applied in the process industries [DNJN11, AO10]. Recently, E-MPC has been found effective within process optimization. In E-MPC the RTO layer is not required for computing targets to the MPC, as the higher-level objective, economics, is directly implemented in the objective function of the MPC.

Fig. 6.1 illustrates the components of the E-MPC and the signal paths between these and the dryer. In the E-MPC control strategy we manipulate the same

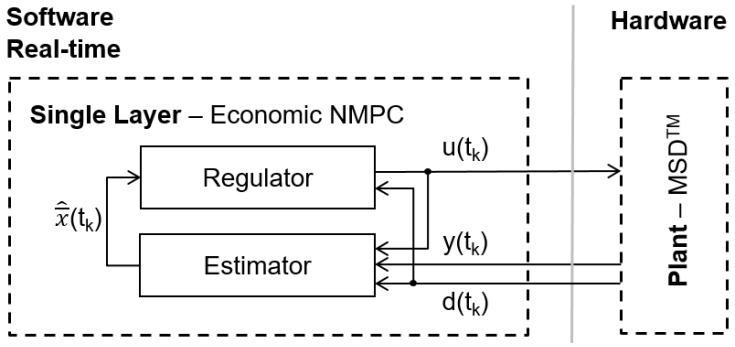

Figure 6.1: Illustration of the E-MPC, that combines a state estimator and a regulator for economic optimization of the dryer operation.

four inputs as in the MPC with RTO strategy based on the same set of measured outputs and disturbances.

The measurement vector, y, the output vector, z, the input vector, u, and the main disturbance vector, d, are

$$y = \begin{bmatrix} T_{\mathrm{SD}} & T_{\mathrm{SFB}} & Y_{\mathrm{ab}} & T_{\mathrm{VFBh}} & T_{\mathrm{VFBc}} & S_{\mathrm{cd}} \end{bmatrix}^T \tag{6.1a}$$

$$z = \begin{bmatrix} T_{\mathrm{SD}} & T_{\mathrm{SFB}} & Y_{\mathrm{ab}} & S_{\mathrm{cd}} \end{bmatrix}^T \tag{6.1b}$$

$$u = \begin{bmatrix} F_{\mathrm{f}} & T_{\mathrm{main}} & T_{\mathrm{sfb}} & T_{\mathrm{vfbh}} \end{bmatrix}^T \tag{6.1c}$$

$$d = \begin{bmatrix} S_{\mathrm{f}} & T_{\mathrm{f}} & Y_{\mathrm{amb}} \end{bmatrix}^T \tag{6.1d}$$

Fig. 2.1 provides an overview of the spray dryer, the symbols and the naming convention of the outputs, inputs and disturbances.

Algorithm 5 lists the on-line computations in the E-MPC algorithm consisting of a regulator and a state estimator. The state estimator consists of a filter and a one-step-ahead predictor step. The sample time is $T_s = 30$ s. As described in Chapter 5, the state estimator provides the initial state of the dynamic model, which in combination with the model is used in the regulator to optimize the future input trajectory. The optimization in the regulator results in a sequence of inputs for a finite horizon, out of which only the first input is applied to the dryer. This procedure is repeated at each sample instant. The repeated optimization procedure provides feedback and form a closed-loop input trajectory. This enables the E-MPC to counteract model uncertainties, model mismatch and unknown disturbances etc.

The discrete-time nonlinear regulator problem may be solved using single-shooting

Algorithm 5 E-MPC Algorithm

Require: y_k, d_k, $\hat{\bar{x}}_{k|k-1}$, $\bar{P}_{k|k-1}$, u_{k-1}
Filter:
Compute the one-step ahead measurement prediction and the output matrix
$\hat{y}_{k|k-1} = \bar{h}_{\mathrm{y}}(\hat{\bar{x}}_{k|k-1}), \quad \bar{C}_{\mathrm{y},k} = \frac{d\bar{h}_y}{d\bar{x}}(\hat{\bar{x}}_{k|k-1})$
Compute the filtered state
$R_{\mathrm{e},k} = \bar{C}_{\mathrm{y},k}\bar{P}_{k|k-1}\bar{C}^T_{\mathrm{y},k} + R_{\mathrm{v,k}}$
$\bar{K}_{\mathrm{fx},k} = \bar{P}_{k|k-1}\bar{C}^T_{\mathrm{y},k}R^{-1}_{\mathrm{e},k}$
$\hat{\bar{x}}_{k|k} = \hat{\bar{x}}_{k|k-1} + \bar{K}_{\mathrm{fx},k}(y_k - \hat{y}_{k|k-1})$
$\bar{P}_{k|k} = \bar{P}_{k|k-1} - \bar{K}_{\mathrm{fx},k}R_{\mathrm{e},k}\bar{K}^T_{\mathrm{fx},k}$
Regulator:
$u_k = \mu(\hat{\bar{x}}_{k|k},\, u_{k-1},\, d_k)$
One-step predictor:
Compute the predicted state, $\hat{\bar{x}}_{k+1|k} = \bar{F}(\hat{\bar{x}}_{k|k}, u_k, d_k)$, and state sensitivity, $\bar{A}_k = \frac{\partial \bar{F}}{\partial \bar{x}}(\hat{\bar{x}}_{k|k}, u_k, d_k)$ using ESDIRK
$[\hat{\bar{x}}_{k+1|k}, \bar{A}_k] = \mathrm{ESDIRK}(t_k, t_{k+1}, \hat{\bar{x}}_{k|k},\, u_k,\, d_k)$
$\bar{P}_{k+1|k} = \bar{A}_k\bar{P}_{k|k}\bar{A}^T_k + \bar{G}\bar{R}_{\mathrm{w}}\bar{G}^T$
return u_k, $\hat{\bar{x}}_{k+1|k}$, $\bar{P}_{k+1|k}$

(control vector parametrization) [SSBM05], multiple-shooting [BP84, CJ12] or the simultaneous method [Bie84]. In this thesis both the single-shooting and the multiple-shooting method are investigated. We use an efficient ODE/DAE solver, the explicit singly diagonally implicit Runge-Kutta (ESDIRK) method, with sensitivity computation capabilities to speed up the computational time. The sensitivity capability also makes the ESDIRK method well suited for the state estimator.

6.2 Model

The E-MPC is based on the complexity reduced nonlinear model in Section 2.5 that is different from the simulation model in Section 2.4. Offset-free estimation of the measurements and offset-free control of the controlled variables at steady-state are achieved by augmenting the model. The state vector, x, is augmented by a vector of integrated disturbance states, x_{d}. The augmented state vector is $\bar{x} = [x; x_{\mathrm{d}}] \in \mathbb{R}^{n_{\bar{x}}}$. The regulator and state estimator are based on the augmented model

$$\bar{x}_{k+1} = \bar{F}(\bar{x}_k, u_k, d_k) + \bar{G}\bar{w}_k \tag{6.2a}$$
$$y_k = \bar{h}_{\mathrm{y}}(\bar{x}_k) + v_k \tag{6.2b}$$

$$z_k = \bar{h}_z(\bar{x}_k) \tag{6.2c}$$

where $u_k \in \mathbb{R}^{n_u}$ is the input vector, $d_k \in \mathbb{R}^{n_d}$ is the measured disturbance vector and $y_k \in \mathbb{R}^{n_y}$ is the measurement vector that may vary in size. $z_k \in \mathbb{R}^{n_z}$ is the outputs.

The operator $\bar{F}(\cdot)$ denotes the state integration of the augmented model, $\bar{x}_{k+1}$, of

$$\bar{x}(t_k) = \bar{x}_k \tag{6.3a}$$

$$\frac{d}{dt}\bar{x}(t) = \bar{f}(\bar{x}(t), u_k, d_k, \theta) \quad t_k \leq t \leq t_{k+1} \tag{6.3b}$$

$$\bar{x}_{k+1} = \bar{x}(t_{k+1}) \tag{6.3c}$$

with

$$\bar{x} = \begin{bmatrix} x \\ x_\mathrm{d} \end{bmatrix} \qquad \bar{f}(\bar{x}, u, d, \theta) = \begin{bmatrix} f(x, u, d, \theta) + B_\mathrm{d} x_\mathrm{d} \\ 0 \end{bmatrix}$$

$\bar{x}_{k+1}$ is computed using the ESDIRK3(4) method with variable step-size. The ESDIRK method is well suited for the EKF, as both the state integration and state sensitivity are utilized in the state estimator [JKTM07]. The augmented output functions are

$$\bar{h}_\mathrm{y}(\bar{x}_k) = h_\mathrm{y}(x_k) + C_\mathrm{d} x_{\mathrm{d},k} \tag{6.4a}$$

$$\bar{h}_\mathrm{z}(\bar{x}_k) = h_\mathrm{z}(x_k) + C_{\mathrm{d,z}} x_{\mathrm{d},k} \tag{6.4b}$$

$\bar{h}_\mathrm{y}(\bar{x}_k)$ is the measured output equations and $\bar{h}_\mathrm{z}(\bar{x}_k)$ is the output equations. $\bar{h}_\mathrm{z}(\bar{x}_k)$ is formed by row selection of $\bar{h}_\mathrm{y}(\bar{x}_k)$. $\bar{G} = I$ is the noise to state matrix, selected such that all states are exposed to state noise. The state and measurement noise covariances are $\bar{w}_k \sim N_\mathrm{iid}(0, \bar{R}_\mathrm{w})$ and $v_k \sim N_\mathrm{iid}(0, R_\mathrm{v})$ and must be estimated. The noise-terms are assumed to be uncorrelated.

6.3 State Estimation

The Extended Kalman Filter (EKF) is used to estimate the state, $\hat{\bar{x}}_{k|k}$, in the augmented nonlinear control model based on the measurements, y_k, and the inputs, u_k. The EKF utilizes many of the same principles as the Kalman filter. However, it linearizes the nonlinear model around the current state estimate at each time step allowing the model to be solved as a Linear Time Varying (LTV) model. The use of the augmented control model ensures offset-free output estimation (and control) at steady-state, in the presence of plant/model mismatch and/or un-modeled disturbances according to [PR03] and [PGA15].

In Paper B, Paper G and Paper H we select pure input disturbances, i.e. $C_d = 0$ and B_d such that the energy- and the vapor mass balances are subject to the disturbance integration.

Algorithm 5 provides the state estimator equations. The filtering part corrects $\hat{\bar{x}}_{k|k}$, using the latest measurement, y_k, after which it is used in the regulator as the initial state. The predictor part uses the model to predict $\hat{\bar{x}}_{k+1|k}$.

Maximum Likelihood (ML) Tuning
The unknown noise variances, $\bar{R}_{\mathrm{w}}$ and R_{v}, are estimated by the Maximum Likelihood (ML) method in the same manner as described in Section 5.3. The likelihood function, $V_{\mathrm{ML}}(\bar{\theta})$ in (5.5) is determined recursively by means of the EKF in Algorithm 5 without the regulator step. $\bar{\theta}$ is $\bar{\theta} = [\bar{\theta}_{\mathrm{w}}; \theta_{\mathrm{v}}]$ and we define the noise covariances $\bar{R}_{\mathrm{w}} = \mathrm{diag}(\bar{\theta}_{\mathrm{w}})$ and $R_{\mathrm{v}} = \mathrm{diag}(\theta_{\mathrm{v}})$.

6.4 Regulator

In a receding horizon manner, the inputs in the E-MPC are obtained by the solution of the following finite dimensional discrete optimal control problem

$$\min_{x,u,s} \ \phi = \phi_{\mathrm{e}} + \phi_{\mathrm{s}} + \phi_{\Delta \mathrm{u}}, \tag{6.5a}$$

$$\text{s.t.} \quad [x_k;\ x_{\mathrm{d},k}] = \hat{\bar{x}}_{k|k}, \quad x(t_k) = x_k, \tag{6.5b}$$

$$\frac{d}{dt}x(t) = f(x(t), u_{k+j}, d_k, \theta) + B_{\mathrm{d}} x_{\mathrm{d},k}, \quad t \in \mathcal{T}_k \tag{6.5c}$$

$$z(t) = h_{\mathrm{z}}(x(t)) + C_{\mathrm{d,z}} x_{\mathrm{d},k}, \quad t \in \mathcal{T}_k \tag{6.5d}$$

$$u_{\min} \leq u_{k+j} \leq u_{\max}, \quad j \in \mathcal{N}_{\mathrm{u}} \tag{6.5e}$$

$$c(z(t_{k+j})) + s_{k+j} \geq 0, \quad j \in \mathcal{N}_{\mathrm{z}} \tag{6.5f}$$

$$s_{k+j} \geq 0, \quad j \in \mathcal{N}_{\mathrm{z}} \tag{6.5g}$$

$x(t)$ is the state vector, u_k is the input vector, d_k is the measured disturbance vector and $s_k \in \mathbb{R}^{n_s}$ is the vector of slack variables related to the soft output constraints. The objective function, ϕ, consists of an economic term

$$\phi_{\mathrm{e}} = -\int_{t_k}^{t_k+T} p(z(t), u_{k+j}, d_k) dt \tag{6.6}$$

measuring the profit of operation, an $\ell_2 - \ell_1$ penalty term

$$\phi_{\mathrm{s}} = \sum_{j=1}^{N} \frac{1}{2} \left\| s_{k+j} \right\|_{2,S_W}^2 + \left\| s_{k+j} \right\|_{1,s_w} \tag{6.7}$$

penalizing violation of the point-wise output constraints, (6.5f), and an input-rate of movement regularization term

$$\phi_{\Delta \mathrm{u}} = \frac{1}{2} \sum_{j=0}^{N-1} \|\Delta u_{k+j}\|^2_{\mathrm{Q}_{\Delta \mathrm{u}}} = \frac{1}{2} \sum_{j=0}^{N-1} \|u_{k+j} - u_{k+j-1}\|^2_{\mathrm{Q}_{\Delta \mathrm{u}}} \tag{6.8}$$

that prevents the optimal profile of inputs from large variations from sample to sample [PJ09, HLJB12]. The profit rate, $p(z(t), u_{k+j}, d_k)$, is identical to the profit rate used by the RTO. p is computed using (2.16a) and the complexity reduced nonlinear model in Section 2.5. The objective function and the nonlinear model dynamics are integrated using the ESDIRK3(4) method as described below. The associated objective and state sensitivities are computed as well by the ESDIRK method. The inputs are parametrized using a piecewise constant function, $u(t) = u_{k+j}$ with $t_{k+j} \leq t < t_{k+j+1},\ j \in \mathcal{N}_u$. The constraints (6.5e) are input constraints and corresponds to (2.5.4). The estimated current state, $\hat{\hat{x}}_{k|k}$, is assigned to the initial state by (6.5b). To avoid violation of the output constraints, while maintaining feasibility of (6.5) at all time, we implement the $\ell_2 - \ell_1$ soft output constraints in (6.5f)-(6.5g) [MRRS00]. The $\ell_2 - \ell_1$ penalty function is the same as for the RTO. The constraint function, $c(z)$, for the output constraints are provided in Section 2.5.4. No forecasts are available for the disturbances, therefore we use the same-as-now forecasts. The sampling time of the E-MPC is $T_\mathrm{s} = 30$ s. The control and prediction horizon is $T = 25$ min leading to $N = T/T_\mathrm{s} = 50$. The horizon is selected such that a steady-state is reach within the horizon and the turnpike property has no effect on the first input. $\mathcal{T}_k = [t_k,\, t_k + T]$ denotes the time interval. $\mathcal{N}_u = \{0, 1, \ldots, N-1\}$ and $\mathcal{N}_\mathrm{z} = \{1, 2, \ldots, N\}$. The solution to (6.5) provides an optimal trajectory, $\{u_{k+j}\}_{j=0}^{N-1}$, of which only the first input, u_k, is implemented on the process.

The ESDIRK3(4) method

The ESDIRK method, based on [KJTJ04, CJ12, Cap13], is used to integrate the model as well as the profit of operation in (6.5a). The method is a special implicit Runge-Kutta method that is computationally efficient for stiff systems, both A- and L-stable, and is implemented with an embedded error estimator [KJTJ04]. The numerical solution of the initial value problem in (6.5) may in each integration step be denoted

$$\phi_{\mathrm{e},j} = -\int_{t_k}^{t_k+T_s} p(z(t), u_{k+j}, d_k)dt = -h_n \sum_{i=1}^{4} b_i p(z(T_i), u_{k+j}, d_k) \tag{6.9}$$

$$\begin{aligned} X_i - h_n\gamma(f(X_i, u_{k+j}, d_k, \theta) + B_\mathrm{d} x_{\mathrm{d},k}) = \\ X_1 + h_n \sum_{j=1}^{i-1} a_{ij}(f(X_j, u_{k+j}, d_k, \theta) + B_\mathrm{d} x_{\mathrm{d},k}) \end{aligned} \tag{6.10}$$

with $i = 2, 3, 4$. $x_{k+j} = X_1$ and X_i denote the state solution at time $T_i =$

$t_n + c_i h_n$ for $i \in \{1, 2, 3, 4\}$. $x_{k+j+1} = X_4$ is the numerical solution at time $t_n + h_n$. a, b, c and γ are the Runge-Kutta Butcher Tableau values. The main computational effort in the ESDIRK method is the solution of the implicit equations (6.10) using a Newton based method. The ESDIRK method also provides sensitivity computation capabilities. The details of the computation of the state and stage cost sensitivities are described in [KJTJ04, CJ12, Cap13]. The scheme has been implemented with variable integration step-size, h_n, with an error accuracy of 10^{-4}. Each integration step-size, h_n, is chosen to be smaller than or equal to the sample time, T_s.

6.4.1 Optimization Methods

The nonlinear optimization problem (NLP) in (6.5) may be solved using a single-shooting, a multiple-shooting or a collocation method. In Paper D, Paper F and Paper G we use the single-shooting method and in Paper B and Paper H we use the multiple-shooting method. We found that the two methods have almost equal execution time for this E-MPC problem. The single-shooting method is advantageous for systems with a relatively large number of states compared to the number of inputs. The method progress towards a solution by iterating between solving the model and solving a reduced size optimization problem. We speed up the computations by computing the gradients by the discrete adjoint method, but many other methods exist. Single-shooting may be costly if evaluation of the problem functions are costly, e.g. if an implicit discretization scheme must be applied. In addition single-shooting lacks robustness when applied to unstable processes [MBF04]. The multiple-shooting method is an alternative and popular choice, as it requires few internal iterations and have good stability properties. Gradients may be constructed directly from the sensitivities given by the ODE/DAE solver. The gradients are highly sparse which must be exploited. Both single-shooting and multiple-shooting methods can use state-of-the-art ODE/DAE solvers [KJTJ04, CJ12, Cap13].

We use the multiple-shooting method with an NLP-solver from IPOPT for the simulation study described in this chapter. IPOPT is based on an interior-point algorithm. Alternatively, the Matlab® function `fmincon` [Mat15] can be used for solution of the NLP. We experience the lowest computation times using the IPOPT method.

The solution of (6.5) is defined by the function

$$u_k = \mu(\hat{\tilde{x}}_{k|k}, u_{k-1}, d_k) \tag{6.11}$$

in which u_k is the first u_k^* of U_k^*. The function defines the on-line computations of the regulator, provided in Algorithm 6, and used in Algorithm 5.

Algorithm 6 Regulator Algorithm for multiple-shooting, $\mu(\cdot)$

Require: $\tilde{X}_{\text{init}}$, $\hat{\tilde{x}}_{k|k}$, u_{k-1}, d_k
  Solve NLP:
  $\tilde{X}^* = \text{NLPSolver}(\text{problem}(\tilde{X}_{\text{init}},u_{k-1},d_k,\hat{\tilde{x}}_{k|k}))$
  $u_k = \text{unpack}(\tilde{X}^*)$
  return u_k

Require: $[\phi, c_{eq}, c_{ineq}]$=problem$(\tilde{X},u_{k-1},d_k,\hat{\tilde{x}}_{k|k})$
  $[U, X, S] = \text{unpack}(\tilde{X})$
  $[x_k;\ x_{\text{d},k}] = \hat{\tilde{x}}_{k|k}$
  $\phi_e = 0$
  for $j = 0 : N-1$
    Compute the state prediction and profit function using ESDIRK
    $[x_{k+j+1}, \phi_{e,j}] = \text{ESDIRK}(t_k,t_{k+1},X_j,\ U_j,\ d_k,\ x_{\text{d},k})$
    $z_{k+j} = h_{\text{z}}(X_j) + C_{\text{d,z}}x_{\text{d},k}$
    $\phi_e = \phi_e + \phi_{e,j}$
  end
  $z_{k+N} = h_{\text{z}}(X_N) + C_{\text{d,z}}x_{\text{d},k}$
  Compute the profit of operation including relaxation
  $\phi = \phi_e + \phi_s(S) + \phi_{\Delta u}(U, u_{k-1}))$
  Compute the equality and inequality constraints
  $c_{eq} = \{x_{k+j}\}_{j=0}^{N} - X = 0$
  $c_{ineq} = [\{c(Z_j)\}_{j=1}^{N} + S \geq 0;\ S \geq 0;\ U_{\min} \leq U \leq U_{\max}]$

6.5 Closed-loop Simulation

The performance of the E-MPC control strategy has been investigated by a closed-loop simulation. Fig. 6.2 shows the measured outputs and the inputs of the closed-loop simulation. Fig. 4.2 shows the disturbances. The E-MPC operates the inputs of the dryer such that the cost of operation is minimized at all time. The optimum is reached when T_{SD} reaches the glass transition temperature, $\bar{T}_g^{\text{SD}}$, i.e. the point at which the powder turns sticky and Y_{ab} is at its maximum value and the moisture content of the powder, S_{cd}, reaches its maximum value $S_{\max}$. The reason is simple, it maximizes the throughput, F_{f}, while meeting the residual moisture specification i.e. product quality. The optimum is achieved while the energy consumption is minimized from the inlet air heaters, i.e. by minimizing T_{main}, T_{sfb} and T_{vfbh} within the given constraints. The most efficient operation is achieved when drying as much as possible in the fluid beds, i.e. in the SFB and VFB stages. This is clearly seen from the simulation where the SFB and VFB air temperatures, T_{sfb} and T_{vfbh}, are

Table 6.1: Average KPIs for the E-MPC controller.

KPIs	Unit	E-MPC	% inc. to PI
Product flow rate	F_{p}	66.81 kg/hr	9.61 %
Energy consumption	Q_{tot}	90.4 kW	3.63 %
Specific energy consum.	$\frac{Q_{\mathrm{tot}}}{F_{\mathrm{p}}}$	4.88 MJ/kg	-5.44 %
Residual moisture	$1 - S$	3.49 %	3.37 %
Energy efficiency	η	42.5 %	5.52 %
Profit of operation	p	135.19 €/hr	9.69 %

maximized until the residual moisture reaches the upper limit. This leads to a high SFB stage temperature that is controlled close to its maximum temperature $T_{\mathrm{SFB}} \leq 75.5°\mathrm{C}$, however it does not reach it.

The simulation also shows that an increase in the ambient air humidity, Y_{amb}, or decrease in feed solid concentration, S_{f}, have the same effect i.e. causing the powder to turn more moist and sticky inside the dryer. The E-MPC compensates in both cases by decreasing the feed rate, F_{f}, and the inlet air temperatures accordingly to maintain the optimal temperatures in the stages. Consequently, the economically most favorable conditions for the dryer is obtained at low ambient air humidity while drying a feed with a high content of solids.

Table 6.1 shows the key performance indicators (KPIs) of the closed-loop simulation presented in Fig. 6.2. Compared to the PI control strategy, the E-MPC provides on average an increased product flow rate of 9.61% and a decreased specific energy consumption of 5.44%. The energy consumption is increased due to the increased product flow rate. The powder moisture content is increased by 3.37% (0.114 p.p.) and the energy efficiency is increased by 5.52% (2.22 p.p.). The profit of operation is improved by 9.69%. These numbers surpass both the performance of the MPC with RTO strategy and the conventional PI control strategy.

6.6 Summary

In this chapter, we described the E-MPC control strategy and performed a closed-loop simulation.

- We described the nonlinear state estimator and the nonlinear regulator that together forms a complete E-MPC control strategy. Tuning of the state estimator was also considered.

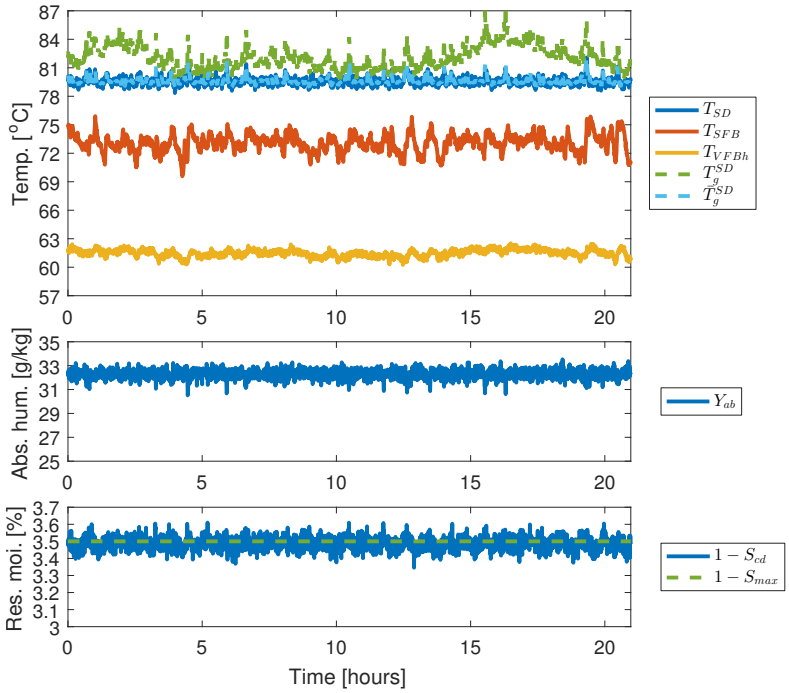

(a) Measured output variables.

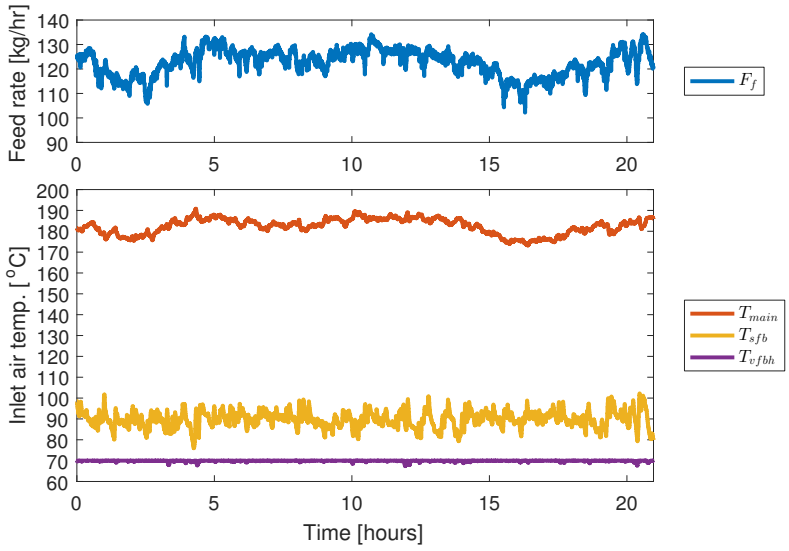

(b) Input variables.

Figure 6.2: Simulation of the E-MPC subject to the disturbance scenario given in Fig. 4.2.

- We designed an E-MPC that controls the residual moisture content and avoids that the powder sticks to the walls of the chamber.
- Compared to the conventional PI control strategy, the product flow rate is improved by 9.61%, the specific energy consumption is decreased by 5.44%, and the powder moisture content is improved by 3.37%.
- We showed by a closed-loop simulation that the E-MPC surpasses the performance of the PI control and MPC with RTO strategies. E-MPC improves the profit of operation by 9.69%.

Chapter 7

Application of MPC to an Industrial Spray Dryer

In this chapter, we describe the application of MPC with an RTO layer to an industrial four-stage spray dryer. We provide an industrially recorded closed-loop experiment and show that the profit of operation is improved significantly by the application of MPC.

The chapter provides a summary of Paper I.

The spray dryer in question is a GEA Multi-Stage Dryer (MSD$^{\text{TM}}$-1250) that produces enriched milk powder. It is one of the largest dryers installed in the dairy industry. The dryer is supplied with 169 tons/hr of air and consumes 7.4 MW of energy to heat the air by combustion of natural gas. The nominal evaporation capacity is approximately 7000 kg/hr of water. The MPC solution, based on the MPC with an RTO layer, which is applied in this study, also forms the basis of a control solution currently being commercialized and marketed as DRYCONTROL$^{\text{TM}}$ by GEA Process Engineering A/S.

7.1 PLC, Industrial PC and SCADA Setup

The dryer was erected in 2015, and is equipped with standard field instruments as well as the latest innovations within advanced field instruments. Fig. 7.1 illustrates the communication paths between the PLC and the advanced field instruments, the PLC and the industrial PC, and the PLC and the SCADA system. The residual moisture content is measured at the VFB powder outlet and the exhaust air humidity is measured by extracting air from the exhaust air duct. The challenge from a control point of view is that these measurements may be unavailable for longer periods due to in-process maintenance, automatically detected sensor errors and slow sample frequencies. The PLC handles the communication between the standard field instruments, the advanced field instruments and controls the actuators. The industrial PC, which runs our MPC algorithm, is located in the PLC panel. The communication between the PLC and the industrial PC is performed via the OPC communication protocol, which is a well proven industrial standard. The SCADA system handles and conveys the operator instructions to the PLC as well as presents the current state of the spray dryer. Fig. 7.2 shows the SCADA system from which the operators handle the standard control system and the MPC solution. In the SCADA system the operator can turn the MPC solution on and off, adjust the constraints in the recipe system and see the optimal targets which the MPC is heading towards. The task for the operator is thus changed from defining targets for the PID controllers to defining ranges (constraints) for the manipulated variables and targets of the MPC solution. The inputs and outputs of the MPC solution are scaled and validated before being sent to the PLC and after being received from the PLC. Bumpless transfer is implemented to ensure a smooth transition between the MPC and the conventional PI control strategy. Interlocks are implemented to accommodate emergency shut downs.

7.2 MPC Program

The MPC program implements the MPC algorithm and the additional features needed to provide a standalone MPC solution. The MPC code is compiled only once to a standalone executable program using Matlab®. The MPC program is used for all applications. The individual specification of each application is made by configuring an XML file. The MPC program reads this XML file as part of its initialization/start-up routine. This XML file is also referred to as the definition file.

Fig. 7.3 shows an overview of the MPC program, which is composed of several

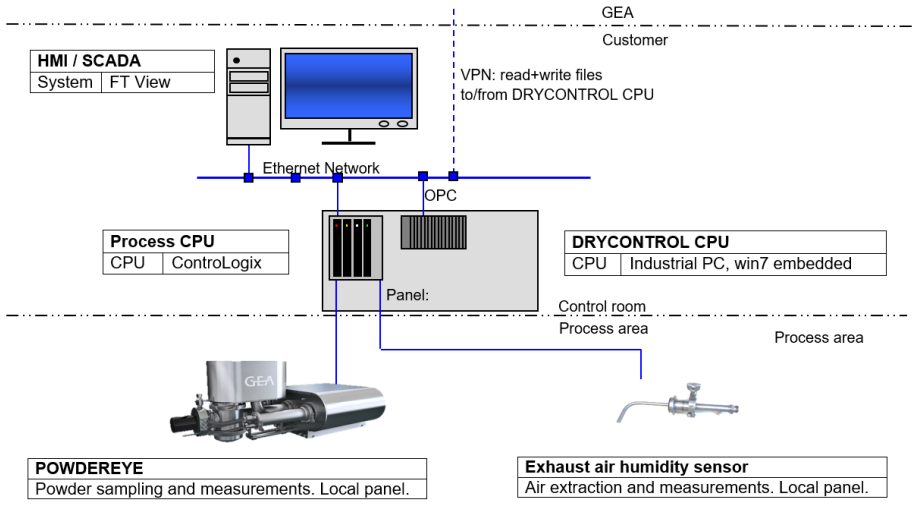

Figure 7.1: Overview of the communication paths from the advanced field instruments to the PLC, MPC as well as the SCADA system.

modules that in combination provides a fully functioning MPC solution. The core of the program is the MPC algorithm, around which several support modules are needed; i.e. the connection module, the manager module, the logger module and the add-on modules.

The MPC program starts up by parsing the XML definition file and initializes the described modules. First, the OPC connection is started and a connection to the relevant tags in the OPC server is established. This module handles the transfer of data to and from the PLC. A watch dog is setup to ensure proper handling of connection losses. The manager module is started to handle errors i.e. present these in the SCADA system as well as storing them in a log file. It also makes sure that dependent modules are started in the correct order. The logger stores the value of all the OPC tags at a fixed rate to a CSV file. The logged OPC values facilitate performance assessment and troubleshooting. The add-on module handles the reading, validation and calculation required for the advanced instruments before these can be used in the MPC algorithm. The state estimator, regulator and RTO module are started to provide the MPC with RTO control solution. The program is mainly intended for MPC use, but simpler control solutions are also supported such as least-squares soft-sensoring and PID regulators.

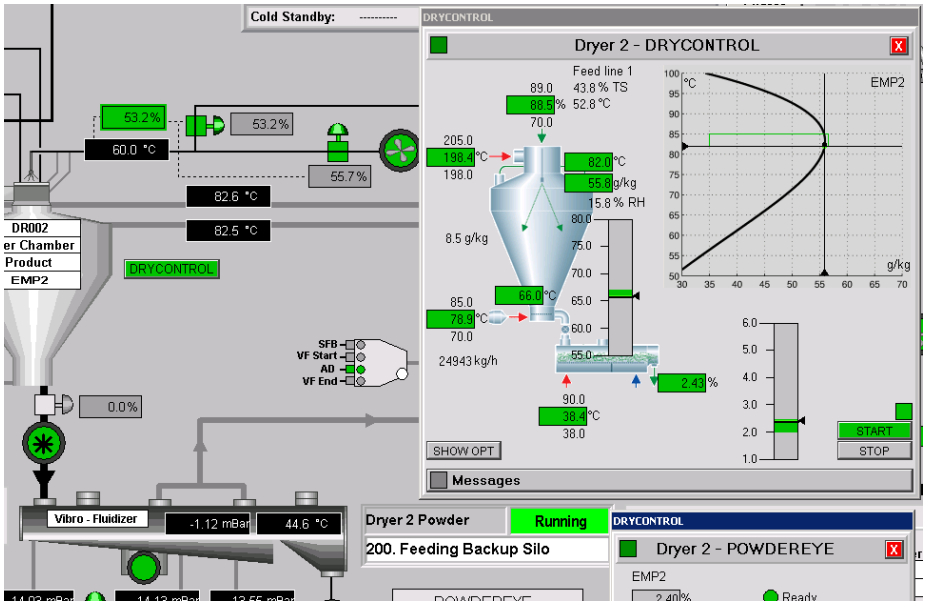

Figure 7.2: The SCADA system for control of the spray dryer along with the MPC faceplate.

7.2.1 MPC Algorithm

The MPC algorithm in the MPC program is based on the earlier described MPC with an RTO layer from Chapter 5, Paper B and Paper H. The performance of this controller compares well to the more advanced E-MPC solution while being simpler to implement, proved reliable and requires a minimum of computational power. The MPC algorithm combines a state estimator, a regulator and an RTO layer as presented in Algorithm 2, Fig. 5.1 in Chapter 5 and Fig. 7.3.

7.2.1.1 State Estimator Module

The state estimator module, which may also act as a standalone soft-sensor, is based on a linear time-varying Kalman filter. The time-varying Kalman filter is used to estimate the initial state in the regulator, $\hat{\hat{x}}_{k|k}$. Offset-free output estimation (and control) at steady-state is provided by augmenting the identified state-space model with integrating output disturbances, i.e. $C_d = I$ and $B_d = 0$ [PR03,PGA15]. The output disturbance model is favored compared to the input

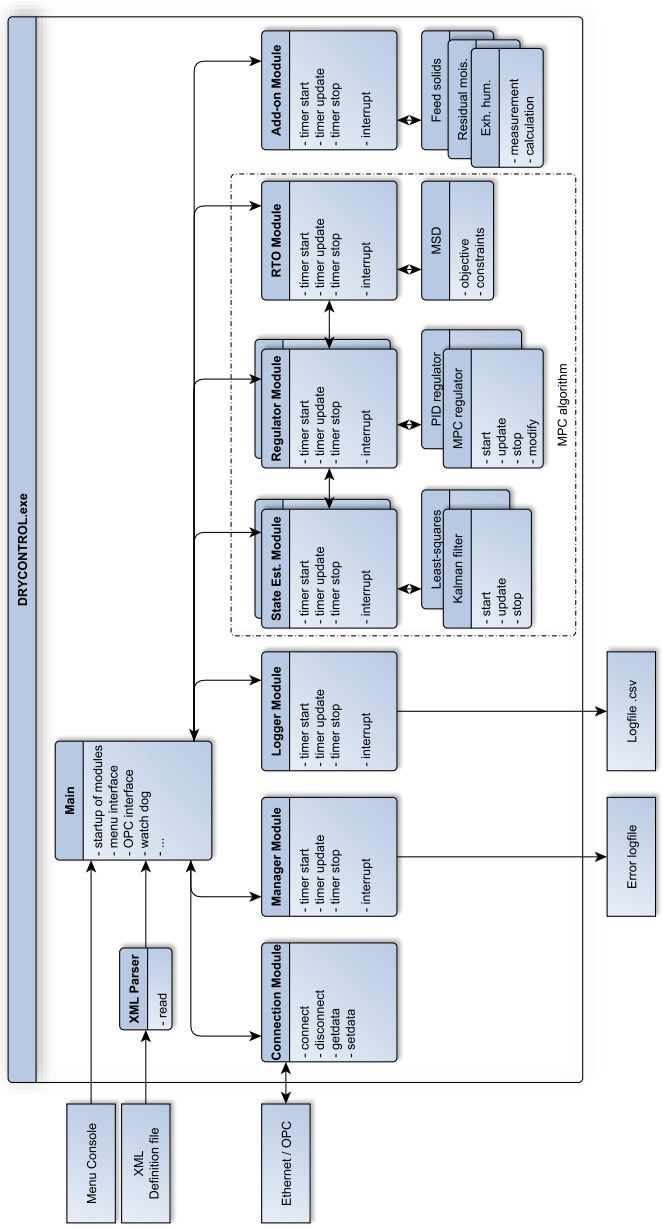

Figure 7.3: Overview of the structure in the MPC program (i.e. DRYCONTROL^{TM}).

disturbances as the model errors seem to mainly show as step changes in the outputs.

As in Section 5.2, the augmented model is

$$\bar{x}_{k+1} = \bar{A}\bar{x}_k + \bar{B}u_k + \bar{E}d_k + \bar{G}\bar{w}_k + \bar{\sigma}_{\mathrm{x}} \tag{7.1a}$$

$$y_k = \bar{C}_{\mathrm{y}}\bar{x}_k + \sigma_{\mathrm{y}} + v_k \tag{7.1b}$$

$$z_k = \bar{C}_{\mathrm{z}}\bar{x}_k + \sigma_{\mathrm{z}} \tag{7.1c}$$

where $\bar{x}_k \in \mathbb{R}^{n_{\bar{x}}}$ is the augmented state vector, $u_k \in \mathbb{R}^{n_u}$ is the input vector, $d_k \in \mathbb{R}^{n_d}$ is the measured disturbance vector and $y_k \in \mathbb{R}^{n_y}$ is the measurement vector that vary in size. $z_k \in \mathbb{R}^{n_z}$ is the controlled output vector. $\bar{G}$ is selected such that only the integrating disturbance states are subject to state noise. $\bar{w}_k$ and v_k are assumed uncorrelated with $\bar{w}_k \sim N_{\mathrm{iid}}\left(0, \bar{R}_w\right)$ and $v_k \sim N_{\mathrm{iid}}(0, R_v)$. The noise covariances are estimated according to Section 5.3.1.

7.2.1.2 Regulator Module

The regulator is formed as an output tracking problem with input constraints

$$\min_{\{u_{k+j}\}_{j=0}^{N-1}} \quad \phi = \frac{1}{2}\sum_{j=1}^{N} \|z_{k+j} - r_k\|_{Q_z}^2 + \frac{1}{2}\sum_{j=0}^{N-1} \|\Delta u_{k+j}\|_{S_u}^2 \tag{7.2a}$$

$$\text{s.t.} \quad \bar{x}_k = \hat{\bar{x}}_{k|k}, \tag{7.2b}$$

$$\bar{x}_{k+j+1} = \bar{A}\bar{x}_{k+j} + \bar{B}u_{k+j} + \bar{E}d_k + \bar{\sigma}_{\mathrm{x}}, \quad j \in \mathcal{N}_u \tag{7.2c}$$

$$z_{k+j} = \bar{C}_{\mathrm{z}}\bar{x}_{k+j} + \sigma_{\mathrm{z}}, \quad j \in \mathcal{N}_z \tag{7.2d}$$

$$u_{\min} \le u_{k+j} \le u_{\max}, \quad j \in \mathcal{N}_u \tag{7.2e}$$

in which $\Delta u_{k+j} = u_{k+j} - u_{k+j-1}$ and $\mathcal{N}_z = \{1, 2 \ldots, N\}$, $\mathcal{N}_u = \{0, 1 \ldots, N-1\}$. N is the control and prediction horizon. The estimated current state, $\hat{\bar{x}}_{k|k}$, is assigned to the initial state by (7.2b). (7.2c) and (7.2d) are the augmented state-space constraints from (7.1). (7.2e) are the input constraints. No forecasts are available for the target, r_k, and the measured disturbances, d_k. Therefore we use the same-as-now predictions in (7.2). The tracking problem in (7.2) is solved by formulating the corresponding convex quadratic problem as described in Section 5.4.

7.2.1.3 RTO Module

The RTO layer computes the target, r_k, in the regulator to achieve better economic performance. The RTO algorithm is described in details in Section 5.5.

r_k is computed by

$$\min_{u_{\mathrm{ss}}, z_{\mathrm{ss}}, s} \quad \phi_{\mathrm{ss}} = -p(z_{\mathrm{ss}}, u_{\mathrm{ss}}, d_k) + \|s\|^2_{2,S_W} \tag{7.3a}$$

$$\text{s.t.} \quad [0\ I]\bar{x}_{\mathrm{ss}} = [0\ I]\hat{\bar{x}}_{k|k} \tag{7.3b}$$

$$\bar{x}_{\mathrm{ss}} = \bar{A}\bar{x}_{\mathrm{ss}} + \bar{B}u_{\mathrm{ss}} + \bar{E}d_k + \bar{\sigma}_{\mathrm{x}} \tag{7.3c}$$

$$z_{\mathrm{ss}} = \bar{C}_{\mathrm{z}}\bar{x}_{\mathrm{ss}} + \sigma_{\mathrm{z}} \tag{7.3d}$$

$$u_{\min} + \delta_u \leq u_{\mathrm{ss}} \leq u_{\max} - \delta_u \tag{7.3e}$$

$$c(z_{\mathrm{ss}}) + s \geq 0 \tag{7.3f}$$

$$s \geq 0 \tag{7.3g}$$

The target is set to the optimal controlled output value, $r_k = z_{ss}$, when (7.3) is solved. At the samples between the intervals, (7.3) is not solved and the current target is maintained.

The objective function, ϕ_{ss}, is the sum of the profit function, $p(z_{\mathrm{ss}}, u_{\mathrm{ss}}, d_k)$, and a penalty function, $\|s\|^2_{2,S_W}$, that penalizes violations of the output constraints. The nonlinear profit function $p(z_{\mathrm{ss}}, u_{\mathrm{ss}}, d_k)$ is tailored to the dryer and product being dried as described in Paper H and Paper I. The integrating disturbance states, $x_{d,k} = [0\ I]\hat{\bar{x}}_{k|k}$, are fixed to their current values by (7.3b). The linear model is used in the constraints (7.3c)-(7.3d) to determine the steady-state relation between the inputs, u_{ss}, and the controlled outputs, z_{ss}. $u_{\min}$ and $u_{\max}$ define the process input constraints. δ_u contains a back-off in the manipulated variables to maintain controllability in the regulator. The nonlinear process constraints, $c(z_{\mathrm{ss}})$, contains the stickiness constraints of the powder and the operator defined limits on the controlled outputs. This function is tailored to the dryer and product being dried as described in Paper H and Paper I. Together these constraints provide a region in which safe operation is guaranteed. We allowed only to constraint the controlled outputs of the Kalman filter to stay within the stickiness constraint as the given constraints already have back-off incorporated. We use the Matlab® function, `fmincon`, using the SQP method for solution of (7.3).

7.2.2 Add-on Module

An add-on module computes the feed solids concentration and handles the reading, validation and calculation required for the advanced field instruments. The feed concentration, S_{f}, is computed from measurements of the feed density and the feed temperature. This is possible as the feed composition and the density of the feed components are approximately known. The exhaust air humidity sensor provides a relative air humidity and a temperature measurement of the

extracted air from the exhaust air duct. The temperature and relative air humidity are used to compute the absolute air humidity, Y. The module computes the absolute air humidity when the instrument readings are within its ranges. Otherwise the measurement is ignored. POWDEREYE^{TM} is a system for in-line powder analysis and is designed specifically for spray dryers. The system allows producers of food and dairy powders to perform the most important product quality tests (i.e. residual moisture content, poured and tapped density of the powder and detection of scorched particles) during spray drying in a single in-line operation [DS14]. The module reads and scales the residual moisture measurement if no warnings are present at the instrument. If there is a warning, such as an empty sample cup, the measurement is ignored.

7.3 XML Definition File

The definition file defines the modules in the MPC program. The file identifies the tag names in the OPC server and defines the process inputs, outputs and disturbances in the MPC algorithm. It contains the state-space models for each recipe of produced products. It specifies the control objective, i.e. targets, constraints and tuning parameters. The file also specifies the auxiliary features, such as handling of the advanced instruments. The design of this file is the design and modeling step of the MPC strategy. The file is formatted according to the XML standard, making it easy to read and parse in the program.

7.3.1 Process Outputs, Inputs and Disturbances

The controlled outputs in the MPC are the exhaust air temperature, T_{exh}, and the absolute exhaust air humidity, Y, to avoid deposits of sticky particles on the spray dryer surfaces. The SFB powder temperature, T_{powder}, is controlled to avoid lumps of powder to form in the SFB. The reisudal moisture content of the final powder, S, is controlled to keep it below and close to the maximum limit. The inputs are the feed flow, F_{f}, the temperature target to the main air heater, $T_{\text{main,sp}}$, the temperature target to the SFB air heater, $T_{\text{sfb,sp}}$, and the temperature target to the VFB air heater, $T_{\text{vfbh,sp}}$. The inputs provide strong controllability of the outputs. The disturbances are the feed solids concentration S_{f}, the absolute ambient air humidity, Y_{amb}, and the number of active nozzles, N_{nozz}, in the feed line.

The measurement and output vector, $y = z$, the input vector, u, and the dis-

turbance vector, d, are

$$y = \begin{bmatrix} T_{\text{exh}} & Y & T_{\text{powder}} & S \end{bmatrix}^T \tag{7.4a}$$

$$u = \begin{bmatrix} F_{\text{f}} & T_{\text{main,sp}} & T_{\text{sfb,sp}} & T_{\text{vfbh,sp}} \end{bmatrix}^T \tag{7.4b}$$

$$d = \begin{bmatrix} S_{\text{f}} & Y_{\text{amb}} & N_{\text{nozz}} \end{bmatrix}^T \tag{7.4c}$$

7.3.2 Model Identification

The MPC relies on a model for estimation of the states and prediction in the regulator. The model is divided into two sub-models; an actuator model and a dryer model. The approach is advantageous as it provides flexibility in tuning of the PID parameters in the actuators, as the tuning can be changed without the need for identification of the full control model.

We identify a continuous-time transfer function model described by

$$\bar{U}(s) = G_a(s)U(s) \tag{7.5a}$$

$$Y(s) = G_m(s)\bar{U}(s) + G_d D(s) \tag{7.5b}$$

$$z(t_k) = y(t_k) \tag{7.5c}$$

in which $U(s)$ is the inputs, $\bar{U}(s)$ is the actuated intermediate values and $Z(s)$ is the controlled outputs. $D(s)$ is the disturbances that affects the controlled outputs.

$G_a(s)$ is the actuator model, $G_m(s)$ is the dryer model and $G_d(s)$ is the disturbance model. These consists of a matrix of transfer functions of the form

$$g_{a,ii}(s) = \frac{K_{a,ii}}{\tau_{a,ii}s + 1} e^{-\theta_{a,ii}s} \tag{7.5d}$$

$$g_{m,ji}(s) = \frac{K_{m,ji}}{\tau_{m,ji}s + 1} e^{-\theta_{m,ji}s} \tag{7.5e}$$

$$g_{d,jk}(s) = \frac{K_{d,jk}}{\tau_{d,jk}s + 1} e^{-\theta_{d,jk}s} \tag{7.5f}$$

where i is the input, k is the disturbance and j is the output. The parameters in the above model are obtained by least-squares minimization of the residuals between the simulated and recorded response. $G_a(s)$ is identified from 4 estimation datasets. $G_m(s)$ and $G_d(s)$ are identified from 10 estimation datasets. The estimation datasets were also used for validation.

Fig. 7.4 presents a dataset used for validation of the combined model in (7.5). The model response is a simulation in which no feedback from the data is implemented. The model fits the data well. The datasets used for identification

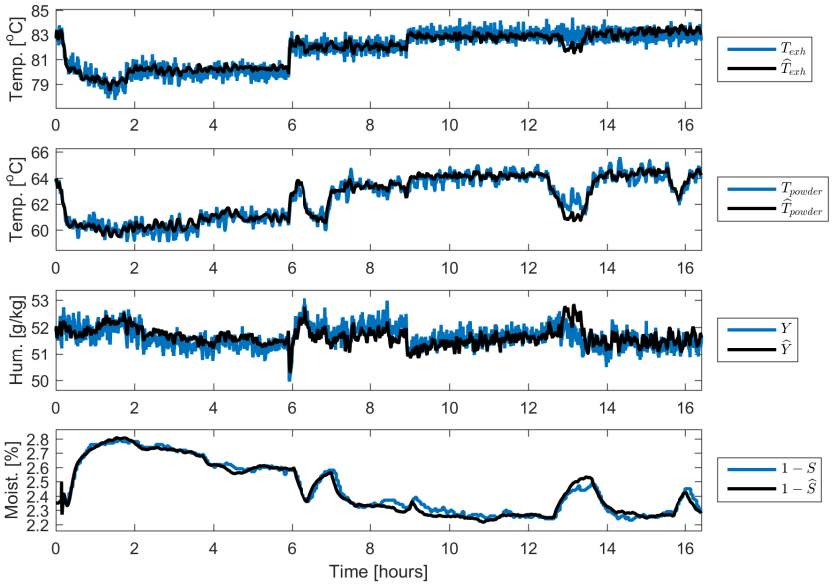

Figure 7.4: Comparison of a validation dataset (blue) and the corresponding simulation (black) of the combined model in (7.5). The model fits the data well.

consist of both open-loop and closed-loop data. Fig. 7.5 shows the unit-step responses of the combined model, $U(s)$ to $Z(s)$. The process model in (7.5) is transformed to a discrete time state-space model, $(A,B,E,C_{\mathrm{y}},C_{\mathrm{z}})$, using a zero-order-hold assumption on the inputs and disturbances. Thereby we can make a balanced realization from the Hankel matrix of the impulse response matrices.

The lumped control model presented in Section 2.5 and Paper G can potentially also be used in the MPC and the RTO layer. Currently, the model describes drying of maltodextrin on the smaller MSD-20 spray dryer and modifications must therefore be performed in order to make it fit this dryer. Instead, we decided to use the more general black-box data driven model in (7.5).

7.3.3 Regulator and RTO Tuning

The tuning parameters in the objective function, $Q_z = \mathrm{diag}([30\ 15\ 30\ 800])$ and $S_u = \mathrm{diag}([45\ 30\ 30\ 7.5])$, are selected to achieve a good compromise between a fast closed-loop response and robust performance. The highest weight is set on control of the residual moisture content. The control and prediction horizon is,

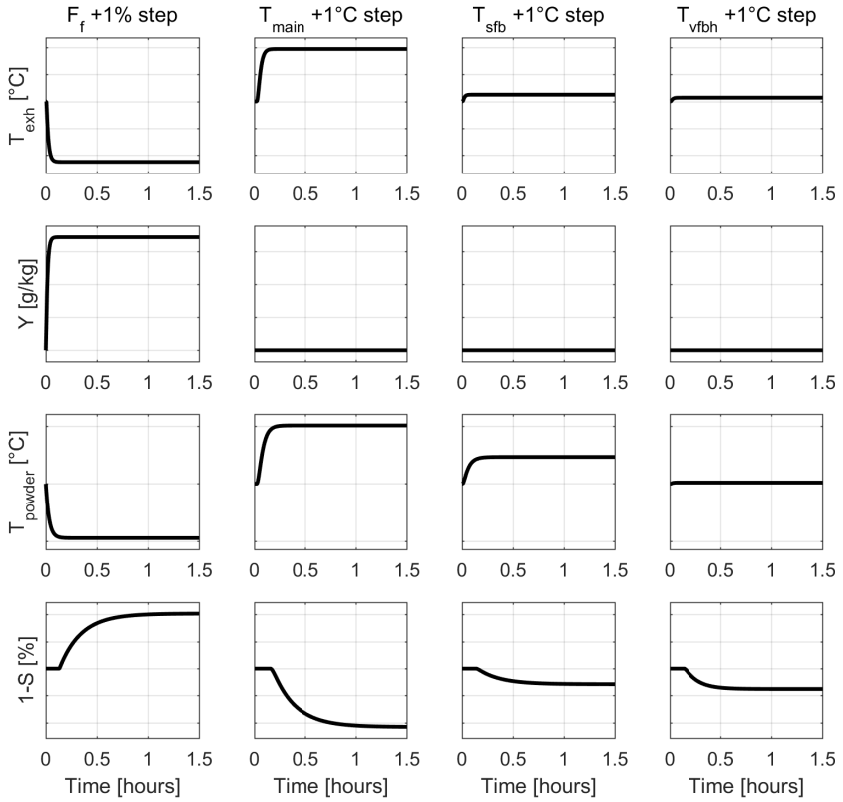

Figure 7.5: Unit-step responses of the identified model in (7.5).

$N = 60$ min/20 s $= 180$. The sample rate of the MPC is 20 s. The RTO problem is solved at a sample rate of 30 s. The fast sample rate of the RTO means that a steady-state is not reached before the RTO computes a new target for the MPC. The soft constraint penalty is $s_{\mathrm{W}} = \mathrm{diag}([10^5\ 10^5\ 10^5\ 10^5])$. The input and output constraints in the MPC and RTO layer are determined by the operators in the recipe handling system. The back-off in the manipulated temperatures, δ_u, is selected to be 5°C to maintain controllability in the regulator.

7.4 Closed-loop Performance

The performance of the MPC has been validated against the conventional PI control strategy in several experiments. Two of these experiments are presented

in Paper I. We present a single closed-loop experiment that illustrates the functionality of the MPC with RTO strategy.

7.4.1 Experiment

Fig. 7.6 shows the measured (and controlled) outputs and the targets. Fig. 7.7 shows the inputs and Fig. 7.8 shows the disturbances. The data series starts shortly after the dryer has been running on cold standby for a longer period. The residual moisture content, S, at time 13:15, therefore initially violates the upper limit. The produced powder is then stored for later rework. The MPC is turned on as soon as the production is within safe limits, but still in the transient start-up phase. After being turned on the MPC stabilizes the production in less than 30 minutes. The closed-loop experiment shows that the MPC is able to control the outputs T_{exh}, Y, T_{powder} and S, to its targets. The disturbances are rejected by small adjustments to the inputs. The targets that are generated by the RTO layer are feasible and is frequently updated in accordance to the disturbances.

The economics of drying is optimized by increasing the product flow rate, and thereby the feed flow rate, F_{f}, while minimizing the inlet air temperatures, $T_{\text{main,sp}}$, $T_{\text{sfb,sp}}$ and $T_{\text{vfbh,sp}}$, accordingly. T_{exh} is minimized until the lower temperature limit at 80°C is reached and Y is increased to maximize the evaporation rate. In this experiment the heaters reach their upper limit and cannot supply more heat for evaporation. Thus, the stickiness of the powder is not the limiting constraint. The residual moisture content, S, is maximized to increase the yield and thereby profit. The RTO layer also seeks to maximize the profit of operation by minimizing the energy consumption by shifting the drying from the top of the spray dryer to the more energy efficient fluid bed stages. This is observed as the SFB powder layer temperature is high and the SFB inlet air temperature has reached its upper limit. Drying in the VFB stage is avoided as this would decrease the residual moisture content, S, below its maximum limit and reduce the product flow rate. In order to increase the profit of operation further, the bottleneck of the performance i.e. the maximum temperatures on the heaters, $T^{\text{max}}_{\text{main,sp}}$ and $T^{\text{max}}_{\text{sfb,sp}}$, must be addressed. Currently, the heaters are almost constantly operating at their upper limits. These upper limits were not obtained from product and dryer specific limits, rather they are a result of operator related experience. It should thus be possible to further increase the profit of operation by challenging these limits.

At time 14:35 the feed solids concentration suddenly changes due to an evaporator swap. The swap leads to an increased amount of water in the feed, S_{f}. The MPC decreases the production capacity accordingly to maintain correct

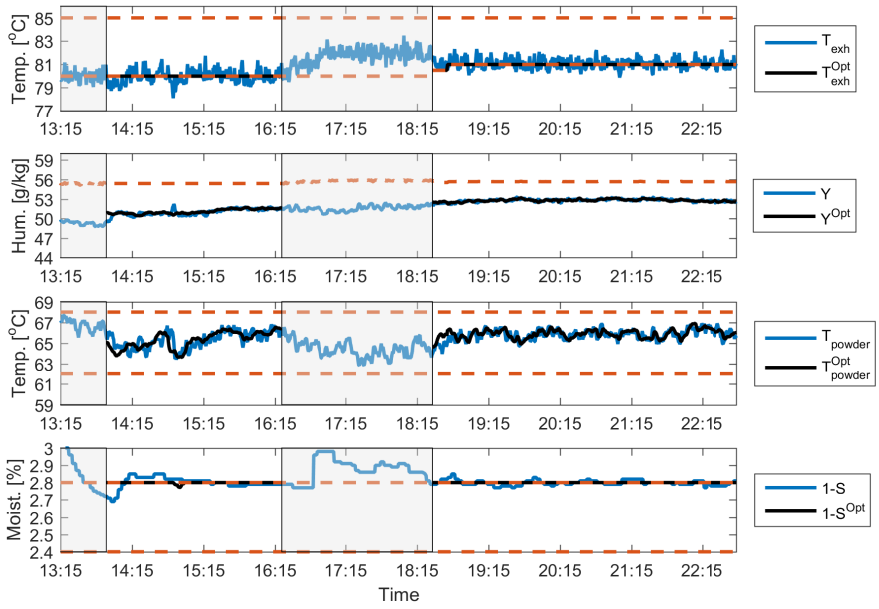

Figure 7.6: Measured and controlled outputs. The gray-shaded area denote PI control in action. Red dashed lines are constraints.

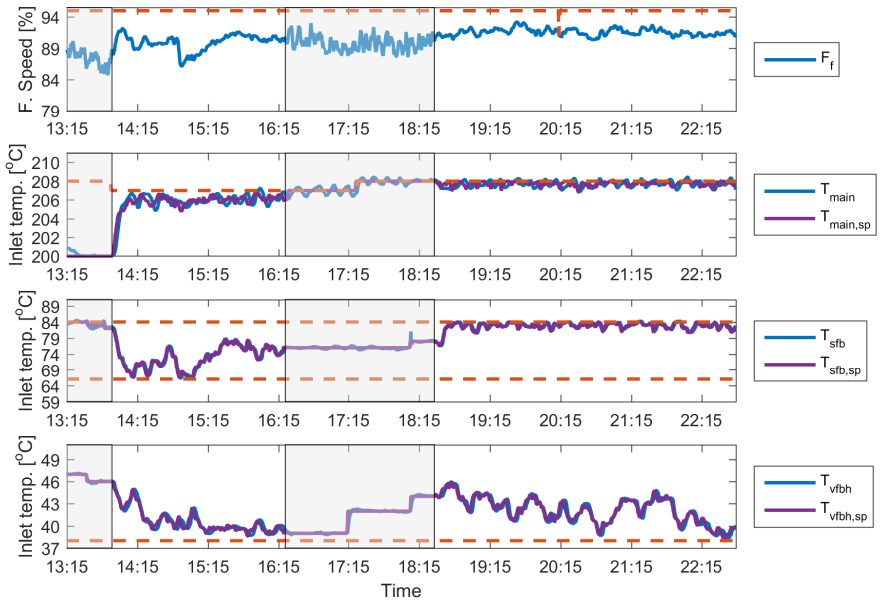

Figure 7.7: Input variables. Red dashed lines are constraints.

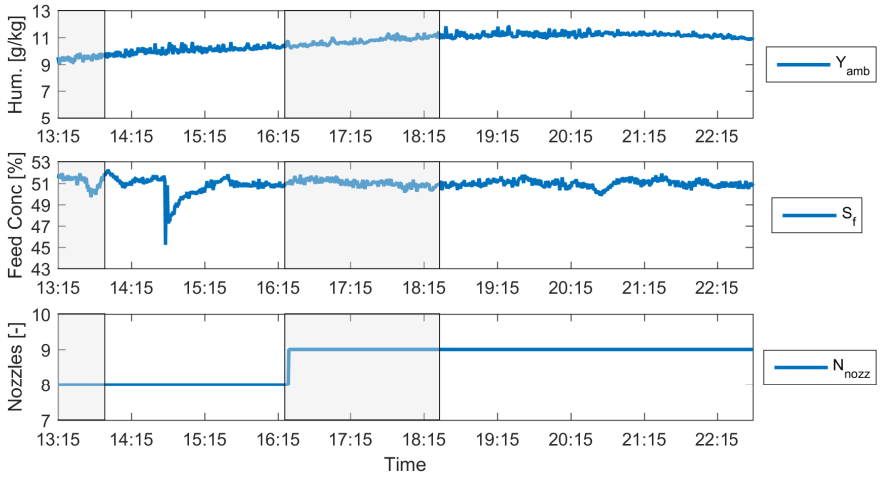

Figure 7.8: Measured disturbances.

residual moisture levels and prevent the powder from sticking to the chamber walls. The varying ambient air humidity is also handled, but the maximum exhaust air humidity is never reached and no correcting action has to be made.

At 16:20 the operator observes high nozzle pressures. In an attempt to handle the situation, the MPC is turned off by the operator. After 2 hours in conventional operation, the MPC is turned on again with $T^{\max}_{\text{main,sp}}$ increased by 1°C to allow an extra nozzle to be activated. During the period with conventional operation, the upper limiting residual moisture content is violated.

During the experiment the MPC maintain T_{exh} and Y within the constraints, which relate to stickiness of the powder, and the residual moisture content, S, below its maximum limit.

7.4.2 Economic Benefit

Table 7.1 shows the average key performance indicators (KPIs) of an experiment with the conventional PI control strategy and the presented MPC experiment in Fig. 7.6. Compared to the MPC strategy, the PI control strategy provides on average a lower average product flow rate and residual moisture content in the powder. This leads to a decreased profit of operation. On average the MPC improves the product flow rate by 4.44% (322 kg/hr) and the residual moisture content by 6.31% (0.166 p.p.). The energy consumption is increased by

Table 7.1: Average KPI values.

KPIs	Unit	PI	MPC	% inc. to PI
Product flow rate	F_{p}	7,177 kg/hr	7,499 kg/hr	4.44%
Energy consumption	Q_{tot}	7.40 MW	7.49 MW	1.23%
Specific energy consum.	$\frac{Q_{\mathrm{tot}}}{F_{\mathrm{p}}}$	3.71 MJ/kg	3.60 MJ/kg	-3.10%
Residual moisture	$1-S$	2.633 %	2.799 %	6.31%
Energy efficiency	η	63.4 %	62.6 %	-1.28%

1.23%, however, more importantly the specific energy consumption is decreased by 3.10%. The MPC decreases the energy efficiency by 1.28% (0.8 p.p.). This decrease is due to a significantly higher ambient air humidity during this experiment compared to the PI control experiment. The powder must therefore be dried more extensively to meet the residual moisture limit, at the expense of an increased energy consumption and decreased energy efficiency. In Paper I we show that for a comparable experiment the energy efficiency is increased by 1 p.p.

The annual profit increase from the residual moisture content improvements equates to approx.

$$\begin{aligned} &= 0.166 \text{ p.p.} \cdot 7400 \text{ kg/hr} \cdot 7200 \text{ hr/year} \cdot 2.5 \text{ €/kg} \\ &= 221,112 \text{ €/year} \end{aligned}$$

The annual energy savings equates to approx.

$$\begin{aligned} &= 1 \text{ p.p.} \cdot 7.40 \text{ MW} \cdot 7200 \text{ hr/year} \cdot 12.906 \text{ €/(MWhr)} \\ &= 6,886 \text{ €/year} \end{aligned}$$

assuming the price of natural gas and the energy improvement achieved in Paper I. We exclude the profit related to increased production, as it may be limited by up- and down stream process capacity as well as the market demand. In total, the profit of operation is increased by approximately 228,000 €/year.

7.5 Summary

In this chapter, we described the industrial application of MPC to a Multi-Stage Dryer (MSD$^{\mathrm{TM}}$-1250) for drying of enriched milk powder.

- We described the implementation of a complete MPC with RTO control strategy applied to an industrial spray dryer.

- The MPC provides significantly better control of the residual moisture content compared to conventional PI control and avoids that the powder sticks to the walls of the chamber.
- The performance of the MPC was documented by industrial experiments. Compared to the PI control strategy, the product flow rate is improved by 4.44% (322 kg/hr) and the residual moisture content is improved by 6.31% (0.166 p.p.).
- Estimated from our experiments, the annual economic benefit from the residual moisture content and energy improvements equates to approximately 228,000 €/year. In this number we exclude the profit related to increased production, although the increase is significant.
- The MPC program is commercialized and marketed as DRYCONTROL^{TM} by GEA Process Engineering A/S. The MPC developed in this project forms an advanced control solution that can be used to improve the performance of several other processes over the coming years.

Chapter 8

Conclusions and Perspectives

In this thesis, we have developed and applied Model Predictive Control (MPC) strategies to optimize the operation of spray dryers. In that effort, we developed simulation and control models of a GEA MSD^{TM}-20 four-stage spray dryer. The models were used to facilitate development and comparison of two MPC strategies. 1) A linear MPC with a Real-Time Optimization layer (MPC with RTO) and 2) An Economic Nonlinear MPC (E-MPC) with economic costs directly in the objective function of the controller. These were both tailored for the spray drying process to maximize the profit of operation, by maximizing the production rate while minimizing the energy consumption. Simulations show that both MPC strategies provide control of the dryer such that the produced powder is within the given quality specifications while avoiding that the powder sticks to the walls of the chamber. We compared the performance of the conventional PI control strategy to the performance of the MPC strategies by both simulation and an industrial experiment. The MPC control strategies improves the profit of operation by up to 9.69% in simulations and by approximately 228,000 €/year in the industrial experiment. Thereby, we conclude that the MPC strategies can be used to optimize the spray dryer operation compared the PI control strategy.

8.1 Spray Dryer Modeling

In Chapter 2, we developed a detailed first-principles dynamic model for simulation of the four-stage spray dryer and a simpler lumped dynamic model for design of the control strategies. The models describe the evolution of the air temperature, air humidity and the powder moisture contents in the dryer. The model parameters are identified from experiments conducted on the MSD^{TM}-20 four-stage spray dryer. The models fit the experimental data well in a wide range of operating points. The models also provide the key performance indicators (KPIs) such as the profit of operation, the energy consumption, the energy efficiency, the product flow rate and the stickiness of the powder in the spray dryer. The KPIs can be calculated directly from measurements.

Future work in this area should investigate simplification of the product drying rate terms and heat exchange term between the SD and SFB stages in the simulation model. Also, the models should be investigated for simulation of larger industrial sized four-stage spray dryers, such as the MSD^{TM}-1250, and drying of more complex products.

8.2 Model Predictive Control

In Chapter 5 and Chapter 6, we developed and compared two MPC strategies. Both control strategies automatically adjust the dryer to variations in the feed and the ambient air humidity, to maximize the profit of operation while the energy consumption is minimized, the residual moisture content in the powder is controlled and sticky powder is avoided. The MPC with RTO and the E-MPC both improve the profit of operation significantly compared to the conventional PI control strategy. By simulation we showed that the MPC with RTO improves the profit of operation by 8.71% and the E-MPC improves the profit of operation by 9.69%. Thus, the E-MPC outperforms both the PI and the MPC with RTO control strategies. The MPC rely on a state estimator (soft-sensor) for estimation of the current state of the dryer. The tuning of these state estimators are important and we investigated the Maximum Likelihood (ML) and Autocovariance Least Squares (ALS) methods for automated tuning of these. We favored the ML method for its ability to handle missing observations well.

Future work in this area should be focused on speeding up the computational time of the E-MPC implementation, such that it can be used for real-time implementations. Several nonlinear MPC frameworks exists, e.g. CasADi or ACADO, which could be applied.

8.3 Industrial Application of MPC

In Chapter 7, we demonstrated that the proposed MPC with RTO is applicable to an industrial GEA MSD$^{\text{TM}}$-1250 dryer producing enriched milk powder. We documented the MPC setup as well as the KPIs obtained during the demonstration experiments. The MPC solution functions well and is used in the daily operation. Compared to the conventional PI control strategy, the product flow rate is improved by 4.44%, the residual moisture content is improved by 6.31% (0.166 p.p.) and the specific energy consumption is decreased by 3.10%. We estimate that the profit of operation is increased by approximately 228,000 €/year, excluding the profit related to increased production.

Future work in this area should focus on the system identification part. The time available for experiments are often limited which reduces the available data for identification. System identification may take considerably time and is thus costly. The use of physics-based models that incorporate a priori knowledge, such as the presented control model from Chapter 5, may be beneficial to reduce the time and costs needed for identification while providing high quality models.

8.4 Commercial Outlook

The MPC with RTO control strategy is today marketed by GEA Process Engineering A/S as DRYCONTROL$^{\text{TM}}$. The MPC algorithm forms a control package which is part of a general control solution platform. We hope to further develop the control package and use it to improve the performance of several other processes in the coming years. The principle of squeeze and shift may apply to many processes in the food industry, e.g. falling film evaporators, potentially leading to further energy savings and improved product quality. These processes are yet to be investigated.

Bibliography

[AAR12] D. Angeli, R. Amrit, and J. B. Rawlings. On average performance and stability of economic model predictive control. *IEEE Transactions on Automatic Control*, 57(7):1615–1626, 2012.

[AG10] V. Adetola and M. Guay. Integration of real-time optimization and model predictive control. *Journal of Process Control*, 20(1):125–133, 2010.

[ÅH06] K. J. Åström and T. Hägglund. *Advanced PID control*. Instrument Society of America, NC, USA, 2006.

[ÅJPJ08] B. M. Åkesson, J. B. Jørgensen, N. K. Poulsen, and S. B. Jørgensen. A generalized autocovariance least–squares method for Kalman filter tuning. *Journal of Process Control*, 18(7–8):769–779, 2008.

[AK03] K. B. Ariyur and M. Krstić. *Real–Time Optimization by Extremum-Seeking Control*. John Wiley and Sons, NY, USA, 2003.

[Amr11] R. Amrit. *Optimizing Process Economics in Model Predictive Control*. PhD thesis, University of Wisconsin–Madison, 2011.

[AO10] L. A. Alvarez and D. Odloak. Robust integration of real time optimization with linear model predictive control. *Computers and Chemical Engineering*, 34(12):1937–1944, 2010.

[ARB13] R. Amrit, J. B. Rawlings, and L. T. Biegler. Optimizing process economics online using model predictive control. *Computers and Chemical Engineering*, 58:334–343, 2013.

[Årz12] K.-E. Årzén. Real-time systems – handout material provided by The Faculty of Engineering, Lund University, 2012.

[BB06] R. A. Bartlett and L. T. Biegler. QPSchur: A dual, active–set, schur–complement method for large–scale and structured convex quadratic programming. *Optimization and Engineering*, 7(1):5–32, 2006.

[BBH04] P. Boonyai, B. Bhandari, and T. Howes. Stickiness measurement techniques for food powders: A review. *Powder Technology*, 145(1):34–46, 2004.

[Bie84] L. T. Biegler. Solution of dynamic optimization problems by successive quadratic programming and orthogonal collocation. *Computers and Chemical Engineering*, 8(3):243–248, 1984.

[BJ04] D. R. Brouwer and J. D. Jansen. Dynamic optimization of waterflooding with smart wells using optimal control theory. *SPE Journal*, 9(4):391–402, 2004.

[BP84] H. G. Bock and K. J. Plitt. A multiple shooting algorithm for direct solution of optimal control problems. *9th IFAC World Congress Budapest*, pages 242–247, 1984.

[BSM06] S. Basu, U. S. Shivhare, and A. S. Mujumdar. Models for sorption isotherms for foods: A review. *Drying Technology*, 24(8):917–930, 2006.

[BV04] S. Boyd and L. Vandenberghe. *Convex Optimization*. Cambridge University Press, NY, USA, 2004.

[Cap13] A. Capolei. *Nonlinear Model Predictive Control for Oil Reservoirs Management*. PhD thesis, Technical University of Denmark, 2013.

[CD75] P. S. R. K. Chintapalli and J. M. Douglas. The use of economic performance measures to synthesize optimal control systems. *Industrial and Engineering Chemistry Fundamentals*, 14(1):1–10, 1975.

[Chi14] N. Chism. Future state 2030: The global megatrends shaping governments. *KPMG International*, 2014.

[CJ12] A. Capolei and J. B. Jørgensen. Solution of constrained optimal control problems using multiple shooting and ESDIRK methods. *American Control Conference*, pages 295–300, 2012.

[Cla] Clal. Italian dairy economic consulting firm. `http://www.clal.it/en/index.php?section=confronto_smp&check=1`. Accessed: 2015-11-26.

[Cla88] D. W. Clarke. Application of generalized predictive control to industrial processes. *Control Systems Magazine*, 8(2):49–55, 1988.

[CPO01] X. D. Chen, W. Pirini, and M. Ozilgen. The reaction engineering approach to modelling drying of thin layer of pulped kiwifruit flesh under conditions of small biot numbers. *Chemical Engineering and Processing: Process Intensification*, 40(4):311–320, 2001.

[CSZ+12] C. Conte, T. Summers, M. N. Zeilinger, M. Morari, and C. N. Jones. Computational aspects of distributed optimization in model predictive control. *Conference on Decision and Control*, pages 6819–6824, 2012.

[DHN09] M. L. Darby, M. Harmse, and M. Nikolaou. MPC: Current practice and challenges. *Control Engineering Practice*, 7(1):86–98, 2009.

[DNJN11] M. L. Darby, M. Nikolaou, J. Jones, and D. Nicholson. RTO: An overview and assessment of current practice. *Journal of Process Control*, 21(6):874–884, 2011.

[DS14] K. N. Dyvelkov and J. Sloth. *Microencapsulation in the Food Industry*, chapter 6, pages 57–63. Academic Press, 2014.

[Dug15] J. Duggan. China's middle class turns to organics after food safety scares. *Guardian sustainable business*, 2015.

[EH01] T. F. Edgar and D. M. Himmelblau. *Optimization of Chemical Processes (2nd Edition)*. McGraw-Hill, NY, USA, 2001.

[Eng07] S. Engell. Feedback control for optimal process operation. *Journal of Process Control*, 17(3):203–219, 2007.

[ESJ09] K. Edlund, L. E. Sokoler, and J. B. Jørgensen. A primal-dual interior-point linear programming algorithm for MPC. *48th Conference on Decision and Control, held jointly with 28th Chinese Control Conference*, pages 351–356, 2009.

[EY15] EY. Megatrends 2015: Making sense of a world in motion. *EMEIA Marketing Agency*, pages 1–53, 2015.

[FASdJ10] M. Fox, C. Akkerman, H. Straatsma, and P. de Jong. Energy reduction by high dry matter concentration and drying. *Spray Drying, NIZO food research*, pages 6–8, 2010.

[FCB15] G. François, S. Costello, and D. Bonvin. Application of real-time optimization methods to energy systems in the presence of uncertainties and disturbances. *TMC Academic Journal*, 9(2):20–41, 2015.

[FJ13] G. Frison and J. B. Jørgensen. A fast condensing method for solution of linear-quadratic control problems. *Conference on Decision and Control*, pages 7715–7720, 2013.

[FKJB14] T. Faulwasser, M. Korda, C. Jones, and D. Bonvin. Turnpike and dissipativity properties in dynamic real-time optimization and economic MPC. *Conference on Decision and Control*, pages 2734–2739, 2014.

[FKP+14] H. J. Ferreau, C. Kirches, A. Potschka, H. G. Bock, and M. Diehl. qpOASES: A parametric active–set algorithm for quadratic programming. *Mathematical Programming Computation*, 6(4):327–363, 2014.

[Flo] SPX Flow. Integrated dairy process – powder and butter diagram. `http://www.spxflow.com/en/industries/food-and-beverage/food-sector/Integrated-Dairy-Process-Powder-Butter/InteractiveSystem/`. Accessed: 2015-11-19.

[FOS01] J. M. Frías, J. C. Oliveira, and K. Schittkowski. Modeling and parameter identification of a maltodextrin DE 12 drying process in a convection oven. *Applied Mathematical Modelling*, 25(6):449–462, 2001.

[FSD13] J. V. Frasch, S. Sager, and M. Diehl. A parallel quadratic programming method for dynamic optimization problems. *Mathematical Programming Computation*, pages 289–329, 2013.

[GEA] GEA. GEA at a glance. `http://www.gea.com/global/en/binaries/GEA%20at%20a%20Glance%20-%20August%202015_tcm11-27984.pdf`. Accessed: 2014-02-03.

[GJC+94] R. Govaerts, A. Johnson, R. Crezee, G. Reyman, and P. L. S. Swinkels. Control of an industrial spray-drying unit. *Control Engineering Practice*, 2(1):69–85, 1994.

[Grü12] L. Grüne. NMPC without terminal constraints. *Conference on Nonlinear Model Predictive Control*, 4(1):1–13, 2012.

[Grü13] L. Grüne. Economic receding horizon control without terminal constraints. *Automatica*, 49(3):725–734, 2013.

[Hal14] R. Halvgaard. *Model Predictive Control for Smart Energy Systems*. PhD thesis, Technical University of Denmark, 2014.

[HAPB07] L. Hassini, S. Azzouz, R. Peczalski, and A. Belghith. Estimation of potato moisture diffusivity from convective drying kinetics with correction for shrinkage. *Journal of Food Engineering*, 79(1):47–56, 2007.

[HFOS10] S. A. Hogan, M. H. Famelart, D. J. O'Callaghan, and P. Schuck. A novel technique for determining glass-rubber transition in dairy powders. *Journal of Food Engineering*, 99(1):76–82, 2010.

[HLJB12] T. G. Hovgaard, L. F. S. Larsen, J. B. Jørgensen, and S. Boyd. Fast nonconvex model predictive control for commercial refrigeration. *Nonlinear Model Predictice Control Conference*, 4:514–521, 2012.

[HPJJ10] J. K. Huusom, N. K. Poulsen, S. B. Jørgensen, and J. B. Jørgensen. Tuning of methods for offset free MPC based on ARX model representations. *American Control Conference*, pages 2255–2360, 2010.

[HPJJ12] J. K. Huusom, N. K. Poulsen, S. B. Jørgensen, and J. B. Jørgensen. Tuning SISO offset-free model predictive control based on ARX models. *Journal of Process Control*, 22(10):1997–2007, 2012.

[HPM+12] R. Halvgaard, N. K. Poulsen, H. Madsen, J. B. Jørgensen, F. Marra, and D. E. M. Bondy. Electric vehicle charge planning using economic model predictive control. *International Electric Vehicle Conference*, pages 1–6, 2012.

[JJ07a] J. B. Jørgensen and S. B. Jørgensen. Comparison of prediction-error–modelling criteria. *American Control Conference*, pages 140–146, 2007.

[JJ07b] J. B. Jørgensen and S. B. Jørgensen. MPC–relevant prediction-error identification. *American Control Conference*, pages 128–133, 2007.

[JKTM07] J. B. Jørgensen, M. R. Kristensen, P. G. Thomsen, and H. Madsen. A computationally efficient and robust implementation of the continuous–discrete extendedKalman filter. *American Control Conference*, pages 3706–3712, 2007.

[Jør05] J. B. Jørgensen. *Moving Horizon Estimation and Control*. PhD thesis, Technical University of Denmark, 2005.

[JRH11] J. B. Jørgensen, J. B. Rawlings, and J. K. Huusom. Finite horizon MPC for systems in innovation form. *Conference on Decision and Control*, pages 1896–1903, 2011.

[JRJ04] J. B. Jørgensen, J. B. Rawlings, and S. B. Jørgensen. Numerical methods for large scale moving horizon estimation and control. *International Symposium on Dynamics and Control Process Systems*, 2004.

[Kie97] F. Kieviet. *Modelling Quality in Spray Drying*. PhD thesis, Eindhoven University of Technology, 1997.

[KJTJ04] M. R. Kristensen, J. B. Jørgensen, P. G. Thomsen, and S. B. Jørgensen. An ESDIRK method with sensitivity analysis capabilities. *Computers and Chemical Engineering*, 28(12):2695–2707, 2004.

[KM07] J. Kent and J. McLeod. Spray-dryer optimization. `http://www.powderbulksolids.com/article/spray-dryer-optimization`, 2007. Accessed: 2016-06-09.

[KMJ04] N. R. Kristensen, H. Madsen, and S. B. Jørgensen. A method for systematic improvement of stochastic grey-box models. *Computers and Chemical Engineering*, 28(8):1431–1449, 2004.

[KP10] T. Kajiyama and K. J. Park. Influence of air parameters on spray drying energy consumption. *Revista Brasileira De Produtos Agroindustriais*, 12(1):45–54, 2010.

[Kud12] T. Kudra. Energy performance of convective dryers. *Drying Technology*, 30(11–12):1190–1198, 2012.

[Lar06] L. F. S. Larsen. *Model Based Control of Refrigeration Systems*. PhD thesis, Aalborg University, 2006.

[Lew21] W. K. Lewis. The rate of drying of solid materials. *Journal of Industrial and Engineering Chemistry*, 13:427–432, 1921.

[Mac02] J. M. Maciejowski. *Predictive Control: With Constraints*. Pearson Education. Prentice Hall, NJ, USA, 2002.

[Mal69] E. Malinvaud. First order certainty equivalence. *Econometrica*, 37(4):706, 1969.

[Mas02] K. Masters. *Spray Drying Handbook*. SprayDryConsult International ApS, Charlottenlund, Denmark, 2002.

[Mat15] MathWorks Inc. Matlab 8.6.0 (r2015b), 2015.

[MBF04] F. Martinsen, L. T. Biegler, and B. A. Foss. Application of optimization algorithms to nonlinear MPC. *Journal of Process Control*, 14(8):853–865, 2004.

[MCH10] Z. Ma, D. Callaway, and I. Hiskens. Decentralized charging control for large populations of plug-in electric vehicles: Application of the nash certainty equivalence principle. *International Conference on Control Applications*, pages 191–195, 2010.

[MRRS00] D. Q. Mayne, J. B. Rawlings, C. V. Rao, and P. O. M. Scokaert. Constrained model predictive control: Stability and optimality. *Automatica*, 36(6):789–814, 2000.

[Muj12] A. S. Mujumdar. *Industrial Transfer Processes.* dept. of Mechanical Engineering, National University of Singapore, City of Singapore, Singapore, 2012.

[Mur07] S. Murray. The world's biggest industry. *Forbes*, 2007.

[Nes09] Y. Nesterov. Primal-dual subgradient methods for convex problems. *Mathematical Programming*, 120(1):221–259, 2009.

[Nie13] P. S. Nielsen. Method of controlling a spray dryer apparatus by regulating an inlet air flow rate, and a spray dryer apparatus, 2013. US Patent App. 12/520,036. URL: `https://www.google.com/patents/US8402672`.

[NW06] J. Nocedal and S. J. Wright. *Numerical Optimization, 2nd edition.* Springer, NY, USA, 2006.

[OC05] D. O'Callaghan and P. Cunningham. Modern process control techniques in the production of dried milk products – a review. *Le Lait*, 85:335–342, 2005.

[ORR06] B. J. Odelson, M. R. Rajamani, and J. B. Rawlings. A new autocovariance least-squares method for estimating noise covariances. *Automatica*, 42(2):303–308, 2006.

[PCF95] J. R. Pérez-Correa and F. Farias. Modelling and control of a spray dryer: A simulation study. *Food Control*, 6(4):219–227, 1995.

[PCLA09] K. C. Patel, X. D. Chen, S. X. Q. Lin, and B. Adhikari. A composite reaction engineering approach to drying of aqueous droplets containing sucrose, maltodextrin (DE6) and their mixtures. *AIChE Journal*, 55(1):217–231, 2009.

[PEH+13] M. K. Petersen, K. Edlund, L. H. Hansen, J. Bendtsen, and J. Stoustrup. A taxonomy for modeling flexibility and a computationally efficient algorithm for dispatch in smart grids. *American Control Conference*, pages 1150–1156, 2013.

[PGA15] G. Pannocchia, M. Gabiccini, and A. Artoni. Offset-free MPC explained: Novelties, subtleties, and applications. *Conference on Nonlinear Model Predictive Control*, pages 342–351, 2015.

[PJ09] G. Prasath and J. B. Jørgensen. Soft constraints for robust MPC of uncertain systems. *International Symposium on Advanced Control of Chemical Processes*, pages 225–230, 2009.

[PR03] G. Pannocchia and J. B. Rawlings. Disturbance models for offset-free model predictive control. *AIChE Journal*, 49(2):426–437, 2003.

[QB03] S. J. Qin and T. A. Badgwell. A survey of industrial model predictive control technology. *Control Engineering Practice*, 11(7):733–764, 2003.

[RA09] J. B. Rawlings and R. Amrit. Optimizing process economic performance using model predictive control. *Lecture Notes in Control and Information Sciences*, 384:119–138, 2009.

[RAB12] J. B. Rawlings, D. Angeli, and C. N. Bates. Fundamentals of economic model predictive control. *Conference on Decision and Control*, pages 3851–3861, 2012.

[Raw00] J. B. Rawlings. Tutorial overview of model predictive control. *IEEE Control Systems*, 20(3):38–52, 2000.

[RJM09] S. Richter, C. N. Jones, and M. Morari. Real-time input-constrained MPC using fast gradient methods. *48th Conference on Decision and Control, held jointly with 28th Chinese Control Conference*, pages 7387–7393, 2009.

[RM09] J. B. Rawlings and D. Q. Mayne. *Model Predictive Control: Theory and design*. Nob Hill Pub. cop., WI, USA, 2009.

[Roc] Rockwell Automation. Advanced process control for improved yield and throughput. `https://www.rockwellautomation.com/resources/downloads/rockwellautomation/pdf/events/automation-fair/2012/psug/ed18-apcforimprovedyieldandthroughput_psug2012.pdf`. Accessed: 2016-06-09.

[RR09] M. R. Rajamani and J. B. Rawlings. Estimation of the disturbance structure from data using semidefinite programming and optimal weighting. *Automatica*, 45(1):142–148, 2009.

[RWR98] C. V. Rao, S. J. Wright, and J. B. Rawlings. Application of interior-point methods to model predictive control. *Journal of Optimization Theory and Applications*, 99(3):723–757, 1998.

[SB11] H. Schwartzbach and A. P. Birkmire. Controlled humidity drying, 2011. WO Patent App. PCT/DK2011/050,209. URL: `http://www.google.com/patents/WO2011154014A1`.

[SEJ15] L. E. Sokoler, K. Edlund, and J. B. Jørgensen. Application of economic MPC to frequency control in a single–area power system. *Conference on Decision and Control*, pages 2635–2642, 2015.

[SESJ13] L. E. Sokoler, K. Edlund, L. Standardi, and J. B. Jørgensen. A decomposition algorithm for optimal control of distributed energy system. *Innovative Smart Grid Technologies Europe*, pages 1–5, 2013.

[SH08] V. S. Shabde and K. A. Hoo. Optimum controller design for a spray drying process. *Control Engineering Practice*, 16(5):541–552, 2008.

[Sha06] V. S. Shabde. *Optimal design and control of a spray drying process that manufactures hollow micro-particles.* PhD thesis, Texas Tech University, 2006.

[Sko00] S. Skogestad. Plantwide control: The search for the self-optimizing control structure. *Journal of Process Control*, 10(5):487–507, 2000.

[Sko03] S. Skogestad. Simple analytic rules for model reduction and PID controller tuning. *Journal of Process Control*, 13(4):291–309, 2003.

[SMTR12] J. Stoustrup, S. A. Meybodi, F. Tahersima, and H. Rasmussen. Economic COP optimization of a heat pump with hierarchical model predictive control. *Conference on Decision and Control*, pages 7583–7588, 2012.

[SPJS13] L. Standardi, N. K. Poulsen, J. B. Jørgensen, and L. E. Sokoler. Computational efficiency of economic MPC for power systems operation. *Innovative Smart Grid Technologies Europe*, pages 1–5, 2013.

[SSBM05] M. Schlegel, K. Stockmann, T. Binder, and W. Marquardt. Dynamic optimization using adaptive control vector parameterization. *Computers and Chemical Engineering*, 29(8):1731–1751, 2005.

[SSF+13] L. E. Sokoler, A. Skajaa, G. Frison, R. Halvgaard, and J. B. Jørgensen. A warm-started homogeneous and self-dual interior-point method for linear economic model predictive control. *Conference on Decision and Control*, pages 3677–3683, 2013.

[Sta15] L. Standardi. *Economic Model Predictive Control for Large-Scale and Distributed Energy Systems*. PhD thesis, Technical University of Denmark, 2015.

[The57] H. Theil. A note on certainty equivalence in dynamic planning. *Econometrica*, 25(2):346–349, 1957.

[TIKT11] L. W. Tan, M. N. Ibrahim, R. Kamil, and F. S. Taip. Empirical modeling for spray drying process of sticky and non-sticky products. *Procedia Food Science*, 1:690–697, 2011.

[TTA09] L. W. Tan, F. S. Taip, and N. A. Aziz. Simulation and control of spray drying using nozzle atomizer spray dryer. *International Journal of Engineering and Technology*, 9(10):1–7, 2009.

[Vai] Vaisala. +20% increase in production capacity with zero increase in energy consumption. `http://www.vaisala.com/VaisalaDocuments/SuccessStories/CEN-TIA-G-Valio-Customer-Story-B211288EN-A.pdf`. Accessed: 2014-02-12.

[VdJ03] R. E. M. Verdurmen and P. de Jong. Optimising product quality and process control for powdered dairy products. *Dairy Processing: Improving Quality*, pages 333–365, 2003.

[VFF15] G. N. A. Vieira, F. B. Freire, and J. T. Freire. Control of the moisture content of milk powder produced in a spouted bed dryer using a grey–box inferential controller. *Drying Technology*, 33(15–16):1920–1928, 2015.

[VJTS10] C. Völcker, J. B. Jørgensen, P. G. Thomsen, and E. H. Stenby. Adaptive step size control in implicit Runge–Kutta methods for reservoir simulation. *International Symposium on Dynamics and Control of Process Systems*, pages 509–514, 2010.

[WB10] Y. Wang and S. P. Boyd. Fast model predictive control using online optimization. *Transactions on Control Systems Technology*, 18(2), 2010.

[WDM+08a] M. W. Woo, W. R. W. Daud, A. S. Mujumdar, M. Z. M. Talib, W. Z. Hua, and S. M. Tasirin. Comparative study of droplet drying models for CFD modelling. *Chemical Engineering Research and Design*, 86(9):1038–1048, 2008.

[WDM+08b] M. W. Woo, W. R. W. Daud, A. S. Mujumdar, Z. Wu, M. Z. M. Talib, and S. M. Tasirin. CFD evaluation of droplet drying models in a spray dryer fitted with a rotary atomizer. *Drying Technology*, 26:1180–1198, 2008.

[Wit71] H. S. Witsenhausen. Separation of estimation and control for discrete time systems. *IEEE*, 59(11):1557–1566, 1971.

[Wri97] S. Wright. Applying new optimization algorithms to model predictive control. *International Conference on Chemical Process Control*, pages 147–155, 1997.

[YSW01] H. Yang, N. Sakai, and M. Watanabe. Drying model with noniisotropic shrinkage deformation undergoing simultaneous heat and mass transfer. *Drying Technology*, 19(7):1441–1460, 2001.

[ZGD13] M. Zanon, S. Gros, and M. Diehl. A lyapunov function for periodic economic optimizing model predictive control. *Conference on Decision and Control*, pages 5107–5112, 2013.

[ZGS+88] I. Zbicinski, S. Grabowski, C. Strumillo, L. Kiraly, and W. Krzanowski. Mathematical modelling of spray drying. *Computers and Chemical Engineering*, 12(2–3):209–214, 1988.

[ZPC91] C. A. Zaror and J. R. Pérez-Correa. Model based control of centrifugal atomizer spray drying. *Food Control*, 2(3):170–175, 1991.

Appendix A

Experiment Data

A.1 Estimation Experiment

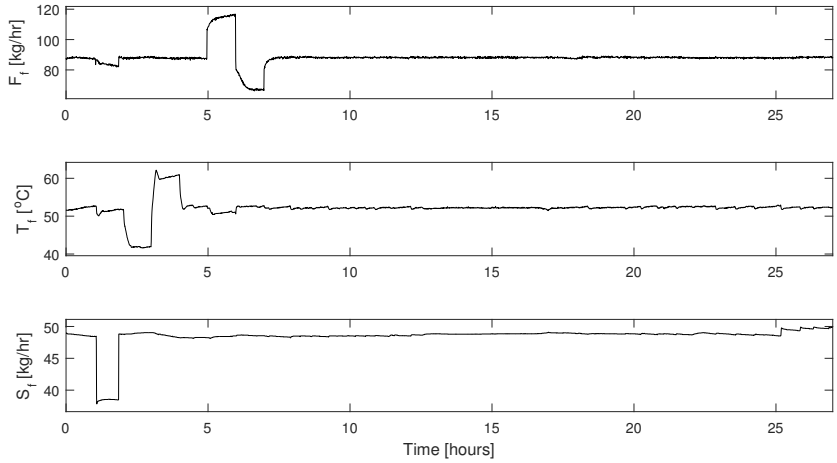

Figure A.2: The input vector, u, for the feed inlet.

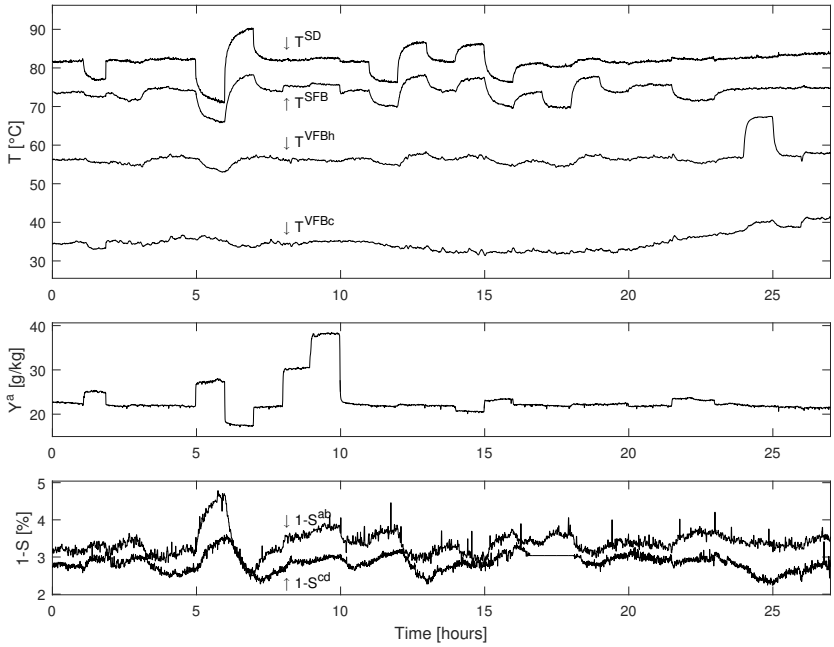

Figure A.1: The measurement vector, y.

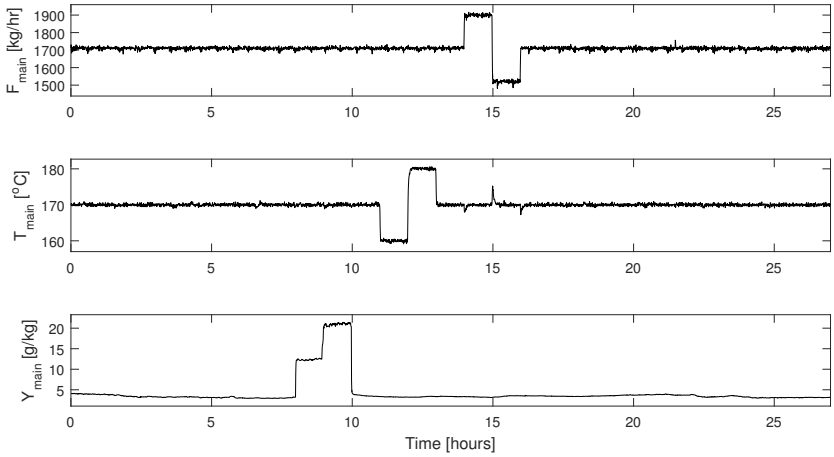

Figure A.3: The input vector, u, for the main air inlet.

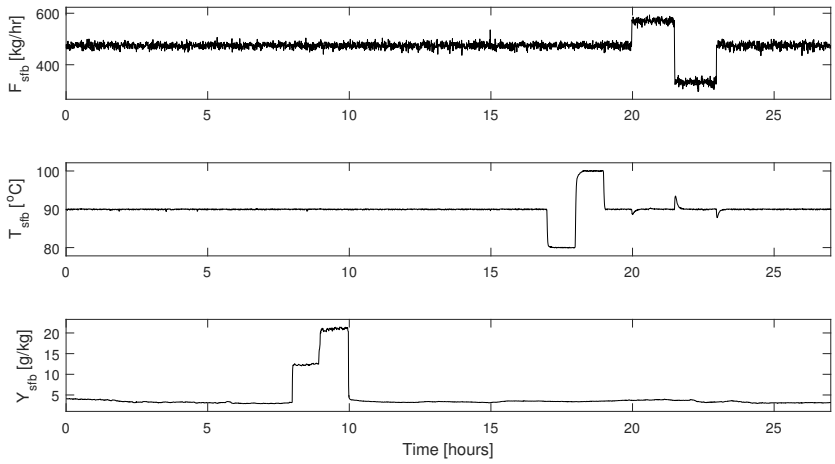

Figure A.4: The input vector, u, for the sfb air inlet.

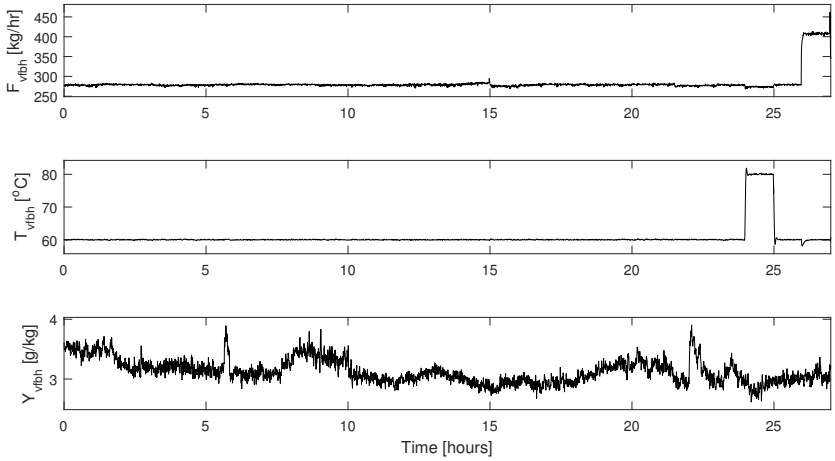

Figure A.5: The input vector, u, for the vfbh air inlet.

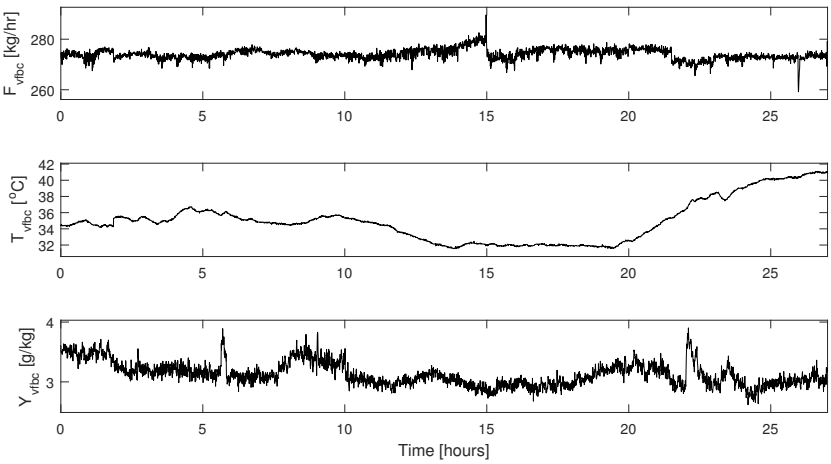

Figure A.6: The input vector, u, for the vfbc air inlet.

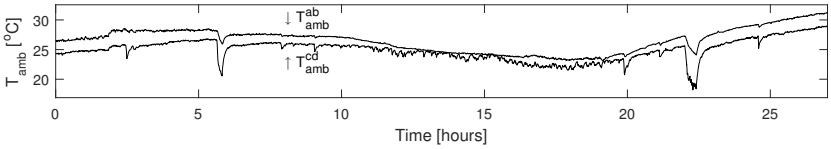

Figure A.7: The disturbance vector, d.

A.2 Validation Experiment

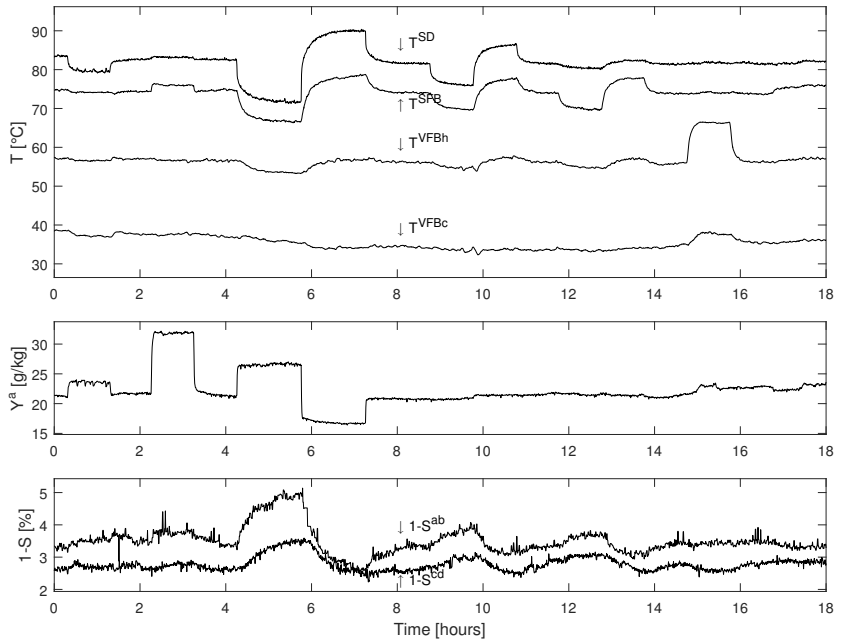

Figure A.8: The measurement vector, y.

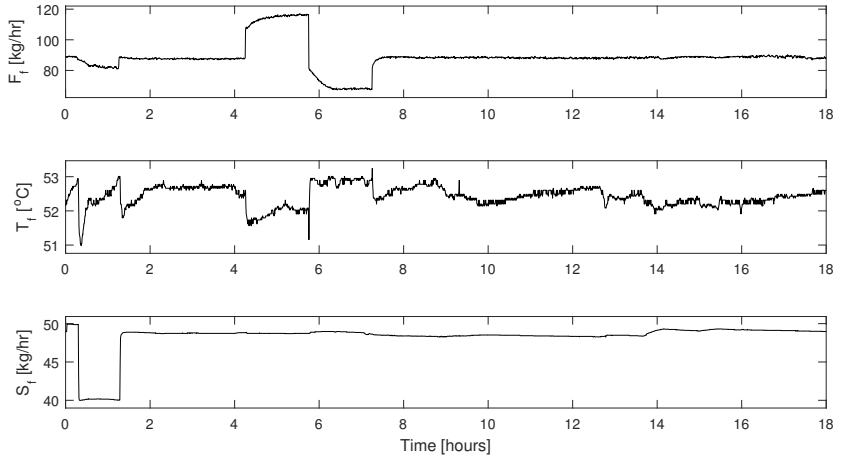

Figure A.9: The input vector, u, for the feed inlet.

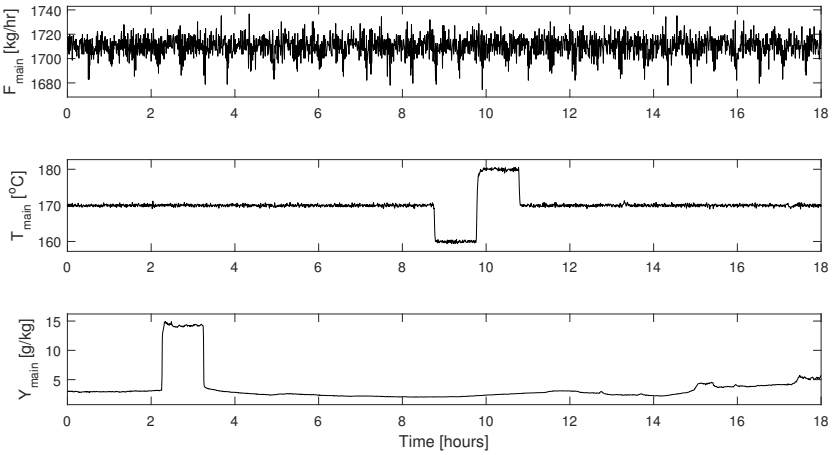

Figure A.10: The input vector, u, for the main air inlet.

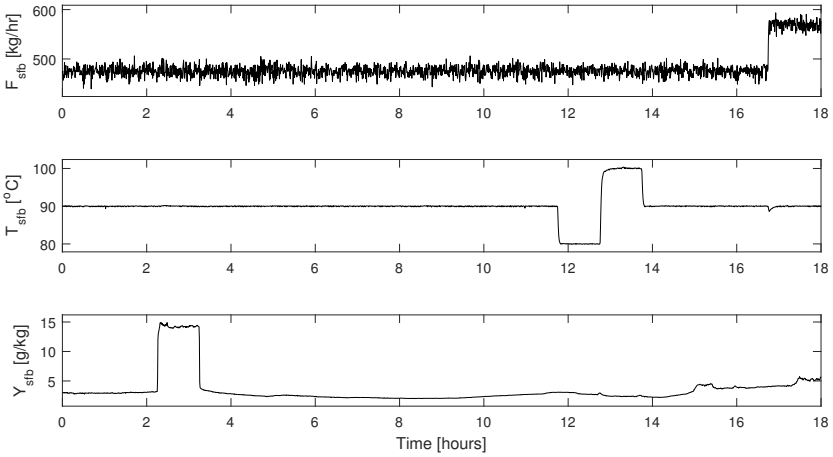

Figure A.11: The input vector, u, for the sfb air inlet.

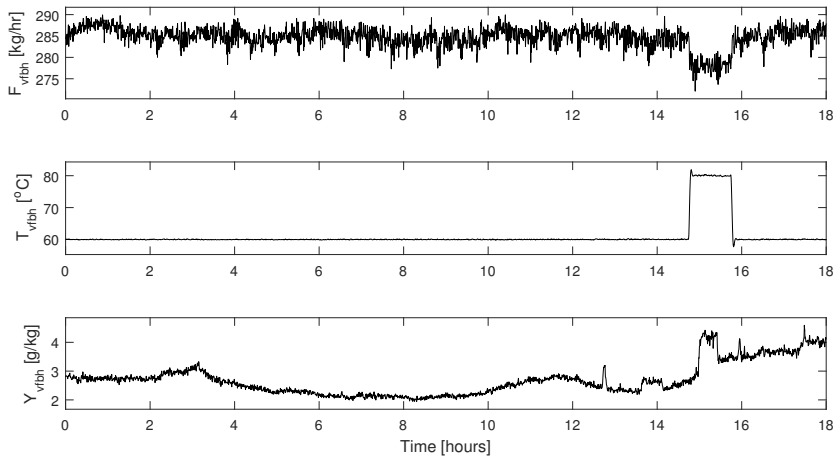

Figure A.12: The input vector, u, for the vfbh air inlet.

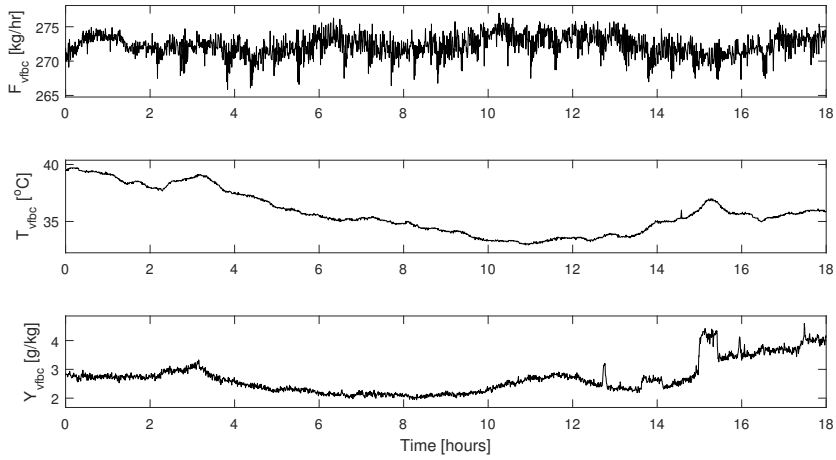

Figure A.13: The input vector, u, for the vfbc air inlet.

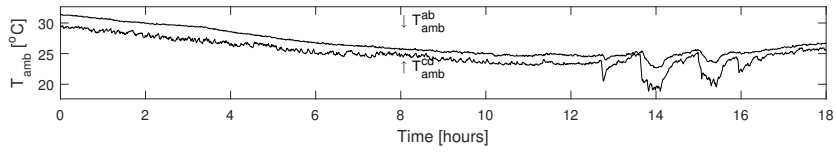

Figure A.14: The disturbance vector, d.

Part II

Papers

Paper A

An experimentally validated simulation model for a four stage spray dryer

---

Submitted to *Journal of Process Control, 2016*.

An experimentally validated simulation model for a four-stage spray dryer

Lars Norbert Petersen[a,b], Niels Kjølstad Poulsen[a], Hans Henrik Niemann[c], Christer Utzen[b], John Bagterp Jørgensen[a,*]

[a]*Department of Applied Mathematics and Computer Science, Technical University of Denmark, DK-2800 Kgs. Lyngby, Denmark*
[b]*GEA Process Engineering A/S, DK-2860 Søborg, Denmark*
[c]*Department of Electrical Engineering, Technical University of Denmark, DK-2800 Kgs. Lyngby, Denmark*

Abstract

In this paper, we develop a dynamic model of an industrial type medium size four-stage spray dryer. The purpose of the model is to enable simulations of the spray dryer at different operating points, such that the model facilitates development and comparison of control strategies. The dryer is divided into four consecutive stages: a primary spray drying stage, two heated fluid bed stages, and a cooling fluid bed stage. Each of these stages in the model is assumed ideally mixed and the dynamics are described by mass- and energy balances. These balance equations are coupled with constitutive equations such as the water evaporation rate, the heat transfer rates, and an equation for the stickiness of the powder (glass transition temperature). Laboratory data is used to model the equilibrium moisture content and the glass transition temperature of the powder. The resulting mathematical model is an index-1 differential algebraic equation (DAE) model with 12 states, 9 inputs, 8 disturbances, and 30 parameters. The parameters in the model are identified from well-excited experimental data obtained from the industrial type spray dryer. The simulated outputs of the model are validated using independent well-excited experimental data from the same spray dryer. The simulated temperatures, humidities, and residual moistures in the spray dryer compare well to the validation data. The model also provides the profit of operation, the production rate, the energy consumption, and the energy efficiency. In addition, it computes stickiness of the powder in different stages of the spray dryer. These facilities make the model well suited as a simulation model for comparison of the process economics associated to different control strategies.

Keywords: Spray drying, Multi-stage dryer, Process simulation, Process modeling, Experimental data

1. Introduction

Spray drying is a processing technique for drying of liquids or slurries. A spray dryer produces a free flowing powder. Spray drying is widely used in the food, chemical and pharmaceutical industries [1]. The main purpose of drying foodstuffs is to increase the shelf life as well as to reduce cost of transportation over long distances. Examples of spray dried foods are instant coffee, coffee whitener, eggs, milk, soups, baby foods, sweeteners, and cheese in powdered form [2]. Also, many powders occur in cooking. Chemicals are often dried to form non-dusty agglomerates that are easier to handle. These may be agrochemicals used in cultivation as well as optical brighteners used in households and many more. Pharmaceuticals are dried for the production of tablets. Aspirin, paracetamol and vitamins are typical examples.

In this paper, we consider a spray dryer with both an integrated and an external fluid bed. This is the preferred type of dryer for production of food powders. It provides product flexibility and the best energy efficiency compared to other spray dryers. It is a challenge and non-trivial to operate a spray dryer in an optimal way. One must maximize energy efficiency and production while minimizing down time [3]. These two goals are often conflicting, as increased production and efficiency may lead to an increase in the hours lost on process-related problems such as plugging, powder build-up, cleaning in place (CIP), etc. Constantly changing external disturbances, such as the ambient air humidity and feed composition, are the main reason that the powder turn sticky and deposits starts to build up on the dryer walls. The operator must perform frequent adjustments to the spray dryer to avoid depositions. These adjustments are hardly ever performed, as the operator have other important tasks to perform. Instead the spray dryer is operated in a conservative non-optimal way. Thus, automatic control systems to perform the adjustments are needed. To facilitate development of automatic control systems, a dynamic model is desirable to simulate the spray drying process and compare control algorithms in terms of economically related key performance indicators.

1.1. Process description

Fig. 1 illustrates a modern four-stage spray dryer with an integrated (static) fluid bed and an external (vibrating) fluid bed. The spray dryer consists of the primary spray drying stage (SD), the static fluid bed stage (SFB), the hot vibrating fluid bed stage (VFBh), and the cold vibrating fluid bed stage (VFBc). The main hot air is let into the upper section of the primary

*Corresponding author
Email addresses: lnpe@dtu.dk (Lars Norbert Petersen), nkpo@dtu.dk (Niels Kjølstad Poulsen), hhn@elektro.dtu.dk (Hans Henrik Niemann), christer.utzen@gea.com (Christer Utzen), jbjo@dtu.dk (John Bagterp Jørgensen)

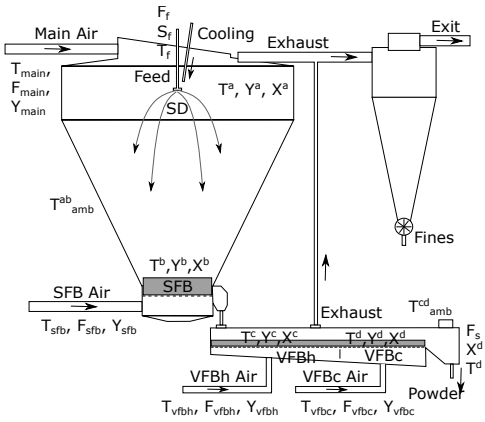

Figure 1: Principle diagram of the four-stage spray dryer with both an integrated fluid bed and an external fluid bed.

spray drying stage (SD) around the high pressure nozzles. The nozzles disperse the liquid feed into droplets. The heat is transferred from the hot air to the droplets. Due to this heat transfer, water evaporates from the droplets. In that process, the air temperature and the residual moisture of the droplets decrease. During drying, there is a transfer of evaporated water from the droplets to the air in the dryer. The rate of this transfer depends on the type and composition of the feed, the air temperature, the air humidity inside the dryer, and the air pressure. The dried product then enters the SFB and is dried further while being fluidized by hot air. After drying in the SFB, the powder is transported to the external vibrating fluid bed (VFB) for gentle drying and cooled to the temperature desired for handling and storage. The drying air from the chamber and VFB is passed through a cyclone, separating the powder contained in the air. The fine powder is returned to the chamber to form agglomerated powder particles. The air is also passed through a bag filter, not shown in Fig. 1, to remove any particles left before the air can be discharged.

1.2. Available mathematical models of spray dryers

Mathematical models of spray dryers exist as detailed computational fluid dynamics (CFD) models for static design oriented simulation [4–6], and as models for dynamic simulation. The models for dynamic simulation are linear models for control design that are also used for closed-loop simulation [7–9] and lumped first-principles engineering models [10–15]. The purpose of the dynamic simulation models is often to facilitate analysis and synthesis of advanced control schemes.

Clarke [7] designs a Generalized Predictive Controller (GPC) for a spray dryer and base the controller on the CARIMA model, but does not provide a simulation model. Tan *et al* [8, 9] provide continuous transfer functions of first order with a delay that they use for controller design as well as closed loop simulation. They report models for spray drying of full cream milk [8] as well as spray drying of whole milk and orange juice [9].

A lumped first-principles model of a single stage spray dryer is developed in [10, 11]. Mass and energy balances describe air temperature, the mean particle size and the residual moisture content of the powder. A mathematical model based on mass, energy and momentum equations are formulated and solved in [12]. The model describes the moisture content and particle size of a single spray dried powder particle. In [13] a dynamic model of a single stage spray dryer is developed from first-principles and is validated experimentally to assist in control simulation studies. The model simulates the moisture content and particle size of the powder as well as the exhaust air temperature and humidity. Reference [14] extends the model in [13] by adding variable inlet droplet size and density of the milk powder particles. Reference [15] develops a single stage dynamic model for the simulation of the residual moisture control and air temperatures in an industrial detergent spray drying process. The above first-principles models simulate single stage spray dryers. Four-stage spray dryer models are available [16, 17]. Reference [16] describes the air temperatures inside the dryer, the final residual moisture content, and the particle size of the produced powder. Powder residual moisture sensors are often not available. Therefore, the above models are based on irregularly sampled off-line laboratory measurements of the residual moisture. Reference [17] describes a lumped first-principles model for a four-stage spray dryer that is validated against in-line powder samples and describes the air temperature, air humidity and residual moisture content of the powder.

1.3. Key contributions

The novelties of the model proposed in this paper are: 1) It is an experimentally validated dynamic model that enables simulation of the four-stage spray dryer at different operating points. The model is a first-principles engineering model and is divided into an SD, an SFB, a VFBh, and a VFBc stage. Each stage describes the evolution of the temperatures, the air humidities as well as the residual moistures of the powder. The model is validated against an experiment with in-line measurements of the residual moisture content of the powder; 2) It provides the key performance indicators such as the profit of operation, the production rate, the energy consumption rate, and the energy efficiency; 3) It offers stickiness constraints of the powder in each stage of the spray dryer.

To the authors knowledge, there does not exist such a dynamic model for simulation of the four-stage spray dryer that is experimentally validated, provides key economic performance indicators, and stickiness constraints. These facilities make the model well suited as a simulation model for comparison of the process economics associated to different control strategies.

1.4. Organization

The paper is organized as follows. Section 2 presents the model. Identification of the model parameters is described in Section 3. Section 4 validates the model using independent experimental data. Simulations with the model are performed in Section 5. Section 5 also reports the simulated stickiness constraints and the key performance indicators. Conclusions are provided in Section 6.

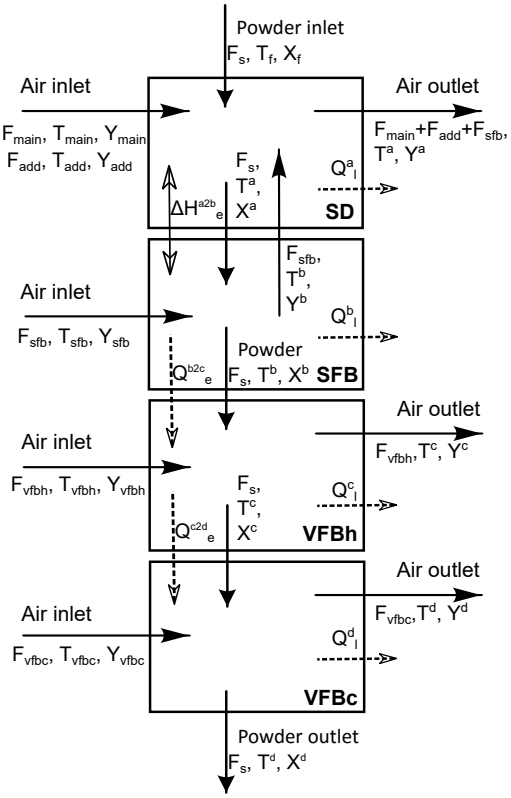

Figure 2: Diagram of the inflows and outflows of air and powder to the stages of the four-stage spray dryer. The diagram also shows the energy exchange.

2. The four-stage spray dryer model

In this section, we derive the four-stage spray dryer model from first engineering principles [18, 19]. The dryer considered in this paper is the GEA Niro Multi-Stage Dryer size 20 (MSD^{TM}-20) operating at standard conditions with a single spray nozzle. The model and experiments are based on drying of Maltodextrin DE-18. Maltodextrin is a starch based polysaccharide that is used as a food additive. Maltodextrin DE-18 is used because the feed can be re-wetted and the composition is well defined.

To simplify the notation, we refer to the SD, SFB, VFBh and VFBc stages by the superscript a, b, c and d. Fig. 1 illustrates the spray drying process and provides the notation for the inputs, the disturbances and the states. Fig. 2 shows a diagram of the mass and energy connections in the model. The diagram illustrates the inflows and outflows of air, powder and energy in the SD, SFB, VFBh and VFBc stages. Fig. 3 illustrates the mass and energy flows used in the modeling of each stage. Altogether, Fig. 1- 3 provide an overview of the symbols and naming convention used for the mathematical model of the four-stage spray dryer.

Mass balances for powder moisture (water in the powder) and

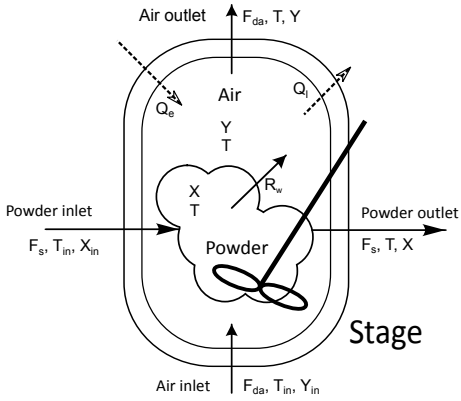

Figure 3: Sketch of a general single stage. The three states, X, Y and T are shown along with the inlet and outlet flows of product and air steams. The flows are given as dry mass flows.

water in the vapor phase as well as an energy balance constitute the conservation equations of the model for each stage of the spray dryer. The constitutive equations are the evaporation rate of water and the heat flow equations. The evaporation rate of water from the powder depends on two properties: the diffusion coefficient and the equilibrium moisture. We provide models for these properties.

2.1. Assumptions

To simplify the modeling of the complex phenomena of drying we apply the following assumptions

A1 The air is an ideal gas and satisfies the ideal gas law.

A2 The hold-ups of dry air and solid powder are constant. This is a good approximation for continuous operation.

A3 The pressure in the dryer is constant and equal to the standard atmospheric pressure.

A4 The stages are assumed well stirred, i.e. the temperature of the stage air and powder are identical within each stage.

A5 The kinetic and potential energy of the powder and the air are negligible compared to the internal energy.

2.2. SD stage

The evolution of the powder moisture content, X^a, the air humidity, Y^a, and the temperature, T^a, in the SD stage are determined by the conservation equations

$$\frac{dm^a_w}{dt} = \overbrace{X_f F_s}^{\text{water in}} - \overbrace{X^a F_s}^{\text{water out}} - \overbrace{R^a_w}^{\text{water evaporation rate}} \tag{1a}$$

$$\frac{dm^a_v}{dt} = \overbrace{Y_{\text{main}} F_{\text{main}} + Y_{\text{add}} F_{\text{add}} + Y^b F_{\text{sfb}}}^{\text{vapor in inlet air}} - \overbrace{Y^a (F_{\text{main}} + F_{\text{add}} + F_{\text{sfb}})}^{\text{vapor in outlet air}} + \overbrace{R^a_w}^{\text{water evaporation rate}} \tag{1b}$$

$$\frac{dU^a}{dt} = \overbrace{h_{a,\text{main}}F_{\text{main}} + h_{a,\text{add}}F_{\text{add}} + h_a^b F_{\text{sfb}}}^{\text{enthalpy of inlet air}} - \overbrace{h_a^a(F_{\text{main}} + F_{\text{sfb}} + F_{\text{add}})}^{\text{enthalpy of outlet air}} + \overbrace{(h_{p,f} - h_p^a)F_s}^{\text{enthalpy of powder flows}} - \overbrace{\Delta H_e^{a2b}}^{\text{enthalpy of mass exchange}} - \overbrace{Q_l^a}^{\text{heat loss}} \tag{1c}$$

where the state variables are the functions

$$m_w^a = X^a m_s^a \tag{2a}$$
$$m_v^a = Y^a m_{da}^a \tag{2b}$$
$$U^a = m_{da}^a(h_a^a - RT^a) + m_s^a h_p^a + m_m^a h_m^a \tag{2c}$$

The mass balance (1a) governs the amount of water in the powder, m_w^a, and (1b) governs the amount of vapor, m_v^a, in the air. The energy balance (1c) governs the accumulated heat, U^a, in the stage. $F_s = F_f S_f$ is the flow of feed solids, $X_f = (1 - S_f)/S_f$ is the dry base feed concentration. R_w^a is the evaporation rate that describes the flow of evaporated water from the powder to the vapor. Y_{main}, Y_{add} and Y^b are the vapor concentration of the main air inlet, the un-modeled air sources, and the SFB stage air outlet, respectively. F_{main}, F_{add} and F_{sfb} are dry base inlet air flows to the stage from the main air inlet, un-modeled air sources, and the SFB stage air outlet, respectively. The relation between humid and dry air flows as well as product flow and product/feed solid flow are given in Appendix A. $h_{a,\text{main}} = h_a(Y_{\text{main}}, T_{\text{main}})$, $h_{a,\text{add}} = h_a(Y_{\text{add}}, T_{\text{add}})$ and $h_a^b = h_a(Y^b, T^b)$ are specific enthalpies of the inlet air flows to the stage. $h_a^a = h_a(Y^a, T^a)$ is the specific enthalpy of the outlet air from the stage. The specific enthalpies of the powder inlet is $h_{p,f} = h_p(X_f, T_f)$ and the powder outlet is $h_p^a = h_p(X^a, T^a)$. T_f is the feed temperature. T_{main}, T_{add} and T^b are temperatures of the inlet air flows. The specific enthalpy is calculated as described in Appendix B. The enthalpies describe the heat exchange due to the flow of mass, i.e. air flows and powder flows. $m_{da}^a = 10$ kg is the mass of dry air, m_s^a is the mass of solids and m_m^a is the mass of metal.

The constitutive equations below defines the relations in the conservation equations. Q_l^a is the heat loss to the surroundings and is modeled by

$$Q_l^a = k_{\text{UA}}^a(T^a - T_{\text{amb}}^{ab}) \tag{3a}$$

in which T_{amb}^{ab} denotes the ambient air temperature. A proportion of the powder in the SFB stage is blown off the fluid bed and back into the SD stage. Thus, there is an exchange of heat and mass. We model this phenomenon in a simplified manner considering the enthalpy of mass exchange only. The enthalpy of mass exchange, ΔH_e^{a2b}, is described by

$$\Delta H_e^{a2b} = k_1(T^a - T^b)F_s + k_2 X_f + k_3 T_f - k_4 \tag{3b}$$

This enthalpy of mass exchange is composed of an enthalpy relation, $k_1(T^a - T^b)F_s$, where k_1 is a heat capacity term, and linear terms to compensate for the dependency on the feed composition. We neglect the heat transfer due to conduction, Q_e^{a2b}, in this stage as it is small compared to ΔH_e^{a2b}.

The product drying rate is governed by the thin layer equation. The thin layer equation models evaporation as a diffusion process [20]

$$R_w^a = k_1^a D_w(X^a - X_{\text{eq}})m_s^a \tag{3c}$$

X^a is the stage moisture content and $X_{\text{eq}} = X_{\text{eq}}(T^a, Y^a)$ is the equilibrium moisture content. The free moisture content, $X^a - X_{\text{eq}}$, describes the moisture content that are free to evaporate. This expression renders a lower bound on the possible moisture removal. The diffusion coefficient, $D_w = D_w(T^a, X^a)$, describes the friction of evaporation and depends on the product being dried [21, 22].

The parameters that are to be identified are k_1^a, k_2^{ab}, k_3^{ab}, k_{UA}^a, k_1, k_2, k_3, k_4, m_m^a, m_s^a, F_{add}, T_{add} and Y_{add}.

2.3. SFB stage

The evolution of the powder moisture content, X^b, the air humidity, Y^b, and the temperature, T^b, in the SFB stage are determined by the conservation equations

$$\frac{dm_w^b}{dt} = \overbrace{X^a F_s}^{\text{water in}} - \overbrace{X^b F_s}^{\text{water out}} - \overbrace{R_w^b}^{\text{water evaporation rate}} \tag{4a}$$

$$\frac{dm_v^b}{dt} = \overbrace{Y_{\text{sfb}}F_{\text{sfb}}}^{\text{vapor in inlet air}} - \overbrace{Y^b F_{\text{sfb}}}^{\text{vapor in outlet air}} + \overbrace{R_w^b}^{\text{water evaporation rate}} \tag{4b}$$

$$\frac{dU^b}{dt} = \overbrace{(h_{a,\text{sfb}} - h_a^b)F_{\text{sfb}}}^{\text{enthalpy of air flows}} + \overbrace{(h_p^a - h_p^b)F_s}^{\text{enthalpy of powder flows}} + \overbrace{\Delta H_e^{a2b}}^{\text{enthalpy of mass exchange}} - \overbrace{Q_e^{b2c}}^{\text{heat exchange}} - \overbrace{Q_l^b}^{\text{heat loss}} \tag{4c}$$

where the state variables are the functions

$$m_w^b = m_s^b X^b \tag{5a}$$
$$m_v^b = m_{da}^b Y^d \tag{5b}$$
$$U^b = m_{da}^b(h_a^b - RT^b) + m_s^b h_p^b + m_m^b h_m^b \tag{5c}$$

The mass balance (4a) governs the amount of water in the powder, m_w^b, and (4b) governs the amount of vapor, m_v^b, in the air. The energy balance (4c) governs the accumulated heat, U^b, in the stage. F_{sfb} is the dry base inlet air flow and Y_{sfb} is the air humidity of the inlet air flow. $h_{a,\text{sfb}} = h_a(Y_{\text{sfb}}, T_{\text{sfb}})$ is the specific enthalpy of the inlet air flow and $h_a^b = h_a(Y^b, T^b)$ is the specific enthalpy of the outlet air flow of the SFB stage. The specific enthalpies of the powder inlet and outlet are $h_p^a = h_p(X^a, T^a)$ and $h_p^b = h_p(X^b, T^b)$. T_{sfb} is the inlet air temperature. $m_{da}^b = 0.5$ kg is the mass of dry air, m_s^b is the mass of solids and m_m^b is the mass of metal.

Next we provide the constitutive equations for the SFB stage. The term

$$Q_e^{b2c} = k_5(T^b - T^c) \tag{6a}$$

describes the heat exchange between the SFB stage and the VFBh stage. The conductive heat loss to the surroundings is modeled as

$$Q_l^b = k_{\mathrm{UA}}^b (T^b - T_{\mathrm{amb}}^{ab}) \tag{6b}$$

The product drying rate is governed by

$$R_w^b = k_1^b D_w (X^b - X_{\mathrm{eq}}) m_s^b \tag{6c}$$

$X_{\mathrm{eq}} = X_{\mathrm{eq}}(T^b, Y^b)$ is the equilibrium moisture content and $D_w = D_w(T^b, X^b)$ is the diffusion coefficient.

The parameters that are to be identified are k_1^b, k_{UA}^b, k_5, m_m^b and m_s^b.

2.4. VFBh stage

The evolution of the powder moisture content, X^c, the air humidity, Y^c, and the temperature, T^c, in the VFBh stage are determined by the conservation equations

$$\frac{dm_w^c}{dt} = \overbrace{X^b F_s}^{\text{water in}} - \overbrace{X^c F_s}^{\text{water out}} - \overbrace{R_w^c}^{\text{water evaporation rate}} \tag{7a}$$

$$\frac{dm_v^c}{dt} = \overbrace{Y_{\mathrm{vfbh}} F_{\mathrm{vfbh}}}^{\text{vapor in inlet air}} - \overbrace{Y^c F_{\mathrm{vfbh}}}^{\text{vapor in outlet air}} + \overbrace{R_w^c}^{\text{water evaporation rate}} \tag{7b}$$

$$\frac{dU^c}{dt} = \overbrace{(h_{a,\mathrm{vfbh}} - h_a^c) F_{\mathrm{vfbh}}}^{\text{enthalpy of air flows}} + \overbrace{(h_p^b - h_p^c) F_s}^{\text{enthalpy of powder flows}} + \overbrace{Q_e^{b2c} - Q_e^{c2d}}^{\text{heat exchange}} - \overbrace{Q_l^c}^{\text{heat loss}} \tag{7c}$$

where the state variables are the functions

$$m_w^c = m_s^c X^c \tag{8a}$$

$$m_v^c = m_{da}^c Y^c \tag{8b}$$

$$U^c = m_{da}^c (h_a^c - R T^c) + m_s^c h_p^c + m_m^c h_m^c \tag{8c}$$

The mass balance (7a) governs the amount of water in the powder, m_w^c, and (7b) governs the amount of vapor, m_v^c, in the air. The energy balance (7c) governs the accumulated heat, U^c, in the stage. F_{vfbh} is the dry base inlet air flow and Y_{vfbh} is the air humidity of the inlet air flow. $h_{a,\mathrm{vfbh}} = h_a(Y_{\mathrm{vfbh}}, T_{\mathrm{vfbh}})$ is the specific enthalpy of the inlet air flow and $h_a^c = h_a(Y^c, T^c)$ is at the specific enthalpy of the outlet air flow of the VFBh stage. The specific enthalpies of the powder inlet and outlet are $h_p^b = h_p\left(X^b, T^b\right)$ and $h_p^c = h_p(X^c, T^c)$. T_{vfbh} is the inlet air temperature. $m_{da}^c = 0.5$ kg is the mass of dry air, m_s^c is the mass of solids and m_m^c is the mass of metal.

Next we describe the constitutive equations of the VFBh stage. The heat conductions are

$$Q_e^{c2d} = k_6 (T^c - T^d) \tag{9a}$$

$$Q_l^c = k_{\mathrm{UA}}^c (T^c - T_{\mathrm{amb}}^{cd}) \tag{9b}$$

Q_e^{c2d} describes the heat exchange between the VFBh stage and the VFBc stage. Q_l^c is the heat loss to the surroundings in which T_{amb}^{cd} is the ambient air temperature. The product drying rate is governed by

$$R_w^c = k_1^c D_w (X^c - X_{\mathrm{eq}}) m_s^c \tag{9c}$$

$X_{\mathrm{eq}} = X_{\mathrm{eq}}(T^c, Y^c)$ is the equilibrium moisture content and $D_w = D_w(T^c, X^c)$ is the diffusion coefficient.

The parameters that are to be identified are k_1^c, k_2^{cd}, k_3^{cd}, k_{UA}^c, k_6, m_m^c and m_s^c.

2.5. VFBc stage

The evolution of the powder moisture content, X^d, the air humidity, Y^d, and the temperature, T^d, in the VFBc stage are determined by the conservation equations

$$\frac{dm_w^d}{dt} = \overbrace{X^c F_s}^{\text{water in}} - \overbrace{X^d F_s}^{\text{water out}} - \overbrace{R_w^d}^{\text{water evaporation rate}} \tag{10a}$$

$$\frac{dm_v^d}{dt} = \overbrace{Y_{\mathrm{vfbc}} F_{\mathrm{vfbc}}}^{\text{vapor in inlet air}} - \overbrace{Y^d F_{\mathrm{vfbc}}}^{\text{vapor in outlet air}} + \overbrace{R_w^d}^{\text{water evaporation rate}} \tag{10b}$$

$$\frac{dU^d}{dt} = \overbrace{(h_{a,\mathrm{vfbc}} - h_a^d) F_{\mathrm{vfbc}}}^{\text{enthalpy of air flows}} + \overbrace{(h_p^c - h_p^d) F_s}^{\text{enthalpy of powder flows}} + \overbrace{Q_e^{c2d}}^{\text{heat exchange}} - \overbrace{Q_l^d}^{\text{heat loss}} \tag{10c}$$

where the state variables are the functions

$$m_w^d = m_s^d X^d \tag{11a}$$

$$m_v^d = m_{da}^d Y^d \tag{11b}$$

$$U^d = m_{da}^d (h_a^d - R T^d) + m_s^d h_p^d + m_m^d h_m^d \tag{11c}$$

The mass balance (10a) governs the amount of water in the powder, m_w^d, and (10b) governs the amount of vapor, m_v^d, in the air. The energy balance (10c) governs the accumulated heat, U^d, in the stage. F_{vfbc} is the dry base inlet air flow and Y_{vfbc} is the air humidity of the inlet air stream. $h_{a,\mathrm{vfbc}} = h_a(Y_{\mathrm{vfbc}}, T_{\mathrm{vfbc}})$ is the specific enthalpy of the inlet air flow and $h_a^d = h_a\left(Y^d, T^d\right)$ is the specific enthalpy of the outlet air flow of the VFBc stage. The specific enthalpies of the powder inlet and outlet are $h_p^c = h_p(X^c, T^c)$ and $h_p^d = h_p\left(X^d, T^d\right)$. T_{vfbc} is the inlet air temperature. $m_{da}^d = 0.5$ kg is the mass of dry air, m_s^d is the mass of solids, and m_m^d is the mass of metal.

The heat conduction and the evaporation rate are the constitutive equations of the VFBc stage. The heat conduction is

$$Q_l^d = k_{\mathrm{UA}}^d (T^d - T_{\mathrm{amb}}^{cd}) \tag{12a}$$

where Q_l^d is the heat loss to the surroundings. The product drying rate is governed by the evaporation rate

$$R_w^d = k_1^d D_w (X^d - X_{\mathrm{eq}}) m_s^d \tag{12b}$$

$X_{\mathrm{eq}} = X_{\mathrm{eq}}(T^d, Y^d)$ is the equilibrium moisture content and $D_w = D_w(T^d, X^d)$ is the diffusion coefficient.

The parameters that are to be identified are k_1^d, k_{UA}^d, m_m^d and m_s^d.

2.6. Diffusion coefficient

The diffusion coefficient, D_w, describes the friction of evaporation and depends on the product being dried [21, 22]. D_w contains an Arrhenius like relation to compensate for temperature dependencies and is a function of the residual moisture. Consequently, the diffusion coefficient is described by

$$D_w(T, X) = \exp\left(-\frac{c_1}{R}\left(\frac{1}{T} - \frac{1}{T_0}\right)\right)\frac{X}{c_2 + X} \tag{13}$$

where T is the stage temperature and X is the stage moisture content. R is the ideal gas constant and T_0 is the reference temperature given in Appendix D. The diffusion coefficient used in the SD and SFB stage is computed with $c_1 = k_2^{ab}$ and $c_2 = k_3^{ab}$ and the diffusion coefficient used in the VFBh and VFBc stage is computed with $c_1 = k_2^{cd}$ and $c_2 = k_3^{cd}$. It was not possible to describe the experimental data accurately using the same set of parameters for all stages.

2.7. Equilibrium moisture content

The equilibrium moisture content, $X_{\text{eq}}(T, Y)$, is a product dependent function that describes the moisture content at which water cannot be evaporated any longer. We use the Guggenheim-Anderson-de Boer (GAB) equations [23] and get

$$X_{\text{eq}}(T, Y) = \frac{C \cdot K \cdot X_m \cdot \text{RH}}{(1 - K \cdot \text{RH})(1 - K \cdot \text{RH} + C \cdot K \cdot \text{RH})} + X_{\text{add}} \tag{14}$$

$X_m = 0.01410 \exp\left(\frac{233.5}{T}\right)$, $C = 1.2646 \cdot 10^{-7} \exp\left(\frac{6618.4}{T}\right)$, and $K = 0.1565 \exp\left(\frac{648.1}{T}\right)$. X_m is the monolayer moisture content. C and K are constants related to monolayer and multilayer properties. X_{add} is an estimated correction term. T is the stage temperature, and RH is the relative humidity of the air calculated as described in Appendix C. The parameters in (14) are identified from already dried powder in the laboratory by *adsorption* isotherms studies. Fig. 4 illustrates the GAB model fit made from 15 data points. Temperatures were fixed at $T = 25°C$, $T = 50°C$ and $T = 75°C$ with relative humidities between RH = 4.5% and RH = 40.1%. In the literature, models already exists for maltodextrin [5, 24, 25]. However, these models do not fit our data well.

2.8. Stickiness

Stickiness of the powder is predicted by the glass transition temperature. The glass transition temperature is calculated by the Gordon–Taylor equation (a mass-proportion-mixing rule) [23, 26, 27].

$$T_g = \frac{T_{\text{gp}} + kZT_{\text{gw}}}{1 + kZ} \tag{15a}$$

$T_{\text{gp}} = 144.8°C$ (maltodextrin DE-18) and $T_{\text{gw}} = -137°C$ (water). The value $k = 6.296$ is estimated from the adsorption isotherm data used in Sec. 2.7. A test indicates whether the powder in Fig. 4 has turned sticky after being exposed to the specific temperature and air humidity conditions for 24 hours.

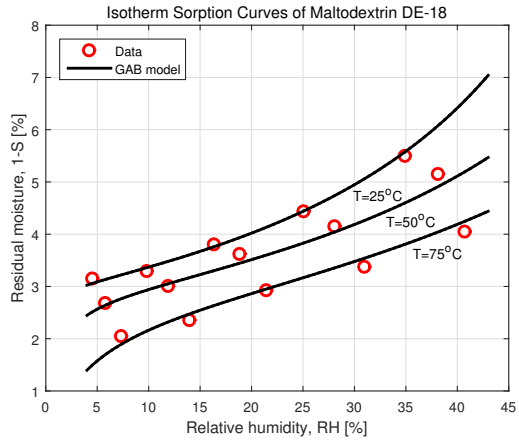

Figure 4: GAB model for calculation of the equilibrium moisture content compared to the laboratory data of maltodextrin DE-18.

Fig. 5 shows the test results and the stickiness model. Powders with a residual moisture content above T_g are sticky. The stickiness model agree well with the measurements. The surface moisture content, Z, in (15a) is

$$Z = \begin{cases} 0.53X^a & \text{for the SD} \\ X^b & \text{for the SFB} \\ X^c & \text{for the VFBh} \\ X^d & \text{for the VFBc} \end{cases} \tag{15b}$$

The surface moisture content, Z, of the powder in the SD stage is subject to a correction term of 0.53. The constant is manually selected and compensates for the crisper surface of the particles that makes the powder less sticky. We did not experience deposits during the trials, thus 0.53 is selected to reflect this fact. The constant can only be exactly determined as a result of dryer specific empirical inspection of the chamber walls after deposits has actually formed [26].

2.9. Key performance indicators

The key performance indicators (KPIs) in spray drying are the profit of operation, the energy consumption rate, the energy efficiency and the product flow rate. The profit of operation is given by the value of the product minus the raw material and energy costs

$$p = p_p F_p - p_f F_f - p_E Q_{tot} \tag{16a}$$

p_p is the unit value of the product, p_f is the unit cost of feed material, and p_E is the unit energy cost. We assume the bulk price of skimmed milk powder (SMP) is $p_p = 2.5$ €/kg, the price of feed is $p_f = 0.1p_p$, and the price of energy is $p_E = 12.906$ €/(MWhr). Q_{tot} is the total energy consumption rate of the dryer

$$\begin{aligned} Q_{tot} &= \Delta H \\ &= F_{\text{main}}(h_{\text{a,main}} - h_{\text{amb}}) + F_{\text{sfb}}(h_{\text{a,sfb}} - h_{\text{amb}}) \\ &\quad + F_{\text{vfbh}}(h_{\text{a,vfbh}} - h_{\text{amb}}) + F_{\text{vfbc}}(h_{\text{a,vfbc}} - h_{\text{amb}}) \end{aligned} \tag{16b}$$

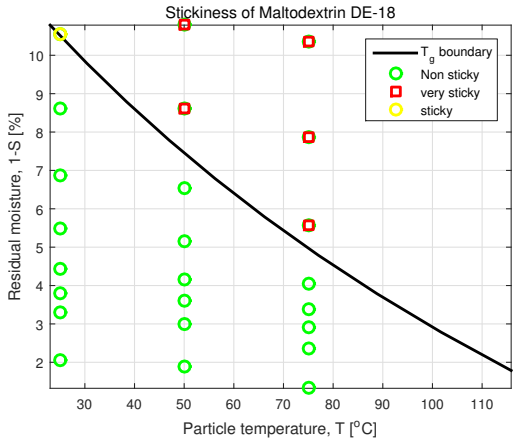

Figure 5: Identification of the stickiness boundary for maltodextrin DE-18.

h_{amb} is the specific enthalpy of the air stream at outdoor temperature and humidity. The energy efficiency is given by the energy required for evaporation relative to the total energy supplied for heating the air [28, 29]

$$\eta = \frac{\lambda(T_0)F_s(X_f - X^d)}{Q_{tot}} \tag{16c}$$

$\lambda(T_0)F_s(X_f - X^d)$ is the energy required for evaporation. The flow rate of powder out of the dryer is given by

$$F_p^d = F_s(1 + X^d) \tag{16d}$$

2.10. Summary

The model, (1) to (14), is a deterministic system of index-1 differential algebraic (DAE) equations in the following form

$$\frac{d}{dt}g(x(t)) = f(x(t), u(t), d(t), \theta) \qquad x(t_0) = x_0 \tag{17a}$$

$$y(t) = h(x(t)) \tag{17b}$$

The index-1 DAE model can be solved efficiently by explicit singly diagonally implicit Runge-Kutta (ESDIRK) methods. We use the ESDIRK4(3) method with variable step-size [30, 31]. The state function $g(x(t))$ represents hold-up of mass and energy and $f(x(t), u(t), d(t), \theta)$ is the flux of mass and energy. $h(x(t))$ is the output equations. θ is the parameter vector that has to be estimated from data.

The measurement vector, y, the controlled input vector, u, the disturbance vector, d, and the states, x, are

$$\begin{aligned}
y(t) &= [T^a \quad T^b \quad T^c \quad T^d \quad Y^a \quad S^b \quad S^d]^T \\
u(t) &= [F_f \quad T_{\text{main}} \quad T_{\text{sfb}} \quad T_{\text{vfbh}}]^T \\
d(t) &= [T_f \quad S_f \quad F_{\text{main}} \quad F_{\text{sfb}} \quad F_{\text{vfbh}} \quad F_{\text{vfbc}} \quad Y_{\text{main}} \quad \dots \\
&\qquad Y_{\text{sfb}} \quad Y_{\text{vfbh}} \quad Y_{\text{vfbc}} \quad T_{\text{vfbc}} \quad T_{\text{amb}}^{ab} \quad T_{\text{amb}}^{cd}]^T \\
x(t) &= [T^a \quad Y^a \quad X^a \quad T^b \quad Y^b \quad X^b \quad \dots \\
&\qquad T^c \quad Y^c \quad X^c \quad T^d \quad Y^d \quad X^d]^T
\end{aligned}$$

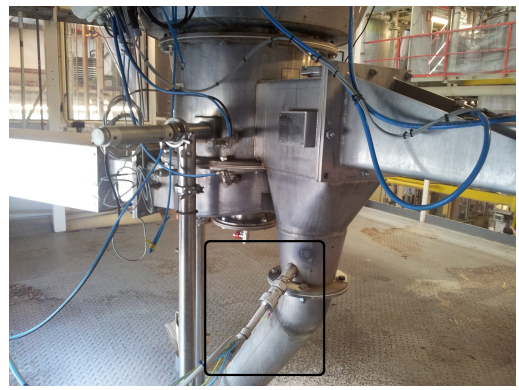

Figure 6: The SFB powder outlet with the in-line NIR analyser and the piston for powder discharge.

The parameter vector, θ, is listed in Table 1. Fig. 1 and Fig. 2 provide an overview of the inputs, disturbances and states.

3. System identification

In this section, we identify the unknown parameters, θ, of the model in (17). Experimental tests have been designed and conducted such that all relevant parameters in the model can be identified.

3.1. Experiment

Two experiments were made in consecutive order without stop. The data from the first experiment is used for estimation, while the data from the second experiment is used for validation.

The nominal input to the spray dryer is a feed flow rate at $F_f = 85$ kg/hr with a feed solids concentration of $S_f = 50\%$. The feed temperature is $T_f = 50°$C. For drying of the feed, we set the main inlet air temperature, T_{main}, to 170°C, the SFB inlet air temperature, T_{sfb}, to 90°C, and the VFBh inlet air temperature, T_{vfbh}, to 60°C. The cooling of the powder is performed with unheated ambient air, T_{vfbc}, at about 35°C. The inlet air flow rates are $F_{\text{main}} = 1700$ kg/h, $F_{\text{sfb}} = 480$ kg/h, $F_{\text{vfbh}} = 280$ kg/h, and $F_{\text{vfbc}} = 280$ kg/h. Ambient air is heated and used for drying, thus the inlet air humidity is equal to the ambient air humidity. The ambient air humidity is measured continuously and is approximately 3 g/kg. The residual moisture contents, $1 - S^b$ and $1 - S^d$, are measured using two Foss Analytical ProFoss$^{\text{TM}}$ in-line analyzers placed at the SFB and VFBc powder outlets. Fig. 6 shows the position of the residual moisture measurement in the SFB stage and Fig. 7 shows the position of the residual moisture measurement in the VFBc stage. We note that all the inlet air mass-flow meters have an offset in the readings. This offset is identified from water and air mass balances of the spray dryer using measurements of the air flow rates and the moistures. We estimated the offset to be 5%, which we subtracted from the readings before these are used in the model.

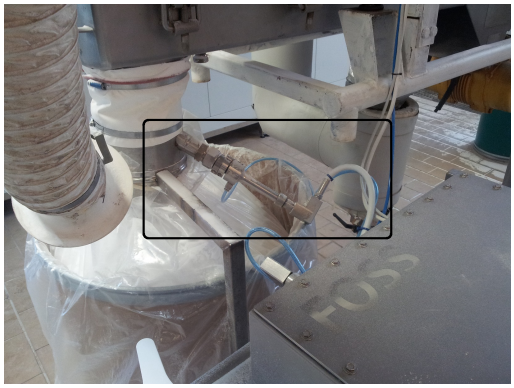

Figure 7: The VFB powder outlet with the in-line NIR analyser and the collection of produced powder.

A number of steps are performed in the experiments to excite the spray dryer outputs. Appendix F describes the steps in the inputs to the spray dryer. During the first experiment, the feed flow rate, F_f, is varied between 65 kg/hr and 120 kg/hr. The feed solid concentration, S_f, is stepped from 50% to 40% and back. We tried a 60% feed solid concentration, but the spray from the nozzle collapsed. This part of the data has therefore been cut out of the estimation experiment. The feed temperature, T_f, is reduced to 42°C, stepped to 60°C and back. The ambient air humidity in the SD and SFB stages, Y_{main} and Y_{sfb}, are stepped from approximately 3 g/kg to 15 g/kg and 25 g/kg in two steps by opening a vapor nozzle in the air ducts. The main inlet air temperature, T_{main}, is stepped ±10 °C from 170°C. The SFB inlet air temperature, T_{sfb}, is stepped ±10 °C from 90°C. The VFBh inlet air temperature, T_{vfbh}, is stepped +20°C from 60°C. The inlet air flow rates are stepped F_{main} = ±200 kg/h, F_{sfb} = ±100 kg/h and F_{vfbh} = +130 kg/h from their nominal values. The second experiment is made from a repetition of the above experiment program, but omitting the steps in the inlet air flow rates and the feed temperature. The excitation steps are also provided in Appendix F. The data from both experiments are well excited and covers a large operation range. This ensures that the model is valid in a large range of operating points. The estimation experiment lasts 28 hours and the validation experiment lasts 17 hours.

3.2. Method

The unknown parameter vector, θ, in the model is identified by minimization of the sum of squared simulation errors. This procedure is performed by solving

$$\hat{\theta} = \arg\min_{\theta} \frac{1}{2} \sum_{k=1}^{N} \|y(t_k) - \hat{y}(t_k, \theta)\|_2^2 \tag{18}$$

in which $y(t_k)$ is the measured output and $\hat{y}(t_k, \theta)$ is the simulated output from (17). $y(t_k) - \hat{y}(t_k, \theta)$ is the simulation error (residual). The outputs of the model have units of comparable size, i.e. °C, g/kg and %, and we can therefore use unit-scaling. Table 1 provides the estimated parameters, $\hat{\theta}$, the standard deviations, $\sigma_{\hat{\theta}}$, and the associated 95% confidence interval. The $100(1-\alpha)$% confidence interval is calculated by

$$\hat{\theta} \pm t_{N-p}(1-\alpha/2)\sqrt{\text{diag}\,(\Sigma_{\hat{\theta}})} \tag{19}$$

in which $\Sigma_{\hat{\theta}}$ is the estimated co-variance matrix of the estimated parameters, $\hat{\theta}$. $N-p$ is the number of observations minus the number of parameters. We compute the covariance of the estimated parameters, $\Sigma_{\hat{\theta}}$, from the residual mean square error, $\|y-\hat{y}\|_2^2$, and the Jacobian, J, of $\hat{y}(t_k, \hat{\theta})$ using the expression [32]

$$\Sigma_{\hat{\theta}} = \frac{\|y-\hat{y}\|_2^2}{N-p}\left(J^T J\right)^{-1} \tag{20}$$

The estimated mean and covariance, $\hat{\theta}$ and $\Sigma_{\hat{\theta}}$, defines the distribution of the parameters, i.e. $\theta \sim N(\hat{\theta}, \Sigma_{\hat{\theta}})$. Knowledge of this distribution enables Monte Carlo simulations that can be used to qualify and quantify the uncertainty of the responses simulated by the model.

As is evident in Table 1, the parameters, T_{add}, Y_{add}, k_3^{cd}, m_m^c, and k_1^d, are uncertain. The other parameters are estimated with reasonable uncertainty for engineering purposes. The following parameters are negative: k_3^{cd}, k_6 and k_1^d. k_3^{cd} is a parameter, c_2, in (13). As k_3^{cd} is very uncertain it could as well be zero such that (13) simplifies. Negativity of k_1^d implies that the evaporation rate (12b) is negative and that water condenses instead of evaporates at the VFBc stage. This is as expected. From physical reasoning negativity of k_6 is problematic as it indicates heat flow (9a) from the VFBc to the VFBh; nevertheless it provides the best fit to data.

4. Validation

In this section, we asses the quality of the model by comparing the simulated outputs to the estimation and validation experiment.

Fig. 8 shows the outputs of the estimation experiment which is used to identify the parameters. Fig. 9 shows the validation experiment. The simulations are shown for 15 realizations of $\theta \sim N(\hat{\theta}, \Sigma_{\hat{\theta}})$. The simulations are performed using the full estimated co-variance matrix, $\Sigma_{\hat{\theta}}$. Table 1 only provide the diagonal elements of $\Sigma_{\hat{\theta}}$, i.e. $\sigma_{\hat{\theta}} = \sqrt{\text{diag}(\Sigma_{\hat{\theta}})}$.

The simulation shows good agreement with the estimation experiment. The transients and the steady-states are well described by the model. The stage temperatures, T^a, T^b, T^c and T^d, and the air humidity in the SD stage, Y^a, fit the data well. The powder moisture contents, $1-S^b$ and $1-S^d$, also fit the data well. The moisture content is difficult to estimate at low residual moisture contents, due to an increasing dependency on the equilibrium moisture content, X_{eq}, in (14). The equilibrium moisture content is estimated for data obtained from a laboratory experiment, which does not exactly match the conditions in the spray dryer. Therefore, we expect some deviation, when the equilibrium moisture content becomes significant in the residual moisture simulation. The VFBc stage is not sealed from

Table 1: Estimated parameters, $\hat{\theta}$, for the four-stage model, divided into the SD, SFB, VFBh and VFBc stage parameters.

Symbol	$\hat{\theta}$	$\sigma_{\hat{\theta}} = \sqrt{\text{diag}(\Sigma_{\hat{\theta}_i})}$	± 95% CL	$\lvert 95\%\ \text{CL}/\hat{\theta}\rvert \cdot 100\%$	Prefix	Unit
k_1^a	1140.6	97.018	±190.22	17	10^{-4}	-
k_2^{ab}	33.104	1.6796	±3.2931	10		-
k_3^{ab}	20.912	1.92	±3.7646	18	10^{-2}	-
k_{UA}^a	181.93	0.889	±1.7424	1	10^{-3}	W/K
k_1	17.899	0.5155	±1.0107	6		W/(K kg)
k_2	1.5788	0.0778	±0.1525	10		W
k_3	59.494	2.7368	±5.366	9	10^{-3}	W/K
k_4	23.789	0.9130	±1.7901	8		W
m_m^a	171.01	9.0916	±17.826	10		kg
m_s^a	0.95172	0.0811	±0.15897	17		kg
F_{add}	149.45	1.9114	±3.7478	3		kg/h
T_{add}	0.27301	0.1096	±0.21481	79		°C
Y_{add}	0.20698	0.1012	±0.19845	96		g/kg
k_1^b	10.52	0.8674	±1.7008	16	10^{-4}	-
k_{UA}^b	0.60952	0.1035	±0.20301	33	10^{-3}	W/K
k_5	8.1977	0.6142	±1.2042	15	10^{-3}	W/K
m_m^b	0.66861	0.1085	±0.2127	32		kg
m_s^b	32.092	1.0314	±2.0223	6		kg
k_1^c	16.535	1.5767	±3.0914	19	10^{-4}	-
k_2^{cd}	13.061	1.3442	± 2.6356	20		-
k_3^{cd}	-0.04827	0.1100	±0.21574	447	10^{-2}	-
k_{UA}^c	30.207	0.4736	± 0.9285	3	10^{-3}	W/K
k_6	-11.107	0.4001	±0.78448	7	10^{-3}	W/K
m_m^c	0.01224	0.1052	±0.20624	1685		kg
m_s^c	13.206	0.5498	±1.078	8		kg
k_1^d	-0.34606	0.1042	±0.20428	59	10^{-4}	-
k_{UA}^d	22.473	0.8771	±1.7197	8	10^{-3}	W/K
m_m^d	3.9403	0.3877	±0.76013	19		kg
m_s^d	4.4197	0.4778	±0.9368	21		kg
X_{add}	6.5473	0.3132	±0.61408	9	10^{-3}	kg/kg

the surrounding air, because the powder has to be emptied from the VFBc stage. The ambient air is therefore dragged into the VFBc stage and dilutes the drying air. $1 - S^d$ may therefore be subject to an unknown disturbance that leads to variations in the residual moisture content. Note, that the communication to the sensor measuring S^d dropped out in the period t=16.5 hours and t=18.2 hours due to a malfunction.

The simulation also shows good agreement with the validation experiment. The transients and the steady-states are well described by the model. The temperatures and air humidity, T^a, T^b, T^c, T^d and Y^a, fit the data well during both disturbance and input steps. The powder moisture contents, $1 - S^b$ and $1 - S^d$, are estimated well. The largest in-accuracy is present at low residual moisture contents.

The normalized root mean square error (NSE) and mean square error (MSE) are used to qualitatively evaluate the model. The NSE and MSE are calculated by

$$\text{NSE} = 1 - \frac{\|\hat{y}(\hat{\theta}) - y\|_2}{\|\hat{y}(\hat{\theta}) - \frac{1}{N}\sum_{k=1}^{N}(\hat{y}(\hat{\theta})_k)\|_2} \tag{21}$$

$$\text{MSE} = \frac{\|\hat{y}(\hat{\theta}) - y\|_2^2}{N - 1} \tag{22}$$

where N is the total number of measurements. NSE vary between $-\infty$ (bad fit) to 100% (perfect fit). The MSE vary between ∞ (bad fit) and 0 (perfect fit). The NSE is independent of the units and the absolute value of $\hat{y}(\theta)$. It is therefore easier to interpret the MSE. Table 2 shows the NSE values and the MSE values for the estimation experiment and the validation experiment. The NSE values indicate, that the simulated air temperatures and air humidities describe the data well, as the values are often above 80%. The simulated residual moisture

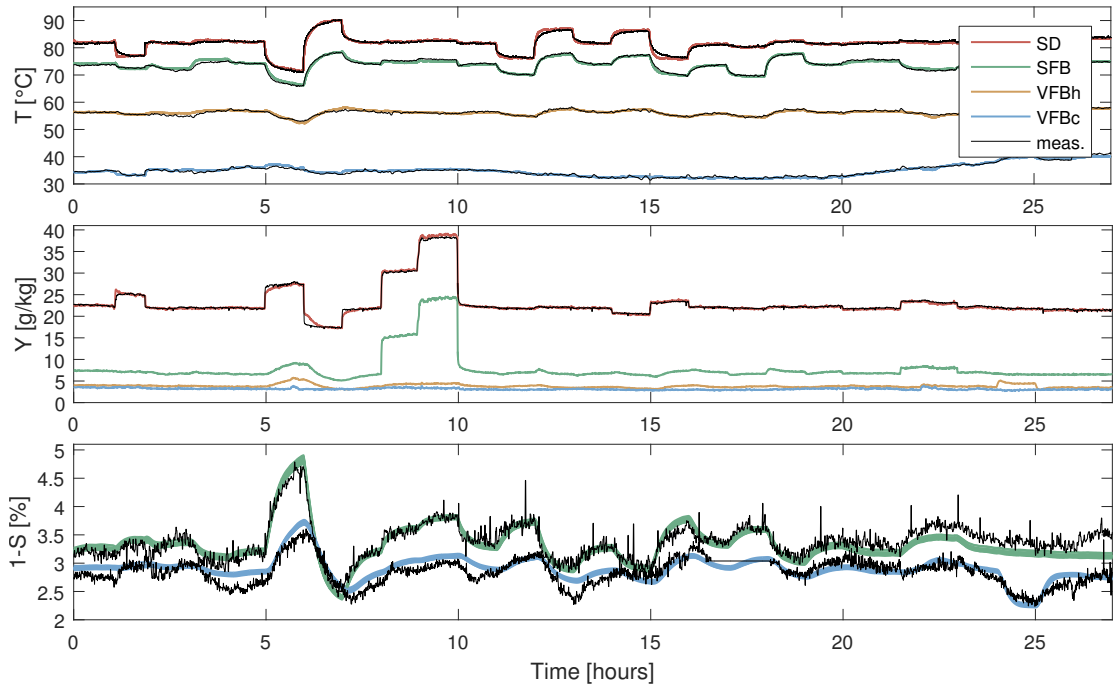

Figure 8: The estimation experiment and the simulated output of the estimated model. T and Y are the temperatures and absolute humidities of the air. $1 - S$ is the residual moisture contents. The transients and the steady-states are well described by the model.

Table 2: Fit quality shown for the estimation and the validation experiments.

Fit of	Est. NSE	Val. NSE	Est. MSE	Val. MSE
T^a	82.6 %	85.8 %	26.7	28.7
T^b	79.7 %	84.6 %	22.9	18.7
T^c	81.6 %	86.6 %	16.7	11.0
T^d	79.4 %	67.0 %	21.8	29.3
Y^a	90.7 %	88.4 %	11.5	13.1
X^b	48.4 %	43.3 %	2.7	6.2
X^d	40.1 %	42.9 %	1.9	1.7

contents provide the poorest description of the data. Further development of the model may therefore be able to increase the simulation accuracy of the residual moisture content.

5. Simulation

The primary objective of the four-stage spray dryer model is to facilitate evaluation and comparison of different control strategies by simulation. Therefore, we simulate stickiness for the estimation experiment to validate that the model correctly predicts safe non-fouling operation. We also simulate KPIs such as profit and energy consumption. To illustrate the properties of the model, we simulate the outputs of the model for steps in the inputs and for selected disturbances.

5.1. Stickiness

Fig. 10 illustrates the simulated residual moisture and temperature of the powder in each stage during the estimation experiment. The stickiness constraint is estimated by (15) and shown with the dashed line in Fig. 10. Fig. 10 shows that drying in the SD stage is closest to the stickiness constraint and therefore most critical. This is due to the high residual moisture of the powder and the high temperature in the SD stage. Unfortunately, stickiness of the powder in the SD stage cannot be measured during operation. During the two experiments, there were no signs of deposits on the chamber walls. Accordingly, we verify that the 0.53 correction term (15b) is an adequate estimate. In some cases, this estimate may be too restrictive and further experiments are needed to identify more accurate and less restrictive values of the correction term.

5.2. Key performance indicators

Fig. 11 shows the simulated KPIs of the spray dryer during the estimation experiment. The KPIs are the profit rate, the production rate, F_p, the energy efficiency, η, and the total energy consumption rate, Q_{tot}. The profit rate of operation is the most important performance indicator of industrial dryers and an important indicator when evaluating different control strategies. The profit rate is mainly affected by the product flow rate as the price of the produced powder is significantly higher than the energy price. Consequently, the rate of consumed energy and the energy efficiency are secondary objectives compared to

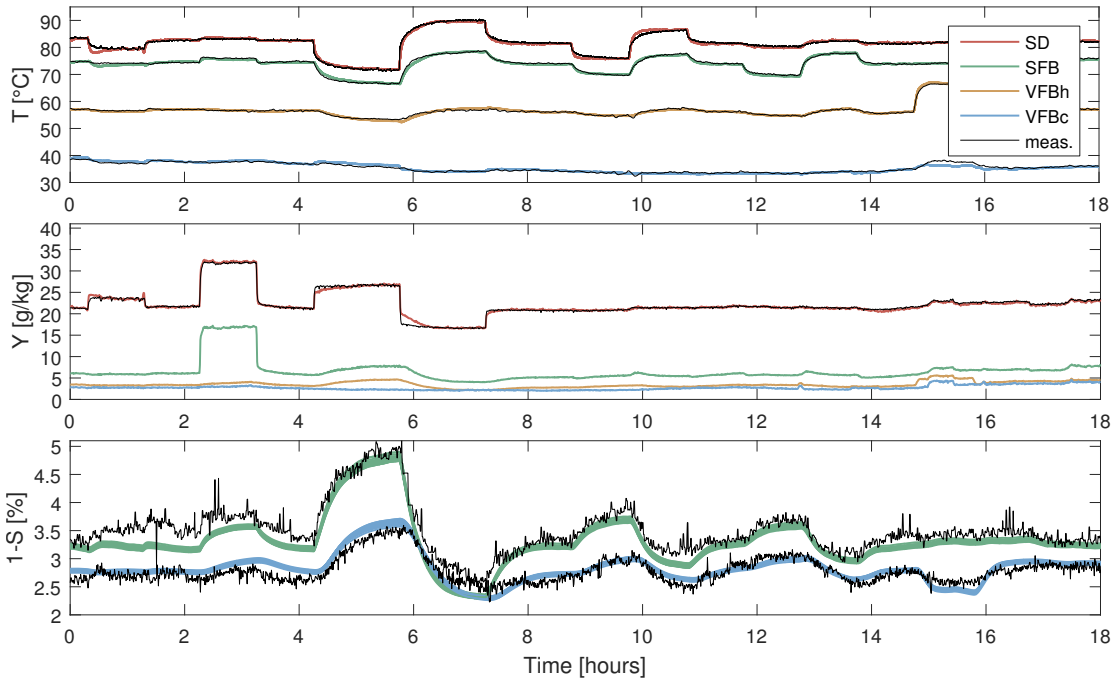

Figure 9: The validation experiment and the simulated output of the estimated model. T and Y are the temperatures and absolute humidities of the air. $1 - S$ is the residual moisture contents. The simulated model outputs agree well with the measured data.

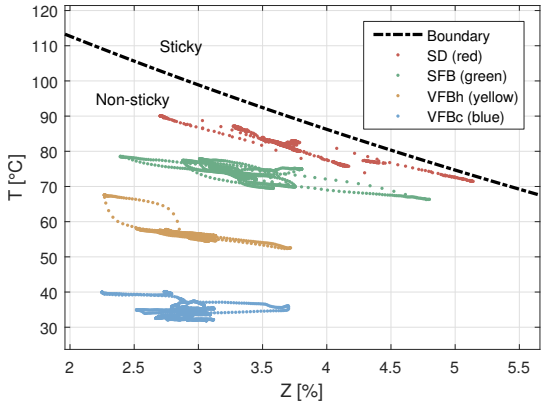

Figure 10: The simulated stickiness constraint and stickiness of the powder in each stage during the estimation experiment.

the profit rate. It should be noted that the energy efficiency of this small dryer is approximately 40%, which is low compared to industrially sized dryers that may achieve efficiencies of approximately 55%. The total energy consumption rate, Q_{tot}, is approximately 83 kW. The energy consumption rate is mainly affected by adjusting the inlet air flow rates and temperatures to the dryer. The ambient temperature and air humidity naturally also has an effect on the energy consumption rate. Increasing ambient air temperatures decreases the energy consumption rate.

5.3. Step responses of the inputs

Fig. 12 reports the step responses of the simulated outputs to the inputs of the four-stage spray dryer. The inputs are the feed flow rate, F_{f}, the temperature in the main hot air inlet, T_{main}, the temperature in the hot air inlet to the SFB, T_{sfb}, and the temperature in the hot air inlet to the VFBh, T_{vfbh}. The outputs are the temperature and the air humidity in each of the four stages of the spray dryer, as well as the measured residual moisture of the powder in the SFB stage and the VFBc stage (the final powder product). We do not to plot the SD stage and the VFBh stage residual moistures as they are not measurable in the four-stage spray dryer.

As is evident in the first row of Fig. 12, a 20 kg/hr increase in the feed flow rate, F_{f}, has a significant effect on the temperatures, the air humidities, and the residual moistures in the spray dryer. When the feed flow rate increases, the temperatures decrease, the air humidities increase, and the residual moistures in the powder increase. The temperatures decrease because more feed, consisting of water and solid, need to be heated and more water is evaporated with the same amount of inlet energy. The air humidities increase as a consequence of the increased evaporation of water from the powder. The residual moistures of the powder increase because the energy supplied is unaltered and the amount of water in the feed is increased. The plots

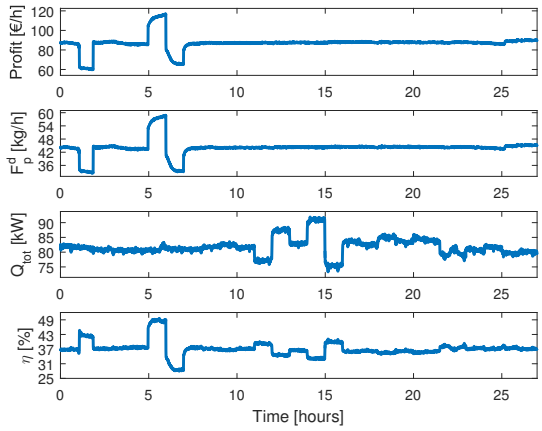

Figure 11: Simulated KPIs for the estimation experiment. The KPIs are the profit rate of operation, the product flow rate, the energy efficiency, and the total energy consumption rate. The profit rate of operation is highly correlated to the product flow rate.

in the second row of Fig. 12 indicate the step responses to a 10°C increase in the temperature of the main hot air inlet, T_{main}. T_{main} significantly affects the temperature in the SD stage and the temperature in the SFB stage. It also decreases the residual moisture of the powder at the SFB stage and the residual moisture at the VFBc stage. T_{main} hardly affects the temperature in the VFBh stage and the temperature in the VFBc stage. T_{main} only has a marginal effect on the air humidities. The third row of plots in Fig. 12 shows the step responses to a 10°C increase of the temperature in the inlet air to the SFB, T_{sfb}. T_{sfb} influences the temperature in the SD stage and the temperature in the SFB stage. This is due to the mixing of the air in these two stages of the four-stage spray dryer. T_{sfb} has hardly any effect on the temperature in the VFBh stage and the temperature in the VFBc stage. Similarly, T_{sfb} does not have any significant effect on the air humidities. Increasing T_{sfb} decreases the powder moisture content in the SFB stage as well as in the final product at the VFBc stage. The last row of plots in Fig. 12 illustrates the step responses to a 10°C increase in the temperature of the hot air inlet to the VFBh stage, T_{vfbh}. T_{vfbh} affects the temperature and the air humidity at the VFBh stage. The air humidity is increased due to the increased evaporation from the powder, resulting in a decreased powder moisture of the final product at the VFBc stage. It does not affect any of the variables in the SD stage nor the SFB stage of the four-stage spray dryer. This is as expected given the design and flows of the four-stage spray dryer.

5.4. Step responses of the disturbances

Fig. 13 reports the step responses of the simulated outputs to the main disturbances of the four-stage spray dryer. The main disturbances are the ambient air humidity, Y_{amb}, the feed solid concentration, S_{f}, and the feed temperature, T_{f}. These disturbances vary during production and a controller must adjust the inputs to compensate for these disturbances. The air humidity varies due to changing weather conditions and the feed varies due to variations in the upstream processes.

The first row of plots in Fig. 13 shows the responses to a 5 g/kg step increase in the ambient air humidity. This increase simultaneously affects all inlet air humidities, i.e. $Y_{\text{main}} = Y_{\text{sfb}} = Y_{\text{vfbh}} = Y_{\text{vfbc}} = Y_{\text{amb}}$. The ambient air humidity has a direct effect on the air humidity in all stages, but only a very small effect on the temperatures. An increased air humidity in the inlet air streams also leads to an increase in the residual moisture of the powder in both the SFB stage and the VFBc stage. The second row of plots in Fig. 13 illustrates the response to a step increase in the feed solid concentration, S_{f}. This increases the air temperatures. In particular, an increase in the feed solid concentration incrases the temperature in the SD stage and the temperature in the SFB stage. A increase in the feed solid concentration decreases the SD air humidity and the residual moisture of the powder in the SFB stage as well as in the VFBc stage. The third row of plots in Fig. 13 demonstrates that the feed temperature, T_{f}, has an effect on the residual moisture of the powder in the SFB stage and also in the VFBc stage. It also affects the temperature at the SFB stage, but hardly affects the temperatures at the other stages. The feed temperature only has a very limited effect on the air humidities.

6. Conclusions

In this paper, we model a medium sized GEA Niro Multi-Stage Dryer size 20 (MSD$^{\text{TM}}$-20). The model is based on four consecutive stages; a primary spray drying stage, two heated fluid bed stages, and a cooling fluid bed stage. In each stage, the model simulates the dynamic responses of the temperatures, the air humidities, and the residual moisture contents of the powder. Deposits caused by stickiness of the powder is predicted using the glass-transition temperature. The model also provides the key performance indicators including the profit of operation. The model is a first-principles engineering model, based on mass- and energy balances, and takes the form of an index-1 DAE model.

The model parameters are estimated from an estimation experiment and validated against a validation experiment. The experiments were both well excited and the model fits the experimental data well. The model provides simulations for a broad operating range, making it ideal as basis for development of control solutions as well as for evaluating the control performance in a production rate and energy efficiency point of view.

Acknowledgement

This work was funded in part by 1) the Danish Ministry of Higher Education and Science in the industrial PhD project "Economic Model Predictive Control for Spray Drying Plants" (12-128720); 2) GEA Process Engineering A/S, DK-2860 Søborg, Denmark; 3) EUDP 64013-0558 in the IEA Annex for Energy Efficient Process Control.

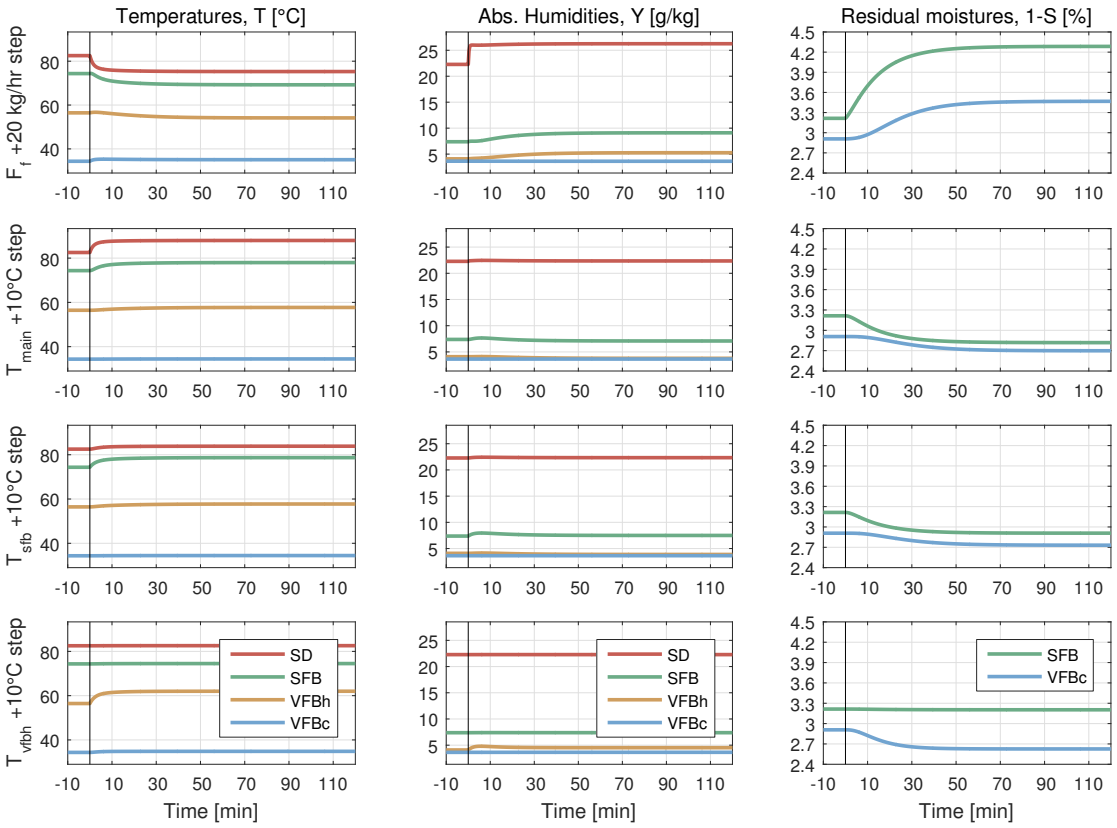

Figure 12: Simulated responses to steps in the inputs. The system outputs shows the response to a step in the feed flow rate, F_{f}, the main inlet air temperature, T_{main}, the SFB inlet air temperature, T_{sfb}, and the VFBh inlet air temperature, T_{vfbh}. The vertical line indicates when the steps are applied and this time is set to t=0.

Appendix A. Basis conversion

The solids feed flow rate, F_s, and total mass feed flow rate, F, are related by

$$F_s = SF \qquad F = \frac{1}{S}F_s \tag{A.1}$$

The dry basis residual moisture content, X, and wet basis solid content, S, are related by

$$X = \frac{1-S}{S} \qquad S = \frac{1}{1+X} \tag{A.2}$$

The dry air flow rate is determined by

$$F_{da} = F\frac{1}{Y+1} \qquad F = F_{da}(Y+1) \tag{A.3}$$

Appendix B. Specific enthalpy

The specific enthalpy of humid air is

$$h_a = h_{da} + Yh_v \tag{B.1}$$

in which

$$h_{da} = h^0_{da} + C_{da}(T - T_0) \tag{B.2}$$

$$h_v = h^0_v + \lambda(T_0) + C_v(T - T_0) \tag{B.3}$$

C_{da} is the mean heat capacity of dry air and C_v is the mean heat capacity of vapor [33]. $\lambda(T_0)$ is the latent heat of evaporation. The standard enthalpies of formation, h^0_{da} and h^0_v, are computed at T_0 with the phase that this product takes at T_0. The specific enthalpy of feed as well as powder is

$$h_p = h_s + Xh_w \tag{B.4}$$

in which

$$h_s = h^0_s + C_s(T - T_0) \tag{B.5}$$

$$h_w = h^0_w + C_w(T - T_0) \tag{B.6}$$

C_s is the mean heat capacity of solid and C_w is the mean heat capacity of water [33]. The mean heat capacity of maltodextrin, C_s is described in [34][pp. 87]. h^0_s and h^0_w are the standard enthalpies of formation. The specific enthalpy of steel is $h_m = C_m(T - T_0)$. C_m is the mean heat capacity of steel.

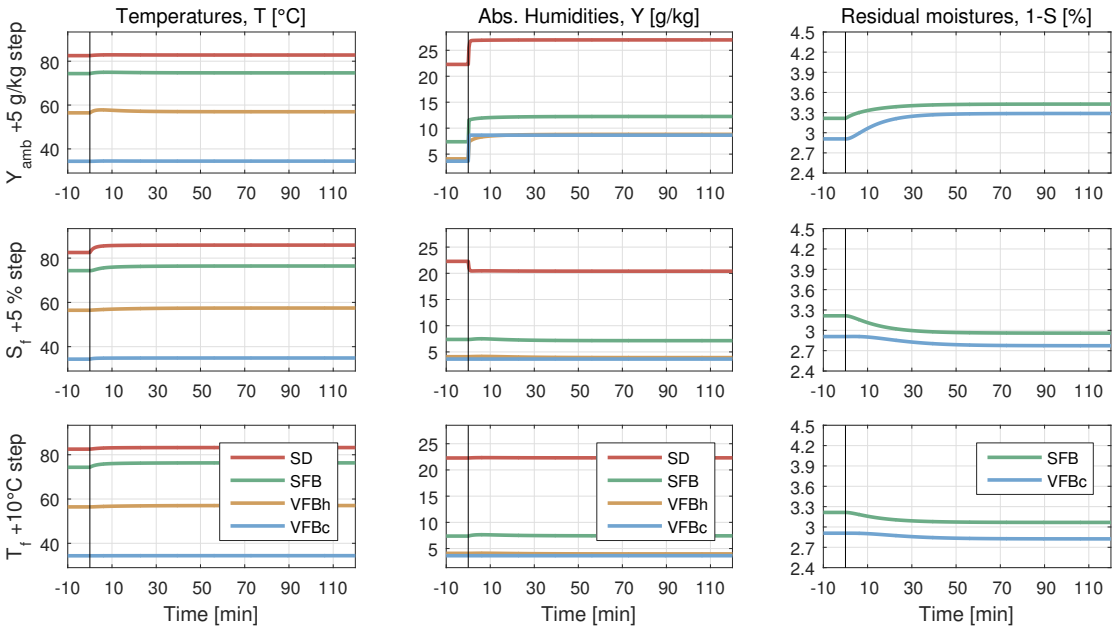

Figure 13: Simulated responses to steps in the selected disturbances. The system outputs shows the response to a step in the ambient air humidity, Y_{amb}, the feed solid concentration, S_{f}, and the feed temperature, T_{f}. The steps are applied after 10 minutes of operation at a steady-state. This is indicated by the vertical line in the figures and the corresponding time is defined as $t = 0$.

Appendix C. Air humidity conversion

The relative air humidity is calculated by

$$\text{RH} = \frac{Y}{\left(\frac{M_v}{M_{da}} + Y\right)} \frac{P_{\text{amb}}}{P_{\text{vsat}}(T)} \tag{C.1}$$

$P_{vsat}(T)$ is the saturated vapor pressure determined by the Antoine equation and P_{amb} is the ambient total pressure. M_v and M_{da} is the molar mass of vapor and dry air respectively. The absolute air humidity, Y, is calculated by

$$Y = \frac{M_v}{M_{da}} \frac{\text{RH}P_{\text{vsat}}(T)}{P_{\text{amb}} - \text{RH}P_{\text{vsat}}(T)} \tag{C.2}$$

Appendix D. Constants

The constants used in the model are listed here
$R = 8.314472 \cdot 10^{-3}$ KJ K^{-1}mol^{-1}, the ideal gas constant.
$M_v = 18.01528 \cdot 10^{-3}$ kg mol^{-1}, the molar mass of vapor.
$M_w = 18.01528 \cdot 10^{-3}$ kg mol^{-1}, the molar mass of water.
$M_{da} = 28.97 \cdot 10^{-3}$ kg mol^{-1}, the molar mass of dry air.
$P_{\text{amb}} = 101325$ Pa, ambient pressure
$T_0 = 25 + 273.15$ K, reference temperature

The mean heat capacities are calculated by [33]

$$C_{\{\cdot\}} = \frac{R}{M}\left(A + \frac{B}{2}T(\tau+1) + \frac{C}{3}T^2(\tau^2+\tau+1) + \frac{D}{\tau T^2}\right) \tag{D.1}$$

A, B, C and D for vapor, water and dry air is
Vapor; $A = 3.470$, $B = 1.450{\cdot}10^{-3}$, C=0, $D = 0.121{\cdot}10^{5}$
Water; $A = 8.712$, $B = 1.25{\cdot}10^{-3}$, $C = -0.18{\cdot}10^{-6}$, $D = 0$
Dry air; $A = 3.355$, $B = 0.575{\cdot}10^{-3}$, $C = 0$, $D = -0.016{\cdot}10^{5}$

The mean heat capacity of Maltodextrin DE-18 and steel are

$$C_s = 1.5488 + 0.0019625T - 5.9399{\cdot}10^{-6}T^2 \tag{D.2}$$

$$C_m = 0.466 \tag{D.3}$$

where T is in °C [34][pp. 87].

The standard enthalpy of formation is given by [33] and [34][pp. 87] $h^0_{da} = 0$ KJ/Kg, $h^0_v = -0.0134$ KJ/Kg, $h^0_w = -0.0159$ KJ/Kg, $h^0_s = 0$ KJ/Kg, $h^0_m = 0$.

The latent heat of vaporization is

$$\lambda(T) = \lambda_{ref}\left(\frac{1 - \frac{T}{\alpha}}{1 - \frac{T_{ref}}{\alpha}}\right)^{\beta} \tag{D.4}$$

in which $\lambda_{ref} = 2257$ KJ/Kg at $T_{ref} = 100 + 273.15$ K and $\alpha = 647.1$ and $\beta = 0.38$ [33].

Appendix E. Steady-states

The steady-state of the model is

$$y_{ss} = [81.713°\text{C} \quad 73.843°\text{C} \quad 56.25°\text{C} \quad 34.491°\text{C} \quad \ldots$$
$$22.266\text{g/kg} \quad 3.2717\% \quad 2.926\%]^T$$

$$x_{ss} = [81.713°C \quad 22.266g/kg \quad 7.6838\% \quad ... \\ 73.843°C \quad 7.9276g/kg \quad 3.3824\% \quad ... \\ 56.25°C \quad 4.1729g/kg \quad 3.015\% \quad ... \\ 34.491°C \quad 3.6126g/kg \quad 3.0142\%]^T$$

given the inputs, u_{ss}, and disturbances, d_{ss}:

$$u_{ss} = [86.951kg/hr \quad 51.15\% \quad 51.65°C \quad ... \\ 1710.1kg/hr \quad 170.14°C \quad 4.0888g/kg \quad ... \\ 479.09kg/hr \quad 89.84°C4.0888g/kg \quad ... \\ 279.52kg/hr \quad 59.95°C \quad 3.6113g/kg \quad ... \\ 274.71kg/hr \quad 34.49°C \quad 3.6113g/kg]^T$$

$$d_{ss} = [26.476°C \quad 24.334°C]^T$$

Appendix F. Steps used for the estimation and validation

Table F.3: The input step-sizes that are used in the experiments.

Input	Estimation Step		Validation Step	
	Down	Up	Down	Up
F_{f}	65 kg/hr	120 kg/hr	70 kg/hr	117 kg/hr
T_{f}	42° C	60° C	-	-
S_{f}	40%	-	40%	-
F_{main}	1500 kg/h	1900 kg/h	-	-
T_{main}	160° C	180° C	160° C	180° C
Y_{main}	-	15 – 25 g/kg	-	15 g/kg
F_{sfb}	330 kg/h	570 kg/h	-	600 kg/h
T_{sfb}	80° C	100° C	80° C	100° C
Y_{sfb}	-	15 – 25 g/kg	-	15 g/kg
F_{vfbh}	-	410 kg/h	-	-
T_{vfbh}	-	80° C	-	80° C

References

[1] A. S. Mujumdar, Handbook of Industrial Drying, Third Edition, CRC Press, 2006.

[2] K. Masters, Spray Drying in Practice, International SprayDryConsult ApS, 2002.

[3] J. Kent, J. McLeod, Spray-dryer optimization, International Powder & Bulk Solids (2007) 12–20.

[4] X. Chen, W. Pirini, M. Ozilgen, The reaction engineering approach to modelling drying of thin layer of pulped kiwifruit flesh under conditions of small Biot numbers, Chemical Engineering and Processing: Process Intensification 40 (4) (2001) 311–320.

[5] K. C. Patel, X. D. Chen, S. X. Q. Lin, B. Adhikari, A composite reaction engineering approach to drying of aqueous droplets containing sucrose, maltodextrin (DE6) and their mixtures, AIChE Journal 55 (1) (2009) 217–231.

[6] M. W. Woo, W. R. W. Daud, A. S. Mujumdar, M. Z. M. Talib, W. Z. Hua, S. M. Tasirin, Comparative study of droplet drying models for CFD modelling, Chemical Engineering Research and Design 86 (9) (2008) 1038–1048.

[7] D. Clarke, Application of generalized predictive control to industrial processes, Control Systems Magazine, IEEE 8 (2) (1988) 49–55.

[8] L. Tan, F. Taip, N. Aziz, Simulation and control of spray drying using nozzle atomizer spray dryer, International Journal of Engineering & Technology 9 (10) (2009) 1–7.

[9] L. W. Tan, M. N. Ibrahim, R. Kamil, F. S. Taip, Empirical modeling for spray drying process of sticky and non-sticky products, Procedia Food Science 1 (2011) 690–697.

[10] V. S. Shabde, K. A. Hoo, Optimum controller design for a spray drying process, Control Engineering Practice 16 (5) (2008) 541–552.

[11] V. S. Shabde, Optimal design and control of a spray drying process that manufactures hollow micro-particles, Ph.D. thesis, Texas Tech University (2006).

[12] I. Zbicinski, S. Grabowski, C. Strumillo, L. Kiraly, W. Krzanowski, Mathematical modelling of spray drying, Computers and Chemical Engineering 12 (2-3) (1988) 209–214.

[13] C. A. Zaror, J. R. Pérez-Correa, Model based control of centrifugal atomizer spray drying, Food Control 2 (3) (1991) 170–175.

[14] J. R. Pérez-Correa, F. Farias, Modelling and control of a spray dryer: A simulation study, Food Control 6 (4) (1995) 219–227.

[15] R. Govaerts, A. Johnson, R. Crezee, G. Reyman, P. Swinkels, Control of an industrial spray-drying unit, Control Engineering Practice 2 (1) (1994) 69–85.

[16] L. N. Petersen, N. K. Poulsen, H. H. Niemann, C. Utzen, J. B. Jørgensen, A grey-box model for spray drying plants, 10th IFAC International Symposium on Dynamics and Control of Process Systems (2013) 559–564.

[17] L. N. Petersen, J. B. Jørgensen, J. B. Rawlings, Economic optimization of spray dryer operation using nonlinear model predictive control with state estimation, 9th International Symposium on Advanced Control of Chemical Processes (2015) 507–513.

[18] N. R. Kristensen, H. Madsen, S. B. Jørgensen, A method for systematic improvement of stochastic grey-box models, Computers & Chemical Engineering 28 (2004) 1431–1449.

[19] D. O. Callaghan, P. Cunningham, Modern process control techniques in the production of dried milk products – a review, Lait 85 (2005) 335–342.

[20] W. K. Lewis, The rate of drying of solid materials, Journal of Industrial and Engineering Chemistry 13 (1921) 427–432.

[21] L. Hassini, S. Azzouz, R. Peczalski, A. Belghith, Estimation of potato moisture diffusivity from convective drying kinetics with correction for shrinkage, Journal of Food Engineering 79 (1) (2007) 47–56.

[22] H. Yang, N. Sakai, M. Watanabe, Drying model with non-isotropic shrinkage deformation undergoing simultaneous heat and mass transfer, Drying Technology 19 (7) (2001) 1441–1460.

[23] S. Basu, U. S. Shivhare, A. S. Mujumdar, Models for sorption isotherms for foods: A review, Drying Technology 24 (8) (2006) 917–930.

[24] M. W. Woo, W. R. W. Daud, A. S. Mujumdar, Z. Wu, M. Z. Meor Talib, S. M. Tasirin, CFD evaluation of droplet drying models in a spray dryer fitted with a rotary atomizer, Drying Technology 26 (2008) 1180–1198.

[25] J. M. Frías, J. C. Oliveira, K. Schittkowski, Modeling and parameter identification of a maltodextrin DE 12 drying process in a convection oven, Applied Mathematical Modelling 25 (6) (2001) 449–462.

[26] S. A. Hogan, M. H. Famelart, D. J. O'Callaghan, P. Schuck, A novel technique for determining glass-rubber transition in dairy powders, Journal of Food Engineering 99 (2010) 76–82.

[27] C. Hennigs, T. K. Kockel, T. A. G. Langrish, New measurements of the sticky behavior of skim milk powder, Drying Technology 19 (3-4) (2001) 471–484.

[28] T. Kudra, Energy performance of convective dryers, Drying Technology 30 (11-12) (2012) 1190–1198.

[29] T. Kajiyama, K. J. Park, Influence of air parameters on spray drying energy consumption, Revista Brasileira De Produtos Agroindustriais, Rbpa 12 (1) (2010) 45–54.

[30] M. R. Kristensen, J. B. Jørgensen, P. G. Thomsen, S. B. Jørgensen, An ESDIRK method with sensitivity analysis capabilities, Computers & Chemical Engineering 28 (12) (2004) 2695–2707.

[31] C. Völcker, J. B. Jørgensen, P. G. Thomsen, E. H. Stenby, Adaptive step size control in implicit Runge-Kutta methods for reservoir simulation, 9th International Symposium on Dynamics and Control of Process Systems (2010) 509–514.

[32] G. A. F. Seber, C. J. Wild, Nonlinear regression, Wiley-Interscience, 2003.

[33] J. Smith, H. Van Ness, M. Abbott, Introduction to chemical engineering thermodynamics, McGraw-Hill chemical engineering series, McGraw-Hill, 2005.

[34] J. Sloth, Opstilling og verificering af en tørringskinetisk model for monodisperse dråber i en spraytørrer, Master's thesis, Technical University of Denmark, Department of Chemical Engineering, Kgs. Lyngby, Denmark (2004).

Paper B

Comparison of Control Strategies for Optimization of Spray Dryer Operation

---

Submitted to *Journal of Process Control, 2016*.

Comparison of three control strategies for optimization of spray dryer operation

Lars Norbert Petersen[a,b], Niels Kjølstad Poulsen[a], Hans Henrik Niemann[c], Christer Utzen[b], John Bagterp Jørgensen[a,*]

[a]*Department of Applied Mathematics and Computer Science, Technical University of Denmark, DK-2800 Kgs. Lyngby, Denmark*
[b]*GEA Process Engineering A/S, DK-2860 Søborg, Denmark*
[c]*Department of Electrical Engineering, Technical University of Denmark, DK-2800 Kgs. Lyngby, Denmark*

Abstract

Spray drying is the preferred process to reduce the water content of many chemicals, pharmaceuticals, and foodstuffs. A significant amount of energy is used in spray drying to remove water and produce a free flowing powder product. In this paper, we present and compare the performance of three controllers for operation of a four-stage spray dryer. The three controllers are a proportional-integral (PI) controller that is used in industrial practice for spray dryer operation, a linear model predictive controller with real-time optimization (MPC with RTO, MPC-RTO), and an economically optimizing nonlinear model predictive controller (E-NMPC). The MPC with RTO is based on the same linear state space model in the MPC and the RTO layer. The E-NMPC consists of a single optimization layer that uses a nonlinear system of ordinary differential equations for its predictions. The PI control strategy has a fixed target that is independent of the disturbances, while the MPC-RTO and the E-NMPC adapt the operating point to the disturbances. The goal of spray dryer operation is to optimize the profit of operation in the presence of feed composition and ambient air humidity variations; i.e. to maximize the production rate, while minimizing the energy consumption, keeping the residual moisture content of the powder below a maximum limit, and avoiding that the powder sticks to the chamber walls. We use an industrially recorded disturbance scenario in order to produce realistic simulations and conclusions. The key performance indicators such as the profit of operation, the product flow rate, the specific energy consumption, the energy efficiency, and the residual moisture content of the produced powder are computed and compared for the three controllers. In this simulation study, we find that the economic performance of the MPC with RTO and E-NMPC is considerably improved compared to the PI control strategy used in industrial practice. The MPC with RTO improves the profit of operation by 8.71%, and the E-NMPC improves the profit of operation by 9.69%. The energy efficiency is improved by 6.06% and 5.52%, respectively.

Keywords: Spray drying, Real-time optimization, Model predictive control, Economic model predictive control, PI control

1. Introduction

The four-stage spray dryer is widely used in the chemical, pharmaceutical and food industries for turning liquid products into free flowing powders. By combining drying in four stages instead of drying in a single stage, four-stage spray dryers have increased energy efficiency and improved product quality. Intensified competition in industries using spray dryers require continuous process innovations to reduce costs and improve product quality. Traditionally, spray dryers are operated using a proportional-integral (PI) control strategy with fixed targets that are independent of disturbances such as the ambient humidity and the feed composition to the spray dryer. The PI control strategy is based on fixed inlet temperatures and a single-input-single-output PI-controller that manipulates the feed flowrate to control the exhaust temperature. In this paper, we demonstrate by closed-loop simulation that the key performance indicators of spray dryer operation using a PI control strategy can be significantly improved by using optimization based controllers adjusting the targets to the disturbances. We investigate two different economically optimizing controllers: 1) a linear model predictive controller with real-time optimization (MPC with RTO, MPC-RTO), and 2) an economic nonlinear model predictive controller (E-NMPC).

The key product qualities in spray drying are the bulk density, the particle size distribution, and the residual moisture content. These product qualities affect the powder reconstitution (sinkability, solubility, dispersability and wetability) in water [1]. Changes in the residual moisture content tend to affect all the other product qualities and have a considerably effect on the profit of operation. It is a challenging and non-trivial task to operate a spray dryer in an economical optimal way and simultaneously meet the product quality specifications. In current industrial practice, a PI control strategy is used for operation of the four-stage spray dryer. This PI based control strategy keeps the inlet and outlet temperatures constant during operation. The approach is simple, but in the presence of changing external disturbances, such as the ambient air humidity and feed composition, the PI control strategy is insufficient. The PI control strategy does not maximize the production rate, it cannot guarantee satisfaction of the residual moisture constraint, and it does

*Corresponding author
Email addresses: lars.n.petersen@gea.com (Lars Norbert Petersen), nkpo@dtu.dk (Niels Kjølstad Poulsen), hhn@elektro.dtu.dk (Hans Henrik Niemann), christer.utzen@gea.com (Christer Utzen), jbjo@dtu.dk (John Bagterp Jørgensen)

not include a stickiness constraint implying that deposits may form due to sticky powder inside the dryer. Furthermore, the inputs and outputs of a spray dryer are highly cross-coupled and long process delays may be present. All these features make it difficult to operate a spray dryer using a PI control strategy [2].

In this paper, we present an MPC-RTO as well as an E-NMPC and apply these controllers to simulate spray dryer operation. By closed-loop simulation, we compare the key performance indicators of the MPC strategies to the PI control strategy that is used in current industrial practice. The goal of spray dryer operation is to optimize the profit in the presence of feed composition and ambient air humidity variations; i.e. the objective is to maximize the production rate, while minimizing the energy consumption rate, keeping the residual moisture content of the powder below a maximum limit, and avoiding that the powder sticks to the chamber walls. The simulations are based on a validated first-principles engineering model of a four-stage spray dryer [2] and uses an industrially recorded disturbance scenario. The MPC-RTO and the E-NMPC have previously been suggested for operation of a four-stage spray dryer [3, 4]. However, the study presented in the current paper represents the first rigorous comparison of the industrially applied PI control strategy to the MPC-RTO and the E-NMPC strategies using the same disturbance scenario. The closed-loop simulations are realistic representations of industrial situations, as the simulations are based on a validated model of an industrial type small scale spray dryer and an industrially recorded disturbance scenario. The MPC-RTO and E-NMPC are based on simpler models that are not identical to the simulation model.

A PI controller is a simple method for controlling a single process value to a specified target. For more complex multivariable processes, linear tracking model predictive control (MPC) is the preferred control methodology in the process industries [5, 6]. MPC provides an integrated solution for controlling processes with multivariate and cross-coupled dynamics, time delays, and constraints on both the inputs and the outputs to a specified target vector [7, 8]. Often MPC is combined with an RTO [9–12]. Together, MPC and RTO form a two-layer structure. The upper-level RTO system provides targets to the lower-level control system to maintain the process operation as close as possible to the economic optimum. The lower-level MPC system brings the process to the target values of the RTO system. Note that the two layer structure consisiting of an RTO and an MPC is different from the two layer MPC for offset free control [13–16]. We apply an RTO, which may be categorized as an explicit iterative optimization method with bias update adaptation [9]. RTO methods, based on explicit iterative optimization, repeatedly solve a model-based optimization problem and are advantageous compared to implicit methods such as the extremum-seeking control [17, 18]. Implicit methods can be slow and require the process to reach steady-state before a new step can be taken. The two-layer structure has some inherent drawbacks. As the optimization is only performed intermittently at a lower sampling rate than the regulation, the adaptation of the operating conditions is slow and assumes that a steady-state can be reached [10]. Recent advances within process optimization focus on optimizing economics directly in the controller [8, 19–21]. This is known as E-NMPC. The advantage of E-NMPC is that it maximizes the profit of operation at all times and it takes both the steady-state and the transient economics into account. The E-NMPC eliminates the RTO layer and the drawbacks of a two-layer structure [22]. The key challenges related to implementation of E-NMPC are the required model accuracy and the need for long control- and prediction-horizons to reach the turnpike solution [20]. A peculiarity of E-NMPC is that the optimal solution is not necessarily a steady-state solution but may be a periodic solution [8, 19, 21].

Mathematical modeling and control of spray dryers have been a subject of research for many decades. PI control is the de facto standard control methodology in the spray drying industry. PI control is reported for drying of full cream milk using a laboratory scale nozzle equipped spray dryer in [23]. Drying of whole milk and orange juice is addressed in [24]. Shabde and Hoo [25] use two PI controllers to control the mean particle size and the residual moisture content of the powder. The controllers are tested by simulation using a first-principles model [26, 27]. Zaror and Pérez-Correa [28] present a feed forward cascade controller to control the exhaust air temperature to indirectly maintain constant product moisture content. Pérez-Correa and Farias [29] extend [28] by controlling the humidity of the exhaust air to indirectly maintain constant product moisture content. Govaerts *et al.* [30] develop a linear quadratic gaussian (LQG) controller for residual moisture control in an industrial detergent spray drying process. The above control strategies concern single-stage spray dryers. Petersen *et al.* [3, 31, 32] report linear and nonlinear MPC algorithms for control of the residual moisture content and the stickiness of the powder in a four-stage spray dryer. Industrial MPC solutions for spray dryers exist and seem to rely on empirically based models and least-squares methods for control of the residual moisture content of the powder. Callaghan and Cunningham [33] provide a thorough review on the status and future of advanced control for spray drying.

The paper is organized as follows. The process and the controllers are presented in Section 2, while Section 3 briefly presents the simulation model. The PI, MPC with RTO, and E-NMPC control strategies are described in Section 4, Section 5, and Section 6. Section 7 compares the control strategies by simulation and the conclusions are provided in Section 8.

2. The process and the controllers

2.1. Process description

Fig. 1 illustrates a modern four-stage spray dryer with an integrated static fluid bed and an external vibrating fluid bed. The spray dryer consists of the primary spray drying stage (SD), the static fluid bed stage (SFB), the hot vibrating fluid bed stage (VFBh), and the cold vibrating fluid bed stage (VFBc).

The hot main air is let into the upper section of the SD around the high pressure nozzles. The nozzles disperse the liquid feed into droplets. The heat is transferred from the hot air to the droplets, which makes the water evaporate from the droplets. In that process the air temperature and the residual moisture of the

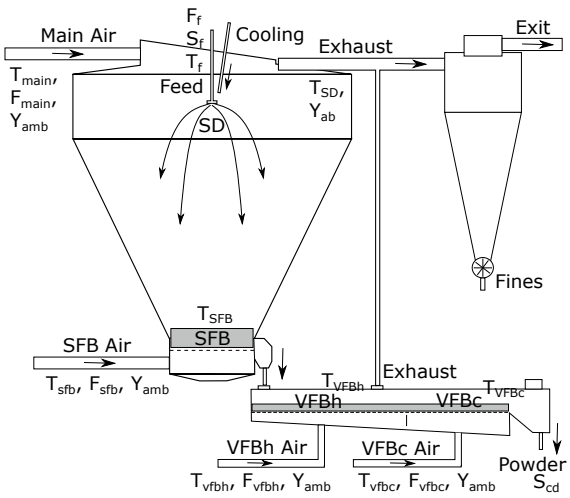

Figure 1: Principle diagram of the four-stage spray dryer with integrated and external fluid beds.

droplets decrease. The dried product then enters the SFB and is dried further while being fluidized by hot air. After drying in the SFB, the powder is transported to the VFB for gentle drying and cooled to the temperature desired for handling and storage. The drying air from the chamber and the VFB is passed through a cyclone and a bag filter. The cyclone separates any powder contained in the air. The filtered powder is returned to the chamber to form agglomerated powder particles.

2.2. Input and outputs

Fig. 1 shows a detailed overview of the manipulated variables, u, the measured disturbances, d, the measurements, y, and the controlled variables, z. The measurements, y, are the stage air temperatures, T_{SD}, T_{SFB}, T_{VFBh} and T_{VFBc}, the absolute air humidity, Y_{ab}, and the final powder residual moisture content, $1 - S_{\mathrm{cd}}$. The controlled variables, z, is a subset of y. The manipulatable inputs, u, are the feed flow rate, F_{f}, the inlet main air temperature, T_{main}, the inlet SFB air temperature, T_{sfb}, and the VFB air temperature, T_{vfbh}. The measured disturbances, d, are the feed temperature, T_{f}, the feed solids concentration, S_{f}, the inlet air flow rates, the ambient air humidity, $Y_{\mathrm{amb}} = Y_{\mathrm{main}} = Y_{\mathrm{sfb}} = Y_{\mathrm{vfbh}} = Y_{\mathrm{vfbc}}$, the VFBc cooling air temperature, T_{vfbc}, and the ambient air temperature, $T_{\mathrm{amb}} = T^{ab}_{\mathrm{amb}} = T^{cd}_{\mathrm{amb}}$. Consequently, the vector of manipulated variables, u, the measured disturbance vector, d, the measurement vector, y, and the vector of controlled variables, z, are

$$u = [F_{\mathrm{f}} \quad T_{\mathrm{main}} \quad T_{\mathrm{sfb}} \quad T_{\mathrm{vfbh}}]^T, \tag{1a}$$

$$d = [T_{\mathrm{f}} \quad S_{\mathrm{f}} \quad F_{\mathrm{main}} \quad F_{\mathrm{sfb}} \quad F_{\mathrm{vfbh}} \quad F_{\mathrm{vfbc}} \quad \ldots \quad Y_{\mathrm{amb}} \quad T_{\mathrm{vfbc}} \quad T_{\mathrm{amb}}]^T, \tag{1b}$$

$$y = [T_{\mathrm{SD}} \quad T_{\mathrm{SFB}} \quad T_{\mathrm{VFBh}} \quad T_{\mathrm{VFBc}} \quad Y_{\mathrm{ab}} \quad S_{\mathrm{cd}}]^T, \tag{1c}$$

$$z = [T_{\mathrm{SD}} \quad T_{\mathrm{SFB}} \quad Y_{\mathrm{ab}} \quad S_{\mathrm{cd}}]^T. \tag{1d}$$

2.3. Key performance indicators

The key performance indicators of spray dryer operation are the profit of operation, p, the product flow rate, F_{p}, the total energy consumption rate, Q_{tot}, the specific energy consumption, $Q_{\mathrm{tot}}/F_{\mathrm{p}}$, the energy efficiency, η, and the residual moisture in the product, $1 - S_{\mathrm{cd}}$.

The profit of operating the spray dryer is given by the value of the product minus the raw material and energy costs,

$$p = p_{\mathrm{p}} F_{\mathrm{p}} - p_{\mathrm{f}} F_{\mathrm{f}} - p_{\mathrm{E}} Q_{\mathrm{tot}}. \tag{2}$$

$p_{\mathrm{p}} = 2.5$ [€/kg] is the unit value of the product, $p_{\mathrm{f}} = 0.1 p_p$ is the unit cost of feed material, and $p_{\mathrm{E}} = 12.906$ [€/(MWhr)] is the unit energy cost. The total energy, $Q_{\mathrm{tot}} = Q_{\mathrm{main}} + Q_{\mathrm{sfb}} + Q_{\mathrm{vfbh}} + Q_{\mathrm{vfbc}}$, supplied to the dryer is the energy to heat the main air stream, Q_{main}, the energy to heat the SFB air stream, Q_{sfb}, the energy to heat the VFBh air stream, Q_{vfbh}, and the energy to heat the VFBc air stream, Q_{vfbc}. In this paper, we do not use the heater for the cold part of the vibrating fluid bed, i.e. $Q_{\mathrm{vfbc}} = 0$ such that $T_{\mathrm{vfbc}} = T_{\mathrm{amb}}$. Each of the other inlet air streams are heated from the ambient temperature, T_{amb}, to their respective setpoints, T_{main}, T_{sfb}, and T_{vfbh}. The computation of Q_{tot} is described in [2]. For the simulations in this paper, the product flow rate is computed as $F_{\mathrm{p}} = F_{\mathrm{f}} S_{\mathrm{f}} / S_{\mathrm{cd}}$ and the specific energy consumption is computed as $Q_{\mathrm{tot}}/F_{\mathrm{p}}$. The energy efficiency is the ratio of energy used for evaporation of water from the powder, $\Delta H_{\mathrm{vap}} = \lambda F_{\mathrm{f}} \frac{S_{\mathrm{cd}} - S_{\mathrm{f}}}{S_{\mathrm{cd}}}$, and the total amount of energy supplied, Q_{tot}, i.e. $\eta = \Delta H_{\mathrm{vap}} / Q_{\mathrm{tot}}$. Reference [2] describes the details for the compuation of the energy efficiency.

2.4. Controllers

In all controllers considered in this paper, the manipulated variables, u, are kept at their setpoints by low level PI controllers. Fig. 2 illustrates the principles of the high-level controllers studied in this paper.

As illustrated in Fig. 2(a), the PI control strategy measures the spray dryer temperature, $y = T_{\mathrm{SD}}$, and controls the spray dryer temperature to the target, r, by manipulating the feed flow rate, $u = F_{\mathrm{f}}$. The inlet temperatures ($T_{\mathrm{main}}, T_{\mathrm{sfb}}, T_{\mathrm{vfbh}}$) are not manipulated in the PI control strategy. Fig. 2(d) illustrates that the outputs, z, in the PI control strategy have fixed constraints for relatively long times of operation as the setpoint, r, is only changed manually. Furthermore, the PI control strategy has a relative large output variance such that the required back-off from the constraint is larger than for the advanced process control strategies (MPC-RTO and E-NMPC).

Fig. 2(b) illustrates that the MPC-RTO is a two layer optimization based controller. Using the measured disturbances, d, the estimated states (the integrating disturbance states), $\hat{\bar{x}}$ ($\hat{x}_d$), the operating profit function, the constraints, and a steady-state linear model, the RTO computes the optimal setpoints, r, for the controlled variables, z, by solving a steady-state optimization problem. The MPC in the MPC-RTO solves a weighted and regularized least-squares problem with constraints using a dynamic linear model. The MPC is based on feedback from the measurements, y, and feed-forward from the measured disturbances, d. The MPC brings the controlled variables, z, to

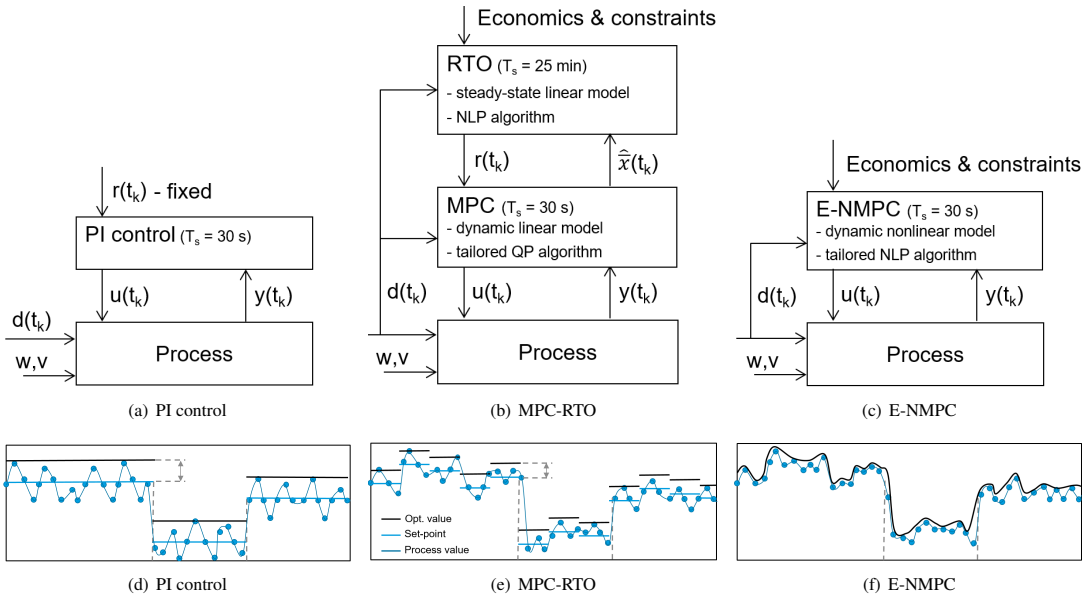

(a) PI control (b) MPC-RTO (c) E-NMPC

(d) PI control (e) MPC-RTO (f) E-NMPC

Figure 2: The diagrams (a-c) illustrates the main computations for the different controllers. The sketches (d-f) illustrates the controlled variables, z, the corresponding setpoints (if relevant), r, and the corresponding constraints for the different controllers.

the targets, r, by manipulating u. As illustrated in Fig. 2(e), the RTO frequently adjusts the setpoints including the corresponding back-off to the variations in the disturbances. The back-off of the MPC-RTO is smaller than the back-off of the PI control strategy due to better regulation by the MPC. The economic value of the MPC-RTO compared to the PI control strategy stems from the adjustment of setpoints to the actual disturbances and less back-off as a consequence of better regulation with less output variance.

Fig. 2(c) illustrates that the E-NMPC is a one layer optimization based controller. Based on the measurements, y, the measured disturbances, d, the profit function, the constraints, and a nonlinear model, E-NMPC computes the manipulated variables, u, at each sample time such that the predicted profit of operation is maximized. Fig. 2(f) shows that E-NMPC does not compute targets, r, directly, but maximizes operating profit subject to constraints. This implies that the optimal controlled variables, z, corresponding to the optimal manipulated variables, u, are adjusted and predicted at each sample time. The back-off in E-NMPC may be implemented directly or by solving stochastic versions of E-NMPC using soft constraints with penalty functions representing the economic cost of violating a constraint. In this paper, we used a certainty-equivalence E-NMPC and did not explicitly consider back-off from the constraints.

3. Simulation model

The simulation model is a first-principles engineering model that is based on mass and energy conservation laws [2]. The model describes drying of maltodextrin DE-18 with a high accuracy in a wide range of operating points. The model may be represented in the discrete stochastic form

$$x_{k+1} = F(x_k, u_k + w_{\mathrm{u},k}, d_k + w_{\mathrm{d},k}, \theta), \tag{3a}$$
$$y_k = h_{\mathrm{y}}(x_k) + v_k, \tag{3b}$$
$$z_k = h_{\mathrm{z}}(x_k), \tag{3c}$$

in which F is an operator representing the solution, x_{k+1}, of the system of differential equations

$$x(t_k) = x_k, \tag{4a}$$
$$\frac{d}{dt} g(x(t)) = f(x(t), u_k + w_{\mathrm{u},k}, d_k + w_{\mathrm{d},k}, \theta), \quad t_k \le t \le t_{k+1}, \tag{4b}$$
$$x_{k+1} = x(t_{k+1}). \tag{4c}$$

Equation (4) is solved using the ESDIRK4(3) method with variable step size [34]. h_{y} is the measurement function and h_{z} is the output function. The model (4) is a deterministic model that has two piecewise stochastic inputs, $u_k + w_{u,k}$ and $d_k + w_{d,k}$, that are constant for $t_k \le t \le t_{k+1}$. The measurement, y, is the measurement function, h_{y}, corrupted by measurement noise, v_k. The process noise, $w_{\mathrm{u},k} \sim N_{\mathrm{iid}}(0, R_{\mathrm{u}})$ and $w_{\mathrm{d},k} \sim N_{\mathrm{iid}}(0, R_{\mathrm{d}})$, and the measurement noise, $v_k \sim N_{\mathrm{iid}}(0, R_{\mathrm{v}})$, are all assumed to be normally distributed. The covariances, (R_{u}, R_{d}, R_{v}), are estimated from the covariances of u, d, and y, respectively.

3.1. Constraints

The maximum capacity of the feed pump limits the feed flow. The inlet temperatures must be higher than the ambient temperature, T_{amb}. To minimize the risk of scorched particles, we also

apply upper limits on the allowable inlet temperatures. Consequently,

$$0\ [\text{kg/hr}] \le F_\text{f} \le 140\ [\text{kg/hr}], \tag{5a}$$
$$T_\text{amb} \le T_\text{main} \le 220\ [^\circ\text{C}], \tag{5b}$$
$$T_\text{amb} \le T_\text{sfb} \le 120\ [^\circ\text{C}], \tag{5c}$$
$$T_\text{amb} \le T_\text{vfbh} \le 70\ [^\circ\text{C}]. \tag{5d}$$

These constraints are hard input constraints. To avoid deposits of sticky particles on the spray dryer surfaces, the stage temperatures must be below the glass transition temperatures, $T_\text{SD} \le T_\text{g}^\text{SD}$, $T_\text{SFB} \le T_\text{g}^\text{SFB}$, $T_\text{VFBh} \le T_\text{g}^\text{VFBh}$, and $T_\text{VFBc} \le T_\text{g}^\text{VFBc} \le 45\ [^\circ\text{C}]$. The glass transition temperatures are determined in [2]. The powder moisture content must be below a maximum limit, $1 - S_\text{cd} \le 1 - S_\text{max} = 3.5\%$. These constraints should be interpreted as soft output constraints. Since, it is difficult on physical grounds to specify what the precise limits should be, we assume that these limits already include the back-off from the real limits.

4. Proportional-integral control

In the following, we briefly present the PI control strategy. This control method is the reference to which advanced controllers should be compared as it is the standard control method used in the spray drying industry. Fig. 2(a) and Fig. 2(d) illustrate the PI control strategy.

4.1. Control principles

PI control offers a simple and industrially accepted method to steer a controlled value to a target and reject disturbances. In the conventional PI control strategy for spray dryers, a number of low level PI controllers keep the inlet temperatures constant during operation. These low level PI controllers maintain the main inlet air temperature, the SFB inlet air temperature, and the VFB inlet air temperature at a fixed setpoint by adjusting the power of the heaters for the respective inlet air streams.

The main controller in the PI control strategy is a high level PI controller that controls the chamber exhaust air temperature, $y = T_\text{SD}$, to a fixed target, $r = T_\text{sp}$, by manipulating the feed flow rate, $u = F_\text{f}$. The target, T_sp, of the high level PI controller and the fixed setpoints for the low level PI controllers are selected such that the profit of operation is maximized, the input constraints are satisfied, and adequate back-off from the stickiness constraints is available such that deposition of particles in the spray dryer is avoided.

4.2. Regulator tuning and discrete-time implementation

The main challenge in using PI control is tuning of the gain and integral action. We used the SIMC tuning method [35]. Using input-output data of the simulation model (3), we approximate the process transfer function with the first order model,

$$Y(s) = \frac{K_\text{p}}{\tau_\text{p} s + 1} U(s), \tag{6}$$

Algorithm 1 PI Algorithm

Require: y_k, r_k, I_k
  $e_k = r_k - y_k$
  $u_k = K_c e_k + I_k$
  $u_k = \min(u_\text{max}, \max(u_\text{min}, u_k))$
  $I_{k+1} = I_k + (T_s K_c/\tau_c)\, e_k$
  return u_k, I_{k+1}

$K_\text{p} = -0.35\ [^\circ\text{C}/(\text{kg/h})]$, and $\tau_\text{p} = 122$ [s]. In continuous-time, the PI control law is

$$E(s) = R(s) - Y(s), \tag{7a}$$
$$U(s) = K_\text{c}\left(1 + \frac{1}{\tau_\text{c} s}\right) E(s) \tag{7b}$$

Aiming for at closed-loop time constant of $\tau_{cl} = 50$ [s], we get the following PI control parameters using the SIMC tuning rule: $K_\text{c} = (1/K_\text{p})\tau_\text{p}/\tau_\text{cl} = -6.97\ [(\text{kg/h})/^\circ\text{C}]$ and $\tau_\text{c} = \min\{\tau_\text{p}, 4\tau_\text{cl}\} = 122$ [s].

Algorithm 1 transforms the continuous-time PI controller (7) to a discrete time PI controller using the explicit Euler method [36]. The implementation outlined in Algorithm 1 provides bumpless parameter changes and handles control signal saturation. Bumpless transfer between manual and automatic mode is obtained by setting $I_0 = u_0 - K_\text{c} e_0$ with $e_0 = r_0 - y_0$, when the PI controller is switched on to automatic mode. In the implementation we do not consider anti-windup nor setpoint weighting. In the PI control strategy for the spray dryer, we use a sample time of $T_\text{s} = 30$ [s], $u_\text{min} = 0$ [kg/hr], and $u_\text{max} = 140$ [kg/hr].

5. Model predictive control with real-time optimization

In the following, we briefly present the MPC-RTO. It consists of a linear MPC and an RTO for determination of the setpoints to the linear MPC. Fig. 2(b) and Fig. 2(e) illustrate the MPC-RTO.

The linear MPC consists of a state estimator and a regulator that in combination based on feedback from the measurements, y, and feedforward from the measured disturbances, d, bring the controlled variables, z, to their targets, r. The RTO adjusts these targets such that the process is operated at the steady-state providing the best economic performance given the process constraint and the disturbances. The process variables (u, d, y, z) are as given in (1). The state estimator, the RTO and the regulator all use the same linear model.

5.1. Linear model

The linear model used in the state estimator, the RTO, and the regulator is a linearization of a nonlinear model with reduced complexity compared to the model used for simulation of the spray dryer. Reference [3] describes the nonlinear model from which the linear model in the MPC-RTO is derived. Compared to the simulation model [2], the nonlinear model that is used to derive the linear model of the MPC-RTO contains fewer states and parameters. This simplifies the parameter estimation and

identification of the model. The model parameters in the complexity reduced model are identified from data produced by the simulation model [2]. These data are generated using the numerical procedure outlined in Section 3. To achieve offset-free output estimation (and control) at steady-state, in the presence of plant/model mismatch and/or un-modeled disturbances, the linear model is augmented with integrating disturbance states on the energy balances and the vapor mass balances [15, 37]. The augmented linear model is

$$\bar{x}_{k+1} = \bar{A}\bar{x}_k + \bar{B}u_k + \bar{E}d_k + \bar{G}\bar{w}_k + \bar{\sigma}_{\mathrm{x}}, \tag{8a}$$

$$y_k = \bar{C}_{\mathrm{y}}\bar{x}_k + \sigma_{\mathrm{y}} + v_k, \tag{8b}$$

$$z_k = \bar{C}_{\mathrm{z}}\bar{x}_k + \sigma_{\mathrm{z}}, \tag{8c}$$

where $\bar{x}_k = [x;\, x_d]_k$ is the augmented state vector, u_k is the manipulatable variables, d_k is the measured disturbances, and y_k is the measurements. z_k is the vector of controlled variables. The augmented process noise is $\bar{w}_k = [w;\, w_{\mathrm{d}}]_k \sim N_{\mathrm{iid}}\left(0, \bar{R}_{\mathrm{w}}\right)$ and the measurement noise is $v_k \sim N_{\mathrm{iid}}(0, R_{\mathrm{v}})$. The augmented state space matrices are

$$\bar{A} = \begin{bmatrix} A & B_{\mathrm{d}} \\ 0 & I \end{bmatrix},\ \bar{B} = \begin{bmatrix} B \\ 0 \end{bmatrix},\ \bar{E} = \begin{bmatrix} E \\ 0 \end{bmatrix},\ \bar{G} = \begin{bmatrix} G & 0 \\ 0 & I \end{bmatrix},\ \bar{\sigma}_{\mathrm{x}} = \begin{bmatrix} \sigma_{\mathrm{x}} \\ 0 \end{bmatrix},$$

$$\bar{C}_{\mathrm{y}} = \begin{bmatrix} C_{\mathrm{y}} & 0 \end{bmatrix},\ \bar{C}_{\mathrm{z}} = \begin{bmatrix} C_{\mathrm{z}} & 0 \end{bmatrix},\ \bar{R}_{\mathrm{w}} = \begin{bmatrix} R_{\mathrm{w}} & 0 \\ 0 & R_{\mathrm{w_d}} \end{bmatrix},$$

where $G = I$ is the noise to state matrix. σ_{x}, σ_{y} and σ_{z} contain the constants related to the linearization of the model, i.e. $\sigma_{\mathrm{x}} = x_{\mathrm{ss}} - Ax_{\mathrm{ss}} - Bu_{\mathrm{ss}} - Ed_{\mathrm{ss}}$, $\sigma_{\mathrm{y}} = y_{\mathrm{ss}} - C_{\mathrm{y}}x_{\mathrm{ss}}$, and $\sigma_{\mathrm{z}} = z_{\mathrm{ss}} - C_{\mathrm{z}}x_{\mathrm{ss}}$.

5.2. State estimator (filter and predictor)

The linear time variant (LTV) Kalman filter is used to estimate the states. The measurement vector, y_k, may vary in size as the exhaust air humidity and residual moisture measurements may be missing for several samples. We use the time variance of the Kalman filter to enable the estimator to handle these missing measurements. The filter part of Algorithm 2 handles missing observations by constructing the measurement related properties ($\bar{C}_{\mathrm{y},k}$, $\sigma_{\mathrm{y},k}$, $R_{\mathrm{v},k}$) from ($\bar{C}_{\mathrm{y}}$, σ_{y}, R_{v}) according to the measurement vector, y_k, at sample k. ($\bar{C}_{\mathrm{y}}$, σ_{y}, R_{v}) denotes the matrices for all possible measurements in (8b), while ($\bar{C}_{\mathrm{y},k}$, $\sigma_{\mathrm{y},k}$, $R_{\mathrm{v},k}$) denotes the matrices corresponding to the actual measurements available at sample k.

Let $\bar{\theta} = [\bar{\theta}_{\mathrm{w}}; \theta_{\mathrm{v}}]$, $\bar{R}_{\mathrm{w}} = \mathrm{diag}(\bar{\theta}_{\mathrm{w}})$, and $R_{\mathrm{v}} = \mathrm{diag}(\theta_{\mathrm{v}})$. The unknown noise covariances, $\bar{R}_{\mathrm{w}}$ and R_{v}, needed for the Kalman filter computations are estimated using the maximum likelihood (ML) method [38]. The negative log likelihood function is [39, 40]

$$V_{\mathrm{ML}}(\bar{\theta}) = \alpha + \frac{1}{2}\sum_{k=1}^{N}\left(\ln[\det(R_{\mathrm{e},k})] + \varepsilon_k^T R_{\mathrm{e},k}^{-1}\varepsilon_k\right) \tag{9}$$

with the innovation, $\varepsilon_k = \varepsilon_k(\bar{\theta}) = y_k - \hat{y}_{k|k-1}(\bar{\theta})$, and its covariance, $R_{\mathrm{e},k} = R_{\mathrm{e},k}(\bar{\theta})$, computed by Kalman filter iterations. $\alpha = Nn_y\ln(\pi)/2$ is a constant independent of $\bar{\theta}$. The ML estimate of the covariances is determined by solving the nonlinear (nonconvex) optimization problem,

$$\min_{\bar{\theta}} V_{\mathrm{ML}}(\bar{\theta}), \tag{10a}$$

$$s.t.\ \ \bar{\theta}_l \le \bar{\theta} \le \bar{\theta}_u, \tag{10b}$$

with the lower and upper bounds, $\bar{\theta}_l$ and $\bar{\theta}_u$. Having the optimal $\bar{\theta} = [\bar{\theta}_{\mathrm{w}}; \theta_{\mathrm{v}}]$ enables computation of the noise covariances, $\bar{R}_{\mathrm{w}} = \mathrm{diag}(\bar{\theta}_{\mathrm{w}})$ and $R_{\mathrm{v}} = \mathrm{diag}(\theta_{\mathrm{v}})$. We use the ML estimation method, instead of the autocovariance least squares (ALS) method [41, 42], because it can easily handle situations with missing observations.

The model (8) and the estimated covariances, $\bar{R}_{\mathrm{w}}$ and R_{v}, enable the computation of the stationary state covariance, $\bar{P}$, of the augmented system by solution of a discrete algebraic Riccati equation. The LTV Kalman filter is initialized using $\bar{P}_{0|-1} = \bar{P}$ and $\hat{\bar{x}}_{0|-1} = \bar{x}_{\mathrm{ss}} = [x_{\mathrm{ss}}; 0]$, where x_{ss} is the steady state also used for linearization of the model.

Knowledge of the model (8), the covariances, $\bar{R}_{\mathrm{w}}$ and R_{v}, and the measurement, y_k, enable the filter to estimate the current states, i.e. computation of $\hat{\bar{x}}_{k|k}$. The filtered state, $\hat{\bar{x}}_{k|k}$, is used by the RTO, the regulator part of the MPC, and the one-step prediction.

5.3. Real-time optimization

Every 25 minutes, the RTO solves the steady-state economic optimization problem,

$$\min_{x_{\mathrm{ss}}, u_{\mathrm{ss}}, z_{\mathrm{ss}}, s} \quad \phi_{\mathrm{ss}} = -p(z_{\mathrm{ss}}, u_{\mathrm{ss}}, d_k) + \rho(s), \tag{11a}$$

$$\text{s.t.} \quad [0\ I]\bar{x}_{\mathrm{ss}} = [0\ I]\hat{\bar{x}}_{k|k}, \tag{11b}$$

$$\bar{x}_{\mathrm{ss}} = \bar{A}\bar{x}_{\mathrm{ss}} + \bar{B}u_{\mathrm{ss}} + \bar{E}d_k + \bar{\sigma}_{\mathrm{x}}, \tag{11c}$$

$$z_{\mathrm{ss}} = \bar{C}_{\mathrm{z}}\bar{x}_{\mathrm{ss}} + \sigma_{\mathrm{z}}, \tag{11d}$$

$$u_{\min} + \delta_{\mathrm{u}} \le u_{\mathrm{ss}} \le u_{\max} - \delta_{\mathrm{u}}, \tag{11e}$$

$$c(z_{\mathrm{ss}}) - \delta_{\mathrm{c}} + s \ge 0, \tag{11f}$$

$$s \ge 0. \tag{11g}$$

The target is set to the optimal controlled variables, $r_k = z_{ss}$, when (11) is solved. At the samples between the 25 minutes intervals, (11) is not solved and the target is set to the previous target, $r_k = r_{k-1}$. We denote this function for the RTO by $r_k = \rho(\hat{\bar{x}}_{k|k}, d_k, r_{k-1}, k)$.

The objective function, ϕ_{ss}, is the sum of the profit function, $p(z_{\mathrm{ss}}, u_{\mathrm{ss}}, d_k)$, and a penalty function, $\rho(s)$, that penalizes violations of output constraints. The profit function, $p(z_{\mathrm{ss}}, u_{\mathrm{ss}}, d_k)$, is computed by (2). In the RTO, Q_{tot} for the profit function is computed using the reduced nonlinear model. The penalty function, $\rho(s)$, is an $\ell_2 - \ell_1$-penalty function defined as

$$\rho(s) = \frac{1}{2}\left\|s\right\|_{2,Q_{\mathrm{s}}}^2 + \left\|s\right\|_{1,q_{\mathrm{s}}}. \tag{12}$$

This penalty function is used to treat the output constraints (11f) as soft constraints.

The integrating disturbance states, x_{d}, are fixed to their current values by (11b). These are not necessarily steady state values. The linear model (8) is used in the constraints (11c)-(11d) to determine the steady state relation between the manipulated variables, u_{ss}, and the controlled variables, z_{ss}. The linear

model (8) is used in the RTO for the spray dryer as the nonlinear effects are mostly related to the output constraints. The input constraints, $u_{\min}$ and $u_{\max}$, are given in (5). δ_u contains a 2.5 [°C] back-off in the input temperatures to avoid saturation and loss of controllability. The function, $c(z_{ss})$, in the soft output constraint (11d) is described in [3]. δ_c contains a 0.05 [°C] back-off in the stickiness constraint and a 0.02% back-off in the residual moisture. These back-offs are selected such that they provide constraint violations that are similar to the PI control strategy and the E-NMPC. The output constraints in (11f) are 75 [°C] $\leq T_{SD} \leq \bar{T}_g^{SD}$, 65 [°C] $\leq T_{SFB} \leq$ 75.5 [°C], and $1 - S_{cd} \leq 1 - S_{max} = 3.5\%$. The glass transition temperature, $\bar{T}_g^{SD}$, is determined as in [3].

5.4. Regulator

The regulator tracks the target, r_k, provided by the RTO and rejects measured disturbances, d_k, as well as unmeasured disturbances by solving the regularized output tracking problem with input constraints. This problem may be formulated as the convex quadratic program (QP),

$$\min_{\{u_{k+j}\}_{j=0}^{N-1}} \quad \phi = \frac{1}{2}\sum_{j=1}^{N} \|z_{k+j} - r_k\|_{Q_z}^2 + \frac{1}{2}\sum_{j=0}^{N-1} \|\Delta u_{k+j}\|_{Q_{\Delta u}}^2, \tag{13a}$$

$$\text{s.t.} \quad \bar{x}_k = \hat{\bar{x}}_{k|k}, \tag{13b}$$

$$\bar{x}_{k+j+1} = \bar{A}\bar{x}_{k+j} + \bar{B}u_{k+j} + \bar{E}d_k + \bar{\sigma}_x, \quad j \in \mathcal{N}_u, \tag{13c}$$

$$z_{k+j} = \bar{C}_z\bar{x}_{k+j} + \sigma_z, \quad j \in \mathcal{N}_z, \tag{13d}$$

$$u_{\min} \leq u_{k+j} \leq u_{\max}, \quad j \in \mathcal{N}_u. \tag{13e}$$

$\Delta u_{k+j} = u_{k+j} - u_{k+j-1}$, $\mathcal{N}_z = \{1, 2 \ldots, N\}$, and $\mathcal{N}_u = \{0, 1 \ldots, N-1\}$. The control and prediction horizon is $N = 30\ \text{min}/T_s = 60$. The control and prediction horizon, N, is selected sufficiently long such that any end effects have no influence on the solution in the beginning of the horizon. No forecasts are available for the target, r_k, and the measured disturbances, d_k. Therefore we use the same-as-now predictions in (13). The values for the input constraints, $u_{\min}$ and $u_{\max}$, are given by (5). The tuning parameters, Q_z and $Q_{\Delta u}$, are selected by trial and error such that an acceptable compromise between robustness and agility is obtained. The highest weight is associated to the residual moisture content.

The solution of (13) provides the sequence $\{u_{k+j}\}_{j=0}^{N-1}$. Only the first variable, u_k, in this sequence is implemented. This combined procedure is denoted $u_k = \mu(r_k, \hat{\bar{x}}_{k|k}, u_{k-1}, d_k)$.

5.5. MPC-RTO algorithm

Algorithm 2 lists the computations in the MPC-RTO algorithm. At every sample, the MPC-RTO assumes that the measurements, y_k, the measured disturbances, d_k, the mean and the covariance of the one-step predicted state, $\hat{\bar{x}}_{k|k-1}$ and $\bar{P}_{k|k-1}$, the previous input, u_{k-1}, and the previous targets, r_{k-1}, are available. Based on that, the LTV filter estimates the current augmented state, $\hat{\bar{x}}_{k|k}$, and its covariance, $\bar{P}_{k|k}$. The RTO computes the optimal target, $r_k = \rho(\hat{\bar{x}}_{k|k}, d_k, r_{k-1}, k)$, as a function of the current estimated states, $\hat{\bar{x}}_{k|k}$, the measured disturbances, d_k, the previous target, r_{k-1}, and the sample instant, k. The dependence on k is used to ensure that the optimization (11) is not performed at every sample but in the case of the spray dryer only at every 50th sample (every 25 minutes). The linear MPC uses the target, r_k, computed by the RTO, the estimated augmented states, $\hat{\bar{x}}_{k|k}$, the previous manipulated variables, u_{k-1}, and the measured disturbances, d_k, to compute the manipulated variables, $u_k = \mu(r_k, \hat{\bar{x}}_{k|k}, u_{k-1}, d_k)$. This value, u_k, is implemented on the process. To prepare the MPC-RTO for the next sample time, the one-step prediction of the augmented states and their covariance are computed using the predictions for linear systems listed in Algorithm 2.

Algorithm 2 MPC-RTO Algorithm

Require: y_k, d_k, $\hat{\bar{x}}_{k|k-1}$, $\bar{P}_{k|k-1}$, u_{k-1}, r_{k-1}

Filter:

Compute the one-step ahead measurement prediction

$\hat{y}_{k|k-1} = \bar{C}_{y,k}\hat{\bar{x}}_{k|k-1} + \sigma_{y,k}$

Compute the innovation and the filtered state

$\varepsilon_k = y_k - \hat{y}_{k|k-1}$

$R_{e,k} = \bar{C}_{y,k}\bar{P}_{k|k-1}\bar{C}_{y,k}^T + R_{v,k}$

$\bar{K}_{fx,k} = \bar{P}_{k|k-1}\bar{C}_{y,k}^T R_{e,k}^{-1}$

$\hat{\bar{x}}_{k|k} = \hat{\bar{x}}_{k|k-1} + \bar{K}_{fx,k}\varepsilon_k$

$\bar{P}_{k|k} = \bar{P}_{k|k-1} - \bar{K}_{fx,k}R_{e,k}\bar{K}_{fx,k}^T$

RTO:

$r_k = \rho(\hat{\bar{x}}_{k|k}, d_k, r_{k-1}, k)$

Regulator:

$u_k = \mu(r_k, \hat{\bar{x}}_{k|k}, u_{k-1}, d_k)$

One-step predictor:

Compute the one-step ahead state and covariance prediction

$\hat{\bar{x}}_{k+1|k} = \bar{A}\hat{\bar{x}}_{k|k} + \bar{B}u_k + \bar{E}d_k + \bar{\sigma}_x$

$\bar{P}_{k+1|k} = \bar{A}\bar{P}_{k|k}\bar{A}^T + \bar{G}\bar{R}_w\bar{G}^T$

return u_k, r_k, $\hat{\bar{x}}_{k+1|k}$, $\bar{P}_{k+1|k}$

6. Economic nonlinear model predictive control

In the following, we briefly present the E-NMPC. E-NMPC uses the economic objective function directly in the control layer. While the RTO in the RTO-MPC uses the economic objective function for steady state optimization, the E-NMPC integrates the economic objective function to capture the effect of transients on the economics. As the economic objective is included directly in the control layer by E-NMPC, the need for intermediate targets is eliminated. The regulator directly seeks to dynamically optimize the economic performance within the given process constraints. The measurements, y, the measured disturbances, d, and the manipulated variables, u, used by the spray dryer E-NMPC are as described by (1). The E-NMPC consists of an extended Kalman filter (EKF) for the filtering and prediction, and a dynamic optimization problem in the regulator for computing the manipulated variables, u_k. The EKF and the regulator in the E-NMPC use an augmented nonlinear model to ensure offset free control.

6.1. Model

The E-NMPC is based on the complexity reduced nonlinear model [3] that is different from the simulation model [2]. The complexity reduced model is denoted by

$$x_{k+1} = F(x_k, u_k, d_k, \theta) + Gw_k, \tag{14a}$$
$$y_k = h_y(x_k) + v_k, \tag{14b}$$
$$z_k = h_z(x_k), \tag{14c}$$

where F denotes the operator that computes the solution, x_{k+1}, of

$$x(t_k) = x_k, \tag{15a}$$
$$\frac{d}{dt}g(x(t)) = f(x(t), u_k, d_k, \theta), \qquad t_k \le t \le t_{k+1}, \tag{15b}$$
$$x_{k+1} = x(t_{k+1}). \tag{15c}$$

This model can be solved using the ESDIRK3(4) method with variable step size [34, 43]. Both the process noise, $w_k \sim N_{\text{iid}}(0, R_{\text{w}})$, and the measurement noise, $v_k \sim N_{\text{iid}}(0, R_{\text{v}})$, are normally distributed stochastic variables.

Offset-free estimation of the measurements and offset-free control at steady-state are achieved by augmenting the model. The state vector, x, is augmented by a vector of integrated disturbance states, x_{d}. The augmented state vector is $\bar{x} = [x; x_{\text{d}}]$. The regulator and state estimator are based on the augmented model,

$$\bar{x}_{k+1} = \bar{F}(\bar{x}_k, u_k, d_k, \theta) + \bar{G}\bar{w}_k, \tag{16a}$$
$$y_k = \bar{h}_{\text{y}}(\bar{x}_k) + v_k, \tag{16b}$$
$$z_k = \bar{h}_{\text{z}}(\bar{x}_k), \tag{16c}$$

where the operator $\bar{F}$ denotes the solution, $\bar{x}_{k+1}$, of

$$\bar{x}(t_k) = \bar{x}_k, \tag{17a}$$
$$\frac{d}{dt}\bar{g}(\bar{x}(t)) = \bar{f}(\bar{x}(t), u_k, d_k, \theta), \quad t_k \le t \le t_{k+1}, \tag{17b}$$
$$\bar{x}_{k+1} = \bar{x}(t_{k+1}) \tag{17c}$$

with

$$\bar{g}(\bar{x}) = \begin{bmatrix} g(x) \\ x_{\text{d}} \end{bmatrix}, \qquad \bar{f}(\bar{x}, u, d, \theta) = \begin{bmatrix} f(x, u, d, \theta) + B_{\text{d}}x_{\text{d}} \\ 0 \end{bmatrix}.$$

The augmented output functions are

$$\bar{h}_{\text{y}}(\bar{x}_k) = h_{\text{y}}(x_k) + C_{\text{y,d}}x_{\text{d},k}, \tag{18a}$$
$$\bar{h}_{\text{z}}(\bar{x}_k) = h_{\text{z}}(x_k) + C_{\text{z,d}}x_{\text{d},k}. \tag{18b}$$

The augmented process noise vector is $\bar{w}_k = [w; w_{\text{d}}]_k \sim N_{\text{iid}}(0, \bar{R}_{\text{w}})$ with

$$\bar{G} = \begin{bmatrix} G & 0 \\ 0 & I \end{bmatrix}, \qquad \bar{R}_{\text{w}} = \begin{bmatrix} R_{\text{w}} & 0 \\ 0 & R_{\text{w}_{\text{d}}} \end{bmatrix}.$$

For the noise and disturbance model used in this paper, we have $G = I$, $C_{\text{y,d}} = 0$, and $C_{\text{z,d}} = 0$. B_{d} is a structural matrix selected such that it puts integrators on the energy balances and the vapor mass balances.

6.2. State estimator for filtering and prediction

The extended Kalman filter (EKF) for the discrete system (16) is used to estimate the filtered state, $\hat{\bar{x}}_{k|k}$, and its covariance, $\bar{P}_{k|k}$, as well as the one-step-ahead predicted state, $\hat{\bar{x}}_{k+1|k}$, and its covariance, $\bar{P}_{k+1|k}$ [44–48]. A number of different approaches for estimating the unknown noise variances, $\bar{R}_{\text{w}}$ and R_{v}, in the EKF exist. These methods include a sensitivity based approach [49, 50], the ALS approach [41, 51, 52], and the ML approach [38–40, 53, 54]. We estimate $\bar{R}_{\text{w}} = \bar{R}_{\text{w}}(\bar{\theta})$ and $R_{\text{v}} = R_{\text{v}}(\bar{\theta})$ by the ML method, i.e. we solve the optimization problem (10) using (9) with the innovation, $\varepsilon_k = \varepsilon_k(\bar{\theta})$, and its covariance, $R_{e,k} = R_{e,k}(\bar{\theta})$, computed by the EKF.

6.3. Discrete-time optimal control problem

In a receding horizon manner, the optimal predicted input profile, $\{u_{k+j}\}_{j=0}^{N-1}$, in the E-NMPC is obtained by the solution of the following finite dimensional discrete optimal control problem,

$$\min_{x,u,z,s} \ \phi = \phi_{\text{e}} + \phi_{\text{s}} + \phi_{\Delta\text{u}}, \tag{19a}$$
$$\text{s.t.} \quad x(t_k) = \hat{x}_{k|k}, \tag{19b}$$
$$\frac{d}{dt}g(x(t)) = f(x(t), u(t), d_k, \theta) + B_{\text{d}}\hat{x}_{\text{d},k|k}, \quad t \in \mathcal{T}_k, \tag{19c}$$
$$z(t) = h_{\text{z}}(x(t)) + C_{\text{z,d}}\hat{x}_{\text{d},k|k}, \qquad t \in \mathcal{T}_k, \tag{19d}$$
$$u(t) = u_{k+j}, \quad t_{k+j} \le t < t_{k+j+1}, \qquad j \in \mathcal{N}_u, \tag{19e}$$
$$u_{\min} \le u_{k+j} \le u_{\max}, \qquad j \in \mathcal{N}_{\text{u}}, \tag{19f}$$
$$c(z(t_{k+j})) + s_{k+j} \ge 0, \qquad j \in \mathcal{N}_{\text{z}}, \tag{19g}$$
$$s_{k+j} \ge 0, \qquad j \in \mathcal{N}_{\text{z}}, \tag{19h}$$

where the objective function, ϕ, consists of an economic term,

$$\phi_{\text{e}} = -\int_{t_k}^{t_k+T} p(z(t), u(t), d_k)dt, \tag{20}$$

measuring the profit of operation, an $\ell_2 - \ell_1$ penalty term,

$$\phi_{\text{s}} = \sum_{j=1}^{N} \rho(s_{k+j}), \tag{21}$$

penalizing violoation of the pointwise output constraints (19g), and an input-rate of movement regularization term,

$$\phi_{\Delta\text{u}} = \frac{1}{2}\sum_{j=0}^{N-1} \left\|\Delta u_{k+j}\right\|_{\text{Q}_{\Delta\text{u}}}^2 = \frac{1}{2}\sum_{j=0}^{N-1} \left\|u_{k+j} - u_{k+j-1}\right\|_{\text{Q}_{\Delta\text{u}}}^2, \tag{22}$$

that prevents the optimal profile of manipulated variables from large variations from sample to sample.

The sampling time of the E-NMPC is $T_{\text{s}} = 30$ [s]. The control and prediction horizon is $T = 25$ min such that $N = T/T_{\text{s}} = 50$. $\mathcal{T}_k = [t_k, t_k + T]$ denotes the time interval. $\mathcal{N}_u = \{0, 1, \ldots, N-1\}$ and $\mathcal{N}_{\text{z}} = \{1, 2, \ldots, N\}$. The profit rate, $p(z(t), u(t), d_k)$, is identical to the profit rate used by the RTO. p is computed using (2) and the complexity reduced nonlinear model [3]. The $\ell_2 - \ell_1$ penalty function is the same as for the RTO. The inputs are parameterized using piecewise constant

Algorithm 3 E-NMPC Algorithm

Require: y_k, d_k, $\hat{\bar{x}}_{k|k-1}$, $\bar{P}_{k|k-1}$, u_{k-1}

Filter:

Compute the one-step ahead measurement prediction

$\hat{y}_{k|k-1} = \bar{h}_{\mathrm{y}}(\hat{\bar{x}}_{k|k-1}), \quad \bar{C}_{\mathrm{y},k} = \frac{d\bar{h}_{\mathrm{y}}}{d\bar{x}}(\hat{\bar{x}}_{k|k-1})$

Compute the innovation and the filtered state

$\varepsilon_k = y_k - \hat{y}_{k|k-1}$

$R_{\mathrm{e},k} = \bar{C}_{\mathrm{y},k}\bar{P}_{k|k-1}\bar{C}_{\mathrm{y},k}^T + R_{\mathrm{v}}$

$\bar{K}_{\mathrm{fx},k} = \bar{P}_{k|k-1}\bar{C}_{\mathrm{y},k}^T R_{\mathrm{e},k}^{-1}$

$\hat{\bar{x}}_{k|k} = \hat{\bar{x}}_{k|k-1} + \bar{K}_{\mathrm{fx},k}\varepsilon_k$

$\bar{P}_{k|k} = \bar{P}_{k|k-1} - \bar{K}_{\mathrm{fx},k}R_{\mathrm{e},k}\bar{K}_{\mathrm{fx},k}^T$

Regulator:

$u_k = \kappa(\hat{\bar{x}}_{k|k}, u_{k-1}, d_k)$

One-step predictor:

Compute the predicted state, $\hat{\bar{x}}_{k+1|k} = \bar{F}(\hat{\bar{x}}_{k|k}, u_k, d_k)$, and the state sensitivity, $\bar{A}_k = \frac{\partial \bar{F}}{\partial \bar{x}}(\hat{\bar{x}}_{k|k}, u_k, d_k)$, using an ESDIRK method with sensitivity computations.

$\bar{P}_{k+1|k} = \bar{A}_k\bar{P}_{k|k}\bar{A}_k^T + \bar{G}\bar{R}_{\mathrm{w}}\bar{G}^T$

return u_k, $\hat{\bar{x}}_{k+1|k}$, $\bar{P}_{k+1|k}$

functions (19e) and constraints (19f) corresponding to (5). The functions, $c(z)$, for the output constraints are discussed in [3]. The solution to (19) provides an optimal trajectory, $\{u_{k+j}\}_{j=0}^{N-1}$, of which only the first manipulated variable, u_k, is implemented on the process. The function generating this manipulated variable is denoted $u_k = \kappa(\hat{\bar{x}}_{k|k}, u_{k-1}, d_k) = \kappa([\hat{x}_{k|k}; \hat{x}_{\mathrm{d},k|k}], u_{k-1}, d_k)$.

6.4. E-NMPC algorithm

Algorithm 3 lists the on-line computations in the E-NMPC algorithm. The computations consist of the filtering in the EKF (filter), the solution of a constrained optimal control problem (regulator), and the one-step prediction using the EKF (one-step predictor). For the spray dryer, the sample time of this E-NMPC algorithm is $T_s = 30$ [s].

The main computational effort in Algorithm 3 is the computation of $u_k = \kappa(\hat{\bar{x}}_{k|k}, u_{k-1}, d_k)$ by solution of the constrained optimal control problem (19). This constrained optimal control problem (19) may be solved using the control vector parametrization method [55], the multiple-shooting method [56, 57], or the simultaneous method [58–60]. Within these classes of algorithms, a number of variations exist on the solution of the quadratic programming subproblem, the SQP strategy, and the sensitivity computations. We solve (19) using the multiple-shooting method [61] and an interior-point optimization algorithm [62] (`IPOPT` interfaced from Matlab®). The gradient computation is performed using forward sensitivities [43, 63].

The one-step ahead prediction, $\hat{\bar{x}}_{k+1|k}$, and the corresponding sensitivities, $\bar{A}_k$, are computed using an ESDIRK method with sensitivity computation capabilities [43, 63]. This enables computation of the one-step ahead state covariance, $\bar{P}_{k+1|k}$, of the augmented system.

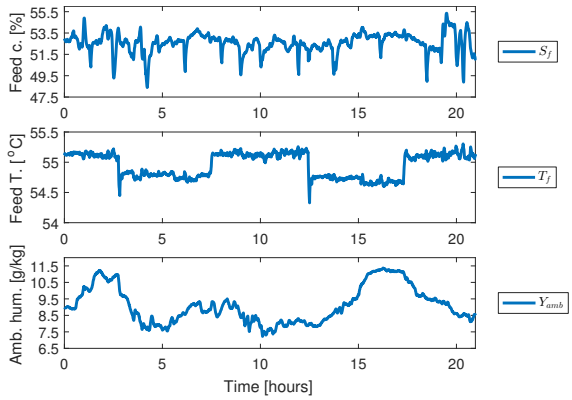

Figure 3: Industrially recorded disturbance scenario. The values of the variables, S_{f}, Y_{amb} and T_{f}, in this disturbance scenario are used in the the closed-loop simulations.

7. Simulation results

In this section, we compare the performance of the PI control strategy, the MPC-RTO strategy, and the E-NMPC strategy by closed-loop simulations.

7.1. Industrially recorded disturbance scenario

Fig. 3 illustrates the disturbance scenario used in the simulations of the three control strategies. The feed solids concentration, S_{f}, the feed temperature, T_{f}, and the ambient air humidity, Y_{amb}, are industrially recorded disturbances. Compared to other dryers, the feed solids concentration, S_{f}, has a relatively large variance, while the feed temperature, T_{f}, is rather stable. The ambient air humidity, Y_{amb}, resembles normal variations from a summer day in northern Europe. The disturbances, F_{main}, F_{sfb}, F_{vfbh}, F_{vfbc}, T_{vfbc} and T_{amb}, are constant. In combination, these disturbances represent a realistic disturbance scenario for the closed-loop simulations.

7.2. Proportional-integral control

Fig. 4 shows the measurements, y, the target, T_{sp}, and the manipulated variables, u, of the spray dryer during the closed-loop simulation of the PI control strategy. The simulation shows that the PI controller is able to maintain a stable exhaust air temperature, T_{SD}, as it was designed for. The exhaust air humidity, Y_{ab}, and the residual moisture content, $1 - S_{\mathrm{cd}}$, are not controlled in the PI control strategy and fluctuate due to the changes in the disturbances, viz. the feed solids concentration, S_{f}, the feed temperature, T_{f}, and the ambient air humidity, Y_{amb}.

As discussed in Section 2.4 and illustrated in Fig. 2, the set-point of the controller is kept constant for long periods and the inlet air temperatures are not manipulated in the PI control strategy. Accordingly, the controller avoids violation of the stickiness constraint and the powder moisture limit by the application of a considerably back-off from the process constraints. The constraints are reached at high ambient air humidities. The

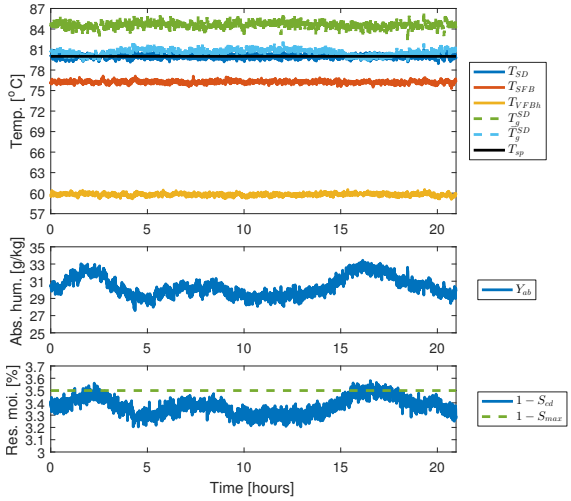

(a) The measured variables, the constraints, and the target.

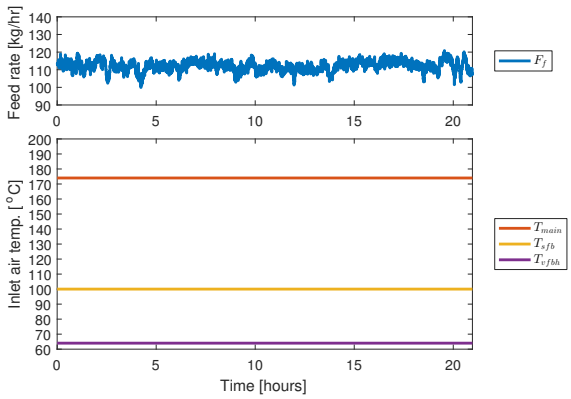

(b) The manipulated variables.

Figure 4: Simulation of the PI control strategy subject to the disturbance scenario given in Fig. 3.

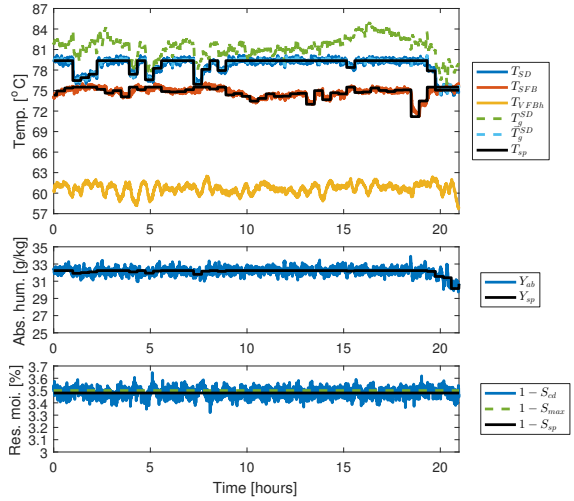

(a) The measured variables, the constraints, and the targets.

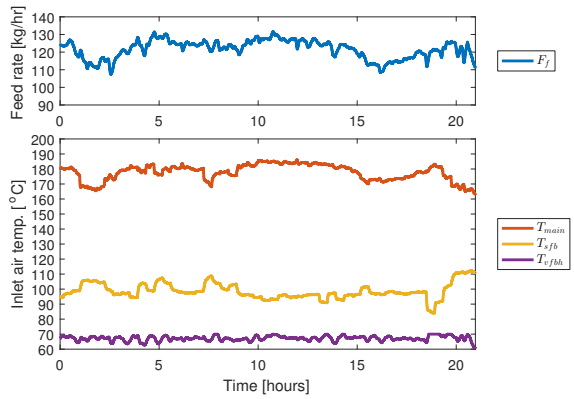

(b) The manipulated variables.

Figure 5: Simulation of the MPC-RTO strategy subject to the disturbance scenario given in Fig. 3.

stickiness constraint, i.e. the constraint related to the glass transition temperature, $\bar{T}_g^{SD}$, is reached at t=2.5 and t=16 hours due to high ambient air humidities. The powder moisture limit is reached at the same time points due to the high ambient air humidities. The controller rejects the effect of the variations in the feed solids concentration on the exhaust air humidity, Y_{ab}, well. The residual moisture content, $1 - S_{cd}$, is affected by all three disturbances. The PI-control strategy only partially and indirectly mitigates the effect of the disturbances on the residual moisture content.

The stickiness constraint determined by the simulation model and the control model, T_g^{SD} and $\bar{T}_g^{SD}$, disagree due to the simplified description of this constraint in the control model. $\bar{T}_g^{SD}$ is conservatively designed compared to T_g^{SD} such that the true simulation constraint is not violated during operation.

Due to the applied back-off, the PI control strategy makes the dryer dry the powder more than necessary to keep the powder moisture below the maximum limit and avoid violation of the stickiness constraint at all time. This more extensive drying decreases the energy efficiency and the yield, i.e. the residual moisture content sold as product, of the production.

7.3. Model predictive control with real-time optimization

Fig. 5 shows the measurements, y, the targets, r, and the manipulated variables, u, of the spray dryer during the closed-loop simulation of the MPC-RTO strategy. The simulation shows that the MPC-RTO strategy is able to steer the controlled variables, z, to the targets, r, computed by the RTO. The controlled variables are the variables related to the stickiness of the powder, T_{SD} and Y_{ab}, the SFB stage temperature, T_{SFB}, and the residual moisture content, $1 - S_{cd}$. The effect of the disturbances on the controlled variables are rejected by adjustments

of the manipulated variables every 30 seconds. Every 25 minutes, the RTO updates the optimal steady state targets based on the measurements, the economic objective, and the process constraints.

As discussed in Section 2.4 and illustrated in Fig. 2, in combination the tracking ability of the MPC and the target updates of the RTO reduce the necessary back-off from the constraints compared to the PI control strategy. The reduced back-off results in an increased profit of operation. The applied back-off is selected to render comparable constraint violations to the other control strategies. As can be seen in Fig. 5(b), the MPC-RTO manipulates F_f relatively smoothly compared to the PI controller (Fig. 4(b)). Making the MPC-RTO more aggressive, like the PI controller, did not significantly reduce the variance of the controlled variables nor the constraint violations. We find that the limiting factor to reduce the applied back-off is the fixed targets, r, that the RTO updates every 25 minutes, only.

Compared to the PI control simulation, the MPC-RTO increases the average product flow rate, F_p. This can be observed by inspection of the manipulated feed flow rate, F_f, in Fig. 4(b) and Fig. 5(b). As a consequence of the higher feed and production rate of the MPC-RTO, the MPC-RTO also increases the average energy supply from the heaters. Fig. 5(b) reveals this by increased inlet air temperatures, T_main, T_sfb and T_vfbh, compared to inlet air temperatures of the PI control strategy (Fig. 4(b)). Drying in the SFB and VFB stages is more energy efficient than drying in the SD stage. Therefore, the MPC-RTO seeks to maximize drying in these fluid bed stages to bring the moisture content of the powder below its maximum limit. The RTO increases the drying in the SFB and VFB stages by selecting an operating point that increases the inlet air temperatures, T_sfb and T_vfbh. Consider Fig. 5(b) as an example illustrating the mechanisms of MPC-RTO. Fig. 5(b) shows how the MPC-RTO manipulates T_vfbh. The RTO selects the operating point such that T_vfbh is at its upper limit except for the back-off, δ_u. The MPC manipulates T_vfbh around this operating point to keep the controlled variables at their targets. At time t=1 to t=2, t=4, t=5 and t=7.5 hours and between t=19 to t=21 hours, the RTO reduces the drying capacity, Y_ab, as the SFB stage temperature, T_SFB, reaches its upper limit at 75.5 [°C]. The reduced capacity results in a simultaneous decrease of the exhaust air temperature, T_SD, to reduce the energy consumption and to avoid violating the stickiness constraint. In comparison to the PI-control strategy, the MPC-RTO increases the average residual moisture content and controls it to be constantly close to the upper limit. The increased residual moisture content improves the process economics in two ways: 1) it reduces the required heat for evaporation and thereby reduces the energy costs; 2) it increases the product flow rate by including more water as part of the product. Thereby, the increased water in the product can be sold at the price of powder.

7.4. Economic nonlinear model predictive control

Fig. 6 shows a simulation of the measurements, y, and the manipulated variables, u, of the spray dryer operated by the E-NMPC. As discussed in Section 2.4 and illustrated in Fig. 2, the manipulated variables determined by the E-NMPC strategy

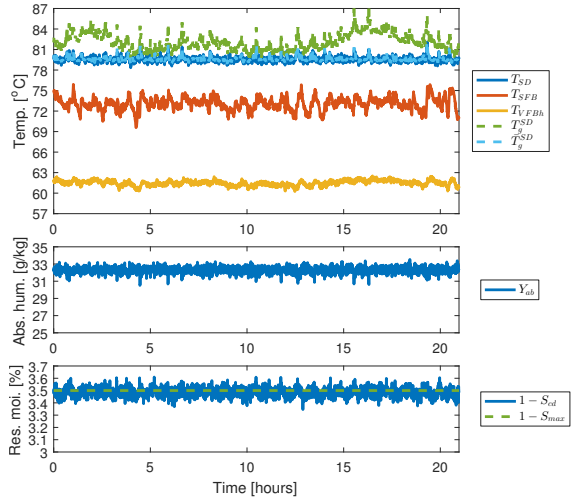

(a) The measured variables and the constraints.

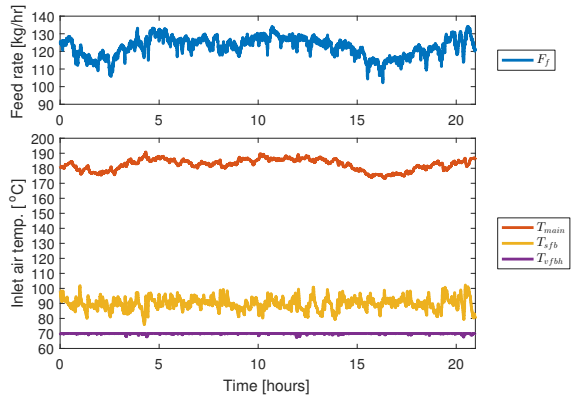

(b) The manipulated variables.

Figure 6: Simulation of the E-NMPC strategy subject to the disturbance scenario given in Fig. 3.

operates the dryer to maximize the predicted profit of operation. The effects of plant-model mismatch and disturbances (known and unknown) are rejected by adjustments of the manipulated variables according to the feedback from measurements and measured disturbances, the economic objective, and the specified process constraints. The dynamic optimization takes place at each sample (30 sec) and this reduces the necessary back-off compared to the MPC-RTO strategy, where the RTO only executes every 25 min.

The E-NMPC strategy seeks to optimize the combined transient and steady-state economics of the spray dryer. For the long control and prediction horizon selected in this study, E-NMPC brings the spray dryer to an optimal steady-state point that is similar to the steady-state operating point selected by the RTO of the MPC-RTO. E-NMPC uses a full nonlinear model, while the RTO uses a linear model for the dynamics and the

same nonlinear model as the E-NMPC for the profit function and the stickiness constraint. Thus, in both simulations, the economic optimum is reached when T_{SD} reaches the point at which the powder turns sticky in the top of the chamber, i.e. the glass transition temperature constraint, $\bar{T}_{\mathrm{g}}^{\mathrm{SD}}$, and when $1 - S_{\mathrm{cd}}$, the moisture content of the powder, reaches $1 - S_{\mathrm{max}}$. In this way, the product flow rate is maximized, the residual moisture is controlled to the specification, and the SFB stage temperature is kept within the constraints. At the same time, the supply of energy is minimized. As in the case of the MPC-RTO, E-NMPC exploits that the most efficient drying occurs in the fluid beds, i.e. the SFB and VFB stages. E-NMPC increases the SFB and VFB air temperatures, T_{sfb} and T_{vfbh}, to bring the residual moisture content just below its maximum limit.

The powder becomes moister and potentially sticky inside the dryer, when the ambient air humidity, Y_{amb}, increases as well as when the feed solid concentration, S_{f}, decreases. The E-NMPC compensates for such variations (increased air humidity and/or descreased feed solid concentration) by decreasing the feed flow rate, F_{f}, and by adjusting the inlet air temperatures. In this way, E-NMPC maintains operation at the optimal production rate using the optimal heat supply.

7.5. Stickiness

The glass transition temperature at the SD stage, $\bar{T}_{\mathrm{g}}^{\mathrm{SD}}$, determines whether the powder sticks in the SD stage of the spray dryer. When the powder temperature in the SD stage, T_{SD}, is below the glass transition temperature in the SD stage, i.e. $T_{\mathrm{SD}} \leq \bar{T}_{\mathrm{g}}^{\mathrm{SD}}$, the powder is non-sticky. Otherwise, the powder is sticky. Reference [3] provides an expression of the glass transition temperature. The glass transition temperature depends on the moisture in the powder. In the simplified, yet reasonably accurate, model used by the MPC-RTO and the E-NMPC, the moisture in the powder at the SD stage is a function of the temperature, T_{SD}, and the air humidity, Y_{ab}. This implies that the estimated sticky and non-sticky regions of the SD stage can be visualized in a 2D-plot. Fig. 7 illustrates the stickiness constraint, $\bar{T}_{\mathrm{g}}^{\mathrm{SD}}$, as well as the phase portrait of the trajectories generated by the PI control strategy, the MPC-RTO, and the E-NMPC. Due to stochastic disturbances, the trajectories produced by all three controllers occasionally violate the stickiness constraint. Therefore, the operating point and stickiness constraint used by the controllers are designed such that they are backed off from the true stickiness constraint of the process.

The PI control strategy does not control the exhaust air humidity, Y_{ab}, directly. In this case, Y_{ab} varies from 27.5 [g/kg] to 34 [g/kg]. Therefore, the operating point of the PI control strategy is selected such that the mean value of Y_{ab} is relatively far from the air humidity stickiness constraint. The consquence is that the production rate is also below the production capacity of the spray dryer.

The MPC-RTO operates the air humidity, Y_{ab}, closer to the constraint limit than the PI control strategy, as it adjusts the operating point every 25 minutes according to the measurements and the measured disturbances. As is evident by Fig. 7, the MPC-RTO does not operate at the maximum air humidity, and consequently not at the maximum production rate, at all times.

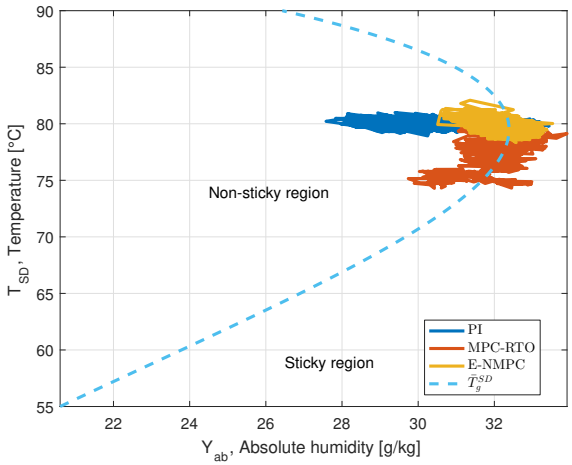

Figure 7: The stickiness constraint from (11f) and (19g) constrains T_{SD} and Y_{ab}. Note, that cost optimal operation is achieved by maximizing Y_{ab} within the non-sticky region.

The RTO problem (11) contains back-offs in the manipulated variables. Due to these back-offs, the temperature of the VFB inlet air stream, T_{vfbh}, is on average decreased compared to the simulation of the E-NMPC strategy (Fig. 6(a)). The MPC-RTO compensates for the decreased VFB inlet air temperature, T_{vfbh}, by increasing the SFB inlet air temperature, T_{sfb}. Consequently, the SFB temperature, T_{SFB}, increases and the upper limit on the SFB temperature, $T_{\mathrm{SFB}} \leq 75.5$ [°C], becomes active (Fig. 5(a)). When the SFB temperature limit is active, the MPC-RTO decreases the production rate as well as the energy supply from the main inlet air and the SFB inlet air, to maintain a stable SFB temperature. Simultaneously, the decreased production rate allows the SD temperature, T_{SD}, to be decreased along the stickiness constraint to save energy and increase the energy efficiency.

The E-NMPC is able to maintain a maximum air humidity and capacity at all time. In the simulation, T_{SD} and Y_{ab} are kept constant at the maximum exhaust air humidity. The E-NMPC is able to do so as no back-off is implemented in the constraints of the manipulated variables and the controlled variables. If for instance the feed solids concentration, S_{f}, had increased further, the E-NMPC would have to decrease the capacity accordingly and in a similarly way to the way MPC-RTO reduces capacity.

7.6. Key performance indicators

Fig. 8 illustrates the product flow rate, F_{p}, the specific energy consumption, $Q_{\mathrm{tot}}/F_{\mathrm{p}}$, the energy efficiency, η, and the profit of operation, p, for the closed-loop simulations of the three control strategies. Table 1 provides the average values of the key performance indicators (KPIs) for the three control strategies.

Fig. 8 and Table 1 show that the performance of the PI control strategy is inferior compared to the performances of the MPC-RTO and the E-NMPC. Compared to the MPC-RTO and the E-NMPC, the PI control strategy has a lower average prod-

Table 1: Average KPI values.

KPI		PI	MPC-RTO	E-NMPC	% increase to PI	
					MPC-RTO	E-NMPC
Product flow rate	F_p [kg/hr]	60.95	66.21	66.81	8.63%	9.61%
Energy consumption rate	Q_{tot} [kW]	87.2	89.1	90.4	2.21%	3.63%
Specific energy consumption	$\frac{Q_{tot}}{F_p}$ [MJ/kg]	5.16	4.81	4.88	-6.72%	-5.44%
Residual moisture	$1 - S_{cd}$ [%]	3.37	3.48	3.49	3.21%	3.37%
Energy efficiency	η [%]	40.2	42.7	42.5	6.06%	5.52%
Profit of operation	p [€/hr]	123.25	133.98	135.19	8.71%	9.69%

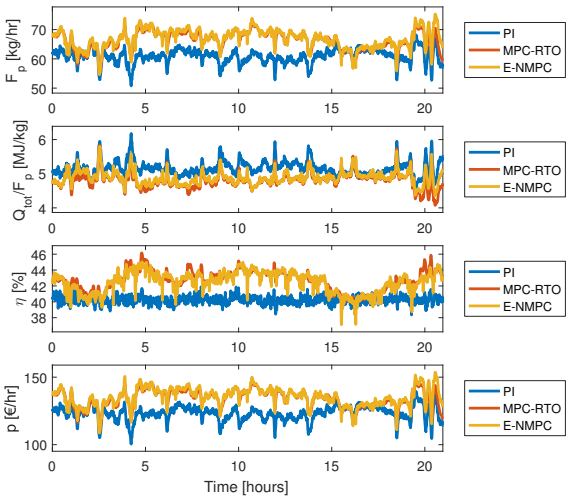

Figure 8: The product flow rate, the specific energy consumption, the energy efficiency, and the profit of operation for the three control strategies.

uct flow rate, a higher specific energy consumption, a lower energy efficiency, and a lower profit of operation. During most of the time in the simulations, the MPC-RTO and the E-NMPC increase both the product flow rate and the energy efficiency considerably. The three controllers perform equally well when the ambient air humidity is high. This illustrates that the benefits arise from the ability of the MPC-RTO and the E-NMPC to utilize the excess capacity available at the low ambient air humidity. The energy efficiency increases as the exhaust air temperature decreases along the stickiness constraint. Thus, the most economic point of operation where Y_{ab} is maximized is not the most energy efficient point of operation. This is also revealed by Table 1. Table 1 shows that MPC-RTO provides the most energy efficient operation. Nevertheless, E-NMPC provides the operation with the largest economic profit. From Table 1, it should be noticed that the increased profit (8.71% and 9.69%) is highly correlated with the increased production rate (8.63% and 9.61%). The residual moisture content is increased by 3.21% and 3.37%, respectively. This contributes significantly to the increased profit of operation as it corresponds to selling water at the price of powder and using less energy for evaporation of the water. The total energy consumption is increased for the MPC-RTO and E-NMPC strategies due to the increased production rate. However, more importantly the specific energy consumption decreases and the energy efficiency increases when using the MPC-RTO and the E-NMPC. MPC-RTO decreases the specific energy consumption by 6.72% and increases the energy efficiency by 6.06%. E-NMPC decreases the specific energy consumption by 5.44% and increases the energy efficiency by 5.52%.

The cumulative increased profit over a year by replacing the standard industrial PI control strategy with the MPC-RTO strategy is (133.98 [€/hr] − 123.25 [€/hr]) · 7200 [hr/year] = 77,000 [€/year]. Similarly, the annual cumulative profit increase by using the E-NMPC instead of the PI control strategy is (135.19 [€/hr] − 123.25 [€/hr]) · 7200 [hr/year] = 86,000 [€/year]. Thus, the profit of operation per year is potentially increased considerably by both model based controllers. These numbers are for an industrial small scale spray dryer with a production capacity around 60 kg/hr. An industrial sized spray dryer for production of skimmed milk powder has a capacity of approximately 7,500 kg/hr. Consequently, industrial sized dryers have a capacity that is more than 100 times larger than the dryer simulated in this paper. Accordingly, the potential economic benefit of replacing existing PI controls strategies with advanced process control is significant.

8. Conclusions

In this paper, we present three control strategies for a four-stage spray dryer and compare their performance based on the product flow rate, the residual moisture content, the specific energy consumption, the energy efficiency, and the profit of operation. The industrially used PI control strategy serves as a benchmark for the performance of the MPC-RTO and the E-NMPC control strategies. Both model based controllers increase the profit of operation by increasing the product flow rate, the residual moisture content, and decreasing the specific energy consumption. The residual moisture content is controlled within specifications, and deposits of sticky powder particles on the spray dryer surfaces are avoided. For the given disturbance scenario, the MPC-RTO increases the profit of operation by 8.71% and the E-NMPC increases the profit of operation by 9.69%. The performance difference between the MPC-RTO and the E-NMPC is mainly due to the necessary back-off in the constraints employed in the RTO layer. The economic value of the MPC-RTO and E-NMPC compared to the PI control strategy stems from the adjustment of the operating point of the dryer to the actual disturbances such that the spray dryer can be operated closer to the process constraints.

Acknowledgement

This work was funded in part by 1) the Danish Ministry of Higher Education and Science in the industrial PhD project "Economic Model Predictive Control for Spray Drying Plants" (12-128720); 2) GEA Process Engineering A/S, DK-2860 Søborg, Denmark; 3) EUDP 64013-0558 in the IEA Annex for Energy Efficient Process Control.

References

[1] W. P. Oliveira, C. R. F. Souza, L. E. Kurozawa, K. J. Park, Spray drying of food and herbal producs, in: M. W. Woo, A. S. Mujumdar, W. R. W. Daud (Eds.), Spray Drying Technology, Singapore, 2010, Ch. 5, pp. 113–156.

[2] L. N. Petersen, N. K. Poulsen, H. H. Niemann, C. Utzen, J. B. Jørgensen, An experimentally validated simulation model for a four-stage spray dryer, Journal of Process Control (in review).

[3] L. N. Petersen, J. B. Jørgensen, J. B. Rawlings, Economic optimization of spray dryer operation using nonlinear model predictive control with state estimation, 9th Symposium on Advanced Control of Chemical Processes (2015) 507–513.

[4] L. N. Petersen, N. K. Poulsen, H. H. Niemann, C. Utzen, J. B. Jørgensen, Comparison of linear and nonlinear model predictive control for optimization of spray dryer operation, 5th Conference on Nonlinear Model Predictive Control (2015) 218–223.

[5] S. J. Qin, T. A. Badgwell, A survey of industrial model predictive control technology, Control Engineering Practice 11 (7) (2003) 733–764.

[6] M. Bauer, I. K. Craig, Economic assessment of advanced process control – A survey and framework, Journal of Process Control 18 (1) (2008) 2–18.

[7] M. L. Darby, M. Harmse, M. Nikolaou, MPC: Current practice and challenges, 7th Symposium on Advanced Control of Chemical Processes 7 (1) (2009) 86–98.

[8] J. B. Rawlings, D. Angeli, C. N. Bates, Fundamentals of economic model predictive control, 51st Conference on Decision and Control (2012) 3851–3861.

[9] G. François, S. Costello, D. Bonvin, Application of real-time optimization methods to energy systems in the presence of uncertainties and disturbances, TMC Academic Journal 9 (2) (2015) 20–41.

[10] S. Engell, Feedback control for optimal process operation, Journal of Process Control 17 (2007) 203–219.

[11] M. L. Darby, M. Nikolaou, J. Jones, D. Nicholson, RTO: An overview and assessment of current practice, Journal of Process Control 21 (6) (2011) 874–884.

[12] T. E. Marlin, A. N. Hrymak, Real-time operations optimization of continuous processes, Chemical Process Control-V Conference (1996) 156–164.

[13] K. R. Muske, J. B. Rawlings, Model predictive control with linear models, AIChE Journal 39 (2) (1993) 262–287.

[14] D. E. Kassmann, T. A. Badgwell, R. B. Hawkins, Robust steady-state target calculation for model predictive control, AIChE Journal 46 (5) (2000) 1007–1024.

[15] G. Pannocchia, J. B. Rawlings, Disturbance models for offset-free model-predictive control, AIChE Journal 49 (2) (2003) 426–437.

[16] C. Ying, B. Joseph, Performance and stability analysis of LP-MPC and QP-MPC cascade control systems, AIChE Journal 45 (7) (1999) 1521–1534.

[17] K. B. Ariyur, M. Krstic, Real–Time Optimization by Extremum-Seeking Control, John Wiley and Sons, 2003.

[18] M. Guay, E. Moshksar, D. Dochain, A constrained extremum-seeking control approach, International Journal of Robust and Nonlinear Control 25 (16) (2015) 3132–3153.

[19] R. Amrit, Optimizing process economics in model predictive control, Ph.D. thesis, University of Wisconsin–Madison (2011).

[20] J. B. Rawlings, R. Amrit, Optimizing process economic performance using model predictive control, Lecture Notes in Control and Information Sciences 384 (2009) 119–138.

[21] D. Angeli, R. Amrit, J. B. Rawlings, On average performance and stability of economic model predictive control, IEEE Transactions on Automatic Control 57 (7) (2012) 1615–1626.

[22] J. B. Rawlings, D. Bonné, J. B. Jørgensen, A. N. Venkat, S. B. Jørgensen, Unreachable setpoints in model predictive control, IEEE Transactions on Automatic Control 53 (9) (2008) 2209–2215.

[23] L. W. Tan, F. S. Taip, N. Abdul Aziz, Simulation and control of spray drying using nozzle atomizer spray dryer, International Journal of Engineering & Technology 9 (10) (2009) 1–7.

[24] L. W. Tan, M. N. Ibrahim, R. Kamil, F. S. Taip, Empirical modeling for spray drying process of sticky and non-sticky products, Procedia Food Science 1 (2011) 690–697.

[25] V. S. Shabde, K. A. Hoo, Optimum controller design for a spray drying process, Control Engineering Practice 16 (5) (2008) 541–552.

[26] V. S. Shabde, K. A. Hoo, Design and operation of a spray dryer for the manufacture of hollow microparticles, Industrial & Engineering Chemistry Research 45 (2006) 8329–8337.

[27] V. S. Shabde, Optimal design and control of a spray drying process that manufacture hollow micro-particles, Ph.D. thesis, Texas Tech University (2006).

[28] C. A. Zaror, J. R. Pérez-Correa, Model based control of centrifugal atomizer spray drying, Food Control 2 (3) (1991) 170–175.

[29] J. R. Pérez-Correa, F. Farias, Modelling and control of a spray dryer: A simulation study, Food Control 6 (4) (1995) 219–227.

[30] R. Govaerts, A. Johnson, R. Crezee, G. Reyman, P. L. S. Swinkels, Control of an industrial spray-drying unit, Control Engineering Practice 2 (1) (1994) 69–85.

[31] L. N. Petersen, N. K. Poulsen, H. H. Niemann, C. Utzen, J. B. Jørgensen, Application of constrained linear MPC to a spray dryer, Multi-Conference on Systems and Control (2014) 2120–2126.

[32] L. N. Petersen, N. K. Poulsen, H. H. Niemann, C. Utzen, J. B. Jørgensen, Economic optimization of spray dryer operation using nonlinear model predictive control, 53rd Conference on Decision and Control (2014) 6794–6800.

[33] D. O'Callaghan, P. Cunningham, Modern process control techniques in the production of dried milk products – a review, Lait 85 (2005) 335–342.

[34] C. Völcker, J. B. Jørgensen, P. G. Thomsen, E. H. Stenby, Adaptive step size control in implicit runge-kutta methods for reservoir simulation, 9th International Symposium on Dynamics and Control of Process Systems (2010) 509–514.

[35] S. Skogestad, Simple analytic rules for model reduction and PID controller tuning, Journal of Process Control 13 (4) (2003) 291–309.

[36] K. J. Åström, T. Hägglund, Advanced PID control, Instrument Society of America, NC, USA, 2006.

[37] G. Pannocchia, M. Gabiccini, A. Artoni, Offset-free MPC explained: novelties, subtleties, and applications, 5th Conference on Nonlinear Model Predictive Control (2015) 342–351.

[38] N. R. Kristensen, H. Madsen, S. B. Jørgensen, A method for systematic improvement of stochastic grey-box models, Computers & Chemical Engineering 28 (8) (2004) 1431–1449.

[39] J. B. Jørgensen, S. B. Jørgensen, MPC-relevant prediction-error identification, The American Control Conference (2007) 2475–2480.

[40] J. B. Jørgensen, S. B. Jørgensen, Comparison of prediction-error-modelling criteria, The American Control Conference (2007) 140–146.

[41] B. J. Odelson, M. R. Rajamani, J. B. Rawlings, A new autocovariance least-squares method for estimating noise covariances, Automatica 42 (2006) 303–308.

[42] B. M. Åkesson, J. B. Jørgensen, N. K. Poulsen, S. B. Jørgensen, A generalized autocovariance least-squares method for Kalman filter tuning, Journal of Process Control 18 (7) (2008) 769–779.

[43] M. R. Kristensen, J. B. Jørgensen, P. G. Thomsen, S. B. Jørgensen, An ESDIRK method with sensitivity analysis capabilities, Computers & Chemical Engineering 28 (12) (2004) 2695–2707.

[44] J. B. Jørgensen, M. R. Kristensen, P. G. Thomsen, H. Madsen, A computationally efficient and robust implementation of the continuous-discrete extended Kalman filter, The American Control Conference (2007) 3706–3712.

[45] J. B. Jørgensen, A critical discussion of the continuous-discrete extended Kalman filter, in: European Congress of Chemical Engineering - 6, Copenhagen, Denmark, 2007.

[46] J. B. Rawlings, D. Q. Mayne, Model Predictive Control: Theory and Design, Nob Hill Publishing, 2009.

[47] E. L. Haseltine, J. B. Rawlings, Critical evaluation of extended Kalman filtering and moving-horizon estimation, Industrial & Engineering Chem-

istry Research 44 (8) (2005) 2451–2460.
[48] J. B. Rawlings, B. R. Bakshi, Particle filtering and moving horizon estimation, Computers & Chemical Engineering 30 (10) (2006) 1529–1541.
[49] J. Valappil, C. Georgakis, Systematic estimation of state noise statistics for extended Kalman filters, AIChE Journal 46 (2) (2000) 292–308.
[50] Z. K. Nagy, R. D. Braatz, Robust nonlinear model predictive control of batch processes, AIChE Journal 49 (7) (2003) 1776–1786.
[51] F. V. Lima, J. B. Rawlings, Nonlinear stochastic modeling to improve state estimation in process monitoring and control, AIChE Journal 57 (4) (2011) 996–1007.
[52] M. A. Zagrobelny, J. B. Rawlings, Practical improvements to autocovariance least-squares, AIChE Journal 61 (6) (2015) 1840–1855.
[53] N. R. Kristensen, H. Madsen, S. B. Jørgensen, Parameter estimation in stochastic grey-box models, Automatica 40 (2) (2004) 225–237.
[54] M. A. Zagrobelny, J. B. Rawlings, Identifying the uncertainty structure using maximum likelihood estimation, The American Control Conference (2015) 422–427.
[55] M. Schlegel, K. Stockmann, T. Binder, W. Marquardt, Dynamic optimization using adaptive control vector parameterization, Computers & Chemical Engineering 29 (8) (2005) 1731–1751.
[56] H. G. Bock, K. J. Plitt, A multiple shooting algorithm for direct solution of optimal control problems, 9th IFAC World Congress Budapest (1984) 242–247.
[57] M. Diehl, H. G. Bock, J. P. Schlöder, R. Findeisen, Z. Nagy, F. Allgöwer, Real-time optimization and nonlinear model predictive control of processes governed by differential-algebraic equations, Journal of Process Control 12 (4) (2002) 577–585.
[58] L. T. Biegler, Solution of dynamic optimization problems by successive quadratic programming and orthogonal collocation, Computers & Chemical Engineering 8 (3) (1984) 243–248.
[59] L. T. Biegler, An overview of simultaneous strategies for dynamic optimization, Chemical Engineering and Processing: Process Intensification 46 (11) (2007) 1043–1053.
[60] L. T. Biegler, X. Yang, G. A. G. Fischer, Advances in sensitivity-based nonlinear model predictive control and dynamic real-time optimization, Journal of Process Control 30 (2015) 104–116.
[61] A. Capolei, J. B. Jørgensen, Solution of constrained optimal control problems using multiple shooting and ESDIRK methods, The American Control Conference (2012) 295–300.
[62] A. Wächter, L. T. Biegler, On the implementation of an interior-point filter line-search algorithm for large-scale nonlinear programming, Mathematical programming 106 (1) (2006) 25–57.
[63] A. Capolei, Nonlinear Model Predictive Control for Oil Reservoirs Management, Ph.D. thesis, Technical University of Denmark (2013).

Paper C

A Grey-Box Model for Spray Drying Plants

Published in *10th IFAC International Symposium on Dynamics and Control of Process Systems (DYCOPS 2013), pp. 559–564, 2013, Mumbai.*

Preprints of the 10th IFAC International Symposium on Dynamics and Control of Process Systems
The International Federation of Automatic Control
December 18-20, 2013. Mumbai, India

A Grey-Box Model for Spray Drying Plants

Lars Norbert Petersen [*,**] **Niels Kjølstad Poulsen** [*]
Hans Henrik Niemann [***] **Christer Utzen** [**]
John Bagterp Jørgensen [*]

[*] *Department of Applied Mathematics and Computer Science, Technical University of Denmark, Kgs. Lyngby, Denmark (e-mail: {lnpe,nkpo,jbjo}@dtu.dk)*
[**] *GEA Process Engineering A/S, Søborg, Denmark (e-mail: christer.utzen@gea.com)*
[***] *Department of Electrical Engineering, Technical University of Denmark, Kgs. Lyngby, Denmark (e-mail: hhn@elektro.dtu.dk)*

Abstract: Multi-stage spray drying is an important and widely used unit operation in the production of food powders. In this paper we develop and present a dynamic model of the complete drying process in a multi-stage spray dryer. The dryer is divided into three stages: The spray stage and two fluid bed stages. Each stage is assumed ideally mixed and described by mass- and energy balances. The model is able to predict the temperature, the residual moisture and the particle size in each stage. Process constraints are also proposed to predict deposits due to stickiness of the powder. The model predictions are compared to datasets gathered at GEA Process Engineering's test facility. The identified grey-box model parameters are identified from data and the resulting model fits the data well. The complexity of the model has been selected such that it is suitable for development of real-time optimization algorithms in an economic optimizing MPC framework.

Keywords: Drying process, Spray drying, Multi-stage dryer, Grey-box model, Modelling and identification, Maltodextrin, Simulation

1. INTRODUCTION

In 2015 the milk quota system in the European Union will be completely liberalized. The expected effect is that the milk volume production will increase significantly. The extra milk will need to be processed to find its way to the market. Analysts expect production of skimmed and whole milk powder to increase by 5-6% while its prices will decline by about 6-7% (IPTS and EuroCARE GmbH, 2009). To accommodate this production expansion, efficient control and optimization of the spray drying process become increasingly important. In this paper we develop a simple first-principle engineering model that can be used to simulate the spray drying processes and facilitate development of efficient control algorithms.

In this paper a grey-box model will be introduced which is based on engineering first principles. It describes the spray drying (SD), the static fluid bed (SFB) and the vibrating fluid bed (VFB) stages of a multi-stage dryer (MSD) plant as illustrated in Fig. 1. The model is validated against data acquired from a MSD at a test-station in Copenhagen (GEA Process Engineering A/S). The model describes the temperatures, the residual moisture and the particle size in each stage of the spray dryer, as well as the stickiness limit.

Conventional control of spray drying plants keeps inlet- and outlet temperatures constant during operation, as a surrogate to controlling the product quality (O'Callaghan and Cunningham, 2005). This approach is simple, but known to be insufficient for control of residual moisture and particle size. The simple approach is often preferred, as product quality is expensive to measure and can lead to sanitary problems. One approach to avoid the use of expensive sensors is to use soft sensors based on readily available measurements and a mathematical model. The importance of good models is therefore evident for both use in controllers and soft sensors as well as in design and validation studies.

Chen and Lin (2005) derived a simple set of differential equations for use in computational fluid dynamics (CFD) to describe the drying of a single particle. In this study, it was shown that the characteristic drying rate curve (CDRC) method did not resemble the experimental trends, and therefore they preferred the reaction engineering approach (REA) method. Langrish (2009) used the REA method for CFD with success on studying wall depositions. Shabde and Hoo (2008) investigated control design and optimization using CFD methods for a single-stage spray dryer, and described a (lumped) model and control for the residual moisture and the particle size. We deemed the models relying on CFD too complex for real-time advanced control and real-time dynamic optimization. Bizmark et al. (2010) introduced a sequential static model for a continuous fluidized bed and Iguaz et al. (2003) formulated a sequential reactor approach, which was used to simulate the dynamic response of a rotary dryer to a change in the input conditions. We come up with a three-stage approach inspired by Bizmark et al. (2010) and Iguaz

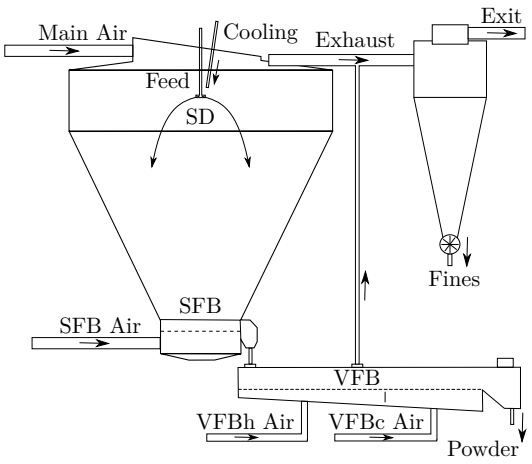

Fig. 1. Diagram of the multi-stage dryer. SD = spray drying, SFB = static fluid bed and VFB = vibrating fluid bed

et al. (2003) and use constitutive equations inspired by Langrish and Kockel (2001).

To our knowledge, no control oriented general dynamic model exist for multi-stage spray dryers. In this work such a general model is proposed.

The paper is organized as follows. In Section 2 we describe the spray drying process and in Section 3 we present the three-stage model. We also give constraints to the residual moisture in order to predict wall deposits. Section 4 contains a brief description of the method for parameter estimation, the estimated parameters, and a validation of the model to data from two experiments. Conclusions are given in Section 5.

2. THE SPRAY DRYING PROCESS

As illustrated in Fig. 1, spray drying is a continuous process which produces a dry powder from a liquid or a slurry. The spray dryer consists most often of a combination of three stages; the actual spray drying (SD), the static fluid bed (SFB) and the vibrating fluid bed (VFB). The main purpose of the SD stage is to reduce stickiness and fouling of the wet feed. The powder then falls to the SFB for further agglomeration and drying. Finally the powder is transported to the external VFB, for gentle drying and is cooled to the temperature desired for handling and storage. Cooling air and fines from the cyclone are returned to the SD stage near the nozzles for forced agglomeration.

The main factors affecting the residual moisture in the powder are the temperature, the relative humidity and the particle size in the stages. Normally, the SD air temperature (exhaust temperature) is automatically controlled by adjusting the feed flow rate while the temperatures in the other stages are manually controlled from the inlet air temperatures set by the operator. The particle size is mainly affected by the nozzle pressure (i.e. feed flow, concentration and viscosity), residual moisture and the SFB inlet air flows. The particle size is often controlled by adjusting inlet air flows and the residual moisture is controlled from the exhaust temperature. Generally, two external disturbances are present in spray drying i.e. the ambient air humidity and the feed composition. The disturbances both affect the residual moisture and the particle size. Also the hold-up of powder in the SFB and VFB can vary and influences the drying.

3. MULTI-STAGE DRYER MODEL

The model structure is derived from engineering first principles and the unknown parameters are identified using a least-squares method. This approach, called grey-box modeling (Ljung, 1999), combines physical knowledge with data-based (statistical) modeling; physical knowledge provides the main structure and statistical modeling provides details on the actual coefficients (Kristensen et al., 2004). Compared to statistical black-box models; this is advantageous since it allows a physical interpretation of the model and often wide valid operation range. Utilizing mass and energy conservation laws, also make it possible to extract otherwise unknown drying conditions inside the drying zones.

We divide the model of the dryer into three stages. The SD, the SFB and the VFB stage. Fig. 2 shows a schematic representation of the three-stage model approach, and Fig. 3 describes the details of a single stage.

For each of the stages, we set up two mass balances (Eq. 1 and 4), one energy balance (Eq. 15) and one particle size balance (Eq. 31) in order to fully describe the drying conditions in each stage. In the following, the derivation of the equations for the stages will be treated generally and when necessary a specific stage is noted in the superscript of the equation.

The experiments were based on drying of maltodextrin DE-18, because milk is expensive, cannot be stored in liquid form and its composition is not well defined. Maltodextrin, though, resemble the same fundamental properties as skim milk.

3.1 Powder moisture

A mass balance for water in the powder yields

$$\frac{dm_w}{dt} = F_{ps_{in}} X_{in} - F_{ps_{out}} X_{out} - R_w m_{ps} \tag{1}$$

X is the dry basis water concentration (kg water/kg dry solid) in the powder and the flux of evaporating water is $R_w m_{ps}$. The hold-up of dry powder is assumed constant, and thus the flow of dry powder entering and leaving is

$$F_{ps_{out}} = F_{ps_{in}} = S_{in} F_{p_{in}} \tag{2}$$

The dry basis concentration of product in- and outlet flows are

$$X_{in} = \frac{1 - S_{in}}{S_{in}} \qquad X_{out} = \frac{m_w}{m_p - m_w} \tag{3}$$

where S_{in} is the concentration (kg solid/kg total) and m_w is the mass of water. m_p is the total mass of the powder.

3.2 Air moisture

The amount of vapour in the air is given by

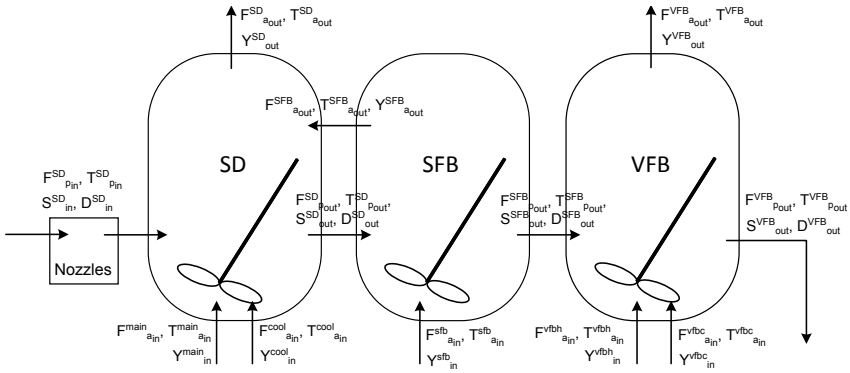

Fig. 2. Princple of the sequential stage model.

$$\frac{dm_v}{dt} = F_{v_{in}} - F_{v_{out}} + R_w m_{ps} \tag{4}$$

The inlet vapour flow, $F_{v_{in}}$, for each stage is

$$F_{v_{in}}^{SD} = Y_{in}^{main} F_{da_{in}}^{main} + Y_{in}^{cool} F_{da_{in}}^{cool} + Y_{out}^{SFB} F_{da_{out}}^{SFB} \tag{5}$$
$$F_{v_{in}}^{SFB} = Y_{in}^{sfb} F_{da_{in}}^{sfb} \tag{6}$$
$$F_{v_{in}}^{VFB} = Y_{in}^{vfbh} F_{da_{in}}^{vfbh} + Y_{in}^{vfbc} F_{da_{in}}^{vfbc} \tag{7}$$

The flow of dry air, $F_{da_{in}}$, is given by

$$F_{da_{in}} = \frac{1}{Y_{in}+1} F_{a_{in}} \tag{8}$$

and the absolute humidity, Y_{in}, of the incoming air is

$$Y_{in} = \frac{M_v}{M_{da}} \frac{\mathrm{RH}_{in} P_{vsat}}{P_{in} - \mathrm{RH}_{in} P_{vsat}} \tag{9}$$

RH_{in} is the relative humidity and P_{vsat} is the saturated vapour pressure from the Antoine equation.

The hold-up of dry air is assumed constant, and thus the dry air flow out of the chamber is equal to the dry air flow into the chamber. The flow of vapour out of the stages is

$$F_{v_{out}}^{SD} = Y_{out}^{SD}(F_{da_{in}}^{main} + F_{da_{in}}^{cool} + F_{da_{out}}^{SFB}) \tag{10}$$
$$F_{v_{out}}^{SFB} = Y_{out}^{SFB} F_{da_{in}}^{sfb} \tag{11}$$
$$F_{v_{out}}^{VFB} = Y_{out}^{VFB}(F_{da_{in}}^{vfbh} + F_{da_{in}}^{vfbc}) \tag{12}$$

The absolute humidity of the stage air, Y_{out}, is given by

$$Y_{out} = \frac{M_{da}}{M_v} \frac{P - P_v}{P_v} \tag{13}$$

Assuming constant total chamber pressure, P, which is controlled by a suction fan. The vapour pressure is given by the ideal gas law

$$P_v = \frac{M_v R T_{a_{out}}}{m_v V} \tag{14}$$

M_v is the molar mass of vapour. V is the stage air volume.

3.3 Energy balance

It is assumed that in each stage the temperature of the air and the product are in equilibrium and identical. This temperature is defined by an energy balance

$$\frac{dU}{dt} = \Delta H + Q + W \tag{15}$$

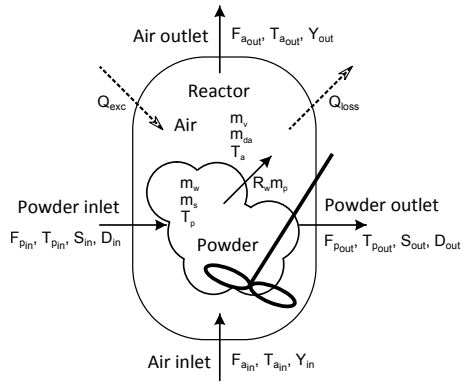

Fig. 3. Sketch of a single stage.

where $W = 0$ and

$$\Delta H = H_{a_{in}} - H_{a_{out}} + H_{p_{in}} - H_{p_{out}} \tag{16}$$
$$Q = -Q_{loss} + Q_{exc} \tag{17}$$

The enthalpy of humid air is

$$H_a = H_{a_0} + F_{da}(C_{da}(T_a - T_{ref}) + Y(\lambda + C_v(T_a - T_{ref}))) \tag{18}$$

where C_{da} and C_v is the specific heat capacity of dry air and vapour respectively. λ is the latent heat of evaporation and $T_{ref} = 25°C$ is the reference temperature.

The enthalpy increase from inlet air in each stage is

$$H_{a_{in}}^{SD} = H_{a_{in}}^{main} + H_{a_{in}}^{cool} + H_{a_{out}}^{SFB} \tag{19}$$
$$H_{a_{in}}^{SFB} = H_{a_{in}}^{sfb} \tag{20}$$
$$H_{a_{in}}^{VFB} = H_{a_{in}}^{vfbh} + H_{a_{in}}^{vfbc} \tag{21}$$

The enthalpy of humid air leaving the stages is simply determined from (18). We denote the enthalpies $H_{a_{out}}^{SD}$, $H_{a_{out}}^{SFB}$ and $H_{a_{out}}^{VFB}$.

The enthalpy of liquid feed as well as powder is

$$H_p = H_{p_0} + F_{ps}(C_s + XC_w)(T_p - T_{ref}) \tag{22}$$

where C_s and C_w is the specific heat capacity of solids and water respectively.

The heat loss is given by

$$Q_{loss} = UA(T_{a_{out}} - T_{indoor}) \quad (23)$$

Since the indoor temperature was not measured, we approximate the indoor temperature by T_{vfbc}.

The SD and SFB stage is subject to exchange of heat, as these are placed inside the same chamber. The heat exchange is

$$Q_{exc}^{SD} = -UA_{exc}(T_{a_{out}}^{SD} - T_{a_{out}}^{SFB}) \quad (24)$$

$$Q_{exc}^{SFB} = UA_{exc}(T_{a_{out}}^{SD} - T_{a_{out}}^{SFB}) \quad (25)$$

The VFB is isolated from the other stages, and thus have zero heat exchange i.e. $Q_{exc}^{VFB} = 0$.

The total energy is given by

$$U = m_p C_p T_{p_{out}} + m_{da} C_{da} T_{a_{out}} + m_v C_{av} T_{a_{out}} + m_{steel} C_{steel} T_{a_{out}} \quad (26)$$

As mentioned the temperature of the air in the chamber, $T_{a_{out}}$ equals $T_{p_{out}}$. The heat capacities are placed in appendix A. In this we assume that the temperature of the steel chamber changes reasonably fast compared to the air temperature. The mass of steel is determined by assuming 3 mm of steel. i.e. $m_{steel}^{SD} = 212.22$ kg, $m_{steel}^{SFB} = 7.80$ kg and $m_{steel}^{VFB} = 8.10$ kg.

3.4 Drying rate equation

The evaporation rate, R_w, is an essential part of the model. According to Iguaz et al. (2003) it should include equilibrium moisture content data and must be determined experimentally under conditions as close as possible to those of the process. We find that the drying kinetics is best described by the lumped-parameter expression (Langrish and Kockel, 2001; Chen and Lin, 2005). Thus, the drying rate is a function of vapour density and the moisture content. The drying rate may be expressed as

$$R_w = K_1(X_{out} - X_{eq})(\rho_{vsat} - \rho_v) \quad (27)$$

where

$$\rho_{vsat} = \frac{M_v P_{vsat}}{RT_{p_{out}}} \qquad \rho_v = \frac{M_v P_v}{RT_{a_{out}}} \quad (28)$$

The last term of (27), $\rho_{vsat} - \rho_v$, describes the driving force of evaporation from the particles to the air, assuming that the surface of the particle is completely covered in water. To describe the friction of evaporation we introduce the term of free moisture, $X_{out} - X_{eq}$. The term decreases towards zero as the residual moisture get closer to the equilibrium moisture content. The constant K_1 corrects for un-modelled effects, such as relative speed between air and particle and other phenomena affecting drying. These phenomena are practically impossible to model without taking a CFD approach. It is, furthermore, necessary to multiply R_w by $F_{p_{in}}^{SD}/0.0241$ in the SD stage in order to correctly render variations in the feed flow.

The equilibrium moisture content, X_{eq}, is described by

$$X_{eq} = A\left(\frac{RH_{a_{out}}}{1 - RH_{a_{out}}}\right)^B \left(\frac{1}{T_{a_{out}} - 273.15}\right)^C \quad (29)$$

X_{eq} is a product dependent function that describe the moisture content where water cannot be extracted from the powder any longer. As the moisture content approaches this value the friction of extracting water from the particles increase to infinite. In theory the moisture content can only be obtained by infinite residence time. Woo et al. (2008), shows that $A = 1.2098$, $B = 0.8535$ and $C = 0.5962$ can be used for maltodextrin DE-18.

3.5 Particle size

The droplets can be produced by either a rotating atomizer or a nozzle. We use a nozzle and the particle size can be described by

$$D_{in}^{SD} = D_0 + a(F_{p_{in}}^{SD} - F_{p0}) + b(T_{p_{in}}^{SD} - T_{p0}) + c(S_{in}^{SD} - S_0) \quad (30)$$

The constants have been manually fitted to

$$a = 4000 \qquad b = -10.1 \qquad c = -600$$
$$F_{p0} = 0.021921 \qquad T_{p0} = 326.35 \qquad S_0 = 0.5$$

The sprayed droplets are subject to shrinkage during drying. If it is assumed that the particles are perfectly spherical before and after the drying and only water is evaporating, we can derive a differential equation for the resulting size of the particles. For each stage we get

$$\dot{D}_{out} = \frac{1}{\tau}\left(\left(\frac{X_{out}+1}{X_{in}+1} \cdot \frac{\rho_{p_{in}}}{\rho_{p_{out}}}\right)^{\frac{1}{3}} D_{in} + K_{ag}(F_a - F_{a0}) - D_{out}\right) \quad (31)$$

Agglomeration is generally difficult to describe and we simply add a term proportional to the air flow rate of the stage. The parameters are

$$\tau^{SD} = 400 \qquad \tau^{SFB} = 200 \qquad \tau^{VFB} = 100$$
$$K_{ag}^{SD} = 100 \qquad K_{ag}^{SFB} = 300 \qquad K_{ag}^{VFB} = 200$$
$$F_{a0}^{SD} = 0.49944 \qquad F_{a0}^{SFB} = 0.14167 \qquad F_{a0}^{VFB} = 0.18046$$

3.6 Stickiness

Stickiness of the produced particles is an important limitation to the achievable performance of the MSD. Sticky particles form depositions on the walls of the spray dryer. Stickiness has been found to depend on product temperature and moisture content. Furthermore, the transition from sticky to non-sticky takes place very quickly, thus we can assume it to have binary state. We will use a mass-proportion-mixing rule, as proposed by (Hennigs et al., 2001; Hogan et al., 2010), to describe the non-sticky region i.e. when the powder is below its glass transition temperature.

$$T_g = \frac{S_{out}T_{gp} + k(1 - S_{out})T_{gw}}{S_{out} + k(1 - S_{out})} \quad (32)$$

$T_{gp} = 144.8°C$ and $T_{gw} = -137°C$ for maltodextrin DE-18 and water respectively. The value $k = 6.296$ is estimated from adsorption isotherm data.

The data of the experiment is produced by studying the stickiness of the powder in an equilibrium state. Meaning that the moisture at the surface is equal to that of the core of the particle. This situation is not present in spray drying, where the rapid evaporation from the surface tend to form a particle with a crisper surface than the core. In practice this means that T_g is higher i.e. that the powder is less sticky inside the spray dryer. To compensate for this, we form a correction term

$$T_{max} = T_g + \Delta T_{adj} \quad (33)$$

The offset depends on the design of the dryer and unknown factors. Normally it is in the range of 10 to 60°C (Hogan

Table 1. Identified parameters.

Symbol	Value	99% Conf.	Unit
K_1	0.027106	±0.00070505	$m^3/(s \cdot kg)$
U^{SD}	6.0576	±0.05556	J/Km^2
U^{SFB}	56.513	±0.67788	J/Km^2
U^{VFB}	151.74	±4.1353	J/Km^2
m_p^{SD}	19.279	±0.45641	kg
m_p^{SFB}	15.954	±1.8596	kg
m_p^{VFB}	3.4953	±3.7004	kg
UA_{exc}	113.76	±3.0285	J/K
D_0	154.39	±0.12645	μm

et al., 2010). It must be determined experimentally for each dryer.

4. SYSTEM IDENTIFICATION

The unknown variables in the grey-box model are identified in order to determine the relation between input and output variables of the MSD. The cost function is the sum of squared prediction errors. The dynamic system is described by the set of ordinary differential equations (ODEs) given in Section 3. Consequently, the grey-box model of the MSD can be written

$$\frac{d}{dt}\mathbf{x}(t) = \mathbf{f}(\mathbf{x}(t), \mathbf{u}(t), \theta)$$
$$\widehat{\mathbf{y}}(t_k) = \mathbf{g}(\mathbf{x}(t_k), \mathbf{u}(t_k), \theta)$$

with the optimization problem given by

$$\mathbf{e}(t_k, \theta) = \mathbf{y}(t_k) - \widehat{\mathbf{y}}(t_k, \theta)$$
$$V_{LS}(\theta) = \frac{1}{2}\sum_{t_k=1}^{N} \|\mathbf{e}(t_k, \theta)\|_{\mathbf{w}}^2$$
$$\widehat{\theta}_{LS} = \arg\min_{\theta \in D_m} V_{LS}(\theta)$$

$\mathbf{y}(t_k)$ and $\widehat{\mathbf{y}}(t_k, \theta)$ are the measured and estimated output at time t_k. We ignore the initial startup trend i.e. only use data points from $t_k > 5.8$ hours. $\mathbf{e}$ is the estimation error (residual) and V_{LS} is the value of the cost function. The weights have been selected to

$$\mathbf{w} = diag([1\ 1\ 1\ 100\ 0.05])$$

The weights are selected such that the magnitude of the residuals are in the same range. The weight on S_{out}^{SFB} could be increased, giving a better fit on this residual. But then the temperature estimates will suffer and vice versa. The outputs and inputs are

$$\mathbf{y} = [T_{a_{out}}^{SD}\ T_{p_{out}}^{SFB}\ T_{a_{out}}^{VFB}\ S_{out}^{SFB}\ D_{out}^{SFB}]^T$$
$$\mathbf{u} = [F^{feed}\ T^{feed}\ S^{feed}\ F^{main}\ T^{main}\ Y^{main}\ F^{cool}\ \ldots$$
$$T^{cool}\ Y^{cool} F^{sfb}\ T^{sfb}\ Y^{sfb}\ F^{vfbh}\ T^{vfbh}\ \ldots$$
$$Y^{vfbh}\ F^{vfbc}\ T^{vfbc}\ Y^{vfbc}\ T_{indoor}]^T$$
$$\mathbf{x} = [m_w^{SD}\ m_v^{SD}\ T_{a_{out}}^{SD}\ D_{out}^{SD}\ m_w^{SFB}\ m_v^{SFB}\ T_{a_{out}}^{SFB}\ \ldots$$
$$D_{out}^{SFB}\ m_w^{VFB}\ m_v^{VFB}\ T_{a_{out}}^{VFB}\ D_{out}^{VFB}]^T$$

The identified parameters are shown in Table 1. The approximate 99% confidence interval in Table 1 is given by $p_i \pm t_{m-n}\hat{\sigma}\sqrt{C_{ii}^{-1}}$ with $m - n = 1525 - 9$ equal to the degrees of freedom, t is the student-T-distribution, $\hat{\sigma}$ is the unbiased estimate of the noise covariance and $C = J^T J$ where J is the Jacobian of the model.

The correlation matrix for the parameters is

$$\begin{bmatrix}
1 & & & & & & & \\
-0.35 & 1 & & & & & & \\
0.19 & -0.95 & 1 & & & & & \\
0.33 & -0.36 & 0.28 & 1 & & & & \\
-0.36 & -0.59 & 0.64 & 0.18 & 1 & & & \\
0.46 & -0.44 & 0.24 & 0.41 & 0.15 & 1 & & \\
0.02 & -0.09 & 0.08 & 0.74 & 0.09 & 0.06 & 1 & \\
0.04 & -0.49 & 0.61 & 0.03 & 0.00 & 0.05 & 0.01 & 1 \\
0.63 & -0.67 & 0.51 & 0.47 & 0.31 & 0.83 & 0.08 & 0.05\ 1
\end{bmatrix}$$

The hold-up of powder in the VFB, m_p^{VFB}, is difficult to estimate, as it is mostly determined from a combination of the measurement of residual moisture in the VFB (unmeasured) and the dynamic change of temperature $T_{a_{out}}^{VFB}$, which is slowly varying.

Fig. 4 shows the estimation data and the corresponding model response. The model response to the validation data is shown in Fig. 5. We removed a constant temperature offset in the validation model response by adjusting the indoor temperature by $\Delta T_{indoor}^{SD} = -10.06°C$, $\Delta T_{indoor}^{SFB} = 14.33°C$ and $\Delta T_{indoor}^{SFB} = 2.745°C$. The reason for these offsets is most likely the changed indoor temperature between trials (the dryer is placed in a tall unheated test-facility) and the non-uniform temperature between top and bottom of the dryer. The indoor temperature was unfortunately not measured.

The estimation dataset (Fig. 4) is made by first changing the SD feed flow from 65 l/h to 75 l/h twice. The inlet air temperature is then changed from 160°C to 150°C and increased to 170°C and back. The SD air flow is then changed from 1800 kg/h to 2000 kg/h and back twice. The second time with the heater in manual, which cause the inlet air temperature to drop slightly. Then the SFB inlet air flow was changed followed by a change in the SFB inlet air temperature.
In the validation dataset (Fig. 5) the SD outlet air temperature is controlled constant at 87°C by the feed flow rate. First the inlet air humidity is changed from 7 to 22 g/kg and back. Next the feed solids content is changed from 50% to 40% and back. Notice the difference in time-scale of the two experiments.

Inspecting Fig. 4 and 5, we conclude that the estimation of temperatures shows a precise fit while the product quality is more difficult to estimate. Disregarding the initial start-up trend of approx. 4-5 hours, in which the dryer is not operating normally, especially the residual moisture is difficult to estimate. The reason is the difficulty of measuring the residual moisture, the indoor temperature change and the discontinuous discharge (especially in the validation data at $t = 4.5$) of powder from the SFB. The estimation of particle size is slightly off, but within reasonable limits. For a greater accuracy we might need to model the nozzle pressure directly and the fines return system.

As a consequence the MSD is now being upgraded with in-line residual moisture sensors, indoor temperature sensors and a new mechanism for discharge of powder from the SFB. A new experiment has already been ordered and will soon be conducted.

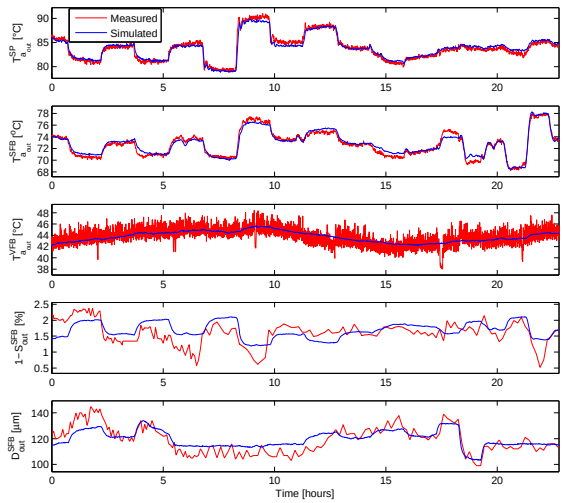

Fig. 4. The estimation dataset. S_{out}^{SFB} and D_{out}^{SFB} are sampled by hand resulting in a low sample frequency.

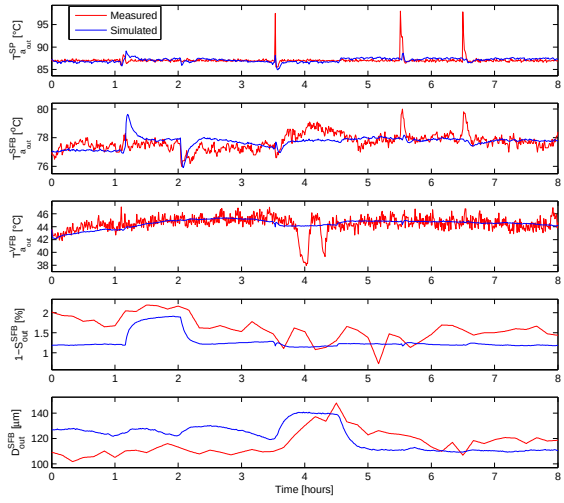

Fig. 5. The validation dataset. The three temperatures are offset corrected. The temperature peak ($t = 3.5$) is due to change of feed tank and the peak at $t = 5.5$ and 6.5 is due to change of nozzle.

5. CONCLUSIONS

In this paper, a mathematical model is proposed for a multi-stage spray dryer. We established a dynamic model consisting of three stages; the actual spray drying (SD), the static fluid bed (SFB) and the vibrating fluid bed (VFB). The stages were described by the same constitutive equation. The model predicts the temperatures within the dryer with high accuracy. The residual moisture and the particle size of the powder is predicted with some expected uncertainty, due to unstable discharge of powder from the SFB stage and varying indoor temperature. We also provided a novel prediction for stickiness of the powder, as a function of powder temperature and residual moisture. The model is general in the sense, that it can be adjusted to describe the drying of any liquid or slurry in a multi-stage spray dryer.

REFERENCES

Bizmark, N., Mostoufi, N., Sotudeh-Gharebagh, R., and Ehsani, H. (2010). Sequential modeling of fluidized bed paddy dryer. *Journal of Food Engineering*, 101, 303–308.

Chen, X.D. and Lin, S.X.Q. (2005). Air drying of milk droplet under constant and time-dependent conditions. *AIChE J.*, 51, 1790–1799.

Hennigs, C., Kockel, T.K., and Langrish, T.A.G. (2001). New measurements of the sticky behavior of skim milk powder. *Drying Technology*, 19, 471–484.

Hogan, S., Famelart, M., O'Callaghan, D., and Schuck, P. (2010). A novel technique for determining glass-rubber transition in dairy powders. *Journal of Food Engineering*, 99, 76–82.

Iguaz, A., Esnoz, A., Martínez, G., López, A., and Vírseda, P. (2003). Mathematical modelling and simulation for the drying process of vegetable wholesale by-products in a rotary dryer. *Journal of Food Engineering*, 59, 151–160.

IPTS and EuroCARE GmbH (2009). Economic impact of the abolition of the milk quota regime. URL `http://ec.europa.eu/agriculture/analysis/external/milkquota/ex_sum_en.pdf`.

Kristensen, N.R., Madsen, H., and Jørgensen, S.B. (2004). A method for systematic improvement of stochastic grey-box models. *Computers and Chemical Engineering*, 28, 1431–1449.

Langrish, T.A.G. and Kockel, T.K. (2001). The assessment of a characteristic drying curve for milk powder for use in computational fluid dynamics modelling. *Chemical Engineering Journal*, 84, 69–74.

Langrish, T.A.G. (2009). Multi-scale mathematical modelling of spray dryers. *Journal of Food Engineering*, 93, 218–228.

Ljung, L. (1999). *System Identification: Theory for the User (2nd Edition)*. Prentice Hall, Linkoping, Sweden.

O'Callaghan, D. and Cunningham, P. (2005). Modern process control techniques in the production of dried milk products - a review. *Lait*, 85, 335–342.

Shabde, V.S. and Hoo, K.A. (2008). Optimum controller design for a spray drying process. *Control Engineering Practice*, 16, 541–552.

Woo, M.W., Daud, W.R.W., Mujumdar, A.S., Wu, Z., Meor Talib, M.Z., and Tasirin, S.M. (2008). CFD evaluation of droplet drying models in a spray dryer fitted with a rotary atomizer. *Drying Technology*, 26, 1180–1198.

Appendix A. PRODUCT RELATED CONSTANTS

The latent heat of evaporation for water is $\lambda = 2260$ KJ. The heat capacity of dry air, vapour, solid maltodextrin DE-18 and water is

$$C_{da} = 1008.6 \qquad C_v = 1883.6$$

$$C_s = 1548.8 + 1.9625T - 5.9399 \cdot 10^{-3}T^2$$

$$C_w = 4176.2 - 0.0909T - 1.3129 \cdot 10^{-3}T^2$$

Paper D

Real-time economic optimization for a fermentation process using Model Predictive Control

Published in *13th European Control Conference (ECC 2014), pp. 1831–1836, 2014, Strasbourg.*

2014 European Control Conference (ECC)
June 24-27, 2014. Strasbourg, France

Real-time economic optimization for a fermentation process using Model Predictive Control

Lars Norbert Petersen[1] and John Bagterp Jørgensen[2]

Abstract— **Fermentation is a widely used process in production of many foods, beverages, and pharmaceuticals. The main goal of the control system is to maximize profit of the fermentation process, and thus this is also the main goal of this paper. We present a simple dynamic model for a fermentation process and demonstrate its usefulness in economic optimization. The model is formulated as an index-1 differential algebraic equation (DAE), which guarantees conservation of mass and energy in discrete form. The optimization is based on recent advances within Economic Nonlinear Model Predictive Control (E-NMPC), and also utilizes the index-1 DAE model. The E-NMPC uses the single-shooting method and the adjoint method for computation of the optimization gradients. The process constraints are relaxed to soft-constraints on the outputs. Finally we derive the analytical solution to the economic optimization problem and compare it with the numerically determined solution.**

I. Introduction

Maximizing profit has been and will always be the primary purpose of optimal process operation. Within conventional process control, the economic optimization considerations of a plant are usually indirectly addressed or addressed in a separate real-time optimization (RTO) layer that performs a steady-state economic optimization of the process variables [1]. Recent advances have focused on optimizing the higher-level objectives, such as economics, directly in the process control layer. Model Predictive Control (MPC) has for long time been the preferred framework in both industry and academia because of its flexibility, performance and ability to handle constraints on the inputs as well as the states [2]. Many researchers have also proposed nonlinear MPC which handles nonlinear systems and constraints. Much research has, therefore, been focused on extending the MPC framework to also handle optimization of process economics. The idea of optimizing economics directly has been reported in many works [1], [3]–[5]. Research has also been performed on stability theory, showing that limit cycles may arise because these are economically favourable [6].

The use of fermentation in industry is widely used, and the ability to control a fermentation process at its optimal state is of considerable interest to many fermentation industries. Optimal control reduces the production costs and increases yield while maintaining proper quality of the product. Optimal open-loop time profiles of the feed rates are well known and used, but these solutions depend heavily upon uncertainties in the initial conditions and system parameters which can lead to large errors and thereby profit loss [7], [8]. Therefore, it is advantageous to develop a closed-loop optimization scheme which attenuates uncertainties and is independent of the initial conditions [8].

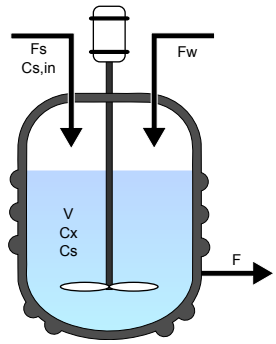

Fig. 1. Simple sketch of the fermentation process.

In this work we address the issue of optimizing the economics directly in the controller. We present a simple fermenter example to demonstrate our results and show the applicability of E-NMPC in a tutorial fashion. The example is simple enough for us to derive the exact solution to the control problem, and thus compare the achieved performance of the discrete nonlinear controller with the analytical solution. We aim at developing an economic nonlinear MPC which optimizes the closed loop performance with respect to an economic objective function for a nonlinear system. We compute the gradients of the optimization problem using the single-shooting method to reduce the computational load. The controller handles both input and (soft) output constraints. The design of the MPC is based on receding horizon control. It is easy to implement and can also easily be used for control of other nonlinear processes to maximize the profit of operation.

We introduce a fermentation model that is based on engineering first principles. It describes the fermentation process as illustrated in Figure 1. The model is partly taken from [9] and describes the fermentation of single cell proteins using Methylococcus Capsulatus. The model is simplified in order to only render the fundamental properties of fermentation. The model describes the hold-up, the biomass concentration and the substrate concentration in a well stirred tank, as a

[1]L. N. Petersen is with the Department of Applied Mathematics and Computer Science, Technical University of Denmark, DK-2800 Kgs. Lyngby, Denmark and GEA Process Engineering A/S, Søborg, Denmark lnpe@dtu.dk

[2]J. B. Jørgensen is with the Department of Applied Mathematics and Computer Science, Technical University of Denmark, DK-2800 Kgs. Lyngby, Denmark jbjo@dtu.dk

function of water- and substrate-inlets.

The paper is organized as follows: In Section II we set-up the control problem including discretization and derivation of the gradients of the optimization problem, in Section III we present the fermentation model. Section IV contains the derivation of the analytical solution to the control problem. In Section V we present simulation studies to show the benefit of optimizing the fermenter operation compared to the analytical solution. Conclusions are given in Section VI.

II. Optimization of Dynamical Systems

In this paper, we consider systems of differential equations in the form

$$\frac{d}{dt}g(x(t)) = f(x(t), u(t), d(t)) \qquad t \in [t_0, t_f[\quad (1)$$

where $x(t_0) = x_0$. The form is natural for a large number of systems in process engineering, petroleum engineering, electrical engineering and mechanical engineering. This system representation is also natural for modelling fermenter dynamics. The state function $g(x(t))$ typically represents mass, energy and momentum and $x(t)$ represents the states. The differential equation may also be represented as the index-1 differential equations

$$\frac{d}{dt}h(t) = f(x(t), u(t), d(t)) \qquad x(t_0) = x_0 \quad (2a)$$
$$h(t) = g(x(t)) \qquad h(t_0) = g(x_0) \quad (2b)$$

There are no numerical difference in these two representations. Assuming dg/dt is non-singular, we can rewrite and get

$$\frac{d}{dt}x(t) = \left(\frac{dg}{dx}(x(t))\right)^{-1} f(x(t), u(t), d(t)) \quad x(t_0) = x_0 \quad (3)$$

which is not numerically equivalent to (2). In particular, the representation in (3) does not guarantee conservation of $g(x(t))$, e.g. mass energy and momentum when solved numerically. We will therefore use the representation in (2) when solving the initial value problem of the fermenter model.

The objective function of our optimization is given in Bolza form

$$\phi = \int_{t_0}^{t_f} l(x(t), u(t), d(t))dt + \bar{l}(x(t_f)) \quad (4)$$

where $l(x(t), u(t), d(t))$ is the stage cost and $\bar{l}(x(t))$ is the end cost. In order to optimize the profit of operation, the cost function must represent the cost (or profit) of operating the system in the period $[t_0, t_f]$

The manipulated variables and states are restricted by the constraints

$$c(x(t), u(t)) \geq 0 \qquad t \in [t_0, t_f[\quad (5a)$$
$$\bar{c}(x(t_f)) \geq 0 \quad (5b)$$

where $c(x(t), u(t))$ are the stage constraints and $\bar{c}(x(t_f))$ is the end constraint.

The optimal trajectory for the manipulated variables, $u(t)$, and the states, $x(t)$, are obtained by solution of the continuous-time constrained optimal control problem in Bolza form

$$\min_{[x(t),u(t)]_{t_0}^{t_f}} \quad \phi = \int_{t_0}^{t_f} l(x(t), u(t), d(t))dt + \bar{l}(x(t_f)) \quad (6a)$$
$$\text{s. t.} \quad x(t_0) = x_0 \quad (6b)$$
$$\frac{d}{dt}g(x(t)) = f(x(t), u(t), d(t)), t \in [t_0, t_f[\quad (6c)$$
$$c(x(t), u(t)) \geq 0, t \in [t_0, t_f[\quad (6d)$$
$$\bar{c}(x(t_f)) \geq 0, \quad (6e)$$

A. Discretization

The continous-time constrained optimal control problem is infinite-dimensional. To solve it numerically it must be approximated by a finite-dimensional optimal control problem. The manipulated variables are made finite-dimensional by approximating the input profile by a piecewise constant profile

$$u(t) = u_k \qquad t_k \leq t < t_{k+1} \qquad k \in \mathcal{K} \quad (7)$$

with this discretization, the dynamics may be represented as

$$\frac{d}{dt}g(x(t)) = f(x(t), u_k, d_k), \qquad t_k \leq t \leq t_{k+1} \quad (8)$$

for $\mathcal{K} = 0, 1, ..., N-1$ where $x(t_k) = x_k$. The numerical solution to (8) can be determined by using a simple Forward Euler method. We write it in the residual form

$$R_k(x_k, x_{k+1}, u_k, d_k) = g(x_{k+1}) - g(x_k) - \Delta t_k f(x_k, u_k, d_k) = 0$$

The discretization of $u(t)$ implies the objective function

$$\sum_{k=0}^{N-1} L_k(x_k, u_k, d_k) + L_N(x_N) \quad (9)$$

where we also use Forward Euler for discretization and get

$$L_k(x_k, u_k, d_k) = \Delta t_k l(x_k, u_k, d_k) \quad (10)$$
$$L_N(x_N) = \bar{l}(x(t_f)) \quad (11)$$

The path constraints are relaxed to point constraints

$$C_k(x_k, u_k) = c_k(x(t_k), u(t_k)) \geq 0 \quad (12)$$
$$C_N(x_N) = \bar{c}(x(t_f)) \geq 0 \quad (13)$$

Consequently, the continuous time constrained optimal control problem in (6) is approximated by the following discrete time constrained optimal control problem

$$\min_{\{x_k\}_{k=0}^{N}, \{u_k\}_{k=0}^{N-1}} \quad \phi = \sum_{k=0}^{N-1} L_k(x_k, u_k, d_k) + L_N(x_N) \quad (14a)$$
$$\text{s. t.} \quad x_0 = \overline{x}_0 \quad (14b)$$
$$R_k(x_k, x_{k+1}, u_k, d_k) = 0, k \in \mathcal{K} \quad (14c)$$
$$C_k(x_k, u_k) \geq 0, k \in \mathcal{K} \quad (14d)$$
$$C_N(x_N) \geq 0, \quad (14e)$$

B. Single-Shooting Optimization

The discrete-time finite-dimensional optimal control problem may be solved using single-shooting (control vector parametrization) [10], multiple shooting [11], [12], or the simultaneous method [13]. In these methods, a sequential quadratic programming (SQP) algorithm is typically used for the optimization. Gradient computation is straightforward in the simultaneous method, while either forward sensitivity computation or the adjoint method [14] is used by the single-shooting and the multiple-shooting methods.

We solve the optimization problem in (14) by the single-shooting method (also called vector parametrization, CVP). In this method the system dynamics (14c) are used to eliminate the state variables and express the objective and constraint function as function of the manipulated variables and initial state only. Given the manipulated inputs, $\{u_k\}_{k=0}^{N-1}$, the initial value, x_0, and the requirement, that the system dynamics are observable, the objective function may be expressed as

$$\begin{aligned}\Psi =&\Psi(\{u_k\}_{k=0}^{N-1}; x_0)\\ =&\{\phi = \sum_{k=0}^{N-1} L_k(x_k, u_k, d_k) + l_N(x_N) : \\ &x_0 = \bar{x}_0,\\ &R_k(x_k, x_{k+1}, u_k, d_k) = 0, k \in \mathcal{K}\}\end{aligned} \tag{15}$$

Similarly, the constraint functions may be parametrized

$$\begin{aligned}\chi_k =&\chi_k(\{u_j\}_{j=0}^{k}; x_0)\\ =&\{ C_k(x_k, u_k) :\\ &x_0 = \bar{x}_0,\\ &R_j(x_j, x_{j+1}, u_j, d_j) = 0, j \in \mathcal{K}\}\end{aligned} \tag{16}$$

$$\begin{aligned}\chi_N =&\chi_k(\{u_j\}_{j=0}^{N-1}; x_0)\\ =&\{ C_N(x_N) :\\ &x_0 = \bar{x}_0,\\ &R_j(x_j, x_{j+1}, u_j, d_j) = 0, j \in \mathcal{K}\}\end{aligned} \tag{17}$$

Using (15)-(17), the discrete time constraint optimal control problem may be expressed as

$$\min_{\{u_k\}_{k=0}^{N-1}} \quad \Psi(\{u_k\}_{k=0}^{N-1}; x_0) \tag{18a}$$

$$\text{s. t.} \quad \chi_k(\{u_j\}_{j=0}^{k}; x_0) \geq 0, k \in \mathcal{K} \tag{18b}$$

$$\chi_N(\{u_j\}_{j=0}^{N-1}; x_0) \geq 0 \tag{18c}$$

where $\mathcal{K} = 0, 1, ..., N-1$. It is a nonlinear optimization problem which is solved by using sequential quadratic programming (SQP). In each iteration a convex quadratic problem is solved for which evaluation of Ψ, $\nabla\Psi$, χ_k, χ_N and $\nabla\chi_k$,$\nabla\chi_N$ of the nonlinear problem has to be determined. Ψ and χ are computed directly from (15) and (16) while $\nabla\Psi$ and $\nabla\chi$ is computed using the adjoint method. The system states in the optimization problem are dependent on the manipulated variables, in such a way that past changes have an influence on all the subsequent states. This means that the gradients have to be determined in each iteration. The adjoint method is an efficient method for computation of these gradients.

The algorithm for the adjoint method is presented in Algorithm 1 and 2.

Algorithm 1 Adjoint method for $\nabla_{u_k}\Psi(\{u_k\}_{k=0}^{N-1}; x_0)$

Solve for λ_N in $\nabla_{x_N} R_{N-1}\lambda_N = \nabla_{x_N} L_N$
for $k = N-1$ **to** 1 **do**
  Compute
  $\nabla_{u_k}\Psi = \nabla_{u_k} L_k - \nabla_{u_k} R_k \lambda_{k+1}$
  Solve for λ_k in
  $\nabla_{x_k} R_{k-1}\lambda_k = \nabla_{x_k} L_k - \nabla_{x_k} R_k \lambda_{k+1}$
end for
Compute
$\nabla_{u_0}\Psi = \nabla_{u_0} L_0 - \nabla_{u_0} R_0 \lambda_1$

Algorithm 2 Adjoint method for $\nabla_{u_k}\chi(u_k; x_0)_{j=0}^{N-1}$

Solve for λ_N in $\nabla_{x_N} R_{N-1}\lambda_N = \nabla_{x_N} C_N$
for $k = N-1$ **to** 1 **do**
  Compute $\nabla_{u_k}\chi = \nabla_{u_k} C_k - \nabla_{u_k} R_k \lambda_{k+1}$
  Solve for λ_k in $\nabla_{x_k} R_{k-1}\lambda_k = \nabla_{x_k} C_k - \nabla_{x_k} R_k \lambda_{k+1}$
end for
Compute $\nabla_{u_0}\chi = \nabla_{u_0} C_0 - \nabla_{u_0} R_0 \lambda_1$

As we use the Forward Euler method the derivatives simply become

$$\nabla_{x_k} R_k = -\nabla_{x_k} g(x_k) - T_s \nabla_{x_k} f(x_k, u_k, d_k) \tag{19}$$

$$\nabla_{x_k} R_{k-1} = \nabla_{x_k} g(x_k) \tag{20}$$

$$\nabla_{u_k} R_k = -T_s \nabla_{u_k} f(x_k, u_k, d_k) \tag{21}$$

and the derivatives for the cost function become

$$\nabla_{x_k} L_k = T_s \nabla_{x_k} l_k \tag{22}$$

$$\nabla_{u_k} L_k = T_s \nabla_{u_k} l_k \tag{23}$$

To solve the problem, we use Matlab's `fmincon` with an SQP algorithm. A local optimum is reported if the KKT conditions are satisfied with relative and absolute tolerance of 10^{-9}. A non-optimal solution is returned if the relative cost function or step size changes less than 10^{-9}. The sample time of the NMPC is $T_s = 0.20$ hours.

C. Soft Constraints

When both inputs and states are subject to constraints, the solution may become infeasible. For example when disturbances, which cannot be rejected within the given constraints, hits the system. A method for dealing with infeasibility is to introduce so-called soft-constraints. The constraints are softened by using slack variables with the $l_2 - l_1$ penalty function

$$\phi_s = \sum_{k=0}^{N-1} \left(\frac{1}{2} s_k^T S_w s_k + s_k diag(S_w) \right) \tag{24}$$

with $s \geq 0$ and (14d) are relaxed to $C_k(x_k, u_k) - s_k \geq 0$. The optimizer will then find a solution which minimises the original cost function (14) while keeping the constraint

TABLE I
KINETIC PARAMETERS

Symbol	Value	Unit
γ_S	1.777	kg substrate/kg biomass
μ_{max}	0.37	1/hr
K_S	0.021	kg/m^3
K_I	0.38	kg/m^3

violations as small as possible. The constraints can also be handled without the need for slack variables as shown in [12].

III. FERMENTATION MODEL

A mathematical model is needed for the optimal control and economic analysis of the fermentation process. The aim of this study is to provide a model of the Methylococcus Capsulatus fermentation process. The process is sketched in Figure 1

It is a model with variable volume, substrate and biomass hold-up that are governed by Haldane growth kinetics. The model is deliberately kept simple to illustrate key principles of fermenter operation.

A. Constitutive Relations

The biomass growth is limited by substrate. The overall reaction mechanism is

$$\gamma_S S \rightarrow X \tag{25}$$

The cell growth model is governed by the Haldane expression. The reaction rate can be written as follows

$$r = \mu C_X \tag{26}$$

where the specific growth rate is

$$\mu = \mu_{max} \frac{C_S}{K_S + C_S + C_S^2/K_I} \tag{27}$$

Consequently, the growth of biomass is only limited by the substrate concentration. The production rates of biomass and substrate are

$$R_X = r, \qquad R_S = -\gamma_s r \tag{28}$$

The parameters belonging to the growth of Methylococcus Capsulatus are shown in table I.

B. Conservation equations

A mass balance for the hold-up in the fermenter is governed, assuming constant and identical density of all feed streams and the fermenter content. The mass balances for the biomass and the substrate are also governed and gives

$$\frac{d}{dt}(\rho V) = \rho F_s + \rho F_w - \rho F \tag{29a}$$

$$\frac{d}{dt}(VC_X) = -FC_X + R_X V \tag{29b}$$

$$\frac{d}{dt}(VC_S) = F_s C_{S,in} - FC_S + R_S V \tag{29c}$$

with $V(t_0) = V_0$, $C_X(t_0) = C_{X,0}$ and $C_S(t_0) = C_{S,0}$. The state functions in the model are the total mass, $m = \rho V$, the mass of biomass, $m_X = VC_X$, and the mass of substrate, $m_S = VC_S$. The state variables of the model are the volume, V, the biomass concentration, C_X, and the substrate concentration, C_S. The manipulated variables are the water inlet flow rate, F_w, the substrate inlet flow rate, F_s, and the outlet flow rate, F. When the fermenter is operated in fed batch mode, the outlet flow rate is zero, i.e. $F = 0$.

C. Objective function - Profit

The profit of operating the fermenter is given as the value of the produced biomass minus the cost of the used substrate. This profit, in the period $[t_0,t_f]$, may be expressed as

$$\phi_p = \int_{t_0}^{t_f} (p_X R_X V - p_S F_S C_{S,in}) dt \tag{30}$$

The price of biomass and substrate is 3000\$ and 0\$ respectively. Often we neglect the price of the substrate, as $p_X \gg p_S$. The end cost, $\bar{l}(x(t_f))$, is equal to zero. Optimal operation of the fermenter seeks to maximize the profit, ϕ_p, by manipulating the fermenter inputs within the operation constraints.

D. Constraints

The fermentation process is subject to operation restrictions. The manipulated variables are restricted by input constraints

$$0 \leq \quad F_s \quad \leq 30 \tag{31}$$

$$0 \leq \quad F_w \quad \leq 30 \tag{32}$$

$$0 \leq \quad F \quad \leq 60 \tag{33}$$

The outputs, the volume and the concentrations, are restricted by the output constraints

$$0 \leq \quad V \quad \leq 60 \tag{34}$$

$$0 \leq \quad C_X \quad \leq 0.2 \tag{35}$$

These are relaxed in the computations as shown in (24). The end constraint, $\bar{c}(x(t_f))$, is equal to zero.

IV. ANALYTICAL SOLUTION

In this section, we develop an analytical solution to the operation of the fermenter described in section III. As the fermenter is initially almost empty, we start up in fed batch mode, and when the tank is filled, it is operated in continuous mode.

We consider operation of the fermenter in a period $[t_0\ t_f]$ where t_0 and t_f is a large number i.e. $t_f \rightarrow \infty$. In the period $[t_0\ t_N]$ the fermenter is operated in fed batch mode and operated in continuous mode when filled in the period $[t_N\ t_f]$. The profit of such an operation is, when neglecting the cost of substrate ($p_X \gg p_S$) for simplicity,

$$\phi_p = p_X \int_{t_0}^{t_N} R_X(t) V(t) dt + p_X \int_{t_N}^{t_f} R_X(t) V(t) dt \tag{36}$$

In order to maximize the production and profit, $R_X(t)$ and $V(t)$ must be maximized in both periods. From sec. III-A we have

$$R_X^* = r^* = \mu(C_S^*)C_X^* \tag{37}$$

Thus, the maximal production of biomass is obtained when the biomass and substrate concentrations are kept constant at their optimal values

$$C_X^* = C_{X,max} \qquad t \in [t_0, t_f] \tag{38}$$
$$C_S^* = \max \mu(C_S) = \sqrt{K_I K_s} \qquad t \in [t_0, t_f] \tag{39}$$

In this case the production rates, R_X and R_S, become constant values which attain their maximal values at

$$R_X^* = r^*, \qquad R_S^* = -\gamma_s r^* \tag{40}$$

such that the total profit of the biomass production (36) can be expressed as

$$\phi_p = p_X R_X^*(V_{max} - V_0) + p_X R_X^* V_{max}(t_f - t_N) \tag{41}$$

A. Fed batch operation

In order to determine the optimal trajectory for the manipulated inputs we set up the model equations, utilizing that the biomass and substrate concentrations are now constant. $F = 0$ in fed batch mode and the density ρ is constant, which reduces the model to

$$\dot{V}(t) = F_s(t) + F_w(t) \qquad V(t_0) = V_0 \tag{42a}$$
$$\dot{V}(t)C_X^* = R_X V(t) \qquad C_X(t_0) = C_X^* \tag{42b}$$
$$\dot{V}(t)C_S^* = F_s C_{S,in} + R_S V(t) \qquad C_S(t_0) = C_S^* \tag{42c}$$

Substitution of (42a) in (42b) and (42c) yields

$$\begin{bmatrix} C_X^* & C_X^* \\ C_S^* - C_{S,in} & C_S^* \end{bmatrix} \begin{bmatrix} F_s(t) \\ F_w(t) \end{bmatrix} = \begin{bmatrix} R_X^* \\ R_S^* \end{bmatrix} V(t) \tag{43}$$

Solving for $\begin{bmatrix} F_s(t) & F_w(t) \end{bmatrix}^T$ we get

$$\begin{bmatrix} F_s(t) \\ F_w(t) \end{bmatrix} = \begin{bmatrix} \frac{C_S^* R_X^*}{C_{S,in} C_X^*} - \frac{R_S^*}{C_{S,in}} \\ -\frac{R_X^*(C_S^* - C_{S,in})}{C_{S,in} C_X^*} + \frac{R_S^*}{C_{S,in}} \end{bmatrix} V(t) \tag{44}$$

As we have restricted F_w to be greater than zero we require

$$R_X^*(C_S^* - C_{S,in}) \leq R_S^* C_X^* \Rightarrow \tag{45}$$
$$C_{S,in} \geq C_S^* + \gamma_s C_X^* \tag{46}$$

As the volume in the fermenter is given by the simple differential equation in (29a), we can now construct the trajectory of the states and the inputs in fed batch operation. The equation becomes

$$\frac{d}{dt}V = F_s + F_w = \frac{R_X^*}{C_X^*} V(t) \qquad V(t_0) = V_0 \tag{47}$$

Leading to the state evolution

$$V(t) = V_0 \exp\left(\frac{R_X^*}{C_X^*} t\right) \tag{48}$$

and the time, t_N, where the fermenter is filled, $V(t_N) = V_{max}$

$$t_N = \frac{C_X^*}{R_X^*} \log\left(\frac{V_{max}}{V_0}\right) \tag{49}$$

Consequently, the optimal operation of the inputs are given by substituting (48) into (44) and the switch to continuous operation is given in (49).

B. Continuous operation

During continuous operation, the production is optimized by letting the state assume its optimal values

$$V^*(t) = V^* = V_{max} \qquad t \in [t_N, t_f] \tag{50}$$
$$C_X^*(t) = C_X^* = C_{X,max} \qquad t \in [t_N, t_f] \tag{51}$$
$$C_S^*(t) = C_S^* = \sqrt{K_I K_s} \qquad t \in [t_N, t_f] \tag{52}$$

Solving for $\begin{bmatrix} F_s(t) & F_w(t) & F(t) \end{bmatrix}^T$ in (29) utilizing the above we get the optimal input trajectory

$$\begin{bmatrix} F_s^*(t) \\ F_w^*(t) \\ F^*(t) \end{bmatrix} = \begin{bmatrix} \frac{C_S^* R_X^*}{C_{S,in} C_X^*} - \frac{R_S^*}{C_{S,in}} \\ -\frac{R_X^*(C_S^* - C_{S,in})}{C_{S,in} C_X^*} + \frac{R_S^*}{C_{S,in}} \\ \frac{R_X^*}{C_X^*} \end{bmatrix} V^* \tag{53}$$

As the volume, biomass and substrate concentration in the fermenter are measured, we can now construct the optimal inputs for continuous operation.

V. Results

We illustrate the applicability of the E-NMPC by considering a combined simulation, in which the fermenter is started in fed batch mode and then goes into continuous mode when it is full. The analytical solution and simulated states, inputs and the value of the objective function to the fermenter are shown in Figure 2, 3 and 4 respectively.

A. Fed batch operation

The fermenter is started in fed batch mode. We, first of all, notice that the controller is able to control the system to the optimal state when comparing with the analytical solution. Furthermore, the volume of the fermenter increases exponentially. The NMPC uses a simple Forward Euler method with constant step size for state prediction, and we, therefore, see a small offset arise in the substrate and biomass concentrations while the volume increases. A reduced sample time will decrease the deviation from the analytical solution. On the other hand, the deviation do not lead to a significant loss of profit. The violations of the constraints are small and by any practical means do not pose a problem.

B. Continuous operation

Continuous mode is reached when production is continued after the fermenter is filled. Again we note that the correct optimal solution is found compared to the analytical solution. The before mentioned small offset in the substrate and biomass concentrations have vanished due to the constant hold-up. Only small numerical errors on the NMPC solution arise. These errors are due to the Forward Euler method, but are also negligible.

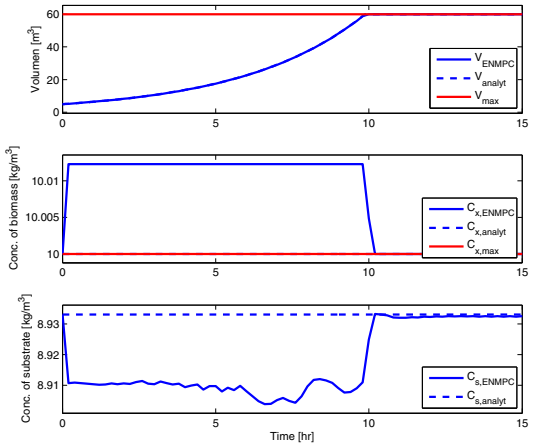

Fig. 2. States of the fermenter. The controller fills the tank and then opens the outlet valve, i.e. starts up in fed batch mode and then continue in continuous mode. The concentrations are kept at almost optimal values during the compete operation.

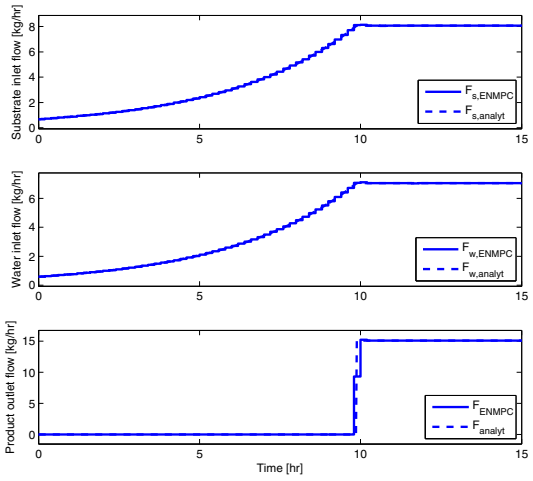

Fig. 3. Inputs to the fermenter. In fed batch mode the flow of water and substrate increases exponentially in order to stabilize the biomass and substrate concentrations. The flows stabilize when the fermenter is filled.

VI. Conclusion

In this paper, we have derived and demonstrated an economically optimizing nonlinear model predictive controller (NMPC) for a fermentation process. The performance of the controller is by any practical means deemed identical to the analytical solution. Only minor economic loss was observed due to the Forward Euler state integration method. A model for the fermentation process of single cell proteins, using Methylococcus Capsulatus, was stated and used directly in the control algorithm. The process was studied under feedback control using the proposed controller in a reseeding

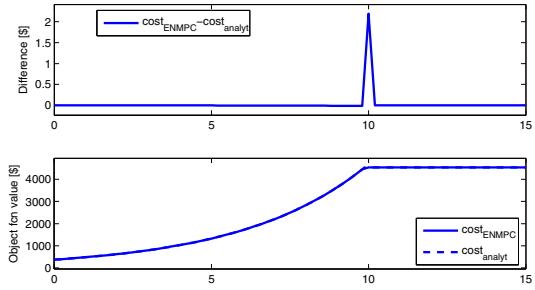

Fig. 4. Objective function of the fermenter compared to the analytical solution. As seen the losses of running an E-NMPC are very small compared to the analytical solution.

horizon setup. The performance of the closed-loop system was studied in fed batch and continuous operation. We have presented a through description of the NMPC algorithm and a fermentation example, which can be used in a tutorial fashion.

References

[1] J. B. Rawlings, C. N. Bates, and D. Angeli, "Fundamentals of economic model predictive control," *Proceedings of the IEEE Conference on Decision and Control*, pp. 3851–3861, 2012.

[2] M. L. Darby, M. Harmse, and M. Nikolaou, "MPC: Current practice and challenges," *IFAC Proceedings Volumes*, vol. 7, no. 1, pp. 86–98, 2009.

[3] R. Amrit, "Optimizing process economics in model predictive control," Ph.D. dissertation, University of WisconsinMadison, September 2011.

[4] R. Halvgaard, N. K. Poulsen, H. Madsen, and J. B. Jørgensen, *Economic Model Predictive Control for Building Climate Control in a Smart Grid*. IEEE, 2012.

[5] T. G. Hovgaard, L. F. Larsen, and J. B. Jørgensen, "Flexible and cost efficient power consumption using economic mpc," *Proceedings of the 50th IEEE Conference on Decision and Control and European Control Conference*, pp. 848–854, 2011.

[6] D. Angeli, R. Amrit, and J. B. Rawlings, "Receding horizon cost optimization for overly constrained nonlinear plants," *Proceedings of the IEEE Conference on Decision and Control*, pp. 7972–7977, 2009.

[7] J. M. Modak and H. C. Lim, "Feedback optimization of fed-batch fermentation," *Biotechnology and Bioengineering*, vol. 30, no. 4, pp. 528–540, 1987.

[8] B. Srinivasan, D. Bonvin, E. Visser, and S. Palanki, "Dynamic optimization of batch processes: II. Role of measurements in handling uncertainty," *Computers & Chemical Engineering*, vol. 27, pp. 27–44, 2003.

[9] D. F. Olsen, J. B. Jørgensen, J. Villadsen, and S. B. Jørgensen, "Modeling and simulation of single cell protein production," vol. 11, no. 1, pp. 502–507, 2010.

[10] M. Schlegel, K. Stockmann, T. Binder, and W. Marquardt, "Dynamic optimization using adaptive control vector parameterization," *Computers & Chemical Engineering*, vol. 29, no. 8, pp. 1731–1751, 2005.

[11] H. G. Bock and K. J. Plitt, "A multiple shooting algorithm for direct solution of optimal control problems," *9th IFAC World Congress Budapest. Pergamon Press*, pp. 242–247, 1984.

[12] A. Capolei and J. B. Jørgensen, "Solution of constrained optimal control problems using multiple shooting and esdirk methods," *Control Conference (ACC), 2012*, pp. 295–300, 2012.

[13] L. T. Biegler, "Solution of dynamic optimization problems by successive quadratic programming and orthogonal collocation," *Computers & Chemical Engineering*, vol. 8, no. 3, pp. 243–248, 1984.

[14] J. B. Jørgensen, "Adjoint sensitivity results for predictive control, state- and parameter-estimation with nonlinear models," *European Control Conference 2007*, pp. 3649–3656, 2007.

Paper E

Application of Constrained Linear MPC to a Spray Dryer

Published in *IEEE Multi-conference on Systems and Control (MSC 2014), pp. 2120–2126, 2014, Antibes.*

2014 IEEE Conference on Control Applications (CCA)
Part of 2014 IEEE Multi-conference on Systems and Control
October 8-10, 2014. Antibes, France

Application of Constrained Linear MPC to a Spray Dryer

Lars Norbert Petersen[1,2], Niels Kjølstad Poulsen[1], Hans Henrik Niemann[3],
Christer Utzen[2] and John Bagterp Jørgensen[1]

Abstract— **In this paper we develop a linear model predictive control (MPC) algorithm for control of a two stage spray dryer. The states are estimated by a stationary Kalman filter. A non-linear first-principle engineering model is developed to simulate the spray drying process. The model is validated against experimental data and able to precisely predict the temperatures, the air humidity and the residual moisture in the dryer. The MPC controls these variables to the target and reject disturbances. Spray drying is a cost-effective method to evaporate water from liquid foods and produces a free flowing powder. The main challenge of spray drying is to meet the residual moisture specification and prevent powder from sticking to the chamber walls. By simulation we compare the performance of the MPC against the conventional PID control strategy. During an industrially recorded disturbance scenario, the MPC increases the production rate by 7.9%, profit of production by 8.2% and the energy efficiency by 4.1% on average.**

I. Introduction

In 2015 the milk quota system in the European Union will be completely liberalized. The expected effect of this liberalization is that the milk production increases significantly. In some countries up to 50% in 2020 [1]. The milk production expansion will mainly affect the milk powder production due to the short shelf life of dairy products. Consequently, the capacity for production of milk powder will need to increase [1]. Industry studies show that advanced control is capable of increasing the capacity of spray dryers by up to 20% [2]. Optimal control is therefore an effective way to leverage the future production increase.

The main objective in controlling a spray dryer is to minimize the energy consumption while bringing the residual moisture in the powder below the specification and avoid that the powder sticks to the chamber walls. The dryers are generally very large. These may have a feed capacity of up to 4.4 million l/day of raw milk and require 7 MW of power. Therefore, even small improvement in operation will have a large impact on the profitability. The challenge is in maintaining optimal operation since to do so the dryer must be constantly adjusted to variations in the feed concentration and ambient air humidity.

Conventional PID control of spray dryers keeps inlet- and outlet temperatures constant during operation. This is a simple approach, but known to be insufficient at controlling the residual moisture and prevent powder from sticking to the chamber walls [3]. The variations in residual moisture of the produced powder reflects that the conventional PID controller cannot reject disturbances such as feed concentration variations and air humidity variations. Still, this conventional control strategy is the de facto standard in the industry. The MPC proposed in this paper constantly adjusts the manipulated variables such that the residual moisture, the exhaust air temperature and exhaust air humidity is controlled to a reference. The temperature and humidity in the dryer are closely correlated to stickiness of powder. Therefore, controlling the temperature and humidity indirectly controls the stickiness and deposits of the powder in the dryer. The residual moisture must be controlled to specifications to avoid bacterial growth and preserve the milk powder. Conventional control must frequently be manually adjusted in order to avoid stickiness of the powder and produce at specified residual moisture content.

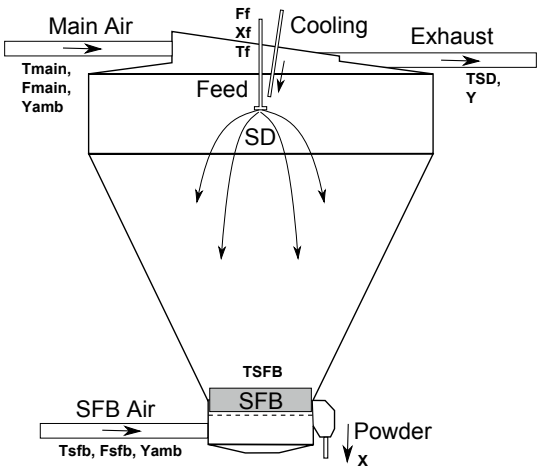

Fig. 1: Illustration of the spray chamber (SD) and the static fluid bed (SFB) stages of a two stage spray dryer. Hot air is let into the upper section of the drying chamber where the nozzles disperse the liquid feed. The droplets dry into powder particles in these two stages.

A. Process Description

The two stage spray dryer is an energy efficient dryer and is often used for production of milk and other food powders. Fig. 1 illustrates the spray chamber (SD) and static fluid

[1] Department of Applied Mathematics and Computer Science, Technical University of Denmark, Kgs. Lyngby, Denmark {lnpe,nkpo,jbjo}@dtu.dk
[2] GEA Process Engineering A/S, Søborg, Denmark christer.utzen@gea.com
[3] Department of Electrical Engineering, Technical University of Denmark, Kgs. Lyngby, Denmark hhn@elektro.dtu.dk

bed stage (SFB). The main hot air is let into the upper section of the drying chamber (SD) around the high pressure nozzles. The nozzles disperse the liquid feed into droplets. The heat is transferred from the hot air to the droplets, and due to this transfer water evaporates from the droplets. In that process, the air temperature and the residual moisture of the droplets decrease. The dried product then enters the static fluid bed (SFB) where it is dried further. After drying in the SFB, the powder is transported to the external vibrating fluid bed (VFB) for gentle drying and cooled to the temperature desired for handling and storage. The VFB is not illustrated in Fig. 1.

B. Modelling and Control

Modelling of the drying process in spray dryers varies in complexity and purpose. First order transfer function models as well as first principles engineering models for control purposes are proposed [4], [5]. [6] proposes a dynamic model for a complete multi-stage dryer. A number of papers present control strategies for spray dryers. The focus varies from pressure control of the chamber pressure to MPC control of the residual moisture based on industrial software [2]. [7] provides a detailed review on the status and future of advanced control for spray dryers. In [5] a feed forward approach is made to help control the residual moisture. Set-point tracking MPC is a standard methodology for optimizing the operation of processes and a recognised control method in both academia and industry due to its ability to handle coupled dynamics, time delays, constraints and feed forward of measured disturbances [8], [9]. In this methodology the economics of operation is optimized in a separate real-time steady-state optimization (RTO) layer [10]. Recent advances has shifted to combine these two layers into a single economically optimizing (E-)MPC layer. [11] use nonlinear (E-)MPC for economic optimization of a two stage spray dryer.

C. Content

In this paper we investigate the potential of optimizing the spray drying process by linear MPC. We compare the linear MPC to the conventional PID based control method. The MPC is composed of an optimal regulator and a state estimator. The regulator has the structure described in [12]–[14], with the modification that we use a deterministic linearised first principles engineering model instead of an innovation form state space model identified from data. The model used for simulation is also based on the non-linear first principles engineering model. The proposed model is identified and validated against two independent experimental datasets provided by GEA Process Engineering A/S.

D. Organization

The paper is organized as follows. In Section II we describe the model and show its accuracy by comparing its output to experimental data. Section III presents the regulator and state estimator. In Section IV we present two simulations to validate the MPC and show the benefit of optimizing the two stage spray dryer. Conclusions are given in Section V.

II. Spray Dryer Model

In this section, we present the first principles engineering model for a Multi-Stage Dryer type 20 (MSD$^{\text{TM}}$-20), i.e. a medium-sized two stage spray dryer, made available by GEA Process Engineering A/S. The dryer has a maximum water evaporation capacity of approximately 125 kg/h. The data for identification is based on drying of sugar water, maltodextrin DE-18. We use maltodextrin, because milk is difficult to handle over longer periods due to natural deterioration and maltodextrin DE-18 has the same drying properties as skim milk [15].

A. Mass- and Energy Balances

The model consists of four states. The states are the spray dryer temperature, T_{SD}, the static fluid bed temperature, T_{SFB}, the humidity in the air of the spray dryer, Y, and the moisture in the powder, X. The lumped energy and mass balances describing the evolution of the states are

$$C_a \frac{dT_{SD}}{dt} = -\lambda R_w + H_{a_{in}} - H_{a_{out}} - Q_{exc} - Q_{la} \tag{1a}$$

$$C_b \frac{dT_{SFB}}{dt} = H_{b_{in}} - H_{b_{out}} + Q_{exc} - Q_{lb} \tag{1b}$$

$$\begin{aligned} m_{da} \frac{dY}{dt} = (F_{main} + F_{sfb})(Y_{amb} - Y) \\ + F_{add}(Y_{add} - Y) + R_w \end{aligned} \tag{1c}$$

$$m_s \frac{dX}{dt} = F_s(X_f - X) - R_w \tag{1d}$$

where

$$\begin{aligned} H_{a_{in}} = F_{main}(c_{da} + c_v Y_{amb})(T_{main} - T_0) + \\ F_{add}(c_{da} + c_v Y_{add})(T_{add} - T_0) \end{aligned} \tag{2a}$$

$$\begin{aligned} H_{a_{out}} = (F_{main} + F_{sfb} + F_{add}) \cdot \\ (c_{da} + c_v Y)(T_{SD} - T_0) \end{aligned} \tag{2b}$$

$$H_{b_{in}} = F_{sfb}(c_{da} + c_v Y_{amb})(T_{sfb} - T_0) \tag{2c}$$

$$H_{b_{out}} = F_{sfb}(c_{da} + c_v Y_{amb})(T_{SFB} - T_0) \tag{2d}$$

$$Q_{exc} = k_1(T_{SD} - T_{SFB}) + k_2 X_f + k_3 T_f - k_4 \tag{2e}$$

$$Q_{la} = k_5(T_{SD} - T_{amb}) \tag{2f}$$

$$Q_{lb} = k_6(T_{SFB} - T_{amb}) \tag{2g}$$

$$F_s = F_f X_f / (X_f + 1) \tag{2h}$$

The air and the product temperatures are assumed in equilibrium in both stages, i.e. T_{SD} and T_{SFB} are each identical to the powder temperatures in the SD- and the SFB-stage, respectively. $H_{a_{in}}$, $H_{a_{out}}$, $H_{b_{in}}$ and $H_{b_{out}}$ are the enthalpies of humid air in and out of the SD and the SFB stage, respectively. The reference temperature is $T_0 = 25°C$. C_a and C_b is the heat capacity of the hold-up of air and powder. F_{main} and F_{sfb} are dry basis inlet air flows. The parameters Y_{add} and F_{add} are used to correct for air leakage and other un-modeled inlet air flows such as nozzle cooling air. Q_{exc} is the heat exchange between the SD and the SFB stages. Q_{la} and Q_{lb} are heat losses to the surroundings. λR_w is the heat of evaporation. We assume that the evaporation only takes place in the SD stage. X_f is the dry base feed concentration and T_f is the feed temperature. m_s is the dry

mass of powder and m_{da} is the mass of dry air. The latent heat of vaporization, λ, and the heat capacities, c_{da} and c_v, are calculated according to [16].

B. Drying Rate

The drying rate of the product, R_w, is an important parameter of the model. The thin layer equation describes the product drying rate, R_w, well [17]

$$R_w = D_{diff}(X - X_{eq})m_s \tag{3}$$

D_{diff} is an experimentally determined constant called the drying constant or diffusivity [18]. It may depend on both the temperature and the moisture of the powder, but in the present study it is assumed constant.

The equilibrium moisture, X_{eq}, describes the moisture content at which water cannot be evaporated from the powder any longer. The Guggenheim-Anderson-de Boer (GAB) relation is used to describe the equilibrium moisture content [19] and is fitted to laboratory data obtained specifically from maltodextrin to get

$$X_{eq} = \frac{C \cdot K \cdot X_m \cdot RH}{(1 - K \cdot RH)(1 - K \cdot RH + C \cdot K \cdot RH)} \tag{4}$$

where $X_m = 0.030723$, $C = 2.6535 \cdot 10^{-7} \exp\left(\frac{6292.1}{T}\right)$ and $K = 0.057882 \exp\left(\frac{945.16}{T}\right)$. X_m, C and K are GAB constants related to monolayer and multilayer properties. In the computation of X_{eq}, $T = T_{SFB}$ and $RH = Y/(18.02/28.97 + Y) \cdot p_c/p_{vapsat}(T)$. p_c is the chamber pressure and p_{vapsat} is the saturated vapor pressure.

C. Performance

The energy efficiency, the profit of operation and the product flow rate are the three key performance indicators (KPIs) for evaluation of the performance of a spray dryer. There are a number of energy efficiency indices to measure the energy performance of a dryer. We adopt the definition given by [20]

$$\eta = \frac{\lambda F_s(X_f - X)}{\Delta H} \tag{5}$$

Here $\lambda F_s(X_f - X)$ is the energy used to evaporate water and ΔH is the total energy supplied to the dryer given by

$$\Delta H = F_{main}(h_{a_{in}} - h_{amb}) + F_{sfb}(h_{b_{in}} - h_{amb}) \tag{6}$$

in which $h_{amb} = (c_{da} + c_v Y_{amb})(T_{amb} - T_0)$. The profit from operating the spray dryer is the value of the product minus the raw material and energy costs.

$$P = p_p F_s(1 + X) - p_f F_s(1 + X_f) - p_H \Delta H \tag{7}$$

The price of the produced powder is $p_p = 4.47$ \$/kg, the price of feed material is $p_f = 0.447$ \$/kg, and the price of energy is $p_H = 3.4873 \cdot 10^{-5}$ \$/KJ. The prices are selected to reflect the industrial prices of natural gas and the price of the powder. The flow rate of powder is $F_p = F_s(1 + X)$.

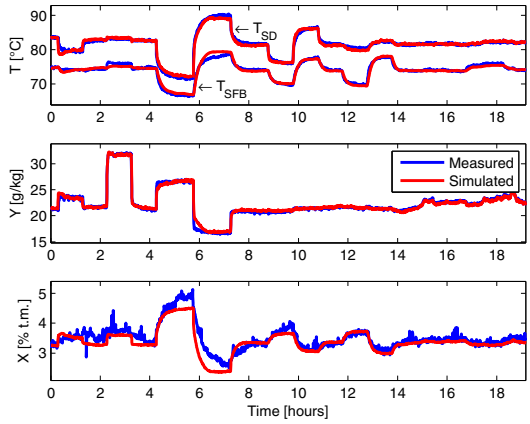

Fig. 2: Model validation dataset. The disturbances i.e. feed concentration and ambient air humidity are altered from $t = 0$ to $t = 4$. The feed flow is altered between $t = 4$ and $t = 8$. The main inlet air temperature, the SFB inlet air temperature and SFB air flow rate is changed between $t = 8$ to $t = 15$.

D. Parameter Estimation

The parameters, θ, in the model (1)-(4) are estimated from data (not shown here) by minimizing the least squares simulation error (not 1-step prediction error). The model is validated against the data in Fig. 2. Generally the model fits the data well. Table I provides the parameters and all parameters are significantly identified. The mass of dry powder and dry air are determined from physical considerations and fixed to $m_{da} = 10$ kg and $m_s = 15$ kg.

The model of the dryer is a deterministic system of ordinary differential equations, i.e.

$$\frac{d\bar{x}(t)}{dt} = f(\bar{x}(t), u(t), d(t), \theta) \tag{8}$$

in which

$$\bar{x} = \begin{bmatrix} T_{SD} & T_{SFB} & Y & X \end{bmatrix}^T \tag{9}$$

$$u = \begin{bmatrix} F_f & T_{main} & T_{sfb} \end{bmatrix}^T \tag{10}$$

$$d = \begin{bmatrix} F_{main} & F_{sfb} & X_f & T_f & T_{amb} & Y_{amb} \end{bmatrix}^T \tag{11}$$

$\bar{x}$ is the state vector, u is the manipulated input vector, d is the disturbance vector and θ is the parameter vector. The measurement vector, y, and the controlled output vector, z, are

$$y = \begin{bmatrix} T_{SD} & T_{SFB} & Y & X \end{bmatrix}^T, \quad z = \begin{bmatrix} T_{SD} & Y & X \end{bmatrix}^T$$

E. Stochastic Model

The deterministic system in (8) is augmented by two stochastic terms. Consequently, the state evolution and measurement equation of the dryer is described by

$$\bar{x}(t_k + T_s) = F(\bar{x}(t_k), u(t_k), d(t_k), \theta) + \bar{w}(t_k) \tag{12a}$$

TABLE I: Estimated parameters for the model (1)-(4)

Symbol	Value	Unit	Symbol	Value	Unit
C_a	68.266	KJ/K	F_{add}	256.46/3600	kg/s
C_b	141.36	KJ/K	Y_{add}	$8.1799{\cdot}10^{-3}$	kg/kg
k_1	0.29268	KW/K	T_{add}	100.03+273.15	K
k_2	1.6207	KW	k_3	0.073198	KW
k_4	31.111	KW	k_5	0.26981	KW/K
k_6	-0.023367	KW/K	D_{diff}	0.091922	

$$y(t_k) = h(\bar{x}(t_k)) + v(t_k) \tag{12b}$$
$$z(t_k) = g(\bar{x}(t_k)) \tag{12c}$$

where $T_s = 10$ s. The state and measurement noise covariances are $\bar{w}(t_k) = N_{iid}(0, \bar{R}_w)$ and $v(t_k) = N_{iid}(0, R_v)$. The two noise-terms are assumed to be uncorrelated. The system is simulated using a 4^{th} and 5^{th} order accurate Runge-Kutta method with variable step size.

III. Model Predictive Control

In this section we present the regulator and the state estimator in the linear MPC.

A. Background and control objectives

The controlled variables are the exhaust air temperature T_{SD}, the absolute air humidity, Y, and the product specific residual moisture content, X. T_{SD} and Y are closely related to the stickiness of the powder. The set-points for T_{SD} and Y are a result of empirical experience, and can only be exactly determined from product and spray dryer specific trials. Generally, there is a lower limit to T_{SD} and an upper limit to Y. A simple RTO layer can be designed to provide such set-points depending on the type of product being dried. The set-point for X is also product specific. The manipulated variables are the feed flow, F_f, the inlet main air temperature, T_{main}, and the inlet SFB air temperature, T_{sfb}. The inlet air flows, the feed concentration X_f, the feed temperature, T_f, the ambient air humidity, Y_{amb}, and the indoor temperature, T_{amb}, are all measured disturbances. The states and disturbances are measurable, also in industrial practice.

B. Plant and Sensors

The non-linear model of the dryer is numerically linearised, by applying small perturbations to the steady-state, and represented in state space form. To guarantee offset-free control of the outputs, z, we augment the process model with a number of integrating disturbances equal to the number of measured outputs y [21]. Thus, the presence of constant unmeasured disturbances and plant model mismatch do not affect the tracking performance. The augmented model has the following form

$$x_{k+1} = Ax_k + Bu_k + Ed_k + \sigma_x + w_k \tag{13a}$$
$$y_k = C_y x_k + \sigma_y + v_k \tag{13b}$$
$$z_k = C_z x_k + \sigma_z \tag{13c}$$

with x, u, d, y and z being the same variables as in (8), but x also including the disturbance states. w and v are distributed by $w_k \sim N_{iid}(0, R_w)$ and $v_k \sim N_{iid}(0, R_v)$. The initial state is, $x_0 \sim N(\hat{x}_0, P_0)$. σ_x, σ_y and σ_z contain the constants related to the linearisation of the model, i.e. $\sigma_x = x_0 - Ax_0 - Bu_0 - Ed_0$, $\sigma_y = y_0 - C_y x_0$ and $\sigma_z = z_0 - C_z x_0$. (A, B) is stabilizable and (C_y, A) is detectable. Thus, we can control and estimate the states of the dryer.

Algorithm 1 MPC algorithm

Require: y_k, d_k, r_k, $\hat{x}_{k|k-1}$, u_{k-1}
Filter:
$e_k = y_k - (C_y \hat{x}_{k|k-1} + \sigma_y)$
$\hat{x}_{k|k} = \hat{x}_{k|k-1} + K_{fx} e_k$
Regulator:
$u_k = \mu(\hat{x}_{k|k}, r_k, d_k, u_{k-1})$
One-step predictor:
$\hat{x}_{k+1|k} = A\hat{x}_{k|k} + Bu_k + Ed_k + \sigma_x$
Return: u_k, $\hat{x}_{k+1|k}$

C. Regulator

The output tracking problem with input and input rate constraints may be formulated as

$$\min_{u_k \in \mathcal{N}_u} \quad \phi \tag{14a}$$
$$s.t. \quad x_{k+j+1|k} = Ax_{k+j|k} + Bu_{k+j|k} + Ed_{k+j|k} + \sigma_x, \quad j \in \mathcal{N}_u \tag{14b}$$
$$z_{k+j|k} = C_z x_{k+j|k} + \sigma_z, \quad j \in \mathcal{N}_z \tag{14c}$$
$$u_{min} \le u_{k+j|k} \le u_{max}, \quad j \in \mathcal{N}_u \tag{14d}$$
$$\Delta u_{min} \le \Delta u_{k+j|k} \le \Delta u_{max}, \quad j \in \mathcal{N}_u \tag{14e}$$

where

$$\phi = \frac{1}{2} \sum_{j=1}^{N_z} \|z_{k+j|k} - r_{k+j|k}\|^2_{Q_z} + \frac{1}{2} \sum_{j=0}^{N_u} \|\Delta u_{k+j|k}\|^2_{S_u}$$

in which $\Delta u_k = u_k - u_{k-1}$ and $\mathcal{N}_z = \{1, 2 \ldots, N_z - 1\}$, $\mathcal{N}_u = \{0, 1 \ldots, N_u - 1\}$. The control and prediction horizons are, $N_z = 20$ min/10 s $= 120$ and $N_u = 120$. These are selected sufficiently long such that any end effects have no influence on the solution in the beginning of the horizon. No forecasts are available for the references and disturbances, so we use the same-as-now forecasts, i.e. $r_{k+j|k} = r_k$ and $d_{k+j|k} = d_k$.

The problem in (14) can be converted to a constrained quadratic problem. Appendix A shows the details of the derivation of the regulator, the tuning parameters Q_z and S_u and the constraints. Algorithm 1 list the on-line computations in the linear MPC algorithm. The computation of $u_k = \mu(\hat{x}_{k|k}, r_k, d_k, u_{k-1})$ is performed by solving (14). The solution of the QP (14) is the computational expensive step in the MPC algorithm. The QP is solved using `quadprog()` in Matlab® and the worst-case execution time is approx. 12.5 msec.

IV. Closed-loop simulations

In this section we demonstrate the performance of the linear MPC and compare it to the performance of a conventional

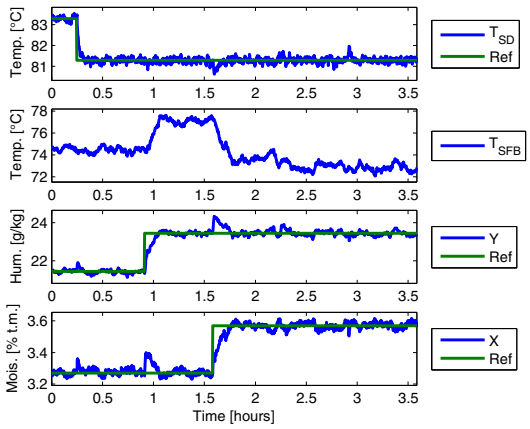

(a) Measured outputs of the system. The controlled variables are shown with the associated reference.

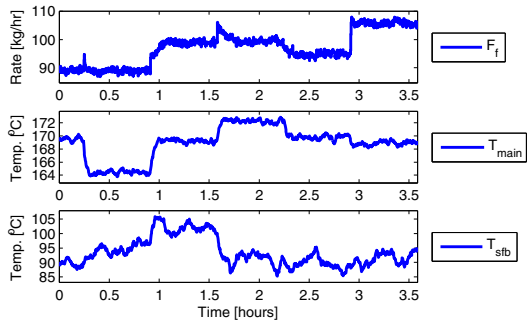

(b) Manipulated inputs to the system.

Fig. 3: Closed-loop simulation showing that the MPC tracks the set-points and rejects the unknown disturbances without steady-state error.

PID controller. The stochastic system model in (12) is used in the simulations.

A. MPC Validation

In the following the MPC will be validated against reference- and disturbance step changes. Fig. 3a shows the measured and controlled variables and Fig. 3b shows the manipulated variables. The ambient air humidity changes from 3 g/kg to 4 g/kg at $t = 2.25$ hours and the feed concentration decreases from 50.6% to 45.6% at $t = 2.92$ hours. The disturbances are treated as unknown to the MPC in this simulation. At $t = 0.25$ to $t = 1.6$ three reference steps are introduced for each controlled variable. The exhaust air temperature and humidity, T_{SD} and Y, change slightly faster than the residual moisture content, X. The MPC tracks the references and rejects disturbances without any offset. The system is controlled to a steady-state within reasonable time. The MPC handles the highly cross coupled system

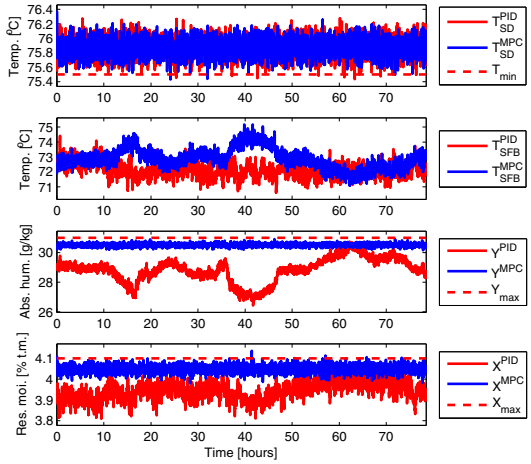

(a) Measured outputs of the system. The controlled variables are shown with the associated reference.

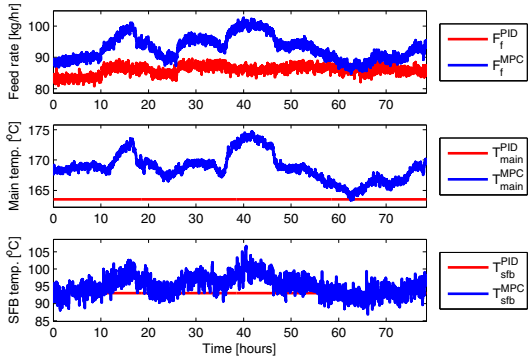

(b) Manipulated inputs to the system.

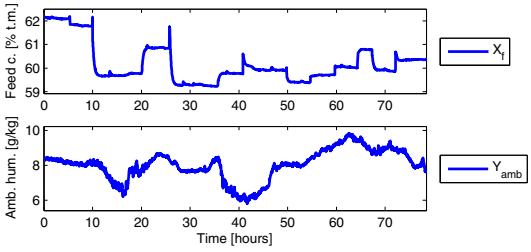

(c) Disturbance inputs to the system. The changes are used in feedforward to the controller i.e. $d_{k+j|k} = d_k$.

Fig. 4: Closed-loop simulation of an industrial disturbance scenario using an MPC and the conventional PID controller. The MPC tracks the set-points and rejects the disturbances.

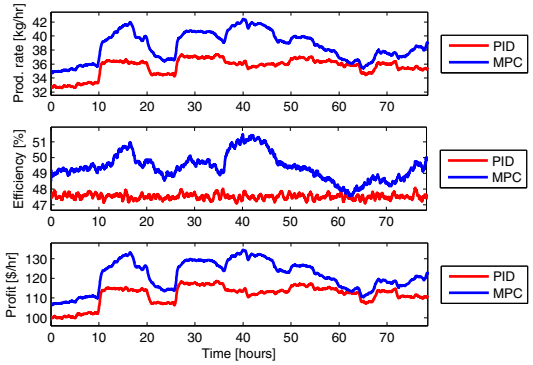

Fig. 5: The production rate, the energy efficiency and the profit of drying during the closed-loop simulation in Fig. 4.

dynamics well. The manipulated variables are kept within the input constraints and input rate constraints. The constraints are expected to become active occasionally as the load on the dryer is increased, i.e. as the feed flow, F_f, and the heat inputs, T_{main} and T_{sfb}, are increased.

B. Industrial scenario

We also perform a closed-loop simulation with a realistic disturbance scenario from an industrial spray dryer. Thereby we can compare the achieved performance of the MPC to the conventional PID controller. Fig. 4 shows the spray dryer operation when controlled by the MPC and the conventional PID controller. Fig. 5 shows the KPIs. The disturbances are known to the MPC as these measurements are normally available in industry. The disturbances are recorded at a spray dryer producing whey protein concentrate in the period 8/13/2013 21:30 to 8/17/2013 04:00.

Fig. 4 shows the measured and controlled outputs, the manipulated variables and the disturbances. The simulation reveal that the proposed MPC is able to maintain a correct and constant residual moisture content, X, as well as maintaining the stickiness related variables, T_{SD} and Y, at their setpoints. The MPC constantly adjusts the feed flow and inlet air temperatures to maintain the controlled variables at their set-points. An increase in the ambient air humidity increases the humidity in the dryer. Thus, the MPC must decrease the feed rate i.e. production. An increase in feed water concentration has the same effect and is also compensated by a decrease in the feed rate i.e. production.

The conventional PID controller maintains a constant exhaust air temperature, T_{SD}, by manipulating the feed rate, F_f. The two inlet air temperatures are fixed. With this control methodology, no correcting action is taken when the ambient air humidity increases. Changes related to the feed concentration are compensated for as the feed water affects the exhaust air temperature. Thus, on average the dryer need to dry the powder more than necessary to satisfy the specifications. The MPC only dries the powder to the specified level.

Fig. 5 shows the production rate, energy efficiency and profit of operation during the simulation. On average the MPC increases the production rate by 7.9%, the energy efficiency by 4.1% and profit of production by 8.2%. Thus, the dryer is used both more energy efficiently and increases the profit of operation significantly.

V. Conclusions

This paper presents a solution to the control problem of a two stage spray dryer. The controller is based on a set-point tracking MPC with output feedback. The states used in the regulator are estimated by a Kalman filter. The regulator and the estimator is designed based on the linearised non-linear system model. The simulations show that the air temperature and air humidity of the outlet air from the dryer can be controlled to a set-point as well as the residual moisture content in the powder. On average during the disturbance scenario the MPC increases the production rate by 7.9%, the energy efficiency by 4.1% and the profit of production by 8.2%. These numbers may be even greater in industry, as the conventional PID controller is often used more conservatively than presented in this paper. Thus, the dryer is used both more efficiently and increases the profit of operation significantly.

GEA Process Engineering A/S is currently implementing and testing the proposed control strategy at industrial scale spray dryers. The control methodology is generally applicable to other foods, chemicals and pharmaceuticals and not limited to two-stage dryers.

References

[1] T. Donnellan, T. Hennessy, M. Fenelon, and D. O'Callaghan, "The potential for scale economies in milk powder processing: an irish case study," *International Journal of Dairy Technology*, vol. 67, no. 1, pp. 129–134, 2014.

[2] Vaisala. (2014, Feb.) +20% increase in production capacity with zero increase in energy consumption. [Online]. Available: http://www.vaisala.com/Vaisala%20Documents/Success%20Stories/CEN-TIA-G-Valio-Customer-Story-B211288EN-A.pdf

[3] D. O'Callaghan and P. Cunningham, "Modern process control techniques in the production of dried milk products - a review," *Lait*, vol. 85, pp. 335–342, 2005.

[4] L. Tan, F. Taip, and N. Aziz, "Simulation and Control of Spray Drying Using Nozzle Atomizer Spray Dryer." *International Journal of Engineering & Technology*, no. 10, pp. 1–7, 2009.

[5] J. Pérez-Correa and F. Fariass, "Modelling and control of a spray dryer: a simulation study," *Food Control*, vol. 6, no. 4, pp. 219–227, 1995.

[6] L. N. Petersen, N. K. Poulsen, H. H. Niemann, C. Utzen, and J. B. Jørgensen, "A Grey-Box Model for Spray Drying Plants," *10th IFAC International Symposium on Dynamics and Control of Process Systems (DYCOPS 2013)*, pp. 559–564, 2013.

[7] D. O. Callaghan and P. Cunningham, "Modern process control techniques in the production of dried milk products a review," *Lait*, vol. 85, pp. 335–342, 2005.

[8] M. L. Darby, M. Harmse, and M. Nikolaou, "MPC: Current practice and challenges," *IFAC Proceedings Volumes*, vol. 7, no. 1, pp. 86–98, 2009.

[9] M. Bauer and I. K. Craig, "Economic assessment of advanced process control – a survey and framework," *Journal of Process Control*, vol. 18, no. 1, pp. 2–18, 2008.

[10] M. R. Naysmith and P. L. Douglas, "Review of real time optimization in the chemical process industries," *Developments in Chemical Engineering and Mineral Processing*, pp. 67–87, 1995.

[11] L. N. Petersen, N. K. Poulsen, H. H. Niemann, C. Utzen, and J. B. Jørgensen, "Economic optimization of spray dryer operation using nonlinear model predictive control," *Proceedings of the IEEE Conference on Decision and Control*, 2014.
[12] G. Prasath and J. B. Jørgensen, "Soft constraints for robust mpc of uncertain systems," *International Symposium on Advanced Control of Chemical Processes*, vol. 7, no. 1, pp. 225–230, 2009.
[13] J. B. Jørgensen, J. B. Rawlings, and J. K. Huusom, "Finite horizon mpc for systems in innovation form," *Proceedings of the IEEE Conference on Decision and Control*, pp. 1896–1903, 2011.
[14] J. K. Huusom, N. K. Poulsen, S. B. Jørgensen, and J. B. Jørgensen, "Tuning of methods for offset free mpc based on arx model representations," *Proceedings of the American Control Conference*, pp. 2255–2360, 2010.
[15] C. Hennigs, T. K. Kockel, and T. A. G. Langrish, "New measurements of the sticky behavior of skim milk powder," *Drying Technology*, vol. 19, no. 3-4, pp. 471–484, 2001.
[16] J. Smith, H. Van Ness, and M. Abbott, *Introduction to chemical engineering thermodynamics*, ser. McGraw-Hill chemical engineering series. McGraw-Hill, 2005.
[17] W. K. Lewis, "The rate of drying of solid materials," *Journal of Industrial and Engineering Chemistry*, vol. 13, pp. 427–432, 1921.
[18] F. F. G. Areed, M. S. El-Kasassy, and K. A. Mahmoud, "Design of neuro-fuzzy controller for a rotary dryer," *International Journal of Computer Applications*, vol. 37, no. 5, p. 34, 2012.
[19] C. E. C. Pérez, R. D. P. Andrade, and L. M. Roberto, "Models of sorption isotherms for food: Uses and limitations," *Vitae*, vol. 18, no. 3, pp. 325–334, 2011.
[20] C. G. J. Baker and K. A. McKenzie, "Energy consumption of industrial spray dryers," *Drying Technology*, vol. 23, no. 1-2, pp. 365–386, 2005.
[21] G. Pannocchia and J. B. Rawlings, "Disturbance models for offset-free model-predictive control," *AIChE Journal*, vol. 49, no. 2, pp. 426–437, 2003.

APPENDIX

In this section we briefly describe the details of the regulator design.

A. Regulator

The tracking problem in Sec. III-C is solved by formulating the corresponding convex quadratic problem. The tracking problem is similar to [12]–[14].

Define the vectors Z, R, U and D as

$$Z = \begin{bmatrix} z_{k+1|k} \\ z_{k+2|k} \\ \vdots \\ z_{k+N_z|k} \end{bmatrix} \quad R = \begin{bmatrix} r_{k+1} \\ r_{k+2} \\ \vdots \\ r_{k+N_z} \end{bmatrix} \quad U = \begin{bmatrix} u_{k|k} \\ u_{k+1|k} \\ \vdots \\ u_{k+N_u|k} \end{bmatrix}$$

$$D = \begin{bmatrix} d_{k|k} & d_{k+1|k} & \dots & d_{k+N_z|k} \end{bmatrix}^T$$

Then the predictions are

$$Z = \Phi_x x_{k|k-1} + \Gamma_u U_k + \Gamma_d D_k + \Omega\Sigma_x + \Sigma_z$$

Using the predictions in vector form we can write the objective function as

$$\begin{aligned} \phi &= \frac{1}{2}\sum_{j=1}^{N_z} \|z_{k+j|k} - r_{k+j|k}\|^2_{Q_z} + \frac{1}{2}\sum_{j=0}^{N_u} \|\Delta u_{k+j|k}\|^2_{S_u} \\ &= \frac{1}{2}\|Z_k - R_k\|^2_{\mathcal{Q}_z} + \frac{1}{2}\|\Lambda U - I_0 u_{k-1}\|^2_{S_u} \\ &= \frac{1}{2}U_k' H U_k + g' U_k + \rho \end{aligned}$$

with

$$\begin{aligned} H &= \Gamma_u^T \mathcal{Q}_z \Gamma_u + \Lambda^T \mathcal{S}_u \Lambda \\ g &= -\Gamma_u^T \mathcal{Q}_z (R_k - b) - \Lambda^T \mathcal{S}_u I_0 u_{k-1} \\ \rho &= \frac{1}{2}\| - b - R_k\|^2_{\mathcal{Q}_z} + \frac{1}{2}\|I_0 u_{k-1}\|^2_{S_u} \end{aligned}$$

where

$$b = -\Phi_x x_{k|k} - \Gamma_d D_k - \Omega\Sigma_x - \Sigma_z$$

The constraints are assumed constant over the prediction horizon and $u_{min} \le u_{k+j|k} \le u_{max}$ and $\Delta u_{min} \le \Delta u_{k+j|k} \le \Delta u_{max}$ may be denoted

$$U_{min} \le U_k \le U_{max} \tag{15}$$
$$b_l \le \Psi U_k \le b_u \tag{16}$$

where

$$b_l = \Delta U_{min} + I_0 u_{k-1}, \quad b_u = \Delta U_{max} + I_0 u_{k-1} \tag{17}$$

We solve the tracking problem by solution to the following convex quadratic problem

$$\min_{U_k} \quad \frac{1}{2}U_k^T H U_k + g^T U_k + \rho \tag{18a}$$
$$s.t. \quad U_{min} \le U_k \le U_{max} \tag{18b}$$
$$b_l \le \Psi U_k \le b_u \tag{18c}$$

The MPC only apply the first u_0^* of U_k^* to the process. The open-loop optimization is repeated at the next sample where it also utilize the new state estimate $\hat{x}_k$.

The regulator is tuned to penalize deviation in the exhaust air temperature and humidity by 10 and the residual moisture content the most by 500. Movements of the feed pump and inlet air temperatures are penalized, so that the feed pump is allowed to change very fast.

$$Q_z = diag(\begin{bmatrix} 10 & 10 & 500 \end{bmatrix}), \quad S_u = diag(\begin{bmatrix} 0.5 & 50 & 50 \end{bmatrix})$$

The maximum capacity of the feed pump limits the feed flow. The inlet temperatures, T_{main} and T_{sfb} must be higher than the ambient temperature, T_{amb}. Furthermore, the risk of powder explosions and the risk of scorched particles puts upper limits on the allowable inlet temperatures. Thus, we have

$$\begin{aligned} 0 \text{ kg/hr} \le & F_f \le 200 \text{ kg/hr} \\ T_{\text{amb}} \le & T_{\text{main}} \le 220^\circ\text{C} \\ T_{\text{amb}} \le & T_{\text{sfb}} \le 120^\circ\text{C} \end{aligned}$$

We do not impose input rate constraints.

Paper F

Economic Optimization of Spray Dryer Operation using Nonlinear Model Predictive Control

Published in *53rd IEEE Conference on Decision and Control (CDC 2014), pp. 6794–6800, 2014, Los Angeles.*

53rd IEEE Conference on Decision and Control
December 15-17, 2014. Los Angeles, California, USA

Economic Optimization of Spray Dryer Operation using Nonlinear Model Predictive Control

Lars Norbert Petersen[1,2], Niels Kjølstad Poulsen[1], Hans Henrik Niemann[3], Christer Utzen[2] and John Bagterp Jørgensen[1]

Abstract— **In this paper we investigate an economically optimizing Nonlinear Model Predictive Control (E-NMPC) for a spray drying process. By simulation we evaluate the economic potential of this E-NMPC compared to a conventional PID based control strategy. Spray drying is the preferred process to reduce the water content for many liquid foodstuffs and produces a free flowing powder. The main challenge in controlling the spray drying process is to meet the residual moisture specifications and avoid that the powder sticks to the chamber walls of the spray dryer. We present a model for a spray dryer that has been validated on experimental data from a pilot plant. We use this model for simulation as well as for prediction in the E-NMPC. The E-NMPC is designed with hard input constraints and soft output constraints. The open-loop optimal control problem in the E-NMPC is solved using the single-shooting method combined with a quasi-Newton Sequential Quadratic Programming (SQP) algorithm and the adjoint method for computation of gradients. The E-NMPC improves the cost of spray drying by 26.7% compared to conventional PI control in our simulations.**

I. Introduction

The production of raw milk has increased due to the liberalization of the milk quota system in the European Union [1]. A large proportion of this milk will be dried into varies types of food powders, due to the short shelf life of milk products and the increased demand for food powders in markets outside Europe. Consequently, a significant increase in production capacity is needed [1]. Application of advanced control is potentially a cost effective way to increase the production capacity. An industry study reveal that advanced control can increase the capacity with 20% [2]. Therefore, optimal control of the spray drying process is important.

The main challenge in controlling the spray dryer is to use a minimum of energy (hot air) to bring the residual moisture in the powder below the specification and to avoid that the powder sticks to the chamber walls. The dryers are generally very large and may require up to 7 MW of energy for heating of the inlet air flows. Therefore, it is not sufficient just to satisfy product specifications; the energy cost of operation must also be minimized. In addition, the operation of the spray dryer must continuously be adjusted to variations in the feed concentration and variations in the ambient air humidity.

[1] Department of Applied Mathematics and Computer Science, Technical University of Denmark, Kgs. Lyngby, Denmark {lnpe,nkpo,jbjo}@dtu.dk
[2] GEA Process Engineering A/S, Søborg, Denmark christer.utzen@gea.com
[3] Department of Electrical Engineering, Technical University of Denmark, Kgs. Lyngby, Denmark hhn@elektro.dtu.dk

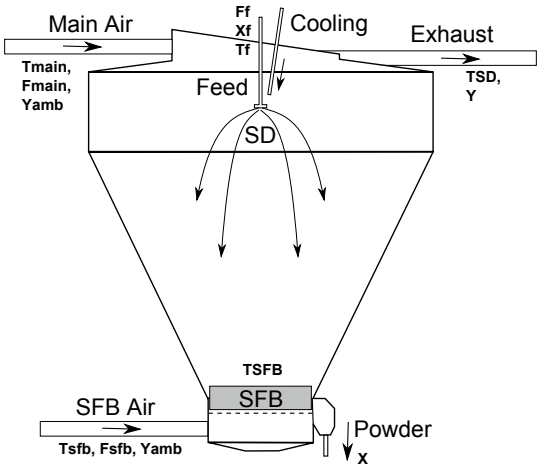

Fig. 1: Principle diagram of the spray dryer. Sprayed droplets and hot air are mixed in the top. The droplets dry into powder and ends in the SFB where the product is dried further. The powder exits the chamber from the SFB.

Conventional set-point based control of spray dryers keeps the inlet and outlet temperatures constant during operation. This approach is simple, but known to be insufficient at controlling the residual moisture. Furthermore, the powder may turn sticky inside the dryer during high ambient air humidities. Thus, operators must constantly adjust the temperature set-points to ensure proper operation. Unfortunately, these corrections are seldom made and the dryer must frequently be stopped for cleaning. This motivates E-NMPC in the presence of feed and ambient air variations. E-NMPC adjusts the manipulated variables such that the residual moisture is below its maximum, fouling of the spray dryer is avoided, and the cost of operation is minimized. E-NMPC is potentially a step towards fully automated operation of spray dryers.

A. Process Description

We consider the spray chamber (SD) and the static fluid bed (SFB) stages of a Multi-Stage Dryer (MSD^{TM}). The spray dryer is an efficient dryer and is widely used in the production of food powders. Fig. 1 illustrates the SD and SFB stages of the spray dryer. The dryer is designed such that the hot inlet air is let into the upper section of

the drying chamber around the high pressure nozzles. The nozzles disperse the liquid feed into droplets. The heat is transferred from the hot air to the droplets, which makes the water evaporate from the droplets. In that process, the air temperature and the residual moisture of the droplets decrease. The dried product then enters the SFB where it is further dried. Next, the powder is transported to a vibrating fluid bed (VFB) for gentle drying and cooled to the temperature desired for handling and storage.

Modelling of spray dryers varies in complexity from complex CFD models to simple steady-state calculations. [3] presents a first principles engineering model for control purposes and [4] proposes a model for a complete MSD™ to facilitate development of advanced controllers. A simpler model for a spray dryer is given in [5] still with a high simulation accuracy.

B. Control and Optimization

Real-time steady-state optimization (RTO) and set-point based model predictive control is a standard methodology for optimizing process operation [6]. Recent advances within process optimization focus on optimizing the higher-level objectives, such as economics, directly in the control layer. This is called economically optimizing NMPC (E-NMPC). Model Predictive Control (MPC) has for a long time been the preferred advanced control methodology in both industry and academia due to its flexibility, performance and ability to handle constraints [7], [8]. The idea of optimizing economics directly is an old idea [9], [10] that has gained significant renewed interest [8], [11]–[13]. Steady as well as non-steady optimal operation may arise as a result of E-NMPC [14].

A number of papers exist, which are related to control of spray dryers. The reported applications varies from pressure control to industrial based MPC solutions for control of the residual moisture [2]. [3] presents a PID temperature controller with feed forward for stabilization of the residual moisture. A linear tracking MPC for a spray dryer is presented in [5]. [15] provides a through review on the status and future of advanced control for spray drying. To our knowledge no papers about E-NMPC for spray dryers has been published.

C. Content

In this paper we investigate by simulation the potential of E-NMPC for a spray drying process. We present a simple model for a spray dryer and use this model to demonstrate the performance of the E-NMPC. The model has been validated from industrial data provided by GEA Process Engineering A/S. We develop an E-NMPC which optimizes an economic objective function using the nonlinear system model. The optimal control problem in the E-NMPC is solved by the single-shooting method using a quasi-Newton SQP algorithm and the adjoint method for the gradients. The controller handles both hard input constraints and soft output constraints. The NMPC algorithm is based on the computational methods described in [16], [17]. Conventional control is simulated with a PID controller to give an estimate of the performance improvement by the proposed E-NMPC.

D. Organization

The paper is organized as follows. In Section II we present the control problem and its transcription to a computationally tractable optimization problem. Section III presents the model of the spray dryer. In Section IV we present a simulation to show the benefit of optimizing the operation. Conclusions are given in Section V.

II. Optimal Control Problem

In this section, we present the continuous-time constrained optimal control problem and its transcription to a discrete optimal control problem. We solve the discrete optimal control problem using the single-shooting method.

A. Continuous-Time Constrained Optimal Control Problem

In a receding horizon manner, the manipulated variables in the E-NMPC considered in this paper are obtained by solution of the following continuous-time constrained optimal control problem in Lagrange form

$$\min_{x(\cdot),u(\cdot),s(\cdot)} \quad \phi = \int_{t_0}^{t_f} [l(x(t),u(t),d(t)) + \phi(s(t))]dt \tag{1a}$$

$$\text{s.t.} \quad x(t_0) = \hat{x}_0 \tag{1b}$$

$$\frac{d}{dt}g(x(t)) = f(x(t),u(t),d(t)), \qquad t \in \mathcal{T} \tag{1c}$$

$$u_{\min} \le u(t) \le u_{\max}, \qquad t \in \mathcal{T} \tag{1d}$$

$$c(x(t),u(t)) + s(t) \ge 0, \qquad t \in \mathcal{T} \tag{1e}$$

$$s(t) \ge 0, \qquad t \in \mathcal{T} \tag{1f}$$

in which $\mathcal{T} = [t_0, t_f[$. $x(t) \in \mathbb{R}^{n_x}$ is the state vector, $u(t) \in \mathbb{R}^{n_u}$ is the manipulated variables, $d(t) \in \mathbb{R}^{n_d}$ is the known disturbance vector, and $s(t) \in \mathbb{R}^{n_s}$ are the slack variables related to the soft output constraints. The initial state $x(t_0) = \hat{x}_0$ and the period $[t_0, t_f]$ are fixed. At each sample time t_0 is the current time and t_f is the prediction and control horizon. The current state, $\hat{x}_0$, is assigned to the initial state by (1b). The stage cost function, $l(x(t),u(t),d(t))$, represents the cost of operation, (1c) represents the process dynamics, and (1d) is hard input constraints. $\phi(s(t)) = \frac{1}{2}\|s(t)\|_{2,S_W} + \|s(t)\|_{1,s_W}$ and (1e)-(1f) represent $\ell_2 - \ell_1$ soft output constraints. The system of differential equations (1c) is different from $\dot{x}(t) = f(x(t),u(t),d(t))$. In (1c), $g(x(t))$ represent state functions that are common in modeling process systems. In particular, we note that it is not advisable from a numerical point of view to use the chain rule to convert (1c) to a system of ordinary differential equations, $\dot{x}(t) = \tilde{f}(x(t),u(t),d(t))$. Rather, the numerical solution procedure should be tailored to the system of differential equations (1c).

B. Transcription

The infinite-dimensional optimal control problem (1) is converted to a numerically tractable finite-dimensional optimal control problem by 1) parametrization of the control

vector, $u(t)$, and the disturbance vector, $d(t)$, 2) point-wise Dirac delta approximation of the soft output constraints, and 3) discretization of the dynamics (1c) and the objective integral. Using these approximations, (1) may be transcribed into the finite dimensional discrete optimal control problem

$$\min_{x,u,s} \quad \phi = \sum_{k=0}^{N-1} L_k(x_k, x_{k+1}, u_k, d_k) + \phi(s_k) \tag{2a}$$

$$\text{s.t.} \quad x_0 = \hat{x}_0 \tag{2b}$$

$$R_k(x_k, x_{k+1}, u_k, d_k) = 0, \qquad k \in \mathcal{N} \tag{2c}$$

$$u_{\min} \leq u_k \leq u_{\max}, \qquad k \in \mathcal{N} \tag{2d}$$

$$c(x_k, u_k) + s_k \geq 0, \qquad k \in \mathcal{N} \tag{2e}$$

$$s_k \geq 0, \qquad k \in \mathcal{N} \tag{2f}$$

with $\mathcal{N} = \{0, 1, \ldots, N-1\}$ and N being the discrete prediction and control horizon. The discrete stage cost, $L_k = L_k(x_k, u_k, d_k)$, and the residual function, $R_k = R_k(x_k, x_{k+1}, u_k, d_k)$, obtained from discretization by the trapezoidal method are

$$L_k = \frac{\Delta t_k}{2}(l(x_k, u_k, d_k) + l(x_{k+1}, u_k, d_k)) \tag{3}$$

$$R_k = g(x_{k+1}) - g(x_k) - \frac{\Delta t_k}{2}\left(f(x_k, u_k, d_k) + f(x_{k+1}, u_k, d_k)\right) \tag{4}$$

for $k \in \mathcal{N}$. No forecasts are available for the disturbances, so we use the same-as-now forecasts, i.e. $d_k = d(t_0)$.

C. Single-Shooting Optimization

The discrete-time finite dimensional optimal control problem (2) may be solved using single-shooting (control vector parametrization) [18], multiple shooting [19], [20], or the simultaneous method [21], [22]. In all these methods, some sequential quadratic programming (SQP) algorithm is typically used for the optimization. Gradient computation is straightforward in the simultaneous method, while either forward sensitivity computation [23] or the adjoint method [16] is used by the single-shooting and the multiple-shooting methods. Furthermore, real-time iteration may be used to reduce the computational delay by the optimal control computation at each sample time [22], [24].

In this paper, the optimal control problem (2) is solved by the single-shooting method using a quasi-Newton SQP optimization algorithm (`fmincon` in Matlab's optimization toolbox) and the adjoint method for gradient computation [17].

III. SPRAY DRYER MODEL

In this section the spray dryer model is presented. It is derived from first engineering principles. The unknown parameters are estimated from data by minimizing the sum of squared simulation errors. The model describes drying of maltodextrin DE-18, which is chosen because milk is difficult to handle over longer periods due to natural deterioration. Maltodextrin DE-18 has almost the same stickiness and properties of drying as milk [25]. The model is also used in [5] for simulation and control of a spray dryer.

A. Conservation Equations

The model used for simulation as well as prediction in the E-NMPC is a lumped model with four states. The four states are the spray dryer temperature, T_{SD}, the static fluid bed temperature, T_{SFB}, the humidity, Y, in the air of the spray dryer, and the moisture, X, in the powder. The evolution of the temperatures, T_{SD} and T_{SFB}, is governed by energy balances, while mass balances determine the evolution of the air and powder moisture, Y and X. The lumped energy and mass balances describing the evolution of the states are

$$C_a \frac{dT_{SD}}{dt} = -\lambda R_w + H_{a_{in}} - H_{a_{out}} - Q_{exc} - Q_{la} \tag{5a}$$

$$C_b \frac{dT_{SFB}}{dt} = H_{b_{in}} - H_{b_{out}} + Q_{exc} - Q_{lb} \tag{5b}$$

$$m_{da} \frac{dY}{dt} = (F_{main} + F_{sfb})(Y_{amb} - Y) + F_{add}(Y_{add} - Y) + R_w \tag{5c}$$

$$m_s \frac{dX}{dt} = F_s(X_f - X) - R_w \tag{5d}$$

where

$$H_{a_{in}} = F_{main}(c_{da} + c_v Y_{amb})(T_{main} - T_0) + F_{add}(c_{da} + c_v Y_{add})(T_{add} - T_0) \tag{6a}$$

$$H_{a_{out}} = (F_{main} + F_{sfb} + F_{add}) \cdot (c_{da} + c_v Y)(T_{SD} - T_0) \tag{6b}$$

$$H_{b_{in}} = F_{sfb}(c_{da} + c_v Y_{amb})(T_{sfb} - T_0) \tag{6c}$$

$$H_{b_{out}} = F_{sfb}(c_{da} + c_v Y_{amb})(T_{SFB} - T_0) \tag{6d}$$

$$Q_{exc} = k_1(T_{SD} - T_{SFB}) + k_2 X_f + k_3 T_f - k_4 \tag{6e}$$

$$Q_{la} = k_5(T_{SD} - T_{amb}) \tag{6f}$$

$$Q_{lb} = k_6(T_{SFB} - T_{amb}) \tag{6g}$$

$$F_s = F_f X_f / (X_f + 1) \tag{6h}$$

In the SD as well as the SFB, it is assumed that the air and the product are in equilibrium i.e. that the temperature of the air, T_{SD} and T_{SFB}, and the temperature of the product are identical. $H_{a_{in}}$, $H_{a_{out}}$, $H_{b_{in}}$ and $H_{b_{out}}$ are the enthalpies of humid air in and out of the SD and the SFB stage, respectively. C_a and C_b are the heat capacity of the hold-up of air and powder. F_{main} and F_{sfb} are the dry base inlet air flows. The parameters Y_{add}, F_{add} and T_{add} are used to correct for air leakages and un-modeled inlet air flows such as nozzle cooling air. Q_{sd} and Q_{sfb} are heat losses to the surroundings. λR_w is the heat of evaporation at T_0. We assume that the evaporation takes place in the SD stage only. The heat of evaporation related to the SFB is modeled through Q_{exc}, that describes the heat exchange between the SD and the SFB stages and corrects for this assumption. m_s is the dry mass of powder and X is the dry base moisture content of the powder. X_f and T_f is the dry base feed concentration and feed temperature. m_{da} is the mass of dry air and Y is the absolute humidity in the dryer. The reference temperature is $T_0 = 25^\circ C$.

B. Drying Rate

The kinetics of the drying is important for the behavior of the model. The thin layer equation describes the product

drying rate, R_w, well [26]

$$R_w = D_{diff}(X - X_{eq})m_s \tag{7}$$

D_{diff} is an empirical constant called the drying constant or diffusivity. It must be experimentally determined [27]. In the present study it is constant, but it may depend on both temperature and powder moisture.

The equilibrium moisture, X_{eq}, of the powder is a product dependent function that describes the moisture content at which water cannot be evaporated any longer. The Guggenheim-Anderson-de Boer (GAB) relation is used to describe the equilibrium moisture [28]. The GAB relation is fitted to laboratory data obtained specifically for maltodextrin to get

$$X_{eq} = \frac{C \cdot K \cdot X_m \cdot RH}{(1 - K \cdot RH)(1 - K \cdot RH + C \cdot K \cdot RH)} \tag{8}$$

in which $X_m = 0.030723$, $C = 2.6535 \cdot 10^{-7} \exp\left(\frac{6292.1}{T}\right)$ and $K = 0.057882 \exp\left(\frac{945.16}{T}\right)$. X_m is the monolayer moisture content. C and K are constants related to monolayer and multi-layer properties. The relative humidity RH is calculated from T_{SFB} and Y. In the computation of X_{eq} for the product drying rate, $T = T_{SFB}$ is used.

C. Stickiness

Stickiness of the produced particles is an important limitation to the achievable performance of the spray dryer. Sticky particles form depositions on the walls of the spray dryer. Stickiness depends on product temperature and moisture content. We use a mass-proportion-mixing rule to describe the glass transition temperature [25], [29]

$$T_g = \frac{T_{gp} + kZT_{gw}}{1 + kZ} \tag{9}$$

in which $T_{gp} = 144.8°C$ (maltodextrin) and $T_{gw} = -137°C$ (water). The value $k = 6.296$ is estimated from adsorption isotherm data. The obtained glass transition temperatures, T_g^{SD} and T_g^{SFB}, are the upper limiting temperatures of which deposits form on the chamber walls of the spray dryer. The moisture content of the powder is

$$Z = \begin{cases} 2.2 \cdot (A_p + B_p\ T_{SD}) exp(C_p\ RH) & \text{for SD} \\ X & \text{for SFB} \end{cases} \tag{10}$$

in which $A_p = 0.0877$, $B_p = -0.00019751$ and $C_p = 2.0498$. The moisture content of the powder in the SD stage is difficult to estimate. Common practice is to use the equilibrium moisture, X_{eq}, as an approximation. We use an exponential function instead of the above GAB model for this purpose, as it renders the transient residual moisture content at low relative humidity better than (8).

TABLE I: Estimated parameters for the model (5)-(10)

Symbol	Value	Unit	Symbol	Value	Unit
C_a	68.266	KJ/K	F_{add}	256.46/3600	kg/s
C_b	141.36	KJ/K	Y_{add}	$8.1799 \cdot 10^{-3}$	kg/kg
k_1	0.29268	KW/K	T_{add}	100.03+273.15	K
k_2	1.6207	KW	k_3	0.073198	KW
k_4	31.111	KW	k_5	0.26981	KW/K
k_6	-0.023367	KW/K	D_{diff}	0.091922	

D. Model and Parameters

The model (5)-(10) of the dryer is a deterministic system of differential equations in the form (1c) in which

$$x = \begin{bmatrix} T_{SD} \\ T_{SFB} \\ Y \\ X \end{bmatrix} \quad u = \begin{bmatrix} F_f \\ T_{main} \\ T_{sfb} \end{bmatrix} \quad d = \begin{bmatrix} F_{main} \\ F_{sfb} \\ X_f \\ T_f \\ T_{amb} \\ Y_{amb} \end{bmatrix} \tag{11}$$

x is the state vector, u is the manipulated input vector, and d is the disturbance vector. The states as well as the disturbances are measurable in industrial practice. Therefore, we do not discuss state estimation in this paper.

The parameters in the model (5)-(10) are estimated using data for a medium-scale spray dryer from GEA Process Engineering A/S. Table I provides the estimated parameters in the model. $m_{da} = 10$ kg and $m_s = 15$ kg are fixed parameters and determined from physical considerations. Generally the model fits the data well on both estimation and validation data.

E. Constraints

The maximum capacity of the feed pump limits the feed flow such that 0 kg/hr $\leq F_f \leq 150$ kg/hr. The inlet temperatures, T_{main} and T_{sfb} must be higher than the ambient temperature, T_{amb}, as the dryer can only heat but not cool. Furthermore, the risk of powder explosions and the risk of scorched particles puts upper limits on the allowable inlet temperatures. Consequently, $T_{\text{amb}} \leq T_{\text{main}} \leq 180°\text{C}$ and $T_{\text{amb}} \leq T_{\text{sfb}} \leq 120°\text{C}$. These constraints are hard input constraints of the form (1d).

To avoid depositions of sticky particles on the spray dryer surfaces, the temperatures T_{SD} and T_{SFB} must be below the glass transition temperatures in the SD stage, $T_{SD} \leq T_g^{SD}$ and the SFB stage, $T_{SFB} \leq T_g^{SFB}$, respectively. The glass transition temperature are determined by (9). Furthermore, the powder moisture must be below a maximum limit, $X \leq X_{\max} = 4.5\%$, that is 4.5% for the case studies in this paper. These constraints are treated as soft output constraints in the form (2e). The soft ℓ_1 penalty is $s_W = 10^5 \cdot [0.1; 0.1; 1.0]$ and the soft ℓ_2 penalty is $S_W = \text{diag}(s_W)$.

F. Objective Function - Profit and Regularization

The profit from operating the spray dryer is the value of the product minus the raw material and energy costs. Since

we consider a minimization problem, maximizing the profit of operation corresponds to the following stage cost

$$l(x(t), u(t), d(t)) = \\ -[p_p F_s(1+X) - p_f F_s(1+X_f) - p_H \Delta H] \quad (12)$$

in which p_p is the unit value of the product, p_f is the unit cost of feed material, p_H is the unit energy cost, and ΔH is the total energy supplied to the dryer given by

$$\Delta H = F_{main}(h_{a_{in}} - h_{amb}) + F_{sfb}(h_{b_{in}} - h_{amb}) \quad (13)$$

in which $h_{amb} = (c_{da} + c_v Y_{amb})(T_{amb} - T_0)$. The price of the produced powder is, $p_p = 4.47$ \$/kg, the price of feed material is, $p_f = 0.447$ \$/kg, and the price of energy is, $p_H = 3.4873 \cdot 10^{-5}$ \$/KJ. The prices are selected to reflect industrial reality meaning that the price of natural gas is almost negligible compared to the price of the powder, i.e. $p_p \gg p_H$. In such scenarios, production maximization is the primary concern while efficient utilization of energy is a secondary consideration.

The energy efficiency of operation and the product flow rate are also key performance indicators (KPIs) for evaluation of the performance of a spray dryer. The energy efficiency is

$$\eta = \frac{\lambda F_s(X_f - X)}{\Delta H} \quad (14)$$

Here $\lambda F_s(X_f - X)$ is the energy used to evaporate water and ΔH is the total energy supplied. The flow rate of produced powder is

$$F_p = F_s(1+X) \quad (15)$$

To obtain smooth solutions the objective function (2a) is extended with a regularization term that penalizes changes in the manipulated variables

$$\phi_{\Delta u} = \sum_{k=0}^{N-1} ||u_k - u_{k-1}|\,|^2_{Q_s} \quad (16)$$

We use $Q_s = \Delta t_k \cdot \text{diag}([0.1; 1; 0.5])$.

The sample time is chosen as $\Delta t_k = 15$ s and we use a control and prediction horizon of $t_f = 10$ min i.e. $N = 40$.

IV. Results

We illustrate the performance of the E-NMPC by a closed-loop simulation and compare it to the conventional PID control method.

A. Simulation

Three step disturbances occur in the simulated scenario. As illustrated in Fig. 2, the feed concentration and the ambient air humidity experience step changes. The step sizes are identified from maximum month-to-month variations in historical data from an industrial dryer.

Fig. 3 shows how E-NMPC operates the spray dryer for this disturbance scenario. Fig. 3a shows the outputs and Fig. 3b shows the manipulated variables. Fig. 3c illustrates the energy efficiency, the production rate and the operational profit rate.

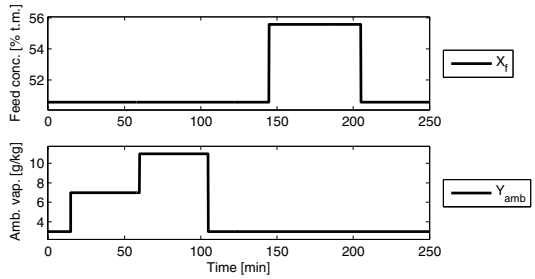

Fig. 2: Disturbance scenario for the case studies.

The E-NMPC controls the dryer such that the profit of operation is maximized. Profit maximization is obtained by maximizing the feed rate, F_f, while minimizing the supply of energy from the main and the SFB inlet air temperatures, T_{main} and T_{SFB}, within the given constraints. The optimum is reached when T_{SD} reaches the glass transition temperature, i.e. the stickiness constraint of the powder, and when X, the powder moisture content, reaches the upper residual moisture specification. During operation the controller always ride these constraints and a standard tracking MPC solution with offline computed set-points may therefore provide similar performance results for this process.

The profit of operation in Fig. 3c is mainly dependent on the production rate and feed concentration. Thus, the energy usage is a secondary objective. Fortunately, the energy efficiency increases with production rate and increasing residual moisture in the powder. The energy efficiency is therefore also maximized when profit is maximized in this case.

An increase in ambient air humidity, Y_{amb}, decreases the evaporation rate, R_w, of the dryer and the powder becomes more moist and sticky. The E-NMPC compensates by decreasing the feed rate, F_f, and the inlet air temperatures, T_{main} and T_{SFB}. Thus, the production capacity is decreased for increasing ambient air humidity. The step increase in feed (water) concentration, X_f, increases the amount of water that has to be evaporated from the feed. The E-NMPC compensates for this by decreasing the feed rate accordingly. Consequently, an increase in feed water concentration also decreases the production capacity of the dryer.

The PID controller maintains a constant exhaust air temperature, T_{SD}, by manipulating the feed rate, F_f. The set-point for the controller, $T^{sp}_{SD} = 75.76°C$, and the two inlet air temperatures are fixed so that profit of operation is maximized without violating the constraints at any time. The model of the spray dryer and the constraints are non-linear. Therefore, it is not a trivial task to determine these optimal set-points. The PID controller does not perform any correcting action to changes in the ambient air humidity. This turns out to be the factor that limits the PID control performance the most. A disturbance in the feed concentration is compensated by decreasing the feed rate and the resulting economic performance is close the performance achieved by the E-NMPC.

On average for the given disturbance scenario the E-NMPC increases the profit of operation by 26.7% compared to the PID controller.

V. CONCLUSIONS

This paper presents an economically optimal control solution for a spray dryer. The controller is based on a nonlinear model predictive controller with an economic objective function (E-NMPC). The E-NMPC provides a control solution that constantly brings the dryer to the most cost optimal state of operation within the given process constraints. The residual moisture specification is controlled within specifications and fouling in the dryer is avoided. A case study is used to simulate and evaluate the performance of the E-NMPC compared to a conventional PID based control strategy. In the simulation the profit of operation is increased by 26.7%. We also find that it is not intuitive to select the most profitable set-points for the conventional PID control. Optimal set-points are therefore hardly never obtained by operators in industrial practice. Accordingly, the economic benefit of E-NMPC may be even larger for industrial spray dryers. Furthermore, a common problem in operation of industrial spray dryers is production stops due to deposition of sticky particles on spray dryer surfaces. Such situations are efficiently avoided by the ability of E-NMPC to include stickiness constraints and compute control profiles that are continuously adapted to variations in the feed and the ambient conditions.

REFERENCES

[1] T. Donnellan, T. Hennessy, M. Fenelon, and D. O'Callaghan, "The potential for scale economies in milk powder processing: an irish case study," *International Journal of Dairy Technology*, vol. 67, no. 1, pp. 129–134, 2014.

[2] Vaisala, "+20% increase in production capacity with zero increase in energy consumption," 2014. [Online]. Available: http://www.vaisala.com/Vaisala\%20Documents/Success\%20Stories/CEN-TIA-G-Valio-Customer-Story-B211288EN-A.pdf

[3] J. Pérez-Correa and F. Fariass, "Modelling and control of a spray dryer : A simulation study," *Food Control*, vol. 6, no. 4, pp. 219–227, 1995.

[4] L. N. Petersen, N. K. Poulsen, H. H. Niemann, C. Utzen, and J. B. Jørgensen, "A Grey-Box Model for Spray Drying Plants," *10th IFAC International Symposium on Dynamics and Control of Process Systems*, pp. 559–564, 2013.

[5] ——, "Application of constrained linear mpc to a spray dryer," *Proceedings of the IEEE Multi-Conference on Systems and Control*, 2014.

[6] M. R. Naysmith and P. L. Douglas, "Review of real time optimization in the chemical process industries," *Developments in Chemical Engineering and Mineral Processing*, pp. 67–87, 1995.

[7] M. L. Darby, M. Harmse, and M. Nikolaou, "MPC: Current practice and challenges," *7th IFAC International Symposium on Advanced Control of Chemical Processes*, vol. 7, no. 1, pp. 86–98, 2009.

[8] M. Bauer and I. K. Craig, "Economic assessment of advanced process control – a survey and framework," *Journal of Process Control*, vol. 18, no. 1, pp. 2–18, 2008.

[9] P. S. R. K. Chintapalli and J. M. Douglas, "The use of economic performance measures to synthesize optimal control systems," *Industrial & Engineering Chemistry Fundamentals*, vol. 14, no. 1, pp. 1–10, 1975.

[10] T. E. Marlin and A. N. Hrymak, "Real-time operations optimization of continuous processes," *Chemical Process Control-V Conference*, pp. 156–164, 1996.

[11] J. B. Rawlings, C. N. Bates, and D. Angeli, "Fundamentals of economic model predictive control," *Proceedings of the IEEE Conference on Decision and Control*, pp. 3851–3861, 2012.

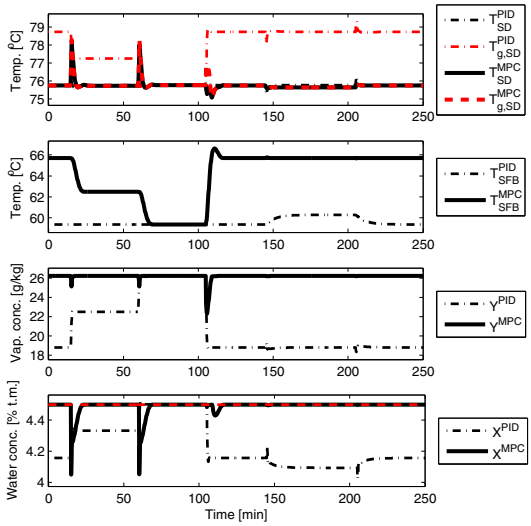

(a) System outputs.

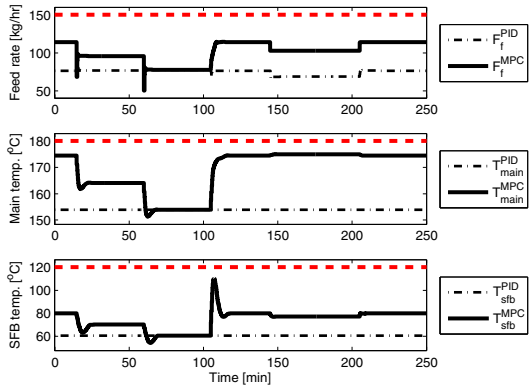

(b) Manipulated variables.

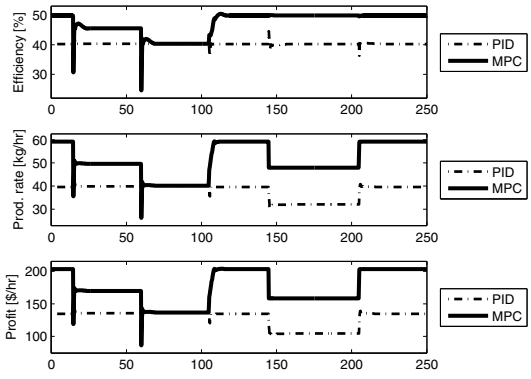

(c) The operational profit rate.

Fig. 3: E-NMPC seeking to maximize profit for the disturbance scenario given in Fig. 2. Red lines indicate constraints.

[12] R. Amrit, "Optimizing process economics in model predictive control," Ph.D. dissertation, University of Wisconsin–Madison, 2011.
[13] T. G. Hovgaard, L. F. Larsen, and J. B. Jørgensen, "Flexible and cost efficient power consumption using economic mpc," *Proceedings of the 50th IEEE Conference on Decision and Control and European Control Conference*, pp. 848–854, 2011.
[14] D. Angeli, R. Amrit, and J. B. Rawlings, "Receding horizon cost optimization for overly constrained nonlinear plants," *Proceedings of the IEEE Conference on Decision and Control*, pp. 7972–7977, 2009.
[15] D. O. Callaghan and P. Cunningham, "Modern process control techniques in the production of dried milk products – a review," *Lait*, vol. 85, pp. 335–342, 2005.
[16] J. B. Jørgensen, "Adjoint sensitivity results for predictive control, state- and parameter-estimation with nonlinear models," *European Control Conference 2007*, pp. 3649–3656, 2007.
[17] L. N. Petersen and J. B. Jørgensen, "Real-time economic optimization for a fermentation process using model predictive control," *13th European Control Conference*, 2014.
[18] M. Schlegel, K. Stockmann, T. Binder, and W. Marquardt, "Dynamic optimization using adaptive control vector parameterization," *Computers & Chemical Engineering*, vol. 29, no. 8, pp. 1731–1751, 2005.
[19] H. G. Bock and K. J. Plitt, "A multiple shooting algorithm for direct solution of optimal control problems," *9th IFAC World Congress Budapest. Pergamon Press*, pp. 242–247, 1984.
[20] A. Capolei and J. B. Jørgensen, "Solution of constrained optimal control problems using multiple shooting and esdirk methods," *Proceedings of the 2012 American Control Conference*, pp. 295–300, 2012.
[21] L. T. Biegler, "Solution of dynamic optimization problems by successive quadratic programming and orthogonal collocation," *Computers & Chemical Engineering*, vol. 8, no. 3, pp. 243–248, 1984.
[22] ——, "A survey on sensitivity-based nonlinear model predictive control," *10th IFAC International Symposium on Dynamics and Control of Process Systems*, pp. 499–510, 2013.
[23] M. R. Kristensen, J. B. Jørgensen, P. G. Thomsen, and S. B. Jørgensen, "An esdirk method with sensitivity analysis capabilities," *Computers & Chemical Engineering*, vol. 28, no. 12, pp. 2695–2707, 2004.
[24] M. Diehl, H. G. Bock, and J. P. Schlöder, "A real-time iteration scheme for nonlinear optimization in optimal feedback control," *SIAM Journal on Control and Optimization*, vol. 43, no. 5, pp. 1714–1736, 2005.
[25] C. Hennigs, T. K. Kockel, and T. A. G. Langrish, "New measurements of the sticky behavior of skim milk powder," *Drying Technology*, vol. 19, no. 3-4, pp. 471–484, 2001.
[26] W. K. Lewis, "The rate of drying of solid materials," *Journal of Industrial and Engineering Chemistry*, vol. 13, pp. 427–432, 1921.
[27] F. F. G. Areed, M. S. El-Kasassy, and K. A. Mahmoud, "Design of neuro-fuzzy controller for a rotary dryer," *International Journal of Computer Applications*, vol. 37, no. 5, pp. 34–41, 2012.
[28] C. E. C. Pérez, R. D. P. Andrade, and L. M. Roberto, "Models of sorption isotherms for food: Uses and limitations," *Vitae*, vol. 18, no. 3, pp. 325–334, 2011.
[29] S. Hogan, M. Famelart, D. O'Callaghan, and P. Schuck, "A novel technique for determining glass-rubber transition in dairy powders," *Journal of Food Engineering*, vol. 99, pp. 76–82, 2010.

Paper G

Economic Optimization of Spray Dryer Operation using Nonlinear Model Predictive Control with State Estimation

Published in *9th International Symposium on Advanced Control of Chemical Processes (ADCHEM 2015), pp. 507–513, 2015, Whistler.*

Available online at www.sciencedirect.com

ScienceDirect

IFAC Papers Online CONFERENCE PAPER ARCHIVE

IFAC-PapersOnLine 48-8 (2015) 507–513

Economic Optimization of Spray Dryer Operation using Nonlinear Model Predictive Control with State Estimation

Lars Norbert Petersen * **John Bagterp Jørgensen** ** **James B. Rawlings** ***

* *GEA Process Engineering A/S, Søborg, Denmark, (e-mail: lars.n.petersen@gea.com)*
** *Department of Applied Mathematics and Computer Science, Technical University of Denmark, Kgs. Lyngby, Denmark, (e-mail: jbjo@dtu.dk)*
*** *Department of Chemical and Biological Engineering, University of Wisconsin-Madison, Madison, USA, (e-mail: rawlings@engr.wisc.edu)*

Abstract:
In this paper, we develop an economically optimizing Nonlinear Model Predictive Controller (E-NMPC) for a complete spray drying plant with multiple stages. In the E-NMPC the initial state is estimated by an extended Kalman Filter (EKF) with noise covariances estimated by an autocovariance least squares method (ALS). We present a model for the spray drying plant and use this model for simulation as well as for prediction in the E-NMPC. The open-loop optimal control problem in the E-NMPC is solved using the single-shooting method combined with a quasi-Newton Sequential Quadratic Programming (SQP) algorithm and the adjoint method for computation of gradients. We evaluate the economic performance when unmeasured disturbances are present. By simulation, we demonstrate that the E-NMPC improves the profit of spray drying by 17% compared to conventional PI control.

Keywords: Nonlinear Model Predictive Control, Optimization, Grey-box model, Spray Drying

1. INTRODUCTION

Spray drying is a processing technique for drying of liquids or slurries into a free flowing powder. Spray drying is a key process in the dairy industry (Mujumdar, 2006), where dairy products are dried into powders to increase the shelf life as well as to reduce cost of transportation over long distances. The quality of dairy powder is, among other factors, characterized by the residual moisture content that must be within the specification. Spray drying is by far the most energy-intensive unit operation in the dairy industry (IDF, 2005). Therefore, maximizing the efficiency of the spray drying process and maintaining the correct residual moisture level are of utmost importance.

The main challenge in controlling the spray dryer is to use a minimum of energy (hot air) to bring the residual moisture in the powder below the specification and to avoid that the powder sticks to the walls of the chamber. This is a challenge, as the operation of the spray dryer must continuously be adjusted to variations in the feed concentration and variations in the ambient air humidity. Application of advanced control is potentially a cost effective way to reduce the energy consumption as well as to increase the production capacity (Petersen et al., 2014b).

Conventional set-point based control of spray dryers keeps the inlet and outlet temperatures constant during operation. This approach is simple, but known to be insufficient for controlling the residual moisture. Furthermore, the powder may turn sticky inside the dryer during high ambient air humidities. This motivates E-NMPC in the presence of feed and ambient air variations. E-NMPC adjusts the manipulated variables in such a way that the residual moisture is below its maximum, fouling of the spray dryer is avoided, and the cost of operation is minimized.

1.1 Process Description

A Multi-Stage Dryer (MSD^{TM}) consists of a spray chamber (SD), a static fluid bed (SFB), and two vibrating fluid bed (VFB) stages. This type of dryer is the most widely used dryer in the production of food powders (Mujumdar and Huang, 2007). Fig. 1 illustrates the stages of the spray dryer as well as the hot air and the powder in- and outlets. The dryer is designed such that the hot inlet air is fed into the upper section of the drying chamber around the high pressure nozzles. The nozzles disperse the liquid feed into droplets. The heat is transferred from the hot air to the droplets, which makes the water evaporate from the droplets. In that process, the air temperature and the residual moisture of the droplets decrease. The dried product then enters the SFB where it is further dried by hot air from below. Next, the powder is transported to the VFBh and VFBc stages for gentle drying and cooled to the temperature desired for handling and storage.

2405-8963
Peer review under responsibility of International Federation of Automatic Control.
10.1016/j.ifacol.2015.09.018

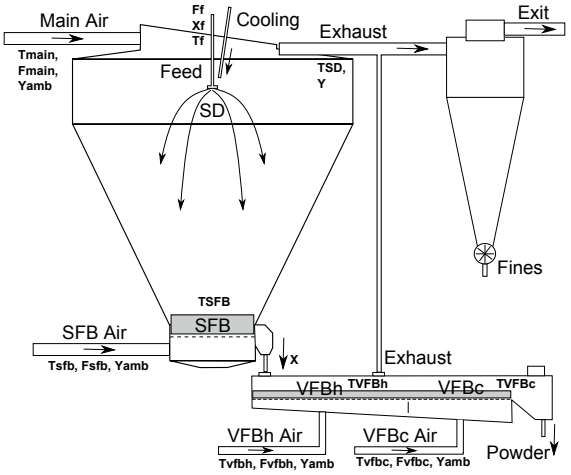

Fig. 1. Diagram of the spray dryer. Sprayed droplets and hot air are mixed in the top. The droplets dry into powder and are dried further in the SFB and VFBh stages and cooled in the VFBc stage.

1.2 Modeling

Dynamic models of spray drying has recently been reported. Petersen et al. (2013) propose a model for a complete spray dryer and Petersen et al. (2014a) presents a model for the SD and SFB stages of the spray dryer. The latter show good simulation accuracy. The model derived in this paper will therefore be based on the model in Petersen et al. (2014a) and extended to also describe the VFB stages.

1.3 Control and State Estimation

The combination of real-time steady-state optimization (RTO) and set-point based model predictive control is a standard methodology for optimizing process operation (Naysmith and Douglas, 1995). Recent advances within process optimization focus on optimizing the higher-level objectives, such as economics, directly in the control layer. This is called economically optimizing Model Predictive Control (E-MPC). For a long time, MPC has been the preferred advanced control methodology in the process industries. Recently, the idea of optimizing economics directly has gained significant renewed interest (Rawlings et al., 2012; Bauer and Craig, 2008). Papers related to control of spray dryers seldom consider an economic objective. Petersen et al. (2014a) discuss a linear tracking MPC, while Petersen et al. (2014b) discuss an E-NMPC for the SD and SFB stages of the spray dryer. Callaghan and Cunningham (2005) provides a thorough review on the status and future of advanced control for spray drying.

The model of the spray dryer is used for simulation as well as for prediction and state estimation in the NMPC. We use the well known extended continuous-discrete Kalman filter (EKF) for state estimation. The performance of the filter is highly dependent on good estimation of the noise covariances, which we will estimate using the Autocovariance Least-Squares (ALS) method described in Rajamani and Rawlings (2009).

1.4 Content & Organization

In this paper, we demonstrate that the profit of operation for a spray drying process can be improved significantly by application of E-NMPC based on an economically optimizing controller and an EKF for state estimation. The noise covariances in the EKF are estimated by the ALS method.

The paper is organized as follows. In Section 2, the model of the spray dryer is presented. Section 3 presents the estimation problem and the ALS method. Section 4 presents the control problem and its transcription to a computationally tractable optimization problem. In Section 5 we present a simulation to show the benefit of optimizing the operation. Conclusions are given in Section 6.

2. SPRAY DRYER MODEL

In this section, the complete spray dryer model is presented. It is derived from first engineering principles and describes drying of maltodextrin DE-18. We use Maltodextrin DE-18 as a substitute to milk, because milk is difficult to handle over longer periods due to natural deterioration.

2.1 Spray Dryer and Static Fluid Bed Model

The evolution of the temperatures, T_{SD} and T_{SFB}, is governed by energy balances, while mass balances determine the evolution of the air and powder moisture, Y_{ab} and X_{ab}. The lumped energy and mass balances describing the evolution of the states are

$$\begin{aligned} C_a \frac{dT_{\mathrm{SD}}}{dt} = &-\lambda R_{aw} + F_{\mathrm{main}} h_{a_{\mathrm{in}}} + F_{\mathrm{sfb}} h_{b_{\mathrm{out}}} - \\ &(F_{\mathrm{main}} + F_{\mathrm{sfb}} + F_{\mathrm{add}}) h_{a_{\mathrm{out}}} + \\ &F_{\mathrm{add}} h_{a_{\mathrm{add}}} + F_s (h_f^p - h_a^p) - Q_{ab} - Q_a \end{aligned} \tag{1a}$$

$$\begin{aligned} C_b \frac{dT_{\mathrm{SFB}}}{dt} = &F_{\mathrm{sfb}} (h_{b_{\mathrm{in}}}^a - h_{b_{\mathrm{out}}}^a) + F_s (h_a^p - h_b^p) + \\ &Q_{ab} - Q_{bc} - Q_b \end{aligned} \tag{1b}$$

$$\begin{aligned} m_a \frac{dY_{ab}}{dt} = &(F_{\mathrm{main}} + F_{\mathrm{sfb}})(Y_{\mathrm{amb}} - Y_{ab}) + \\ &F_{\mathrm{add}} (Y_{\mathrm{add}} - Y_{ab}) + R_{aw} \end{aligned} \tag{1c}$$

$$m_b \frac{dX_{ab}}{dt} = F_s (X_f - X_{ab}) - R_{aw} \tag{1d}$$

where

$$\begin{aligned} h_{a_{\mathrm{in}}}^a &= (c_{da} + c_v Y_{\mathrm{amb}}) T_{\mathrm{main}}, \quad h_{a_{\mathrm{out}}}^a = (c_{da} + c_v Y_{ab}) T_{\mathrm{SD}} \\ h_{b_{\mathrm{in}}}^a &= (c_{da} + c_v Y_{\mathrm{amb}}) T_{\mathrm{sfb}}, \quad h_{b_{\mathrm{out}}}^a = (c_{da} + c_v Y_{\mathrm{amb}}) T_{\mathrm{SFB}} \\ h_{a_{\mathrm{add}}}^a &= (c_{da} + c_v Y_{\mathrm{add}}) T_{\mathrm{add}}, \quad h_f^p = (c_s + c_w X_f) T_f \\ h_a^p &= (c_s + c_w X_{ab}) T_{\mathrm{SD}}, \quad h_b^p = (c_s + c_w X_{ab}) T_{\mathrm{SFB}} \\ Q_{ab} &= k_1 (T_{\mathrm{SD}} - T_{\mathrm{SFB}}) + k_2 X_f + k_3 T_f - k_4 \\ Q_a &= k_5 (T_{\mathrm{SD}} - T_{\mathrm{amb}}), \quad Q_b = k_6 (T_{\mathrm{SFB}} - T_{\mathrm{amb}}) \end{aligned}$$

It is assumed that the air and the product are in equilibrium i.e. that the temperature of the air, T_{SD} and T_{SFB}, and the temperature of the product are identical. $h_{\{\cdot\}}^a$ and $h_{\{\cdot\}}^p$ are the specific enthalpies of the humid air and powder inlets and outlets of the SD and the SFB stages. C_a and C_b are the heat capacities of the hold-up of air and powder. The heat capacities are given at the reference temperature, $T_0 = 25°\mathrm{C}$. λR_{aw} is the heat of evaporation and Q_{ab} describes the heat exchange between the SD and

the SFB stages. F_{main} and F_{sfb} are the dry base inlet air flows. The parameters Y_{add}, F_{add} and T_{add} are used to compensate for air leakages and un-modeled inlet air flows such as nozzle cooling air. Q_a and Q_b are heat losses to the surroundings. $F_s = F_f X_f/(1 - X_f)$ is the flow of feed solids. X_f and T_f are the dry base feed concentration and feed temperature. m_a is the mass of dry air and m_b is the mass of dry powder.

We assume that the evaporation takes place in the SD stage only with the drying rate determined from conditions in the SFB. The product drying rate is governed by the thin layer equation, describing evaporation due to diffusion (Lewis, 1921)

$$R_{aw} = k_7 \frac{k_8}{k_8 + F_s} \left(\frac{T_f}{T_0}\right)^{k_9} (X_{ab} - X_{eq}(T_{\text{SFB}}, Y_{ab}))m_b$$

The equilibrium moisture content, $X_{eq}(T, Y)$, is a nonlinear product dependent function that describes the moisture content at which the water is bounded within the powder particles.

2.2 Vibrating Fluid Bed Model

The evolution of the temperatures, T_{VFBh} and T_{VFBc}, is governed by energy balances, while mass balances govern the evolution of the air humidity, Y_{cd}, and the moisture content, X_{cd}, in the powder.

$$C_{cd}\frac{dT_{\text{VFBh}}}{dt} = -\lambda R_{cw} + F_{\text{vfbh}}(h^a_{c_{\text{in}}} - h^a_{c_{\text{out}}}) + F_s(h^p_b - h^p_c) + Q_{bc} - Q_c \tag{2a}$$

$$C_{cd}\frac{dT_{\text{VFBc}}}{dt} = F_{\text{vfbc}}(h^a_{d_{\text{in}}} - h^a_{d_{\text{out}}}) + F_s(h^p_c - h^p_d) - Q_d \tag{2b}$$

$$m_c\frac{dY_{cd}}{dt} = (F_{\text{vfbh}} + F_{\text{vfbc}})(Y_{\text{amb}} - Y_{\text{cd}}) + R_{cw} \tag{2c}$$

$$m_d\frac{dX_{cd}}{dt} = F_s(X_{ab} - X_{cd}) - R_{cw} \tag{2d}$$

where

$$h^a_{c_{\text{in}}} = (c_{da} + c_v Y_{\text{amb}})T_{\text{vfbh}}, \quad h^a_{c_{\text{out}}} = (c_{da} + c_v Y_{cd})T_{\text{VFBh}}$$
$$h^a_{d_{\text{in}}} = (c_{da} + c_v Y_{\text{amb}})T_{\text{vfbc}}, \quad h^a_{d_{\text{out}}} = (c_{da} + c_v Y_{cd})T_{\text{VFBc}}$$
$$h^p_c = (c_s + c_w X_{cd})T_{\text{VFBh}}, \quad h^p_d = (c_s + c_w X_{cd})T_{\text{VFBc}}$$
$$Q_c = k_{11}(T_{\text{VFBh}} - T_{\text{amb}}), \quad Q_d = k_{12}(T_{\text{VFBc}} - T_{\text{amb}})$$
$$Q_{bc} = k_{10}(T_{\text{SFB}} - T_{\text{VFBh}})$$

$h^a_{\{\cdot\}}$ and $h^p_{\{\cdot\}}$ are the specific enthalpies of humid air and powder in and out of the VFBh and the VFBc stages. C_{cd} is the heat capacity of the hold-up of air and powder in each stage. m_c is the mass of dry air and m_d is the dry mass of powder. F_{vfbh} and F_{vfbc} are the dry base inlet and outlet air flows. Q_{bc} is the exchange of heat between the SFB and VFBh stage. Q_c and Q_d are heat losses to the surroundings. λR_{cw} is the heat of evaporation assumed to take place in the VFBh stage only. The product drying rate is governed from the thin layer equation and a constant term

$$R_{cw} = k_{13}(X_{cd} - X_{eq}(T_{\text{VFBh}}, Y_{cd}))m_d - k_{14}m_d$$

2.3 Stickiness

Stickiness of the produced particles is an important limitation to the achievable performance of the spray dryer. Sticky particles form depositions on the walls of the spray dryer. Stickiness can be predicted by the glass transition temperature given by Boonyai et al. (2004)

$$T_g = \frac{T_{gp} + kZT_{gw}}{1 + kZ} \tag{3}$$

in which $T_{gp} = 144.8°\text{C}$ (maltodextrin) and $T_{gw} = -137°\text{C}$ (water). The value $k = 6.296$ is estimated from adsorption isotherm data. The obtained glass transition temperatures, T_g^{SD} and T_g^{SFB}, are the upper limiting temperatures of which deposits form on the chamber walls of the spray dryer. The moisture content of the powder is

$$Z = \begin{cases} (A_p + B_p\, T_{\text{SD}})e^{C_p\ \text{RH}(T_{\text{SD}}, Y_{ab})} & \text{for SD} \\ X_{ab} & \text{for SFB} \\ X_{cd} & \text{for VFBh} \\ X_{cd} & \text{for VFBc} \end{cases}$$

in which $A_p = 0.193$, $B_p = -0.000435$ and $C_p = 4.51$. $\text{RH}(T_{SD}, Y_{ab})$ is the relative air humidity. The moisture content of the powder in the SD stage is difficult to estimate. Therefore, it is common practice to use an experimentally determined approximation related to the equilibrium moisture, $X_{eq}(T, Y)$.

2.4 Model

The model (1)-(3) of the dryer is a deterministic system of differential equations. In reality, the state and measurement equation of the dryer are corrupted by noise. Consequently, the deterministic system is augmented by two stochastic terms and we have a system of the form

$$x_{k+1} = F(x_k, u_k + w_{u,k}, d_k + w_{d,k}, \theta) \tag{4a}$$
$$y_k = h(x_k) + v_k \tag{4b}$$

The state and measurement noise covariances are $w_{u,k} = N_{iid}(0, T_s R_u)$, $w_{d,k} = N_{iid}(0, T_s R_d)$ and $v_k = N_{iid}(0, R_v)$. T_s is the sample time. The three noise-terms are assumed to be uncorrelated. $F(\cdot)$ is the state integration of $f(x_k, u_k, d_k, \theta)$ using a 3^{rd} and 4^{th} order accurate implicit Runge-Kutta (ESDIRK) method with variable step size (Kristensen et al., 2004). $h(\cdot)$ is the measurement equation.

The state vector, x, the manipulated input vector, u, and the disturbance vector, d are

$$x = \begin{bmatrix} T_{\text{SD}} \\ T_{\text{SFB}} \\ Y_{ab} \\ X_{ab} \\ T_{\text{VFBh}} \\ T_{\text{VFBc}} \\ Y_{cd} \\ X_{cd} \end{bmatrix} \quad u = \begin{bmatrix} F_f \\ T_{\text{main}} \\ T_{\text{sfb}} \\ T_{\text{vfbh}} \\ T_{\text{vfbc}} \end{bmatrix} \quad d = \begin{bmatrix} X_f \\ T_f \\ F_{\text{main}} \\ F_{\text{sfb}} \\ F_{\text{vfbh}} \\ F_{\text{vfbc}} \\ T_{\text{amb}} \\ Y_{\text{amb}} \end{bmatrix} \tag{5}$$

The measurement vector, y, is

$$y = [T_{\text{SD}}\ T_{\text{SFB}}\ Y_{ab}\ T_{\text{VFBh}}\ T_{\text{VFBc}}\ X_{cd}]^{\mathsf{T}} \tag{6}$$

The noise variances, R_u, R_d and R_v, are based on manual inspection of the estimation data. The noise variances are unknown to the state estimator.

2.5 Parameter estimation

The parameters, θ, in the model (4) are estimated using data for a medium-scale spray dryer from GEA Process

Table 1. Estimated param. in model (1)-(3)

Sym.	Value	Unit	Sym.	Value	Unit
C_a	61.634	KJ/K	T_{add}	60.018	°C
C_b	148.26	KJ/K	k_7	$9.401{\cdot}10^{-2}$	-
k_1	0.2725	KW/K	k_8	$1.4887{\cdot}10^{-2}$	-
k_2	1.5017	KW	k_9	8.4203	-
k_3	0.0605	KW/K	C_{cd}	29.244	KW/K
k_4	27.276	KW	k_{10}	$9.561{\cdot}10^{-3}$	KW/K
k_5	0.24735	KW/K	k_{11}	$22.314{\cdot}10^{-3}$	KW/K
k_6	-0.03198	KW/K	k_{12}	$46.818{\cdot}10^{-3}$	KW/K
F_{add}	248.54	kg/hr	k_{13}	$1.9963{\cdot}10^{-3}$	-
Y_{add}	9.4566	g/kg	k_{14}	$13.49{\cdot}10^{-6}$	-

Engineering A/S. Table 1 provides the least squares estimated parameters of the model. $m_a = 7.5$ kg, $m_b = 15$ kg, $m_c = 15$ kg and $m_d = 4$ kg are fixed parameters and determined from physical considerations. Generally the model fits and predicts the data well both for the estimation and validation data, respectively.

2.6 Constraints

The maximum capacity of the feed pump limits the feed flow such that 0 kg/hr $\leq F_f \leq$ 130 kg/hr. The inlet temperatures must be higher than the ambient temperature, T_{amb}, as the dryer can only heat and not cool the air. Furthermore, the risk of powder explosions and the risk of scorched particles creates upper limits on the allowable inlet temperatures. Consequently, $T_{\text{amb}} \leq T_{\text{main}} \leq 200°\text{C}$, $T_{\text{amb}} \leq T_{\text{sfb}} \leq 120°\text{C}$, $T_{\text{amb}} \leq T_{\text{vfbh}} \leq 80°\text{C}$ and $T_{\text{amb}} \leq T_{\text{vfbc}} \leq 80°\text{C}$. These constraints are hard input constraints of the form (9d).

To avoid depositions of sticky particles on the spray dryer surfaces, the temperatures T_{SD}, T_{SFB}, T_{VFBh} and T_{VFBc} must be below the glass transition temperatures in the SD stage, $T_{\text{SD}} \leq T_g^{\text{SD}}$, the SFB stage, $T_{\text{SFB}} \leq T_g^{\text{SFB}}$, the VFBh stage, $T_{\text{VFBh}} \leq T_g^{\text{VFBh}}$ and the VFBc stage, $T_{\text{VFBc}} \leq T_g^{\text{VFBc}} \leq 35°\text{C}$, respectively. The glass transition temperatures are determined by (3). Furthermore, the powder moisture must be below a maximum limit, $X_{cd} \leq X_{\max} = 3.5\%$, that is 3.5% for the case study in this paper. These constraints are treated as soft output constraints in the form (10e). The soft ℓ_1 penalty is $s_W = 10^4 \cdot T_s \cdot [1\ 1\ 1\ 1\ 0.1]$ and the soft ℓ_2 penalty is $S_W = \text{diag}(s_W)$.

2.7 Key Performance Indicators (KPIs)

The profit from operating the spray dryer is the value of the product minus the raw material and energy costs

$$p(x(t), u(t), d(t)) = p_p F_s(1 + X_{cd}) - p_f F_s(1 + X_f) - p_H \Delta H \quad (7)$$

in which p_p is the unit value of the product, p_f is the unit cost of feed material, p_H is the unit energy cost, and ΔH is the total energy supplied to the dryer. ΔH is

$$\Delta H = F_{\text{main}}(h^a_{a_{\text{in}}} - h^a_{\text{amb}}) + F_{\text{sfb}}(h^a_{b_{\text{in}}} - h^a_{\text{amb}}) + F_{\text{vfbh}}(h^a_{c_{\text{in}}} - h^a_{\text{amb}}) + F_{\text{vfbc}}(h^a_{d_{\text{in}}} - h^a_{\text{amb}})$$

in which $h^a_{\text{amb}} = (c_{da} + c_v Y_{\text{amb}})T_{\text{amb}}$. The price of, the produced powder is $p_p = 4.47$ \$/kg, the feed material is $p_f = 0.447$ \$/kg, and the energy is $p_H = 34.873$ \$/GJ. The prices are selected to reflect industrial reality meaning that the price of natural gas is almost negligible compared to the price of the powder, i.e. $p_p \gg p_H$.

The energy efficiency of operation and the product flow rate are also key performance indicators for evaluation of the performance of a spray dryer. The energy efficiency is

$$\eta = \frac{\lambda F_s(X_f - X_{cd})}{\Delta H}$$

Here $\lambda F_s(X_f - X_{cd})$ is the energy used to evaporate water and ΔH is the total energy supplied. The flow rate of the produced powder is

$$F_p = F_s(1 + X_{cd})$$

3. STATE ESTIMATION PROBLEM

In the following, we will use an extended Kalman Filter (EKF), consisting of a filtering part and a one-step predictor part, to estimate the states of the nonlinear stochastic system described in (4).

3.1 Offset-free output estimation

The regulator and state estimator are based on the augmented model in order to achieve offset-free output estimation at steady-state, in the presence of plant/model mismatch and/or un-modeled disturbances (Pannocchia and Rawlings, 2003). We define the augmented model as

$$\bar{x}_{k+1} = \bar{F}(\bar{x}_k, u_k, \bar{d}_k, \bar{\theta}) + \bar{w}_k \quad (8a)$$

$$\bar{y}_k = \bar{h}(\bar{x}_k) + \bar{v}_k \quad (8b)$$

in which $\bar{F}$ is the time integral of $\bar{f}$ and $\bar{h}$ is the output equation. $\bar{x}(t_k)$ is the estimated state, $\bar{d}$ is the measured disturbances and $\bar{\theta}$ is the model parameters that both may differ from the true value in (4). The state and measurement noise covariances are $\bar{w}_k = N_{iid}(0, \bar{R}_w)$ and $\bar{v}_k = N_{iid}(0, \bar{R}_v)$ and estimated in Sec. 3.3 from data. We select pure input disturbances such that the energy- and the vapor mass balances are subject to the disturbance integration.

3.2 State estimator

The EKF utilizes many of the same principles as the Kalman filter. However it linearizes the non-linear model around the current estimate at each time step allowing the system to be solved as a linear time varying (LTV) system.

The estimator consists of a filtering part and a one-step predictor part. The filtering part corrects $\hat{x}_{k|k}$, using the latest measurement, y_k. $\hat{x}_{k|k}$ is used in the controller as the initial state. The predictor part uses the model to predict $\hat{x}_{k+1|k}$. Assuming that the state and measurement noise are uncorrelated, we get the filter equations

$$\hat{x}_{k|k} = \hat{x}_{k|k-1} + K_{fx,k}(y_k - \bar{h}(\hat{x}_{k|k-1}))$$

$$P_{k|k} = P_{k|k-1} - K_{fx,k} R_{e,k} K_{fx,k}$$

where the Kalman gains are

$$R_{e,k} = C_k P_{k|k-1} C_k^{\mathsf{T}} + \bar{R}_v$$

$$K_{fx,k} = P_{k|k-1} C_k^{\mathsf{T}} R_{e,k}^{-1}$$

The one-step predictor is

$$[\hat{x}_{k+1|k}, S_{x,k}] = \text{ESDIRK}(\hat{x}_{k|k-1}, u_k, \bar{d}_k, \bar{\theta})$$

$$P_{k+1|k} = S_{x,k} P_{k|k} S_{x,k}^{\mathsf{T}} + G \bar{R}_w G^{\mathsf{T}}$$

In the above we have $C_k = \frac{d\bar{h}}{d\bar{x}}\Big|_{\hat{x}_{k|k-1}}$ and $G = I$. The state estimator needs a good estimate of the process and measurement noise covariances to work properly. To achieve this we will use the ALS method.

3.3 ALS Estimator tuning

Rajamani and Rawlings (2009) describes a method for estimating the noise covariances based on data, the LTI discrete-time model of the augmented system and an initial guess on the noise sources. We obtain the LTI discrete-time model by linearization and descretization of (8). The estimate of the states are then constructed by the stationary Kalman filter as

$$\hat{x}_{k+1} = \bar{A}\hat{x}_{k|k-1} + \bar{B}u_k + \bar{E}d_k + \bar{A}L(y_k - \bar{C}\hat{x}_{k|k-1})$$

The state estimation error then evolves as

$$\epsilon_{k+1} = (\bar{A} - \bar{A}L\bar{C})\epsilon_k + \begin{bmatrix} I & -\bar{A}L \end{bmatrix} \begin{bmatrix} \bar{w}_k \\ \bar{v}_k \end{bmatrix}$$

In which $\bar{A}$, $\bar{B}$, $\bar{E}$ and $\bar{C}$ are the state, input, disturbance and output LTI system matrices of (8). L is the static Kalman gain constructed from the initial guess of the noise sources and the LTI model. $(\bar{A},\bar{C})$ is detectable and $\bar{A} - \bar{A}L\bar{C}$ is stable. The innovations, $\mathcal{Y}_k$, are constructed by

$$\mathcal{Y}_k = \bar{C}\epsilon_k + v_k$$

and the auto covariance is constructed by $E(\mathcal{Y}_k\mathcal{Y}_{k+1}^T)$. From $\mathcal{Y}_k$, ϵ_{k+1} and the LTI model we can construct a constrained ALS estimation problem, that enforces positive semi-definiteness, to estimate the noise variances by

$$\begin{aligned} \Phi = \min_{\bar{R}_w,\bar{R}_v} \; & \left\| \mathscr{A} \begin{bmatrix} (\bar{R}_w)_s \\ (\bar{R}_v)_s \end{bmatrix} - \hat{b} \right\|_2^2 + \rho \; tr(\bar{R}_w) \\ \text{s.t.} \quad & \bar{R}_w \geq 0, \bar{R}_v \geq 0 \end{aligned}$$

in which $\mathscr{A}$ and $\hat{b}$ are constructed according to Rajamani and Rawlings (2009). The problem is convex and can be solved efficiently even for large datasets. We select the initial state noise covariance $\bar{R}_w = I \cdot 10^{-3}$ and measurement noise $\bar{R}_v = I \cdot 10^{-4}$. The data set used for the estimation is made from an open loop simulation of the nonlinear system with step disturbances in X_f, T_f and Y_{amb}. It contains 650 data points of which the first 10 points are for initialization of the Kalman Filter. The estimated $\bar{R}_w$ and $\bar{R}_v$ in combination with the disturbance structure render a satisfactory performance in the EKF and provides offset-free output estimation.

4. OPTIMAL CONTROL PROBLEM

In this section, we present the continuous-time constrained optimal control problem and its transcription to a discrete time optimal control problem. We solve the discrete optimal control problem using the single-shooting method.

4.1 Continuous-Time Const. Optimal Control Problem

In a receding horizon manner, the manipulated variables in the E-NMPC considered in this paper are obtained by the solution of the following continuous-time constrained optimal control problem in Lagrange form

$$\min_{\bar{x}(\cdot),u(\cdot),s(\cdot)} \phi = \int_{t_0}^{t_f} [-p(\bar{x}(t), u(t), \bar{d}(t)) + \phi(s(t))]dt \quad (9a)$$

$$\text{s.t.} \quad \bar{x}(t_0) = \hat{x}_0, \quad (9b)$$

$$\frac{d\bar{x}(t)}{dt} = \bar{f}(\bar{x}(t), u(t), \bar{d}(t), \bar{\theta}), \quad t \in \mathcal{T} \quad (9c)$$

$$u_{\min} \leq u(t) \leq u_{\max}, \quad t \in \mathcal{T} \quad (9d)$$

$$c(\bar{x}(t)) + s(t) \geq 0, \quad t \in \mathcal{T} \quad (9e)$$

$$s(t) \geq 0, \quad t \in \mathcal{T} \quad (9f)$$

in which $\mathcal{T} = [t_0, t_f[$. $\bar{x}(t) \in \mathbb{R}^{n_x}$ is the state vector, $u(t) \in \mathbb{R}^{n_u}$ is the manipulated variables, $\bar{d}(t) \in \mathbb{R}^{n_d}$ is the known disturbance vector, and $s(t) \in \mathbb{R}^{n_s}$ are the slack variables related to the soft output constraints. The initial state $\bar{x}(t_0) = \hat{x}_0$ and the period $[t_0, t_f[$ are fixed. At each sample time t_0 is the current time and t_f is the prediction and control horizon. The current state, $\hat{x}_0$, is assigned to the initial state by (9b). The stage cost function, $-p(\bar{x}(t), u(t), \bar{d}(t))$, represents the cost of operation, (9c) represents the process dynamics, and (9d) is hard input constraints. $\phi(s(t)) = \frac{1}{2}\|s(t)\|_{2,S_W} + \|s(t)\|_{1,s_W}$ and (9e)-(9f) represent $\ell_2 - \ell_1$ soft output constraints.

4.2 Transcription

The infinite-dimensional optimal control problem (9) is converted to a numerically tractable finite-dimensional optimal control problem by 1) parametrization of the control vector, $u(t)$, and the disturbance vector, $\bar{d}(t)$, 2) point-wise Dirac delta approximation of the soft output constraints, and 3) discretization of the dynamics (9c) and the objective integral. Using these approximations, (9) may be transcribed into the finite dimensional discrete optimal control problem

$$\min_{\bar{x},u,s} \quad \phi = \sum_{k=0}^{N-1} [-P_k(\bar{x}_k, u_k, \bar{d}_k) + \phi(s_k)] + \phi_{\Delta u} \quad (10a)$$

$$\text{s.t.} \quad \bar{x}_0 = \hat{x}_0, \quad (10b)$$

$$R_k(\bar{x}_k, \bar{x}_{k+1}, u_k, \bar{d}_k, \bar{\theta}) = 0, \quad k \in \mathcal{N} \quad (10c)$$

$$u_{\min} \leq u_k \leq u_{\max}, \quad k \in \mathcal{N} \quad (10d)$$

$$c(\bar{x}_k) + s_k \geq 0, \quad k \in \mathcal{N} \quad (10e)$$

$$s_k \geq 0, \quad k \in \mathcal{N} \quad (10f)$$

with $\mathcal{N} = \{0, 1, \ldots, N-1\}$ and N being the discrete prediction and control horizon. The discrete stage cost, $P_k(\bar{x}_k, u_k, \bar{d}_k)$, and the residual function, $R_k = R_k(\bar{x}_k, \bar{x}_{k+1}, u_k, \bar{d}_k, \bar{\theta}) = \bar{x}_{k+1} - \bar{F}(\bar{x}_k, u_k, \bar{d}_k, \bar{\theta})$, are obtained using the ESDIRK3(4) method. The ESDIRK integration method and the computation of the state and stage cost sensitivities are described in Kristensen et al. (2004); Capolei and Jørgensen (2012). The scheme has been implemented with fixed step size using 5 intermediate steps. No forecasts are available for the disturbances, so we use the same-as-now forecasts, i.e. $\bar{d}_k = \bar{d}(t_0)$.

In order to obtain smooth solutions we add the regularization term that penalizes changes in the manipulated variables

$$\phi_{\Delta u} = \sum_{k=0}^{N-1} ||u_k - u_{k-1}||_{Q_s}^2$$

We use $Q_s = T_s \cdot \text{diag}([0.5; 1; 0.5; 0.5; 0.5])$.

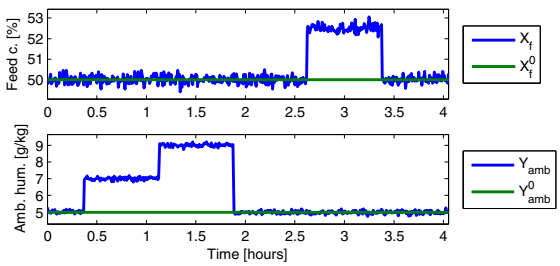

Fig. 2. Disturbance scenario for the case studies.

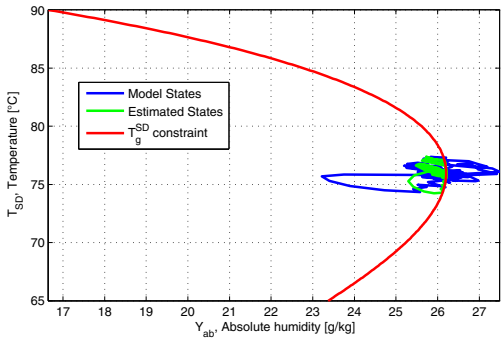

Fig. 3. Active inequality constraint from (3) that constrains T_{SD} and Y_{ab}. Notice, that cost optimal operation is achieved by maximizing Y_{ab} within the non-sticky region.

4.3 Single-Shooting Optimization

In this paper, the optimal control problem (10) is solved by the single-shooting method using a quasi-Newton SQP optimization algorithm (`fmincon` in Matlab's optimization toolbox) and the adjoint method for gradient computation (Petersen and Jørgensen, 2014). The sample time is chosen as $T_s = 30$ s and we use a control and prediction horizon of $t_f = 35$ min i.e. $N = 70$.

5. RESULTS

We illustrate the performance of the E-NMPC by a closed-loop simulation.

5.1 Simulation

Fig. 2 illustrates the feed concentration and the ambient air humidity disturbances considered in the simulated scenario. These renders maximum day-to-day variations.

Fig. 4 shows E-NMPC closed-loop response operation of the spray dryer. Fig. 4(a) shows the outputs and Fig. 4(b) shows the manipulated variables. Fig. 4(c) illustrates the energy efficiency, the production rate and the operational profit rate. Note that the operational profit rate is largely dictated by the production rate.The E-NMPC pushes the system to the constraints in order to maximize profit. In this example, the active constraints are the stickiness constraint in the SD stage, T_g^{SD}, and the maximum allowed residual moisture content in the powder, $X_{\max}$. An increase in ambient air humidity, Y_{amb}, decreases the evaporation rate, R_w, of the dryer and the powder becomes more moist and sticky. The E-NMPC compensates by decreasing the production rate i.e. it decreases the feed rate, F_f, and the inlet air temperatures. A step increase in the feed (water) concentration, X_f, increases the amount of water that has to be evaporated from the feed. The E-NMPC compensates again by decreasing the production rate. Consequently, the economically most favorable conditions for the dryer is obtained at low ambient air humidity and feeds with a high solids content. The sticky temperature, T_g^{SD} in (3), is only a function of the states Y_{ab} and T_{SD}. Thus, we can plot this constrain in 2D. Fig. 3 illustrates T_g^{SD} and shows that one can form a sticky and non-sticky region where cost optimal operation is achieved by maximizing Y_{ab} within the given non-stickiy region. The stickiness constraint, T_g^{SD}, and the residual moisture content, X_{cd}, violates the constraints slightly. A back-off strategy must therefore be implemented to avoid constraint violation at any time.

Cost optimal operation of the plant is not guaranteed to be obtained in general by model based optimization due to plant and model mismatch as well as the presence of unknown disturbances. We obtain almost exact cost optimal plant operation for the disturbance scenario in Fig. 2. This is primarily due to the definition of the active constraints, that do not depend on the unknown disturbances, but only on the measured states T_{SD}, Y_{ab} and X_{cd}.

As illustrated in Fig. 4(c), the profit of operation depends mainly on the production rate, the feed concentration and the residual moisture of the final powder. The energy usage is a secondary objective. Fortunately, the energy efficiency is maximized for a given production rate, but higher efficiencies can be achieved at the sacrifice of production capacity. The PI controller controls the temperature T_{SD} by manipulating the feed flow F_f. Thus, it does not perform any correcting action to compensate for changes in the ambient air humidity. A considerably back-off from the stickiness constraint must therefore be enforced leading to reduced production and profit loss. On average, for the given disturbance scenario, the E-NMPC increases the profit of operation by 17% compared to the conventional PI controller.

6. CONCLUSIONS

This paper presents an economically optimizing control solution for a spray dryer. The E-NMPC provides a control solution that constantly brings the dryer to the most cost optimal state of operation. The residual moisture is controlled within specifications and deposition of sticky particles on spray dryer surfaces are avoided. This is achieved by the ability of the E-NMPC to include stickiness constraints and compute control profiles that are continuously adapted to variations in the feed and the ambient conditions. On average, for the given disturbance scenario, the E-NMPC increases the profit of operation by 17% compared to the conventional PI controller.

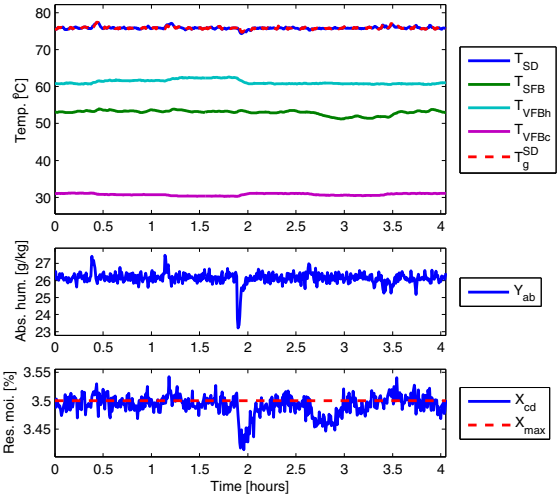

(a) System outputs.

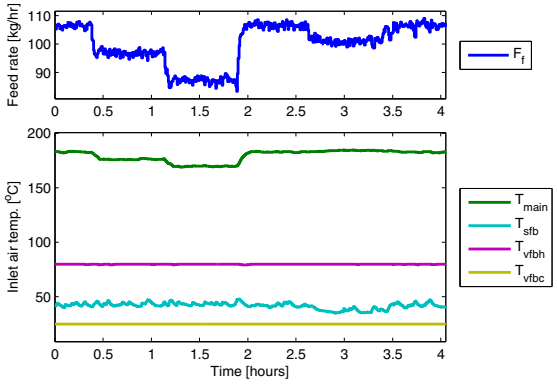

(b) Manipulated variables.

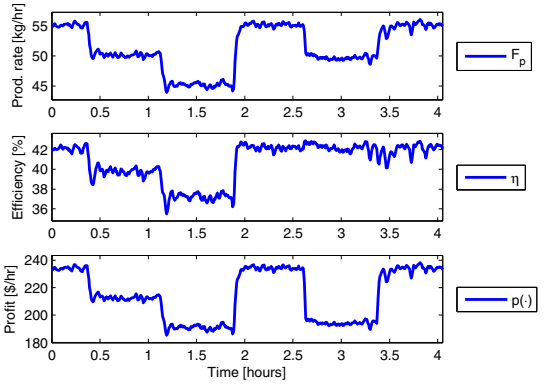

(c) The KPIs and operational profit rate.

Fig. 4. E-NMPC seeking to maximize profit for the disturbance scenario given in Fig. 2. Red lines indicate constraints.

REFERENCES

Bauer, M. and Craig, I.K. (2008). Economic assessment of advanced process control – a survey and framework. *Journal of Process Control*, 18(1), 2–18.

Boonyai, P., Bhandari, B., and Howes, T. (2004). Stickiness measurement techniques for food powders: a review. *Powder Technology*, 145(1), 34 – 46.

Callaghan, D.O. and Cunningham, P. (2005). Modern process control techniques in the production of dried milk products – a review. *Lait*, 85, 335–342.

Capolei, A. and Jørgensen, J.B. (2012). Solution of constrained optimal control problems using multiple shooting and esdirk methods. *Proceedings of the 2012 American Control Conference*, 295–300.

IDF (2005). Energy use in dairy processing. in: Bulletin of the international dairy federation. *International Dairy Federation*, 401.

Kristensen, M.R., Jørgensen, J.B., Thomsen, P.G., and Jørgensen, S.B. (2004). An ESDIRK method with sensitivity analysis capabilities. *Computers & Chemical Engineering*, 28(12), 2695–2707.

Lewis, W.K. (1921). The rate of drying of solid materials. *Journal of Industrial and Engineering Chemistry*, 13, 427–432.

Mujumdar, A.S. and Huang, L.X. (2007). Global R&D needs in drying. *Drying Technology*, 25(4), 647–658.

Mujumdar, A.S. (2006). *Handbook of Industrial Drying, Third Edition*. CRC Press, Boca Raton, FL.

Naysmith, M.R. and Douglas, P.L. (1995). Review of real time optimization in the chemical process industries. *Developments in Chemical Engineering and Mineral Processing*, 67–87.

Pannocchia, G. and Rawlings, J.B. (2003). Disturbance models for offset-free model-predictive control. *AIChE Journal*, 49(2), 426–437.

Petersen, L.N. and Jørgensen, J.B. (2014). Real-time economic optimization for a fermentation process using model predictive control. *13th European Control Conference*.

Petersen, L.N., Poulsen, N.K., Niemann, H.H., Utzen, C., and Jørgensen, J.B. (2013). A Grey-Box Model for Spray Drying Plants. *10th IFAC International Symposium on Dynamics and Control of Process Systems*, 559–564.

Petersen, L.N., Poulsen, N.K., Niemann, H.H., Utzen, C., and Jørgensen, J.B. (2014a). Application of constrained linear mpc to a spray dryer. *Proceedings of the IEEE Multi-Conference on Systems and Control*.

Petersen, L.N., Poulsen, N.K., Niemann, H.H., Utzen, C., and Jørgensen, J.B. (2014b). Economic optimization of spray dryer operation using nonlinear model predictive control. *Proceedings of the IEEE Conference on Decision and Control*.

Rajamani, M.R. and Rawlings, J.B. (2009). Estimation of the disturbance structure from data using semidefinite programming and optimal weighting. *Automatica*, 45(1), 142–148.

Rawlings, J.B., Bates, C.N., and Angeli, D. (2012). Fundamentals of economic model predictive control. *Proceedings of the IEEE Conference on Decision and Control*, 3851–3861.

Paper H

Comparison of Linear and Nonlinear Model Predictive Control for Optimization of Spray Dryer Operation

---

Published in *5th IFAC Conference on Nonlinear Model Predictive Control (NMPC 2015), pp. 218–223, 2015, Seville.*

Available online at www.sciencedirect.com

ScienceDirect

IFAC-PapersOnLine 48-23 (2015) 218–223

IFAC Papers Online CONFERENCE PAPER ARCHIVE

Comparison of Linear and Nonlinear Model Predictive Control for Optimization of Spray Dryer Operation

Lars Norbert Petersen [*,**] **Niels Kjølstad Poulsen** [*]
Hans Henrik Niemann [***] **Christer Utzen** [**]
John Bagterp Jørgensen [*]

[*] *Department of Applied Mathematics and Computer Science, Technical University of Denmark, Kgs. Lyngby, Denmark, (e-mail: {lnpe,nkpo,jbjo}@dtu.dk)*
[**] *GEA Process Engineering A/S, Søborg, Denmark, (e-mail: christer.utzen@gea.com)*
[***] *Department of Electrical Engineering, Technical University of Denmark, Kgs. Lyngby, Denmark, (e-mail: hhn@elektro.dtu.dk)*

Abstract: In this paper, we compare the performance of an economically optimizing Nonlinear Model Predictive Controller (E-NMPC) to a linear tracking Model Predictive Controller (MPC) for a spray drying plant. We find in this simulation study, that the economic performance of the two controllers are almost equal. We evaluate the economic performance with an industrially recorded disturbance scenario, where unmeasured disturbances and model mismatch are present. The state of the spray dryer, used in the E-NMPC and MPC, is estimated using Kalman Filters with noise covariances estimated by a maximum likelihood (ML) method.

Keywords: Model Predictive Control, Optimization, Spray Drying, Simulation

1. INTRODUCTION

Spray drying is a process that turns a liquid product into a free-flowing powder. The most efficient and dominating type of spray dryer is the multi-stage dryer, which combines drying in several stages: Spray drying at the top of the dryer chamber, drying in an integrated static bed at the bottom of the chamber and drying in an external vibrating fluidized bed. Spray drying is a highly energy consuming process. The pressure of environmental issues and demands for better product quality drives the need for innovations within process efficiency and quality control (Govaerts et al., 1994). The key product qualities in spray drying are the bulk density, the particle size distribution and the residual moisture. Research shows that the powder residual moisture content predominate all the other physical parameters. Hence it is of considerable importance to control the moisture content in the powder while minimizing the energy consumption.

The main challenge in controlling the spray dryer is to use a minimum of energy (hot air) to bring the residual moisture in the powder below the specification and to avoid that the powder stick to the walls of the chamber. This is a challenge, as the operation of the spray dryer must continuously be adjusted to variations in the feed and the ambient air humidity. The conventional PID control approach is simple, but known to be insufficient at controlling the moisture and the powder may turn sticky inside the dryer during high ambient air humidities. This motivates more advanced control methods in the presence of feed and ambient air variations.

1.1 Process Description

A multi-stage dryer (MSD^{TM}) consist of a spray chamber (SD), a static fluid bed (SFB) and two vibrating fluid bed (VFB) stages. Fig. 1 illustrates the stages of the spray dryer as well as the hot air and the powder in- and outlets. The hot inlet air is fed into the upper section of the drying chamber around the high pressure nozzles. The nozzles disperse the liquid feed into droplets. The heat is transferred from the hot air to the droplets, which makes most of the water evaporate. The dried product then enters the SFB where it is further dried by hot air from below. Next, the powder is transported to the VFBh and VFBc stages for gentle drying and is cooled to the temperature desired for handling and storage.

1.2 Control

For a long time, linear tracking Model Predictive Control (MPC) has been the preferred advanced control methodology in the process industries. MPC is popular for its flexibility, performance and ability to handle constraints (Darby et al., 2009). Often MPC is combined with an economically optimizing RTO layer (Darby et al., 2011). Recent advances within process optimization focus on optimizing the higher-level objectives, such as economics, directly in the control layer. A popular framework is the economically optimizing Nonlinear Model Predictive Controller (E-NMPC). The discrete-time NMPC problem may be solved using single-shooting (control vector parametrization), multiple shooting (Bock and Plitt, 1984), or the simultaneous method. The multiple-shooting

2405-8963 © 2015, IFAC (International Federation of Automatic Control) Hosting by Elsevier Ltd. All rights reserved.
Peer review under responsibility of International Federation of Automatic Control.
10.1016/j.ifacol.2015.11.286

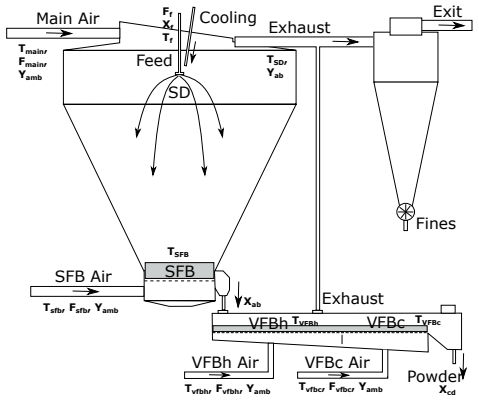

Fig. 1. Diagram of the spray dryer. Sprayed droplets and hot air are mixed in the top. The droplets dry into powder and are dried further in the SFB and VFBh stages and cooled in the VFBc stage.

algorithm is a popular choice, as it has good stability properties and can use state-of-the-art ODE/DAE solvers (Capolei and Jørgensen, 2012). The explicit singly diagonally implicit Runge-Kutta (ESDIRK) method is an example of such a DAE solver with sensitivity computation capabilities. The method is a special implicit Runge-Kutta method that is computationally efficient for particularly stiff systems, both A- and L-stable, and often has an embedded error estimator (Kristensen et al., 2004a). The ESDIRK method is also well suited in combination with a continuous-discrete extended Kalman filter (EKF) for state estimation (Jørgensen et al., 2007).

Some progress has been made towards improving the control of spray dryers. Govaerts et al. (1994) reports a black-box model combined with a cascade PID controller as well as a physics based soft-sensor. A linear MPC and an E-NMPC for a spray dryer is presented in Petersen et al. (2014a) and Petersen et al. (2014b). Shabde and Hoo (2008) synthesizes PI controllers for control of the residual moisture content and the particle size.

1.3 Content & Organization

The aim of this paper is to compare the application of E-NMPC and linear tracking MPC for a multi-stage dryer in an industrially recorded disturbance scenario. The optimal control problem in the E-NMPC is solved using the multiple-shooting method combined with an interior point optimization algorithm (`IPOPT`). The ESDIRK3(4) method, with sensitivity capabilities, is used for state integration of the stiff model. The linear MPC is based on Petersen et al. (2014a) with an RTO layer for calculation of the set-points.

The paper is organized as follows. Section 2 provides a brief description of the spray dryer model. Section 3 presents the EKF used for state estimation and the E-NMPC optimization problem. Section 4 describes the linear tracking MPC. In Section 5 we present a simulation to show the benefit of optimizing the operation and compares the performance of the E-NMPC to the MPC. Conclusions are given in Section 6.

2. SPRAY DRYER MODEL

2.1 Model

The model, described in Petersen et al. (2015), is used for simulation as well as for prediction in the MPCs. It is derived from first engineering principles and describes drying of maltodextrin DE-18 in a small-scale industrial spray dryer. The deterministic model is augmented by two stochastic terms. We have a system of the form

$$x_{k+1} = F(x_k, u_k + w_{\mathrm{u},k}, d_k + w_{\mathrm{d},k}, \theta) \tag{1a}$$

$$y_k = h(x_k) + v_k \tag{1b}$$

The state and measurement noise covariances are $w_{\mathrm{u},k} = N_{\mathrm{iid}}(0, R_{\mathrm{u}})$, $w_{\mathrm{d},k} = N_{\mathrm{iid}}(0, R_{\mathrm{d}})$ and $v_k = N_{\mathrm{iid}}(0, R_{\mathrm{v}})$. The three noise-terms are assumed to be independent and the noise variances, R_{u}, R_{d} and R_{v}, are based on manual inspection of the estimation data. The noise variances are used for simulation and are unknown to the state estimator. $F(\cdot)$ is the state integration of $dx(t)/dt = f(x(t), u(t), d(t), \theta)$. $h(\cdot)$ is the measurement equation. θ are the model parameters. The state vector, x, the manipulated input vector, u, the disturbance vector, d, and the measurement vector, y, are

$$x = [T_{\mathrm{SD}}\ T_{\mathrm{SFB}}\ Y_{\mathrm{ab}}\ X_{\mathrm{ab}}\ T_{\mathrm{VFBh}}\ T_{\mathrm{VFBc}}\ Y_{\mathrm{cd}}\ X_{\mathrm{cd}}]^T \tag{1c}$$

$$u = [F_{\mathrm{f}}\ T_{\mathrm{main}}\ T_{\mathrm{sfb}}\ T_{\mathrm{vfbh}}\ T_{\mathrm{vfbc}}]^T \tag{1d}$$

$$d = [X_{\mathrm{f}}\ T_{\mathrm{f}}\ F_{\mathrm{main}}\ F_{\mathrm{sfb}}\ F_{\mathrm{vfbh}}\ F_{\mathrm{vfbc}}\ T_{\mathrm{amb}}\ Y_{\mathrm{amb}}]^T \tag{1e}$$

$$y = [T_{\mathrm{SD}}\ T_{\mathrm{SFB}}\ Y_{\mathrm{ab}}\ T_{\mathrm{VFBh}}\ T_{\mathrm{VFBc}}\ X_{\mathrm{cd}}]^T \tag{1f}$$

The controlled variables, y, are the stage air temperatures T_{SD}, T_{SFB}, T_{VFBh} and T_{VFBc}, the absolute air humidity, Y_{ab}, and the powder residual moisture content, X_{cd}. The manipulated variables, u, are the feed flow, F_{f}, the inlet main air temperature, T_{main}, the inlet SFB air temperature, T_{sfb}, and the VFB air temperatures, T_{vfbh} and T_{vfbc}. The disturbance variables, d, are the feed concentration, X_{f}, the feed temperature, T_{f}, and the inlet air flows rates. The ambient air temperature and the air humidity, T_{amb} and Y_{amb}.

2.2 Cost of Operation

We will judge the control performance by the profit/cost of operating the spray dryer. The profit is the value of the product minus the raw material and energy costs

$$p(\cdot) = p_{\mathrm{p}} F_{\mathrm{s}}(1 + X_{\mathrm{cd}}) - p_{\mathrm{f}} F_{\mathrm{s}}(1 + X_{\mathrm{f}}) - p_{\mathrm{H}} \Delta H \tag{2}$$

p_{p} is the unit value of the product, p_{f} is the unit cost of feed material, p_{H} is the unit energy cost, and ΔH is the total energy supplied to the dryer. The energy efficiency of operation and the product flow rate are computed as described in Petersen et al. (2015).

2.3 Constraints

The maximum capacity of the feed pump limits the feed flow. The inlet temperatures must be higher than the

ambient temperature, T_{amb}, and the risk scorched particles creates upper limits on the allowable inlet temperatures. Consequently, 0 kg/hr $\leq F_{\text{f}} \leq$ 110 kg/hr, $T_{\text{amb}} \leq T_{\text{main}} \leq$ 175°C, $T_{\text{amb}} \leq T_{\text{sfb}} \leq$ 105°C, 55°C $\leq T_{\text{vfbh}} \leq$ 75°C, and $T_{\text{amb}} \leq T_{\text{vfbc}} \leq$ 50°C. These constraints are hard input constraints of the form (5d) and (9d). To avoid depositions of sticky particles on the spray dryer surfaces, the stage temperatures must be below the glass transition temperatures, $T_{\text{SD}} \leq T_g^{\text{SD}}$, $65° \leq T_{\text{SFB}} \leq T_g^{\text{SFB}} \leq 70°$, $T_{\text{VFBh}} \leq T_g^{\text{VFBh}}$ and $T_{\text{VFBc}} \leq T_g^{\text{VFBc}} \leq$ 35°C. The glass transition temperatures are determined as in Petersen et al. (2015). The powder moisture content must be below a maximum limit, $X_{\text{cd}} \leq X_{\max} = 3.9\%$. These constraints are soft output constraints including back-off from the real limits and is of the form (5e) and (9e).

3. NONLINEAR MODEL PREDICTIVE CONTROL

The E-NMPC control solution is a combination of a state estimator and a regulator, as shown in Algorithm 1.

3.1 Offset-free estimation

To achieve offset-free output estimation (and control) at steady-state, in the presence of plant/model mismatch and/or un-modeled disturbances, the system model in (1) is augmented with integrating disturbance states (Pannocchia and Rawlings, 2003). We select pure input disturbances, i.e. $C_{\text{d}} = 0$ and B_{d} selected such that the energy- and the vapor mass balances are subject to the disturbance integration.

3.2 State estimator

The EKF utilizes many of the same principles as the Kalman filter. However, it linearizes the non-linear model around the current estimate at each time step allowing the system to be solved as a linear time varying (LTV) system. The filter is described in Algorithm 1. The filtering part corrects $\hat{x}_{k|k}$, using the latest measurement, y_k, after which it is used in the controller as the initial state. The predictor part uses the model to predict $\hat{x}_{k+1|k}$.

The regulator and state estimator are based on the augmented model

$$\bar{x}_{k+1} = \bar{F}(\bar{x}_k, u_k, \bar{d}_k, \bar{\theta}) + G\bar{w}_k \tag{3a}$$

$$\bar{y}_k = \bar{h}(\bar{x}_k) + \bar{v}_k \tag{3b}$$

in which $\bar{x}_k$ is the augmented state and $\hat{x}_k$ is the estimated augmented state. $\bar{F}(\cdot)$ is the state integration using the ESDIRK3(4) method with variable step size. $G = I$ is the noise to state matrix. $\bar{h}(\cdot)$ is the measurement equation.The measured disturbances and estimated model parameters may differ from their true value in (1) and we denote these $\bar{d}(t)$ and $\bar{\theta}$. We select $\bar{\theta}$ randomly from $\bar{\theta} \sim N(\theta, \Sigma_\theta)$ where Σ_θ is the estimated covariance of the parameters. The state and measurement noise covariances are $\bar{w}_k = N_{\text{iid}}(0, \bar{R}_{\text{w}})$ and $\bar{v}_k = N_{\text{iid}}(0, \bar{R}_{\text{v}})$ and must be estimated. $\bar{R}_{\text{w}}$ and $\bar{R}_{\text{v}}$ are assumed diagonal.

Estimator tuning The unknown noise variances, $\bar{R}_{\text{w}}$ and $\bar{R}_{\text{v}}$, are estimated using the Maximum Likelihood (ML) method (Kristensen et al., 2004b). Given the model structure, the optimally selected variances maximizes the likelihood function of a sequence of output measurements $\mathcal{Y}_N = [y_N, y_{N-1}, ..., y_1, y_0]$. The likelihood function is $L(\theta; \mathcal{Y}_N)$ and by conditioning on y_0 and taking the negative logarithm we get

$$-\ln(L(\cdot)) = \frac{1}{2}\sum_{k=1}^{N}\left(\ln(\det(R_{e,k|k-1})) + \epsilon_k^T R_{e,k|k-1}^{-1}\epsilon_k\right)$$

with $\epsilon_k = y_k - \hat{y}_{k|k-1}$. The ML estimate of the variances is then determined by solving the nonlinear optimization problem

$$[\bar{R}_{\text{w}}, \bar{R}_{\text{v}}] = \arg\min_{\bar{R}_{\text{w}}, \bar{R}_{\text{v}}} \left\{-\ln(L(\bar{R}_{\text{w}}, \bar{R}_{\text{v}}; \mathcal{Y}_N|y_0))\right\} \tag{4}$$

where ϵ_k and $R_{e,k|k-1}$ are computed recursively by means of the EKF i.e. Algorithm 1 without the regulator computation. We select the initial state noise $\bar{R}_{\text{w}} = I \cdot 0.01$, measurement noise $\bar{R}_{\text{v}} = I \cdot 0.001$, and use generated data from (1).

Algorithm 1 NMPC for the continuous-discrete EKF

Require: y_k, $\bar{d}_k$, $\bar{\theta}$, $\hat{x}_{k|k-1}$, $P_{k|k-1}$, u_{k-1}

Filter:

Compute the one-step ahead measurement prediction and the output matrix

$\hat{y}_{k|k-1} = \bar{h}(\hat{x}_{k|k-1})$, $\quad C_k = \frac{d\bar{h}}{d\bar{x}}\Big|_{t_k, \hat{x}_{k|k-1}}$

Compute the filtered state

$R_{e,k} = C_k P_{k|k-1} C_k^T + \bar{R}_v$

$K_{fx,k} = P_{k|k-1} C_k^T R_{e,k}^{-1}$

$\hat{x}_{k|k} = \hat{x}_{k|k-1} + K_{fx,k}(y_k - \hat{y}_{k|k-1})$

$P_{k|k} = P_{k|k-1} - K_{fx,k} R_{e,k} K_{fx,k}^T$

Regulator:

$u_k = \mu(\hat{x}_{k|k}, u_{k-1}, \bar{d}_k, \bar{\theta})$

One-step predictor:

Compute the predicted state, $\hat{x}_{k+1|k}$, and state sensitivity, $S_{x,k}$ using

$[\hat{x}_{k+1|k}, S_{x,k}] = \text{ESDIRK}(t_k, t_{k+1}, \hat{x}_k, u_k, \bar{d}_k, \bar{\theta})$

$P_{k+1|k} = S_{x,k} P_{k|k} S_{x,k}^T + G\bar{R}_w G^T$

Return: u_k, $\hat{x}_{k+1|k}$, $P_{k+1|k}$

3.3 Discrete-Time Optimal Control Problem

The controlled variables are to be controlled within the given constraints, to maximize profit, by adjusting the manipulated variables. In a receding horizon manner, the manipulated variables in the E-NMPC are obtained by the solution of the following finite dimensional discrete optimal control problem

$$\min_{\bar{x},u,s} \quad \phi = \sum_{k=0}^{N-1}[-P_k(\bar{x}_k, u_k, \bar{d}_k) + \phi(s_k)] + \phi_{\Delta u} \tag{5a}$$

$$\text{s.t.} \quad \bar{x}_0 = \hat{x}_0, \tag{5b}$$

$$\bar{x}_{k+1} - \bar{F}(\bar{x}_k, u_k, \bar{d}_k, \bar{\theta}) = 0, \qquad k \in \mathcal{N} \tag{5c}$$

$$u_{\min} \leq u_k \leq u_{\max}, \qquad k \in \mathcal{N} \tag{5d}$$

$$c(\bar{x}_k) + s_k \geq 0, \qquad k \in \mathcal{N} \tag{5e}$$

$$s_k \geq 0, \qquad k \in \mathcal{N} \tag{5f}$$

with $\mathcal{N} = \{0, 1, \ldots, N-1\}$ and N being the discrete prediction and control horizon. At each sample time, $t(0)$ is the current time. $\bar{x}_k \in \mathbb{R}^{n_x}$ is the state vector, $u_k \in \mathbb{R}^{n_u}$ is the manipulated variables, $\bar{d}_k \in \mathbb{R}^{n_d}$ is the measured

disturbance vector, and $s_k \in \mathbb{R}^{n_s}$ is the vector of slack variables related to the soft output constraints. The estimated current state, $\hat{x}_0$, is assigned to the initial state by (5b). The discrete stage cost, $P_k(\bar{x}_k, u_k, \bar{d}_k)$ in (5a), and the process dynamics residual function, $\bar{x}_{k+1} - \bar{F}(\bar{x}_k, u_k, \bar{d}_k, \bar{\theta})$ in (5c), are obtained using the ESDIRK3(4) method where

$$P_k(\bar{x}_k, u_k, \bar{d}_k) = h_n \sum_{i=1}^{s} b_i p(\bar{X}_i, u_k, \bar{d}_k)$$

$$\bar{F}(\cdot) = h_n \sum_{j=1}^{i-1} a_{ij} f(\bar{X}_j, u_k, \bar{d}_k, \bar{\theta}) + h_n \gamma f(\bar{X}_j, u_k, \bar{d}_k, \bar{\theta})$$

with $\bar{x}_k = \bar{X}_1$ and $\bar{x}_{k+1} = \bar{X}_s$. The computation of the state and stage cost sensitivities are described in (Kristensen et al., 2004a; Capolei and Jørgensen, 2012). The scheme has been implemented with variable step size with an error accuracy of 10^{-4}. (5d) is hard input constraints. $\phi(s_k) = \frac{1}{2} \|s_k\|_{2,S_W} + \|s_k\|_{1,sW}$ and (5e)-(5f) represent $\ell_2 - \ell_1$ soft output constraints. The soft ℓ_1 penalty is $s_W = 10^4 \cdot T_s \cdot [0.1\ 0.1\ 0.1\ 0.1\ 1.0]$ and the soft ℓ_2 penalty is $S_W = \mathrm{diag}(s_W)$.

In order to obtain smooth solutions, we add the regularization term that penalizes changes in the manipulated variables

$$\phi_{\Delta u} = \sum_{k=0}^{N-1} ||u_k - u_{k-1}||_{Q_s}^2 \tag{6}$$

We use $Q_s = T_s \cdot \mathrm{diag}([0.5; 1; 0.5; 0.5; 0.5])$. No forecasts are available for the disturbances, so we use the same-as-now forecasts, i.e. $\bar{d}_k = \bar{d}(t_0)$.

Multiple-Shooting Optimization The optimal control problem (5) is solved by the multiple-shooting method using an interior point method optimization algorithm (`IPOPT` interfaced from Matlab). The gradient computation is performed using forward sensitivities as described in Capolei (2013). The sample time is chosen as $T_s = 30$ s and we use a prediction horizon of 25 min i.e. $N = 50$.

4. LINEAR MODEL PREDICTIVE CONTROL

In the following, we present the linear tracking MPC with an RTO layer.

4.1 State estimator

The linear Kalman filter is used to estimate the states. The regulator and state estimator are based on the linearized model in (3) and we get

$$\bar{x}_{k+1} = A\bar{x}_k + Bu_k + E\bar{d}_k + \sigma_x + \bar{w}_k \tag{7a}$$
$$\bar{y}_k = C_y\bar{x}_k + \sigma_y + \bar{v}_k \tag{7b}$$
$$z_k = C_z\bar{x}_k + \sigma_z \tag{7c}$$

with $\bar{x}$ being the states, u being the manipulated variables, $\bar{d}$ being measured disturbances and z is the controlled variables. σ_x, σ_y and σ_z contain the constants related to the linearisation of the model, i.e. $\sigma_x = \bar{x}_0 - A\bar{x}_0 - Bu_0 - E\bar{d}_0$, $\sigma_y = \bar{y}_0 - C_y\bar{x}_0$ and $\sigma_z = z_0 - C_z\bar{x}_0$.

4.2 Regulator

The controlled variables are the stage air temperatures T_{SD} and T_{SFB}, the absolute air humidity, Y_{ab}, and the powder residual moisture content, X_{cd}. The manipulated variables are F_{f}, T_{main}, T_{sfb} and T_{vfbh} with $T_{\mathrm{vfbc}} = T_{\mathrm{amb}}$.

The output tracking problem with input constraints may be formulated as

$$\min_{u} \quad \phi = \frac{1}{2}\sum_{k=1}^{N_z} \|z_k - r_k\|_{Q_z}^2 + \frac{1}{2}\sum_{k=0}^{N_u} \|\Delta u_k\|_{S_u}^2 \tag{8a}$$
$$\text{s.t.} \quad \bar{x}_0 = \hat{x}_0, \tag{8b}$$
$$\bar{x}_{k+1} = A\bar{x}_k + Bu_k + E\bar{d}_k + \sigma_x, \quad k \in \mathcal{N}_u \tag{8c}$$
$$z_k = C_z\bar{x}_k + \sigma_z, \quad k \in \mathcal{N}_z \tag{8d}$$
$$u_{\min} \le u_k \le u_{\max}, \quad k \in \mathcal{N}_u \tag{8e}$$

in which $\Delta u_k = u_k - u_{k-1}$ and $\mathcal{N}_z = \{1, 2 \ldots, N_z - 1\}$, $\mathcal{N}_u = \{0, 1 \ldots, N_u - 1\}$. The control and prediction horizons are, $N_u = N_z = 25$ min $= 50$. These are selected sufficiently long such that any end effects have no influence on the solution in the beginning of the horizon. No forecasts are available for the references and disturbances, so we use the same-as-now forecasts, i.e. $r_k = r(t_0)$ and $\bar{d}_k = \bar{d}(t_0)$. The tuning parameters Q_z and S_u are selected to achieve fast and robust performance. The problem in (8) can be converted to a constrained quadratic problem and is solved using `quadprog` in Matlab.

4.3 RTO layer

The references, r_k, are computed by solving the steady-state economic optimization problem

$$\min_{\bar{x}_{\mathrm{ss}}, u_{\mathrm{ss}}, s} \quad \phi = -p(\bar{x}_{\mathrm{ss}}, u_{\mathrm{ss}}, \bar{d}_k) + \|s\|_{2,S_W} \tag{9a}$$
$$\text{s.t.} \quad \bar{x}_{\mathrm{ss}} = A\bar{x}_{\mathrm{ss}} + Bu_{\mathrm{ss}} + E\bar{d}_k + \sigma_x \tag{9b}$$
$$z_{\mathrm{ss}} = C_z\bar{x}_{\mathrm{ss}} + \sigma_z \tag{9c}$$
$$u_{\min} \le u_{\mathrm{ss}} \le u_{\max} \tag{9d}$$
$$c(x_{\mathrm{ss}}) + s \ge 0 \tag{9e}$$
$$s \ge 0 \tag{9f}$$

and setting $r_k = z_{\mathrm{ss}} - \delta$. δ contains a 0.1 g/kg back-off in the air humidity and 0.01 % back-off in the residual moisture compared to the E-NMPC, as we want the constraints violation to be equal. The set-point is computed at a sample rate of 5 min. Plant/model mismatch and/or un-modeled disturbances are corrected for by utilizing the estimated offset parameters from the state estimator.

5. RESULTS

We illustrate the performance of the E-NMPC and the linear MPC by two closed-loop simulations.

5.1 Simulation

Fig. 2 illustrates the disturbances considered in the simulated scenario. The feed concentration, X_{f}, the feed temperature, T_{f}, and the ambient air humidity, Y_{amb} are industrially recorded disturbances from a whey protein dairy spray dryer. We simulate an inaccuracy in the measurement of the disturbances and denote the measured disturbances; $\bar{X}_{\mathrm{f}}$, $\bar{T}_{\mathrm{f}}$ and $\bar{Y}_{\mathrm{amb}}$. Fig. 3 illustrates the operational profit rate for the E-NMPC and the linear MPC. Fig. 4 and Fig. 5 illustrates the outputs and the manipulated variables for the E-NMPC and the linear MPC described in Sec. 3 and Sec. 4, respectively. We simulate operator

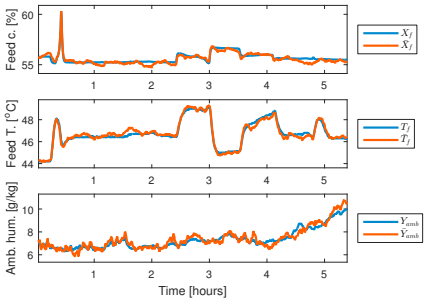

Fig. 2. Disturbance scenario for the case studies.

intervention between time $t = 3$ and $t = 4$ where the lower limit on T_{SFB} is modify from 65°to 68°. We have omitted plotting the VFBc stage temperature, T_{VFBc}, and inlet air temperature, $T_{\mathrm{vfbc}} = 25°C$, to focus on the interesting stage temperatures.

Fig.4 shows that the E-NMPC operates the dryer such that the profit of operation is maximized. The optimum is reached when T_{SD} reaches the glass transition temperature, T_g^{SD}, i.e. the point at which the powder turns sticky in the top of the chamber, T_{SFB} reaches its lower limit at 65°, and when X_{cd}, the moisture content of the powder, reaches X_{max}. The reason is simple, it's the cheapest way to operate while maximizing throughput and meeting the product specification. For the majority of the simulation time, X_{max} can not be reached. Thus, T_{vfbh} is minimized to maximize X_{cd}. T_g^{SD} is only a function of the air humidity, Y_{ab}. Thus, the optimal temperature and air humidity in the chamber are closely connected. Decreasing the air humidity, Y_{ab}, will increase T_g^{SD} and make the powder less sticky.

We perform a closed-loop simulation with the linear tracking MPC and compare the achieved performance to the E-NMPC performance. Fig. 5 shows the controlled outputs, the setpoints and the manipulated variables. The simulation shows that the MPC is able to maintain stable process variables related to stickiness of the powder, T_{SD} and Y_{ab}, at their setpoints. The residual moisture content, X_{cd}, can not be controlled constant and the RTO generated setpoint is fluctuating. This situation is similar to the E-NMPC. Notice, that the manipulated variables are controlled more smoothly than with the E-NMPC. In the E-NMPC we allowed only to restrict the state estimates of the Kalman filters to stay within the constraints. Still, a small back-off from the constraints must be implemented to keep the constraint violating equal for the two controllers.

The computational time for solving the optimization problems in the E-NMPC and MPC are on average 35.2 sec and 0.02 sec, respectively. The algorithms have not been optimized for speed, thus these can be decreased significantly.

Fig. 4 also shows that the noise and disturbances of the system makes both controllers violate the constraints slightly. The constraints includes back-off from the true process constraints, and we therefore choose only to restrict the state estimates of the Kalman filter to stay within the

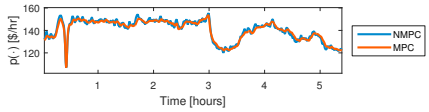

Fig. 3. Key Performance Indicator (KPI) for the E-NMPC (NMPC) and the linear MPC (MPC).

constraints. A more conservative back-off strategy can be implemented, if required, to avoid constraint violation at any time.

Fig. 3 shows that the profit of operation mainly depends on the production rate, which again mainly depends on the feed concentration, the ambient air humidity and the residual moisture of the final powder. The energy usage is a secondary objective. On average, for the given disturbance scenario, the E-NMPC increases the profit of operation by only 0.2% compared to the linear MPC. The profit loss in the MPC solution may be due to tuning differences and slight back-off differences in the setpoints. On average the energy efficiency is increased by 0.05% by the E-NMPC solution. At this point we can not justify an industrial implementation of the E-NMPC based on the economic benefits of the controller. This will to some degree depend on the maintenance requirements for each of the controllers.

6. CONCLUSIONS

This paper presents two economically optimizing control solutions for a spray dryer. The E-NMPC and linear tracking MPC both provides control solutions that constantly brings the dryer to the most cost optimal state of operation. The residual moisture is controlled within specifications and deposition of sticky particles on spray dryer surfaces are avoided. We show that the performance of the E-NMPC is closely mimicked by the simpler linear MPC.

REFERENCES

Bock, H.G. and Plitt, K.J. (1984). A multiple shooting algorithm for direct solution of optimal control problems. *9th IFAC World Congress Budapest. Pergamon Press*, 242–247.

Capolei, A. (2013). *Nonlinear Model Predictive Control for Oil Reservoirs Management*. Ph.D. thesis, Technical University of Denmark.

Capolei, A. and Jørgensen, J.B. (2012). Solution of constrained optimal control problems using multiple shooting and ESDIRK methods. *2012 American Control Conference*, 295–300.

Darby, M.L., Harmse, M., and Nikolaou, M. (2009). MPC: Current practice and challenges. *7th IFAC International Symposium on Advanced Control of Chemical Processes*, 7(1), 86–98.

Darby, M.L., Nikolaou, M., Jones, J., and Nicholson, D. (2011). Rto: An overview and assessment of current practice. *Journal of Process Control*, 21(6), 874–884.

Govaerts, R., Johnson, A., Crezee, R., Reyman, G., and Swinkels, P. (1994). Control of an industrial spray-drying unit. *Control Engineering Practice*, 2(1), 69–85.

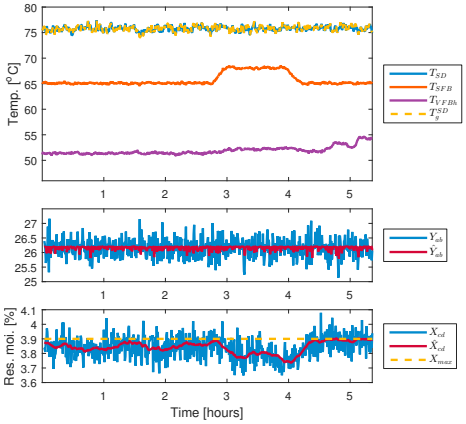

(a) System outputs.

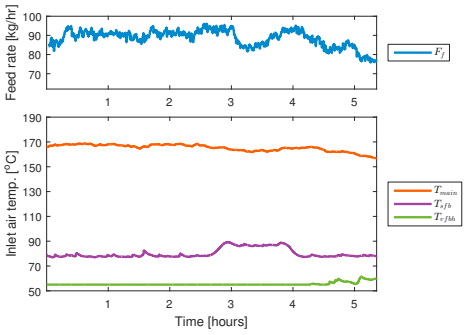

(b) Manipulated variables.

Fig. 4. E-NMPC seeking to maximize profit for the disturbance scenario given in Fig. 2. Dashed lines indicate constraints. T_{VFBc} and T_{vfbc} are omitted in the plot.

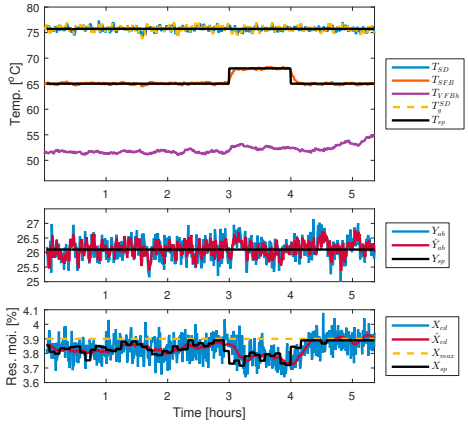

(a) System outputs.

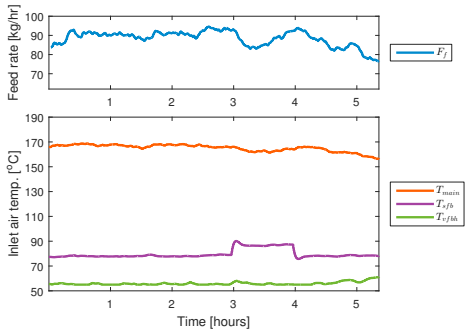

(b) Manipulated variables.

Fig. 5. MPC for the disturbance scenario given in Fig. 2. Dashed line indicate constraints and black lines are setpoints. T_{VFBc} and T_{vfbc} are omitted in the plot.

Jørgensen, J.B., Kristensen, M.R., Thomsen, P.G., and Madsen, H. (2007). A computationally efficient and robust implementation of the continuous-discrete extended kalman filter. *26th American Control Conference*, 3706–3712.

Kristensen, M.R., Jørgensen, J.B., Thomsen, P.G., and Jørgensen, S.B. (2004a). An ESDIRK method with sensitivity analysis capabilities. *Computers & Chemical Engineering*, 28(12), 2695–2707.

Kristensen, N.R., Madsen, H., and Jørgensen, S.B. (2004b). A method for systematic improvement of stochastic grey-box models. *Computers and Chemical Engineering*, 28(8), 1431–1449.

Pannocchia, G. and Rawlings, J.B. (2003). Disturbance models for offset-free model-predictive control. *AIChE Journal*, 49(2), 426–437.

Petersen, L.N., Poulsen, Jørgensen, J.B., and Rawlings, J.B. (2015). Economic optimization of spray dryer operation using nonlinear model predictive control with state estimation. *9th International Symposium on Advanced Control of Chemical Processes*, 507–513.

Petersen, L.N., Poulsen, N.K., Niemann, H.H., Utzen, C., and Jørgensen, J.B. (2014a). Application of Constrained Linear MPC to a spray dryer. *IEEE Multi-Conference on Systems and Control*, 2120–2126.

Petersen, L.N., Poulsen, N.K., Niemann, H.H., Utzen, C., and Jørgensen, J.B. (2014b). Economic optimization of spray dryer operation using nonlinear model predictive control. *53rd IEEE Conference on Decision and Control*, 6794 – 6800.

Shabde, V.S. and Hoo, K.A. (2008). Optimum controller design for a spray drying process. *Control Engineering Practice*, 16, 541–552.

Paper I

Industrial Application of Model Predictive Control to a Milk Powder Spray Drying Plant

Submitted to *15th European Control Conference (ECC 2016), pp. accepted, 2016, Aalborg.*

Industrial Application of Model Predictive Control to a Milk Powder Spray Drying Plant

Lars Norbert Petersen[1,2], Niels Kjølstad Poulsen[1], Hans Henrik Niemann[3], Christer Utzen[2] and John Bagterp Jørgensen[1]

***Abstract*— In this paper, we present our first results from an industrial application of model predictive control (MPC) with real-time steady-state target optimization (RTO) for control of an industrial spray dryer that produces enriched milk powder. The MPC algorithm is based on a continuous-time transfer function model identified from data and states estimated by a time-varying Kalman filter. The RTO layer utilizes the same linear model and a nonlinear economic objective function for calculation of the economically optimized targets. We demonstrate, by industrial application of the MPC, that this method provides significantly better control of the residual moisture content, increases the throughput and decreases the energy consumption compared to conventional PI-control. The MPC operates the spray dryer closer to the residual moisture constraint of the powder product. Thus, the same amount of feed produces more powder product by increasing the average water content. The value of this is 186,000 €/year. In addition, the energy savings account to 6,900 €/year.**

I. Introduction

Spray drying reduces the water content of a product and produces a free flowing powder. It is a processing technique, particularly used in the dairy industry to increase the shelf-life as well as reduce the cost of transportation. The main challenge in controlling the spray dryer is to use a minimum of energy (hot air) to bring the residual moisture in the powder below the specification and to avoid powder sticking to the walls of the drying chamber. In [1] and [2] we identified that application of advanced control is a cost effective way to

- Increase yield and lower specific energy consumption
- Increase throughput while reducing the risk of fouling or blockage due to sticky powder
- Reduce waste by reduced re-work of powder

Three control concepts were investigated by simulation; conventional PI-control, MPC with RTO and economically optimizing nonlinear MPC (NMPC). Based on these simulations we applied the MPC with RTO to an industrial spray dryer [1]. The selected industrial spray dryer produces several dairy related products and is categorized as one of the largest dryers installed in the dairy industry. During the trials enriched skim-milk powder was produced.

[1] Department of Applied Mathematics and Computer Science, Technical University of Denmark, Kgs. Lyngby, Denmark, {lnpe,nkpo,jbjo}@dtu.dk
[2] GEA Process Engineering A/S, Søborg, Denmark, christer.utzen@gea.com
[3] Department of Electrical Engineering, Technical University of Denmark, Kgs. Lyngby, Denmark, hhn@elektro.dtu.dk

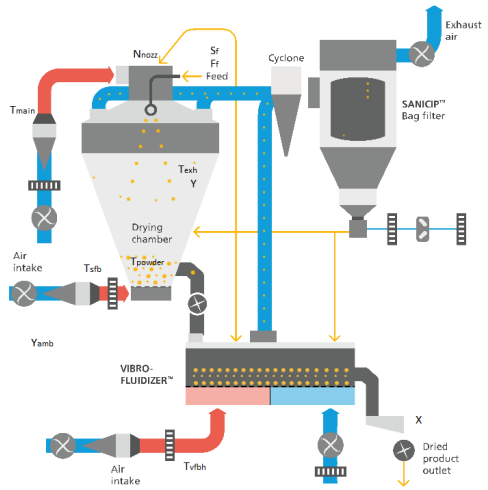

Fig. 1. Diagram of the MSD™. Sprayed droplets are dried into powder in several stages.

A. Process Description

The MSD™ spray dryer combines spray and fluid bed drying technology to ensure the best overall drying efficiency and product quality. Fig. 1 illustrates the stages of the spray dryer as well as the hot air and the powder in- and outlets. A set of nozzles atomize the concentrate and feed it into the drying chamber. The drying air enters vertically through the air disperser at a high velocity and mixes with the atomized concentrate. At this stage, the evaporation takes place instantaneously while the droplets pass through the drying chamber. The air flow leads the particles to the integrated fluid bed at the bottom of the drying chamber for the second stage drying. Finally the powder is led to a VIBRO-FLUIDIZER™ fluid bed for final drying and cooling. A falling film evaporator is placed up stream in the process for pre-concentration of the feed and the powder handling system is down stream for storage and packaging of the produced powder.

For a long time, MPC has been the preferred advanced control methodology in the process industries [3]. The combination of real-time steady-state optimization (RTO) and target based model predictive control (MPC) is a standard methodology for optimizing process operation [4], [5].

Attempts have been made to improve the control of spray

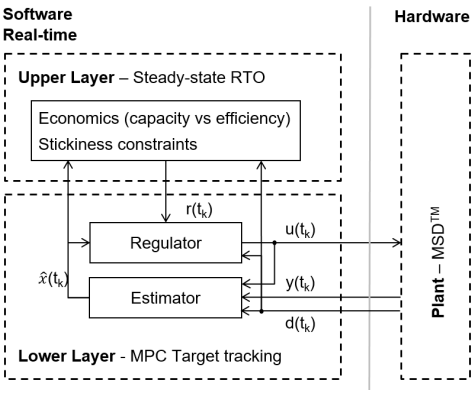

Fig. 2. MPC with steady-state target optimization. The software runs on an industrial PC.

dryers. A feed forward cascade controller is presented in [6], which controls the exhaust temperature by manipulation of the feed rate to indirectly maintain constant product moisture content. [7] extends [6] in the respect that the humidity of the exhaust air is controlled instead of the exhaust air temperature to maintain constant product quality. [8] develop an LQG controller for residual moisture control in an industrial detergent spray drying process. In [6]–[8] the powder moisture was analyzed off-line. Industrial MPC solutions for spray dryers also exist and seem to rely on empirically based step-response models and least-squares methods for estimation of the residual moisture content of the powder. [1] compares a linear tracking MPC with conventional PI-control by simulation and [2] studies an economically optimizing NMPC solution by simulation. In [9] a linear MPC is designed without an RTO layer to be used in industrial spray drying and is validated by simulation.

In this paper, we apply an MPC with RTO to an industrial spray dryer. We describe the industrial setup and present our first results based on industrial data. We conclude that the yield, energy consumption and profit of operation for the spray drying process can be improved significantly by application of MPC compared to conventional PI-control.

B. Organization

The paper is organized as follows. In Section II we present the complete MPC with RTO algorithm. The industrial setup is described in Section III. In Section IV we provide the results of the industrial application and compute the estimated benefits. Conclusions are given in Section V.

II. Model Predictive Control

The MPC is constructed by combining a state estimator, a regulator and an RTO layer as illustrated in Fig. 2.

A. Plant and Sensors

The controlled variables are the exhaust air temperature T_{exh}, the SFB powder temperature T_{powder}, the absolute exhaust air humidity, Y, and the powder outlet residual moisture content, X. The manipulated variables are the feed flow, F_{f}, the inlet main air temperatures, T_{main}, the inlet SFB air temperature, T_{sfb}, and the VFB air temperature, T_{vfbh}. The disturbance variables are the feed solids concentration S_{f}, the absolute ambient air humidity, Y_{amb}, and the number of active nozzles, N_{nozz}.

The measurement vector, y, the manipulated input vector, u, and the disturbance vector, d, are

$$y = \begin{bmatrix} T_{\text{exh}} & T_{\text{powder}} & Y & X \end{bmatrix}^{\mathsf{T}} \tag{1a}$$

$$u = \begin{bmatrix} F_{\text{f}} & T_{\text{main}} & T_{\text{sfb}} & T_{\text{vfbh}} \end{bmatrix}^{\mathsf{T}} \tag{1b}$$

$$d = \begin{bmatrix} S_{\text{f}} & Y_{\text{amb}} & N_{\text{nozz}} \end{bmatrix}^{\mathsf{T}} \tag{1c}$$

Recent developments in sensor technology have made the absolute exhaust air humidity, Y, and the powder outlet residual moisture content, X, available in industrial practice. The sample frequency of these instruments varies up to several minutes and observations may also be unavailable for longer periods which is handled in the MPC by applying a time-varying Kalman filter.

B. Model

We identify a continuous time transfer function model described by

$$\bar{U}(s) = G_a(s)U(s) \tag{2a}$$

$$Z(s) = G_m(s)\bar{U}(s) + G_d D(s) \tag{2b}$$

$$y(t_k) = z(t_k) \tag{2c}$$

in which $U(s)$ is the manipulated variables, $\bar{U}(s)$ is the actuated intermediate values and $Z(s)$ is the controlled variables. $D(s)$ is the disturbances that only affects the controlled variables. $G_a(s)$ is the actuator model, $G_m(s)$ is the dryer model and $G_d(s)$ is the disturbance model. These consist of a matrix of transfer functions of the form

$$g_{a,ii}(s) = \frac{K_{a,ii}}{\tau_{a,ii}s + 1} e^{-\theta_{a,ii}s} \tag{2d}$$

$$g_{m,ji}(s) = \frac{K_{m,ji}}{\tau_{m,ji}s + 1} e^{-\theta_{m,ji}s} \tag{2e}$$

$$g_{d,jk}(s) = \frac{K_{d,jk}}{\tau_{d,jk}s + 1} e^{-\theta_{d,jk}s} \tag{2f}$$

where i is the input, k is the disturbance and j is the output number. The parameters in the above model are obtained by least-squares minimization of the residuals between the simulated and recorded response. The recorded response is sampled every 20 sec with the residual moisture measurement being updated every 3-4 minutes.

Fig. 3 shows the unit step responses of the identified model. Fig. 4 presents 1 out of the 10 datasets used for estimation of the model. The model response is a simulation in which no feedback from the data is implemented. The model fits the data well. The datasets consist of both open-loop step response data and closed-loop data.

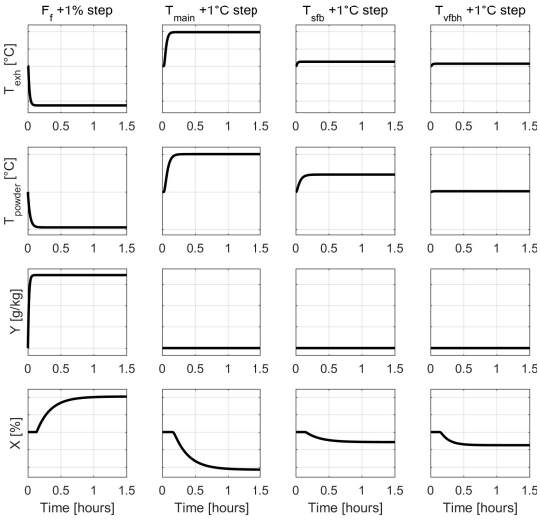

Fig. 3. Unit-step responses of the identified model in (2).

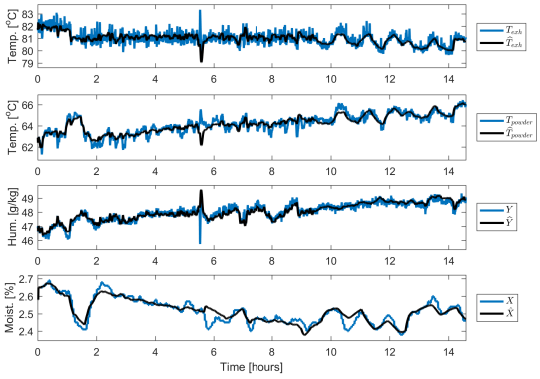

Fig. 4. Comparison of 1 out of 10 estimation datasets (blue) and the corresponding model simulation (black) of (2). The model fits the data well.

C. Offset-free estimation

The process model in (2) is transformed to a discrete time state space model using a sample time of $T_s = 20$ sec and a zero-order-hold assumption on the inputs and disturbances. Thereby we can make a balanced realization from the Hankel matrix of the impulse response matrices. In order to achieve offset-free control at steady-state, in the presence of plant/model mismatch and/or un-modeled disturbances, the linear model is augmented by integrating disturbance states according to the methodology proposed in [10]. We select pure output disturbances, i.e. $C_\mathrm{d} = I$ and $B_\mathrm{d} = 0$.

D. State estimator

The linear time-varying (LTV) Kalman filter (KF) is used to estimate the states. The augmented model used in the state estimator, the regulator and the RTO layer, is

$$x_{k+1} = Ax_k + Bu_k + Ed_k + Gw_k + \sigma_x \tag{3a}$$
$$y_k = C_k x_k + \sigma_k + v_k \tag{3b}$$
$$z_k = Cx_k + \sigma \tag{3c}$$

with x being the augmented states, u being the manipulated variables, d being measured disturbances, y is the measurement variables that may change in size due to the missing observations. z is the controlled variables. G is selected such that state noise is only present at the integrating disturbance states. w and v are $w_k \sim N_{iid}\,(0, R_\mathrm{w})$ and $v_k \sim N_{iid}(0, R_\mathrm{v})$ in which the noise covariances must be estimated. The initial state is, $x_0 \sim N(\tilde{x}_0, P_0)$. σ_x, σ and σ_k are constants $\sigma_x = x_0 - Ax_0 - Bu_0 - Ed_0$, $\sigma = z_0 - Cx_0$ and $\sigma_k = y_{0,k} - C_k x_0$.

E. Estimator tuning

The unknown noise variances, R_w and R_v, are estimated using the Maximum Likelihood (ML) method [11]. Given the model structure, the optimally selected variances maximizes the likelihood function of a sequence of output measurements $\mathcal{Y}_N = [y_N, y_{N-1}, ..., y_1, y_0]$. The likelihood function is $L(R_\mathrm{w}, R_\mathrm{v}; \mathcal{Y}_N)$ and by conditioning on y_0 and taking the negative logarithm we get

$$-\ln(L(\cdot)) = \frac{1}{2}\sum_{k=1}^{N}\left(\ln(\det(R_{e,k|k-1})) + \epsilon_k^T R_{e,k|k-1}^{-1}\epsilon_k\right) + \ln(2\pi)\frac{1}{2}\sum_{k=1}^{N} n_{y,k}$$

with $\epsilon_k = y_k - \hat{y}_{k|k-1}$ and $n_{y,k}$ is the number of measurements. The ML estimate of the variances are then determined by solving the nonlinear optimization problem

$$[R_\mathrm{w}, R_\mathrm{v}] = \arg\min_{R_\mathrm{w}, R_\mathrm{v}} \{-\ln(L(R_\mathrm{w}, R_\mathrm{v}; \mathcal{Y}_N | y_0))\} \tag{4}$$

where ϵ_k and $R_{e,k|k-1}$ are computed recursively by means of the KF, i.e. Algorithm 1 without the regulator and RTO computations, and recorded data from the plant. We select the initial state noise $R_\mathrm{w} = I \cdot 0.01$, measurement noise $R_\mathrm{v} = I \cdot 0.001$ and the state covariance, $P_0 = 10 \cdot \bar{P}$, determined by the solution to the discrete algebraic Riccati equation (DARE)

$$\bar{P} = A\bar{P}A^T + GR_\mathrm{w}G^T - (A\bar{P}C^T)(R_\mathrm{v} + C\bar{P}C^T)^{-1}(A\bar{P}C^T)^T$$

An alternative method for tuning of the estimator is provided in [12].

Algorithm 1 MPC with RTO Algorithm

Require: y_k, d_k, $\hat{x}_{k|k-1}$, $P_{k|k-1}$, u_{k-1}

Filter:

Compute the one-step ahead measurement prediction

$\hat{y}_{k|k-1} = C_k\hat{x}_k + \sigma_k$,

Compute the filtered state

$R_{e,k} = C_k P_{k|k-1} C_k^T + R_{\mathrm{v},k}$

$K_{fx,k} = P_{k|k-1} C_k^T R_{e,k}^{-1}$

$\hat{x}_{k|k} = \hat{x}_{k|k-1} + K_{fx,k}(y_k - \hat{y}_{k|k-1})$

$P_{k|k} = P_{k|k-1} - K_{fx,k} R_{e,k} K_{fx,k}^T$

RTO:

$r_k = \psi(\hat{x}_{k|k},\, d_k)$

Regulator:

$u_k = \mu(r_k,\, \hat{x}_{k|k},\, u_{k-1},\, d_k)$

One-step predictor:

Compute the predicted state, $\hat{x}_{k+1|k}$, using

$\hat{x}_{k+1|k} = A\hat{x}_k + Bu_k + Ed_k + \sigma_x$

$P_{k+1|k} = AP_{k|k}A^T + GR_{\mathrm{w}}G^T$

return u_k, $\hat{x}_{k+1|k}$, $P_{k+1|k}$

F. Regulator

The l_2 output tracking problem with input constraints may be formulated as

$$\min_{U_k} \quad \phi = \frac{1}{2}\sum_{j=1}^{N} \|z_{k+j} - r_k\|_{Q_z}^2 + \frac{1}{2}\sum_{j=0}^{N-1} \|\Delta u_{k+j}\|_{S_u}^2 \tag{5a}$$

$$\text{s.t.} \quad x_k = \hat{x}_{k|k} \tag{5b}$$

$$x_{k+j+1} = Ax_{k+j} + Bu_{k+j}, \quad + Ed_k + \sigma_x \qquad j \in \mathcal{N}_u \tag{5c}$$

$$z_{k+j} = C_{\mathrm{z}} x_{k+j} + \sigma, \qquad j \in \mathcal{N}_z \tag{5d}$$

$$u_{\min} \le u_{k+j} \le u_{\max}, \qquad j \in \mathcal{N}_u \tag{5e}$$

in which $\Delta u_{k+j} = u_{k+j} - u_{k+j-1}$, $\mathcal{N}_z = \{1, 2 \ldots, N\}$ and $\mathcal{N}_u = \{0, 1 \ldots, N-1\}$ [13]. N is the control and prediction horizon. N is selected sufficiently long to avoid any end effects on the solution in the beginning of the horizon. No forecasts are available for the references and disturbances, so we use the same-as-now forecasts, i.e. $r_k = r(t_0)$ and $d_k = d(t_0)$ is applied.

The tracking problem in (5) is solved by formulating the corresponding convex quadratic problem. The tracking problem is similar to [14]–[17]. We choose to solve a condensed QP as the number of states is 55 due to the long process delays and the number of inputs are only 4.

Define the vectors Z, R, U and D as

$$Z_k = \begin{bmatrix} z_{k+1} \\ z_{k+2} \\ \vdots \\ z_{k+N} \end{bmatrix} \quad R_k = \begin{bmatrix} r_k \\ r_k \\ \vdots \\ r_k \end{bmatrix} \quad U_k = \begin{bmatrix} u_k \\ u_{k+1} \\ \vdots \\ u_{k+N} \end{bmatrix} \quad D_k = \begin{bmatrix} d_k \\ d_k \\ \vdots \\ d_k \end{bmatrix}$$

Then the predictions are

$$Z_k = \Phi_x x_k + \Gamma_u U_k + \Gamma_d D_k + \Omega\Sigma_x + \Sigma_z$$

Using the predictions in vector form we can write the objective function as

$$\begin{aligned} \phi &= \frac{1}{2}\sum_{j=1}^{N} \|z_{k+j} - r_k\|_{Q_z}^2 + \frac{1}{2}\sum_{j=0}^{N-1} \|\Delta u_{k+j}\|_{S_u}^2 \\ &= \frac{1}{2}\|Z_k - R_k\|_{\mathcal{Q}_z}^2 + \frac{1}{2}\|U_k - U_{k-1}\|_{\mathcal{S}_u}^2 \\ &= \frac{1}{2}\|\Gamma_u U_k - (R_k + b)\|_{\mathcal{Q}_z}^2 + \frac{1}{2}\|\Lambda U_k - I_0 u_{k-1}\|_{\mathcal{S}_u}^2 \\ &= \frac{1}{2}U_k^T H U_k + g^T U_k + \rho \end{aligned}$$

with

$$\begin{aligned} H &= \Gamma_u^T \mathcal{Q}_z \Gamma_u + \Lambda^T \mathcal{S}_u \Lambda \\ g &= -\Gamma_u^T \mathcal{Q}_z\,(R_k - b) - \Lambda^T \mathcal{S}_u I_0 u_{k-1} \\ \rho &= \frac{1}{2}\| - b - R_k\|_{\mathcal{Q}_z}^2 + \frac{1}{2}\|I_0 u_{k-1}\|_{\mathcal{S}_u}^2 \end{aligned}$$

where

$$b = -\Phi_x x_k - \Gamma_d D_k - \Omega\Sigma_x - \Sigma_z$$

The constraints are assumed constant over the prediction horizon and $u_{min} \le u_{k+j} \le u_{max}$ may be denoted

$$U_{min} \le U_k \le U_{max}$$

We solve the tracking problem by solution of the following convex quadratic problem

$$\min_{U_k} \quad \frac{1}{2}U_k^T H U_k + g^T U_k + \rho \tag{6a}$$

$$\text{s.t.} \quad U_{min} \le U_k \le U_{max} \tag{6b}$$

Given the solution, $U_k^* = \begin{bmatrix}(u_0^*)^T & (u_1^*)^T & \ldots & (u_{N-1}^*)^T\end{bmatrix}^T$, the regulator only apply the first u_0^* to the process. The open-loop optimization is repeated at the next sample where it also utilize the new state estimate $\hat{x}_{k|k}$. We use a tailored interior point QP-solver for solution of (6), based on [18]–[20].

G. RTO

The RTO layer optimizes the reference, r_k, in the regulator to achieve better economic performance. r_k is computed by solving the steady-state economic optimization problem

$$\min_{z_{\mathrm{ss}}, u_{\mathrm{ss}}, s} \quad \phi = -p(z_{\mathrm{ss}}, u_{\mathrm{ss}}, d_k) + \|s\|_{S_W}^2 \tag{7a}$$

$$\text{s.t.} \quad x_{\mathrm{ss}} = Ax_{\mathrm{ss}} + Bu_{\mathrm{ss}} + Ed_k + B_{\mathrm{d}}x_{\mathrm{d}} + \sigma_x \tag{7b}$$

$$z_{\mathrm{ss}} = Cx_{\mathrm{ss}} + C_{\mathrm{d}}x_{\mathrm{d}} + \sigma \tag{7c}$$

$$u_{\min} + \delta \le u_{\mathrm{ss}} \le u_{\max} - \delta \tag{7d}$$

$$c(z_{\mathrm{ss}}) + s \ge 0 \tag{7e}$$

$$s \ge 0 \tag{7f}$$

and setting $r_k = z_{\mathrm{ss}}$. δ contains a 5 °C back-off in the manipulated temperatures to maintain good control properties in the regulator. $p(z_{\mathrm{ss}}, u_{\mathrm{ss}}, d_k)$ is a nonlinear profit function similar to [2]. $c(z_{\mathrm{ss}})$ is the output constraints for each output and includes stickiness constraints of the powder in the top of the dryer [2]. The model (A, B, E, C) and the state x_{ss} are the non-augmented system model. Plant/model mismatch

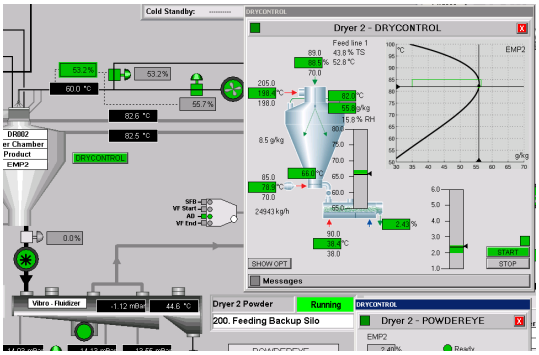

Fig. 5. The SCADA system for control of the spray dryer along with the MPC faceplate.

and/or un-modeled disturbances are corrected for by utilizing the offset corrections estimated by the state estimator, x_{d}, in the RTO.

III. MPC IN AN INDUSTRIAL SETUP

Algorithm 1 lists the on-line computations in the MPC, consisting of a regulator, state estimator with filter and one-step-ahead predictor step and an RTO layer. The tuning parameters Q_z and S_u are fixed and selected to achieve fast and robust performance. The highest weight is set on control of the residual moisture content. The control and prediction horizon is, $N = 60$ min$/20$ s $= 180$. The update interval of the MPC is 20 sec. The long control and prediction horizon is necessary due to the process delays and slow dynamics of the residual moisture content while the relatively fast update interval is necessary due to the fast temperature and air humidity dynamics. The reference, r_k, is computed at a sample rate of 5 min. The constraints in (6b), (7d) and (7e) renders minimum and maximum values to ensure process safety and quality of the powder.

The MPC is implemented using MATLAB® and compiled to a standalone executable program. The MPC interfaces to the PLC system via an OPC connection. The inputs and outputs to the MPC are scaled and validated. Bumpless transfer is implemented to ensure a smooth transition between the MPC and conventional PI controller. Interlocks are implemented to accommodate emergency shut down. The MPC is controlled from the SCADA system as shown in Fig. 5. The operator can turn it on or off, adjust the constraints, and see the optimal targets which the MPC is heading towards.

IV. RESULTS

Fig. 6 and Fig. 7 illustrates the application of the MPC, referred to as MPC trial 1 and MPC trial 2.

The MPC trials in Fig. 6 and Fig. 7 show that the MPC is able to control the process variables to its targets by adjustments to the manipulated variables, even when large disturbances constantly disturb the process. The targets are computed by the RTO layer and are frequently updated. During the trials the MPC was able to maintain T_{exh} and Y close to the constraints that relate to stickiness of the powder and the residual moisture content, X, close to its maximum limit. The constraints are violated particularly in the presence of large disturbances. We only restrict the estimated outputs of the Kalman filter to stay within the process constraint. This is a fair restriction, as the constraints already have back-off incorporated from the true process safety constraints and to avoid process assiduous operation.

In both trial 1 and 2 the MPC handles the large dips in the feed solids concentration well by reducing the capacity accordingly. The dips are due to evaporator swaps upstream in the process. The varying ambient air humidity is also handled, but the maximum exhaust air humidity, $Y_{\max}$, was not reached in these trials. The bottleneck of the dryer performance then becomes the maximum feed rate, $F_{\max}$, in Fig. 6 or the maximum temperatures on the heaters, $T_{\max}^{\mathrm{main}}$ and $T_{\max}^{\mathrm{sfb}}$ in Fig. 7.

The MPC in trial 2, Fig. 7, was turned off by the operator at time 16:20 due to high nozzle pressure. $T_{\max}^{\mathrm{main}}$ was set too low and thus enough energy could not be supplied to the process to keep the last nozzle active. After 2 hours the MPC was turned on again with $T_{\max}^{\mathrm{main}}$ increased by 1°C allowing the control system to keep the extra nozzle active. In the mean time, the operator violates the process constraints.

In general we see, that the RTO layer seeks to maximize the product flow rate by maximizing the feed flow while supplying just the amount of energy needed to avoid that the powder sticks to the chamber walls and the final powder stays within specifications. The energy consumption is further minimized by shifting the drying from the top of the spray dryer to the more efficient fluid bed stages. Drying in the SFB is also preferred opposed to drying in the VFB, as the energy supplied to the SFB is better utilized.

In conventional operation, which uses a PI controller, the exhaust air temperature, T_{exh}, is controlled stable by manipulation of the feed pump speed. The SFB powder temperature, T_{powder}, the exhaust air humidity, Y, and the residual moisture content, X, are un-controlled. Thus, these vary and may violate the process constraints. The task of controlling these are thus up to the operator. The plant operator have many tasks to perform and processes to control at the same time. Process optimization is thus a difficult task for the operator, as it requires constant attention to the process and insight in the spray drying process to adjust the dryer accordingly. Process economics are therefore often a secondary objective. Optimal operation with PI control is therefore hardly ever obtained in practice. With the demonstrated MPC solution, optimal control of the dryer is reduced from a labor intensive task to an automated target tracking MPC problem. The MPC therefore makes the operation of the dryer simpler, improves and stabilizes the powder quality and increasing the energy efficiency.

A. Benefit

Table I shows the key performance indicators (KPIs) of the two presented trials and a reference PI control trial. The PI

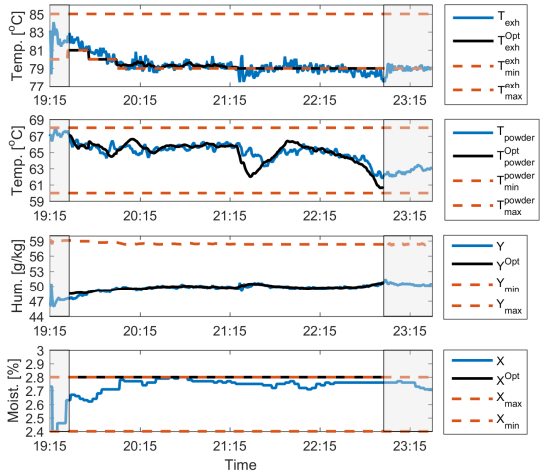

(a) System outputs.

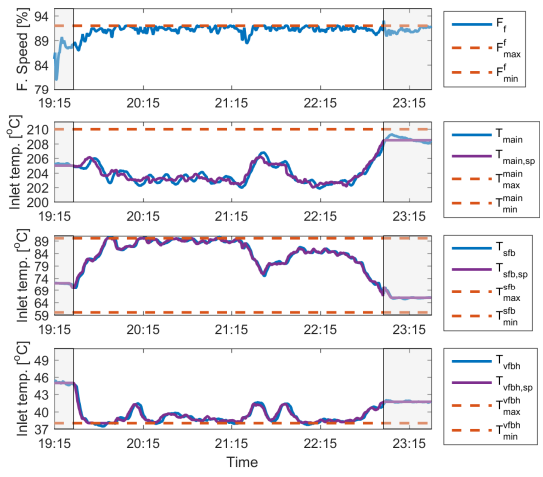

(b) Manipulated variables.

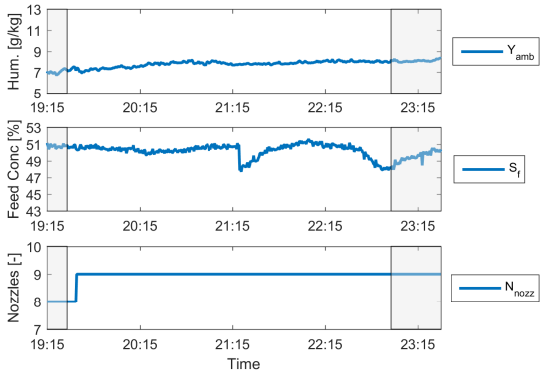

(c) Measured disturbances.

Fig. 6. MPC trial 1 in operation. The grey-shaded area denote PI control in action. Red lines indicate constraints.

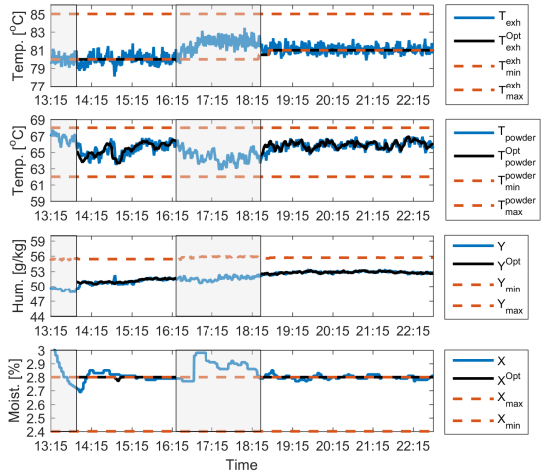

(a) System outputs.

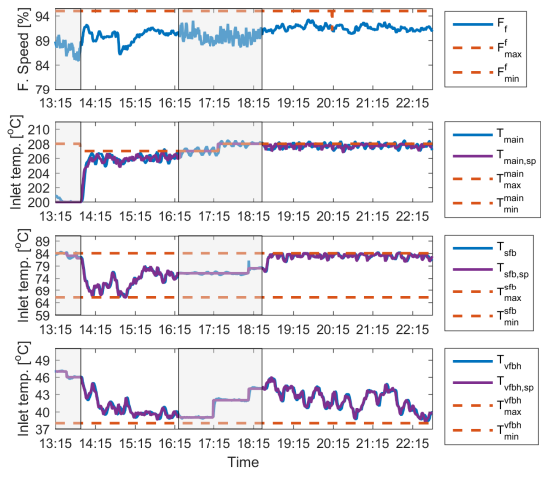

(b) Manipulated variables.

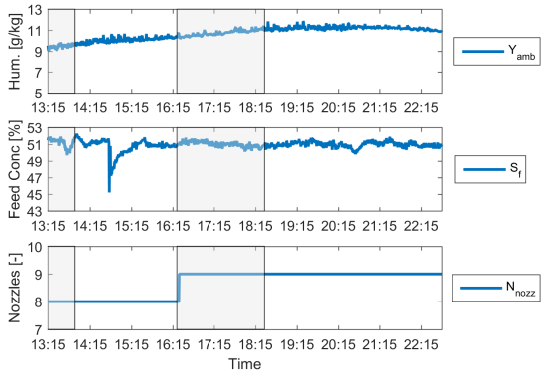

(c) Measured disturbances.

Fig. 7. MPC trial 2 in operation. The grey-shaded area denote PI control in action. Red lines indicate constraints.

TABLE I
AVERAGE KPI VALUES.

KPIs	Unit	PI	MPC 1	MPC 2
Product flow rate	F_p [kg/hr]	7,177	7,416	7,499
Energy consumption	Q_{tot} [MW]	7.41	7.41	7.49
Residual moisture	X [%]	2.633	2.746	2.799
Energy efficiency	η [%]	63.4	64.4	62.6

controller falls out with a lower average product throughput and residual moisture content in the powder. The MPC in trial 1 improves the product flow rate by 239 kg/hr, the energy efficiency by 1% and the residual moisture content by 0.113%. This is achieved without compromising any process constraints. The ambient air humidity is significantly higher in the MPC trial 2. The powder must therefore be dried more extensively to meet the residual moisture limit, at the expense of an increased energy consumption and decreased energy efficiency. The MPC in trial 2 still improves the product flow rate by 322 kg/hr and the residual moisture content by 0.166%. The two MPC trials are both limited by the conservatively chosen tight constraints on the manipulated variables defined by the operators. Either the feed pump speed or the maximum heater temperature constrain the performance. The gains are therefore expected to increase significantly as the operators get more confident in using the MPC and can agree to widen the process constraints on the manipulated variables.

The annual profit increase from the residual moisture content improvements equates to approx.

$$= 0.139\% \cdot 7,400 \text{ kg/hr} \cdot 7,200 \text{ hr/year} \cdot 2.5 \text{ €/kg}$$
$$= 185,614 \text{ €/year}$$

and the annual energy profit increase equates to approx.

$$= 1\% \cdot 7.41 \text{ MW} \cdot 7,200 \text{ hr/year} \cdot 12.906 \text{ €/(MW/hr)}$$
$$= 6,886 \text{ €/year}$$

assuming the price of natural gas and the energy improvement achieved by the MPC in trial 1, where the ambient air humidity is comparable to the PI control trial. We exclude the profit related to increased production, as it may be limited by up- and down stream process capacity as well as the market demand.

V. CONCLUSIONS

We have developed a model predictive controller (MPC) and demonstrated its use on an industrial spray dryer. The performance of the MPC was documented by industrially recorded data and we showed that the MPC provided significantly better control of the residual moisture content i.e. product quality and yield, increased the throughput and energy efficiency compared to conventional PI control. We find evidence that it is difficult to control the dryer using the conventional PI controller, and optimal operation is therefore hardly never obtained by the operators. The MPC reduces the difficult and labor intensive task of process optimization to an automated target tracking MPC problem. The annual profit increase by using MPC is estimated to be, 186,000 €/year from the improved yield and 6,900 €/year from the energy savings.

REFERENCES

[1] L. N. Petersen, J. B. Jørgensen, and J. B. Rawlings, "Economic optimization of spray dryer operation using nonlinear model predictive control with state estimation," *9th International Symposium on Advanced Control of Chemical Processes*, pp. 507–513, 2015.

[2] L. N. Petersen, N. K. Poulsen, H. H. Niemann, C. Utzen, and J. B. Jørgensen, "Comparison of linear and nonlinear model predictive control for optimization of spray dryer operation," *5th IFAC Conference on Nonlinear Model Predictive Control*, pp. 218–223, 2015.

[3] M. L. Darby, M. Harmse, and M. Nikolaou, "MPC: Current practice and challenges," *7th IFAC International Symposium on Advanced Control of Chemical Processes*, vol. 7, no. 1, pp. 86–98, 2009.

[4] M. R. Naysmith and P. L. Douglas, "Review of real time optimization in the chemical process industries," *Developments in Chemical Engineering and Mineral Processing*, pp. 67–87, 1995.

[5] T. E. Marlin and A. N. Hrymak, "Real-time operations optimization of continuous processes," *Chemical Process Control-V Conference*, pp. 156–164, 1996.

[6] J. Pérez-Correa and F. Fariass, "Model based control of centrifugal atomizer spray drying," *Food Control*, vol. 2, no. 3, pp. 170–175, 1991.

[7] ——, "Modelling and control of a spray dryer: a simulation study," *Food Control*, vol. 6, no. 4, pp. 219–227, 1995.

[8] R. Govaerts, A. Johnson, R. Crezee, G. Reyman, and P. Swinkels, "Control of an industrial spray-drying unit," *Control Engineering Practice*, vol. 2, no. 1, pp. 69–85, 1994.

[9] L. N. Petersen, N. K. Poulsen, H. H. Niemann, C. Utzen, and J. B. Jørgensen, "Application of constrained linear MPC to a spray dryer," *The IEEE Multi-Conference on Systems and Control*, 2014.

[10] G. Pannocchia and J. B. Rawlings, "Disturbance models for offset-free model-predictive control," *AIChE Journal*, vol. 49, no. 2, pp. 426–437, 2003.

[11] N. R. Kristensen, H. Madsen, and S. B. Jørgensen, "A method for systematic improvement of stochastic grey-box models," *Computers and Chemical Engineering*, vol. 28, no. 8, pp. 1431–1449, 2004.

[12] D. H. Olesen, J. K. Huusom, and J. B. Jørgensen, "A tuning procedure for ARX-based MPC of multivariate processes," *2013 American Control Conference (ACC)*, pp. 1721–1726, 2013.

[13] J. B. Jørgensen, "Moving horizon estimation and control," Ph.D. dissertation, Technical University of Denmark, 2005.

[14] G. Prasath and J. B. Jørgensen, "Soft Constraints for Robust MPC of Uncertain Systems," *International Symposium on Advanced Control of Chemical Processes*, vol. 7, no. 1, pp. 225–230, 2009.

[15] J. B. Jørgensen, J. B. Rawlings, and J. K. Huusom, "Finite horizon MPC for systems in innovation form," *The IEEE Conference on Decision and Control*, pp. 1896–1903, 2011.

[16] J. K. Huusom, N. K. Poulsen, S. B. Jørgensen, and J. B. Jørgensen, "Tuning of methods for offset free MPC based on ARX model representations," *The American Control Conference*, pp. 2255–2360, 2010.

[17] ——, "Tuning SISO offset-free model predictive control based on ARX models," *Journal of Process Control*, vol. 22, no. 10, pp. 1997 – 2007, 2012.

[18] K. Edlund, L. E. Sokoler, and J. B. Jørgensen, "A Primal-Dual Interior-Point Linear Programming Algorithm for MPC," *48th IEEE Conference on Decision and Control and 28th Chinese Control Conference*, pp. 351–356, 2009.

[19] J. B. Jørgensen, J. B. Rawlings, and S. B. Jørgensen, "Numerical methods for large scale moving horizon estimation and control," *International Symposium on Dynamics and Control Process Systems*, vol. 7, 2004.

[20] J. B. Jørgensen, G. Frison, N. F. Gade-Nielsen, and B. Damman, "Numerical Methods for Solution of the Extended Linear Quadratic Control Problem," *4th IFAC Nonlinear Model Predictive Control Conference*, pp. 187–193, 2002.

[This page intentionally left blank]

[This page intentionally left blank]